CRANFIELD UNIVERSITY

SCHOOL OF INDUSTRIAL AND MANUFACTURING SCIENCE

Ph.D. Thesis

Academic year 1998 - 2003

Didar Singh Dulay

The Application of Electromagnetic NDT Method to the inspection of Non- ferrous Cast Materials

Supervisor: Dr. M. W. B. Lock

March 2003

ABSTRACT

Inspection of non-ferrous cast material is routinely carried out looking for casting defects inherent for the manufacturing process. The NDT methods employed are Radiography and Ultrasonics, primarily for sub-surface or internal defects and Penetrants for surface breaking defects. Electromagnetic techniques have not been used on cast material except maybe for conductivity determination. This limitation resulting from the surface roughness normally associated with cast surfaces and the fact the other techniques mention above have been very successful in finding and evaluating the discontinuities sought.

The possible application of Electromagnetic techniques on surfaces in the as-cast condition of non-ferromagnetic material came about because of specific problems experienced by industry.

Two major investigations were offered namely;

1) Investigation of CNC material - CuNiCr [1.6%Cr] castings exhibiting oxide entrapment in the form of networks.
2) Investigation of NAB - Nickel Aluminium Bronze exhibiting selective phase corrosion on immersion in seawater.

The detection and measurement of both oxide entrapment and phase selective corrosion was difficult and in cases impossible with conventional NDT methods employed for quality control of these material/component types. Time of Flight Diffraction Ultrasonics did give some 50% detectability of phase selective corrosion, but the method was found to be expensive and very time consuming.

The metallurgical properties of the material and morphology of the defects have been studied for both Cupro Nickel Chromium and Nickel Aluminium Bronze cast alloys. An investigation was then conducted to study the effects of eddy current signals and their potential in detecting, both linear and cluster type defects which were predominantly interdendritic with some reported as intergranular in nature.

For inspecting Cupro Nickel Chromium castings two successful eddy current methods have been developed. Detection of surface flaws was achieved by high frequency [2MHz] examination and subsurface flaws by using low frequencies [1-2KHz] but using specifically developed sensors

that provided good penetration but maintained sensitivity to the fine defects.

In the case of Nickel Aluminium Bronze material, the investigation was to look at electromagnetic techniques, which best utilizes the inherent feature of permeability/conductivity associated with this non- ferromagnetic material and any changes that phase selective corrosion may produce. Some meaningful results were obtained using a combination of eddy current excitation with detection via magneto-resistive sensors.

Testing through 30-40mm of material to detect small magnetic variation produced by only 1-2 mm of corrosion penetration was difficult to quantify. Detection and assessment however appeared hopeful when examination was carried out from the corroded surface. With quantifiable samples a meaningful technique using eddy current excitation and magneto-resistive sensor for detection can be developed.

CONTENT **Page**

	Abstract	ii
	Content	iv
	List of Figures	vi
	List of Tables	viii
	Notation	ix
1.	**Introduction**	1
2.	**Standard NDT Inspection Methods**	3
2.1	Visual Inspection	3
2.2	Liquid Penetrant Inspection	4
2.3	Magnetic Particle Inspection	11
2.4	Eddy Current Inspection	17
2.5	Ultrasonic Inspection	31
2.6	Radiography	32
3.	**Study 1- Inspection of CNC [1.6% Cr.] Material Castings to Detect Oxide Entrapments.**	37
3.1	Background	37
3.2	Quality Assurance of CuNiCr Castings to NES 824	39
3.2.1	Dye Penetrant	39
3.2.2	Acceptance Criteria for Penetrant Inspection	39
3.2.3	Radiography	40
3.2.4	Acceptance Criteria for Radiographic Inspection	40
3.3	Metallurgical Examination of Oxide Network Discontinuities	40
3.4	Investigation of Heat Affected Zone Cracking in High Strength Cupro Nickel Chromium NES 824	42
3.4.1	Introduction	42
3.4.2	Chemical Analysis	43
3.4.3	Mechanical properties and Hot Ductility Testing	44
3.4.4	Welding	44
3.4.5	General Discussion	44
3.4.6	Conclusion	45
4.	**Investigation for Suitable NDT Methods**	47
4.1	Consultation with Various UK NDT Agencies	48
4.2	Surface Flaw Detection	49
4.3	Sub-surface Flaw Detection	50
4.3.1	Radiography	50
4.3.2	Ultrasonic	53
4.4	Conclusion	54
5.0	**Development of Surface and Subsurface Eddy Current Techniques**	55
5.1	Experimental Procedures	55

5.2	Results	57
5.3	Conclusion	60
6.0	**Study 2 –Nickel Aluminium Bronze, Detection of Phase Selective Corrosion**	61
6.1	Introduction	61
6.2	Objectives	62
6.3	Nickel Aluminium Bronze	63
6.4	The Form and Shape of the Corrosion	65
7.0	**Evaluations using Eddy Flux Technology**	68
7.1	The Method	68
7.2	Equipment Description	69
7.3	Testing Modes	70
7.4	Eddy Flux Examination	73
8.0	**Magnetic Property Determination and Magnetic Mapping**	78
9.0	**Experimentation with Maxwell Equipment**	81
9.1	Principles of Techniques Applied	82
9.2	Maxwell Examination	85
9.3	Results	88
9.4	Conclusions	94
9.5	Recommendations	94
10.0	**Final Comments**	95
	References	97
	Appendix 1 – Assessment of UT Inspectability of CuNiCr Casting for BAeSEMA.	
	Appendix 2 - Eddy Current Test Equipment	
	Appendix 3 – Eddy Current Test Procedure ECTP5 –Surface Inspection of Cast NES 824 Material.	
	Appendix 4 – Eddy Current Test Procedure ECTP7 – Subsurface Inspection of Cast NES 824 Material	
	Appendix 5 - Ultrasonic Scan of NAB sample NABPC for Babcock Rosyth/MOD	

LIST OF FIGURES

Figure		Page
1	Probability of detection for fluorescent penetrant inspection	5
2	Essential steps for basic penetrant inspection	6
3	Variuos ways of applying penetrant	7
4a	Procedure for solvent removable penetrant process	8
4b	Procedure for water washable penetrant process	8
4c	Procedure for post emulsified penetrant process	8
5	Contrast ratios – brightness of spot V brightness of background	9
6	Atom	11
7	Magnetic force microscopy (MFM) image showing the magnetic domains in a piece of heat-treated carbon steel.	13
8	Magnetic domains in magnetized and un-magnetised material	13
9	Circular magnetization of bar	14
10	Two applications of longitudinal magnetisation	15
11	Flux & Current curve during demagnetisation projected from hysteresis loop	16
12	Induction	17
13	Self induction	18
14	Magnetic field distribution of a coil carrying a current	19
15	Inductive reactance	20
16	Basic circuit for eddy current	21
17	Shows various stages to mutual induction in eddy current inspection	22
18	Different type of electrical circuits	23
19	Impedance circuit	24
20	Penetration of Eddy currents	25
21	Factors affecting eddy current depth of penetration	26
22	Eddy current phase lag	27
23	Impedance plane diagram	28
24	Typical instrument set-up	29
25	Typical eddy current inspection coils	30
26	Types of image quality indicators (IQI's)	34
27	Placement of IQI's	34
28	Construction of X-ray tube head	35
29	Production of X-ray photons	35
30	Linear oxide type defect. X20	41
31	Interdendritic oxide network of defects with band of particulate. X 50	41
32	Zirconium rich particulate. X 200	41
33	Silicon inclusion removed by polishing + associated particulates. X 75	41
34	Section of adapter plate with large linear oxide defect.	47

35	Coarse grain structure - section of adapter plate	**48**
36	Coarse grain structure - section of adapter plate	**48**
37	Anisotropic grain structure	**48**
38	Typical coil arrangement for reflection probe	**56**
39	Picture of cast bends	**57**
40	Eddy current signature [X/Y] from shrinkage defect in the casting	**58**
41	Eddy current signature [X/Y] from oxide network present in the casting.	**58**
42	Eddy current signature [X/Y] indicating the presence of a contaminant having magnetic permeability	**59**
43	Photo's 1, 2 & 3 show various aspects of phase selective corrosion	**61&62**
44	Different precipitate microstructures	**65**
45	Binary phase diagram of NAB	**65**
46	Eddy Flux computer based equipment	**68**
47	Equipment –typical screen display	**69**
48	A schematic of eddy current coil with magneto-resistive sensor	**72**
49	Nickel-Aluminium Bronze Faslane test block NABPC	**73**
50	Eddy Flux signals from NAB sample, Indication1	**74**
51	Eddy Flux signals from NAB sample, Indication2	**75**
52	Eddy Flux signals from NAB sample, Indication3	**75**
53	Small sample with sensor positioned remote to the corrosion surface	**76**
54	Eddy Flux signals from the remanent field when testing from the remote side of corroded surface	**76**
55	Small sample with sensor positioned on the corroded surface	**77**
56	Eddy Flux signals from the remanent field when testing on corroded surface	**77**
57	Maxwell equipment	**81**
58	Simple magnetic flux detection set up with indirect magnetisation	**82**
59	Schematic diagram of a new magneto-resistive probe	**84**
60	Sample 1 mapped for investigation	**86**
61	Sample 2, sections of header mapped for investigation	**87**
62	Area 4	**91**
63	Area 6	**91**
64	Area 7	**91**
65	Area 8	**91**
66	Area 9	**92**
67	Area 10	**92**
68	Area 21	**92**
69	Area 22	**92**
70	Area 23	**92**
71	Area 24	**92**
72	Area 31	**93**
73	Area 32	**93**
74	Area 33	**93**
75	Area 34	**93**

LIST OF TABLES

Table		Page
1.	Comparative properties of nickel aluminium bronze and copper/nickel/chromium	37
2.	Chemical composition of copper nickel chromium castings	38
3.	Impurity levels	38
4.	Summary of the results of scanning 55 cast components in copper/nickel/chromium alloy	57
5.	Analyses of κ_{III} phase (WT%) using analytical electron microscope	66
6.	Correlation of magneto-resistive sensor signals to corrosion evident	89

NOTATION

	Description	Units
CNC	Copper Nickel Chromium	
CuNiCr	Copper Nickel Chromium alloy	
DRA	Defence Research Agency	
GDMS	Glow Discharge Mass Spectrometry	
GMR	Giant Magnetoresistive	
HAZ	Heat affected Zone	
IQI	Image Quality Indicators	
MeV	Million Electron Volts	
MEC	Magnetic measurement by Eddy Currents	
MHz	Million Hertz (cycles per second)	
MIG	Manual Inert Gas	
MFL	Magnetic Flux Leakage	
MFM	Magnetic Force Microscopy	
MMA	Manual Metal Arc	
NAB	Nickel Aluminium Bronze	
NDT	Non-destructive Testing	
NES	Naval Engineering Standard	
TIG	Tungsten Inert Gas	
T.O.F.D	Time Of Flight Diffraction	
μ_p	Magnetic Permeability	H/m (Henry per meter)
μ	Linear Attenuation Coefficient	cm^{-1}
ρ	Density	gm/cm^3
δ	Skin Depth	cm
ω	Angular frequency	Hz
σ	Conductivity	MS/m (Mega Siemens per meter)

1.0 INTRODUCTION

Cast nickel aluminium bronze (NAB) has been used in the seawater system of Naval vessels for thirty years or more.

Whilst the properties of NAB are adequate for many other commercial applications the demanding conditions in naval sea water systems have produced unusually high level of preferential phase attack [Phase Selective Corrosion] in the complex microstructure of the alloy. This resulted in a short life span of component and costly revalidation programme and replacement castings.

When NAB was first introduced in naval applications, a number of problems were experienced resulting in a series of in-depth studies into castability, weldability, heat treatment, composition, microstructure and corrosion resistance. These led to major improvement, especially in the quality of castings.

However, it became clear that the inherent corrosion resistance of the alloy could not be improved sufficiently to provide the service life naval vessels then required.

A review of possible alternative material in 1970`s [1] indicated that cupro nickel alloys offered the most promising prospect of meeting the requirement of a replacement alloy.

Experience and results from Cu-Ni pipe work already used in naval vessel, showing resistance to marine fouling and with mechanical and electrical properties broadly similar to NAB made the use of such an alloy as a casting replacement material desirable. Although for the past twenty years or so, cast copper-nickel has been considered with varying degrees of interest, it was only with the modernization of the UK foundry industry and the replacement of fuel-fired with electric furnaces that they became a serious possibility.

Electric furnaces provided the means of rapid melting, less contamination by furnace atmosphere, this being significant as cupro-nickel alloys have higher melting temperatures and are more susceptible to sulphur pick-up than NAB.

Of the alloys considered, the 30% Ni-alloys possessed the best corrosion resistance and of two possible high strength alloys available, that containing 1.6% chromium was finally chosen.

Essentially, the cast CNC alloy has good strength, good impact properties and moderate ductility. In seawater, it has very good general and crevice corrosion resistance is resistant to biofouling and also to stress corrosion cracking.

Production of castings for naval use proceeded after exhaustive trials. Quality Assessment of castings was carried out to naval specifications, namely that of,

Penetrant inspection for surface flaw detection and Radiography for internal flaw detection.

However subsequent machining of certified material, identified discontinuities that were not reported during casting acceptance tests. The severity of some of the discontinuities and their apparent un-detectability with standard NDT techniques for castings caused concern and prompted a study.

Due to the apparent unacceptability of the new CNC material and in an effort to prolong the life of existing NAB castings, a second study was suggested to look at detectability by NDT methods of the Phase Selective Corrosion.

The objectives of this research and study are to:

- Look at the material form and structure
- Understand the morphology of the discontinuity
- Find suitable and practical NDT techniques that can assist in finding and evaluating:
    - Surface orientated discontinuities
    - Sub –surface discontinuities
- Investigate the applicability of selected techniques for in-situ component inspection.

2.0 STANDARD NDT INSPECTION METHODS

The practice of NDT methodology [2] for quality assessment has existed in many different forms for centuries, providing as it does, the means to assess the condition of an object without compromising its performance.

NDT methods can be scientifically categorised as Optical, Acoustical, Electromagnetic. Thermal, Radiographic and Cross-interactive. Of the many techniques and exotic variations that are sometimes presented, the industry has, in the main, confined NDT to the following:

1) Visual
2) Penetrant
3) Magnetic
4) Eddy Current
5) Ultrasonic
6) Radiographic

Of these, the visual, penetrant and radiographic techniques dominate the casting industry.

2.1 Visual Inspection

Visual inspection of each casting ensures that none of its required features has been omitted or malformed by moulding errors, short running or mistakes in cleaning. Most surface discontinuities and roughness can be observed at this stage. An early visual inspection is essential to ensure that obvious scrap is not passed on for expensive finishing or further inspection operations. Some commercial parts require only visual inspection.

Visual inspection involves a wide variety of equipment and ranges from examination with the naked eye to the use of interference micro-scopes. The eye can be aided by the use of hand held or self-supporting magnifiers, pocket microscopes, stereoscopic microscopes and rigid and flexible borescopes.

The latest developments in visual inspection procedures for examining component appearance are mainly based on vision systems that use electronic cameras coupled to computer assisted image processing systems.

2.2 Liquid Penetrant Inspection

Penetrant inspection is a very versatile method of detecting discontinuities which are open to the surfaces of essentially non-porous materials. It can be used successfully regardless of component size and can tolerate very complicated geometry. The major restriction on penetrant testing is that it is suitable for seeking only those defects which are open to the surface and must therefore have maximum access to them. This means that surfaces must be thoroughly cleaned and dried before application of the penetrant.

Penetrant inspection can give valuable information at all stages in the production and use of components, from production of the new material, through the various stages of manufacture to the finished form, and then on into their useful life.

Liquid penetrant inspection should not be confined only to as-cast surfaces. For example, it is not unusual for castings to exhibit cracks, frequently intergranular, on machined surfaces. A pattern of cracks of this type may be the result of intergranular cracking throughout the material, because of an error in composition or heat treatment, or the cracks may be on the surface only, as a result of machining or grinding. Surface cracking may remain because of an insufficient machining allowance, which did not allow for complete removal of imperfections produced on the as cast surface, or it may result from faulty machining techniques. If imperfections of this type are detected by visual inspection, liquid penetrant inspection will reveal their full extent.

The penetrant material can be applied in a number of different ways, which include spraying, brushing, or immersing the parts in a penetrant bath. The method of penetrant application has little effect on the inspection sensitivity but an electrostatic spraying method is reported to produce slightly better results than other methods. Once the part is covered in penetrant it must be allowed to dwell so the penetrant has time to enter any defect present.

There are basically two dwell mode options, immersion-dwell (keeping the part immersed in the penetrant during the dwell period) or drain-dwell (letting the part drain during the dwell period). Prior to a study by Sherwin, the immersion-dwell mode was generally considered to be more sensitive but recognized to be less economical because more penetrant was washed away and emulsifiers were contaminated more rapidly. The reasoning for thinking this method was more sensitive was that the penetrant was more migratory and more likely to fill flaws when kept completely fluid and not allowed to loose volatile constituents by evaporation. However, Sherwin showed that if the specimens are allowed to drain-dwell, the sensitivity is higher because the evaporation increases the dyestuff concentration of the penetrant on the specimen. Sherwin also cautions that the samples being inspected should be placed outside the penetrant tank wall so that vapors from the tank do not accumulate and dilute the dyestuff concentration of the penetrant on the specimen.

The nature of the defect can have a large affect on sensitivity of a liquid penetrant inspection. Sensitivity is defined as the smallest defect that can be detected with a high degree of reliability. Typically, the crack length at the sample surface is used to define size of the defect. A survey of any probability-of-detection curve for penetrant inspection will quickly lead one to the conclusion that crack length has a definite effect on sensitivity. However, the crack length alone does not determine whether a flaw will be seen or go undetected. The volume of the defect is likely to be the more important feature. The flaw must be of sufficient volume so that enough penetrant will bleed back out to a size that is detectable by the eye or that will satisfy the dimensional thresholds of fluorescence.

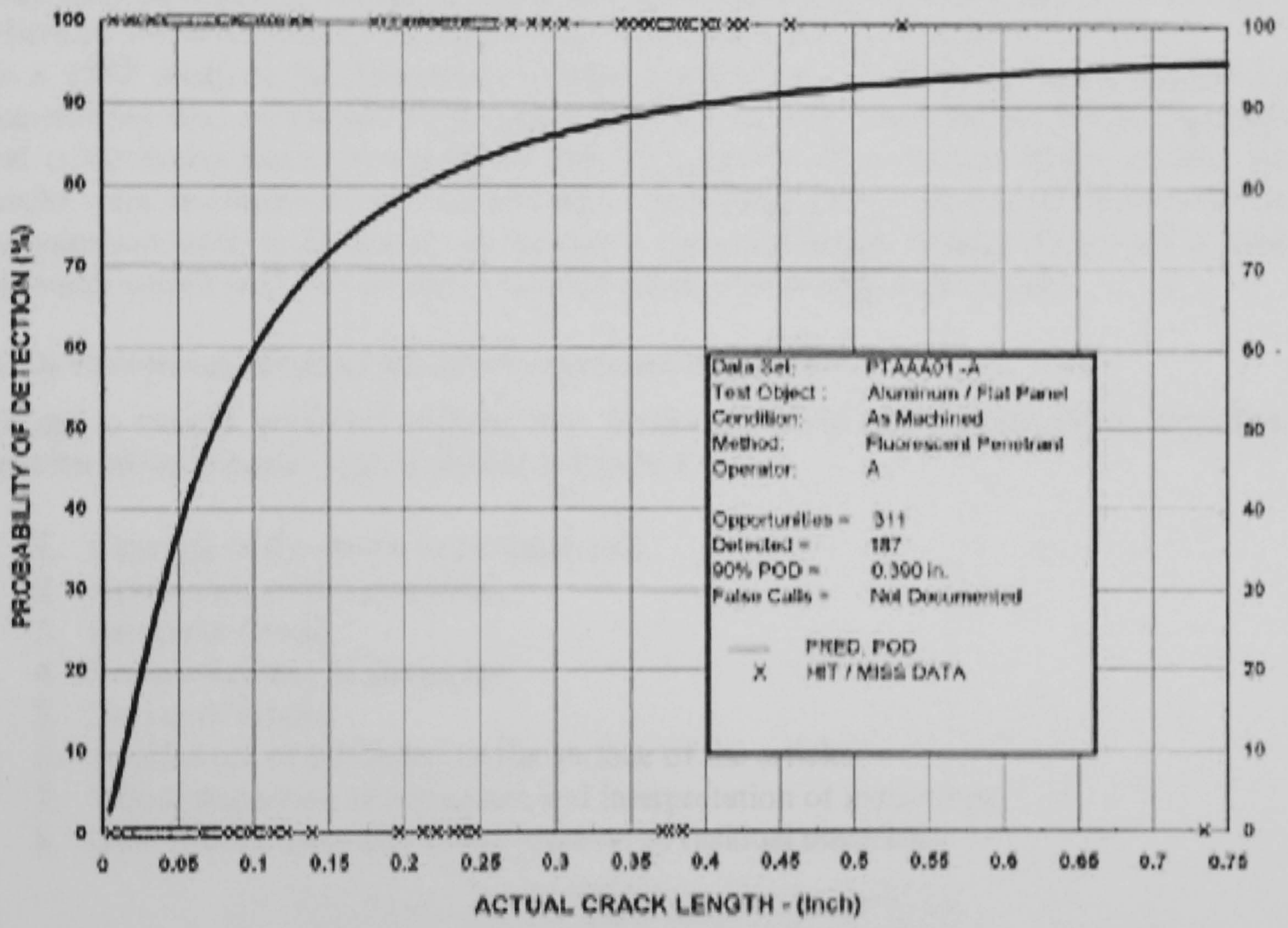

Figure 1 Probability of Detection for Fluorescent Penetrant Inspection

Above is an example of fluorescent penetrant inspection probability of detection (POD) curve from the Nondestructive Evaluation (NDE) Capabilities Data Book. Please note that this curve is specific to one set of inspection conditions and should not be interpreted to apply to other inspection situations [3].

In general, penetrant inspections are more effective at finding small round defects than small linear defects. Small round defects are generally easier to detect for several reasons. First, they are typically volumetric defects that can trap significant amounts of penetrant. Second, round defects fill with penetrant faster than linear defects. One research effort found that elliptical flaw with length to width ratio of 100, will take the penetrant nearly

10 times longer to fill than a cylindrical flaw with the same volume. Deeper flaws will trap more penetrant than shallow flaws, and they are less prone to over washing. Flaws with narrow surface openings are less prone to over washing. The surface roughness of the part primarily affects the removability of a penetrant. Rough surfaces tend to trap more penetrant in the various tool marks, scratches, and pits that make up the surface. Removing the penetrant from the surface of the part is more difficult and a higher level of background fluorescence or over washing may occur.

The surface roughness that the fracture faces is a factor in the speed at which a penetrant enters a defect. In general, the penetrant spreads faster over a surface as the surface roughness increases. It should be noted that a particular penetrant may spread slower than others on a smooth surface but faster than the rest on a rougher surface.

In a 1987 study at the University College London [4], the effect of crack closure on detectability was evaluated. Researchers used a four-point bend fixture to place tension and compression loads on specimens that were fabricated to contain fatigue cracks. All cracks were detected with no load and with tensile loads placed on the parts. However, as compressive loads were placed on the parts, the crack length steadily decreased as load increased until a load was reached when the crack was no longer detectable.

Basic Processing Steps of a Liquid Penetrant Inspection

Except in certain penetrant systems that require no developer, the penetrant inspection process involves basic steps as shown in Figure 1.

1. Cleaning of the article to be inspected.
2. Application of the penetrant.
3. Penetrant Dwell
4. Removal of excess penetrant.
5. Drying of article.
6. Application of developer to the surface of the article.
7. Visual inspection of the article and interpretation of indications.
8. (Not shown) Post-inspection removal of residual materials.

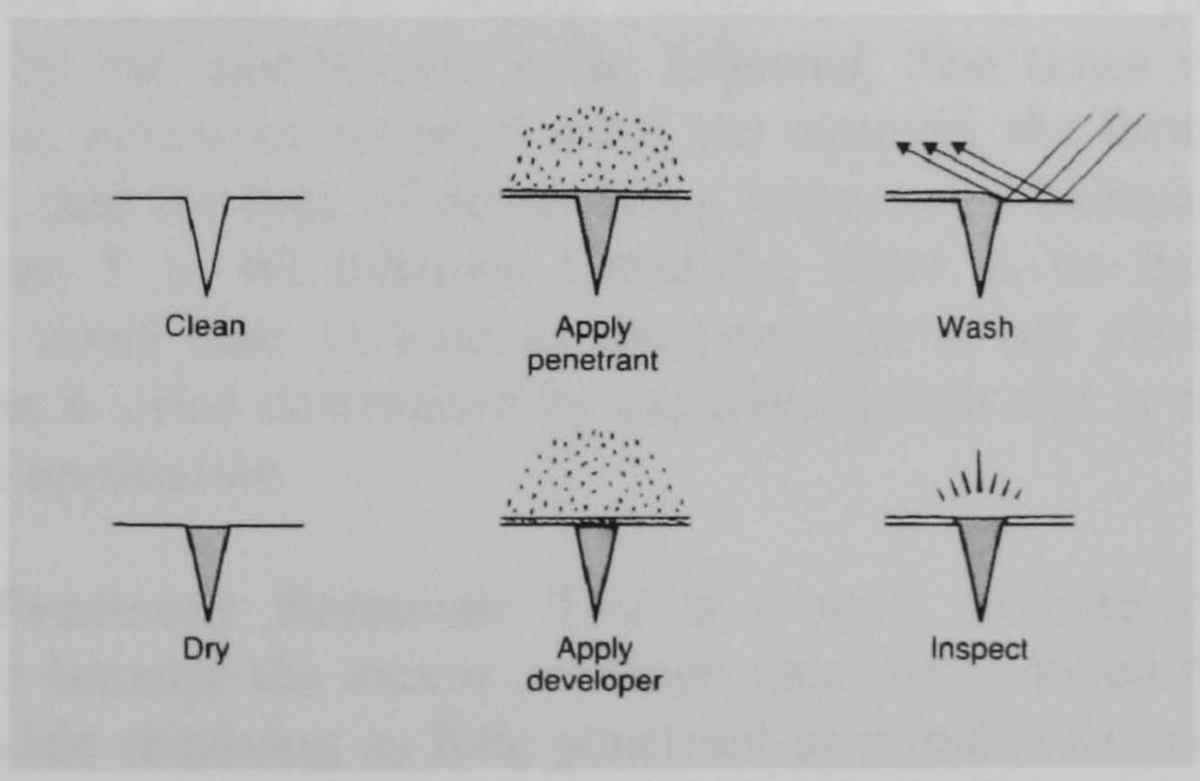

Figure 2 Essential steps for basic penetrant inspection

The illustration shows the steps diagrammatically; the details of each step depend on the particular penetrant system being used. For instance, the post emulsifiable penetrant method requires the addition of an emulsifying agent as part of the wash operation for removal of excess penetrant.

1. **Surface Preparation:** One of the most critical steps of a liquid penetrant inspection is the surface preparation. The surface must be free of oil, grease, water, or other contaminants that may prevent penetrant from entering flaws. The sample may also require etching if mechanical operations such as machining, sanding, or grit blasting have been performed. These and other mechanical operations can smear the surface of the sample, thus closing the defects

2. **Penetrant Application:** Once the surface has been thoroughly cleaned and dried, the penetrant material is applied by spraying, brushing, or immersing the parts in a penetrant bath.

Figure 3. Variuos ways of applying penetrant

3. **Penetrant Dwell:** The penetrant is left on the surface for a sufficient time to allow as much penetrant as possible to be drawn from or to seep into a defect. Penetrant dwell time is the total time that the penetrant is in contact with the part surface. Dwell times are usually recommended by the penetrant producers or required by the specification being followed. The times vary depending on the application, penetrant materials used, the material, the form of the material being inspected, and the type of defect being inspected. Minimum dwell times typically range from 5 to 60 minutes. Generally, there is no harm in using a longer penetrant dwell time as long as the penetrant is not allowed to dry. The ideal dwell time is often determined by experimentation and is often very specific to a particular application

4. **Excess Penetrant Removal:** This is a most delicate part of the inspection procedure because the excess penetrant must be removed from the surface of the sample while removing as little penetrant as possible from defects. Depending on the penetrant system used, this step may involve cleaning with a solvent, direct rinsing with water, or first treated with an emulsifier and then rinsing with water.

5. **Drying:** This is necessary if dry developers are to be employed. Drying is usually carried out using hot air recirculated drying ovens operating at temperatures of 70°C ± 10°C. Drying at these temperatures should be kept to a minimum, typical times being in the order of 20 minutes for small mass objects. Ambient air can be used but contamination of drying surface would need to be controlled.

6. **Developer Application:** A thin layer of developer is then applied to the sample to draw penetrant trapped in flaws back to the surface where it will be visible. Developers come in a variety of forms that may be applied by dusting (dry powdered), dipping, or spraying (wet developers

   Indication Development: The developer is allowed to stand on the part surface for a period of time sufficient to permit the extraction of the trapped penetrant out of any surface flaws. This development time is usually a minimum of 10 minutes and significantly longer times may be necessary for tight cracks

7. **Inspection:** Inspection is then performed under appropriate lighting to detect indications from any flaws which may be present

8. **Clean Surface:** The final step in the process is to thoroughly clean the part surface to remove the developer from the parts that were found to be acceptable

Flow charts illustrating the sequence of steps for the most commonly used penetrant systems are shown in Figure 4a, b and c. [5]

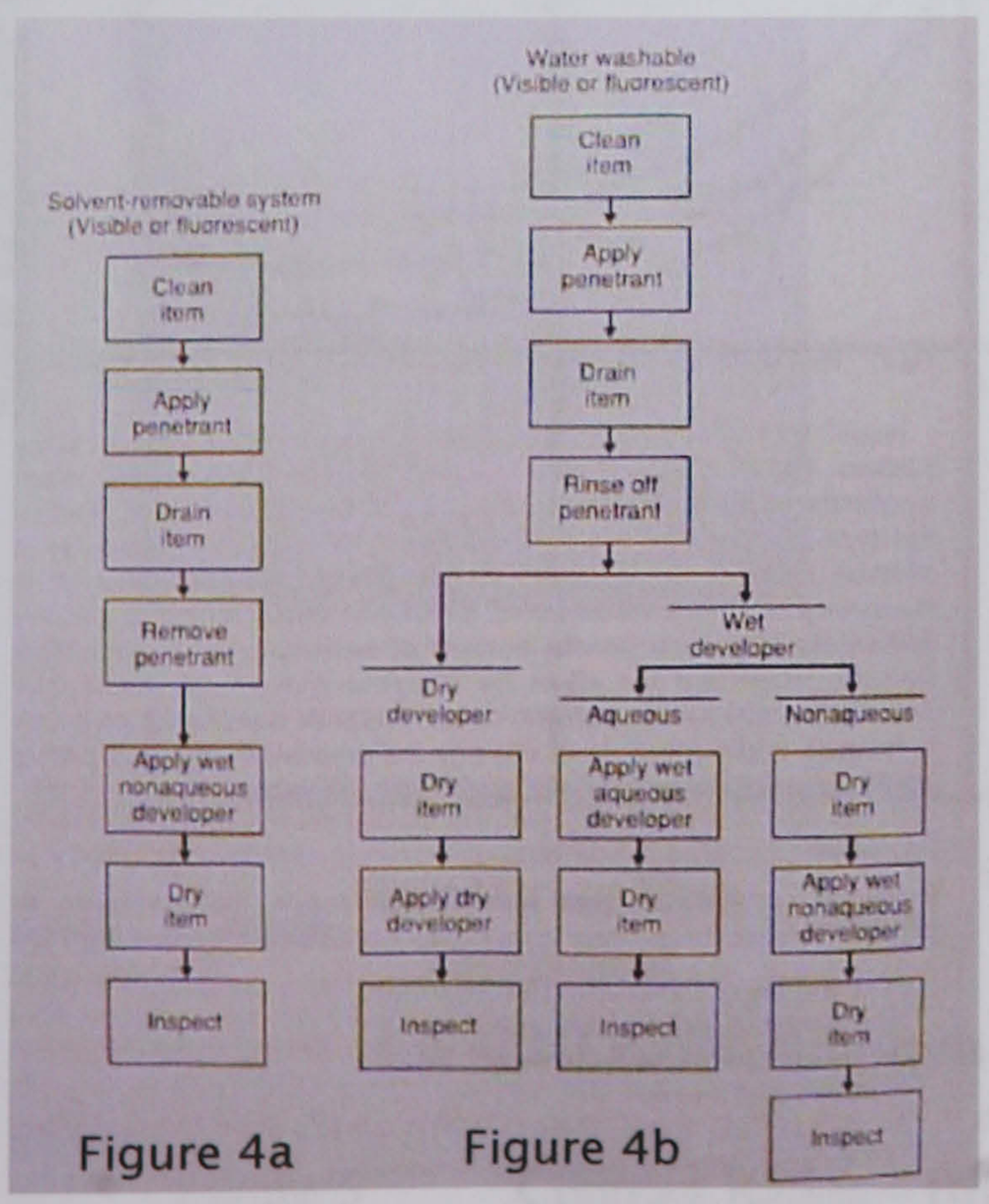

Figure 4a Figure 4b

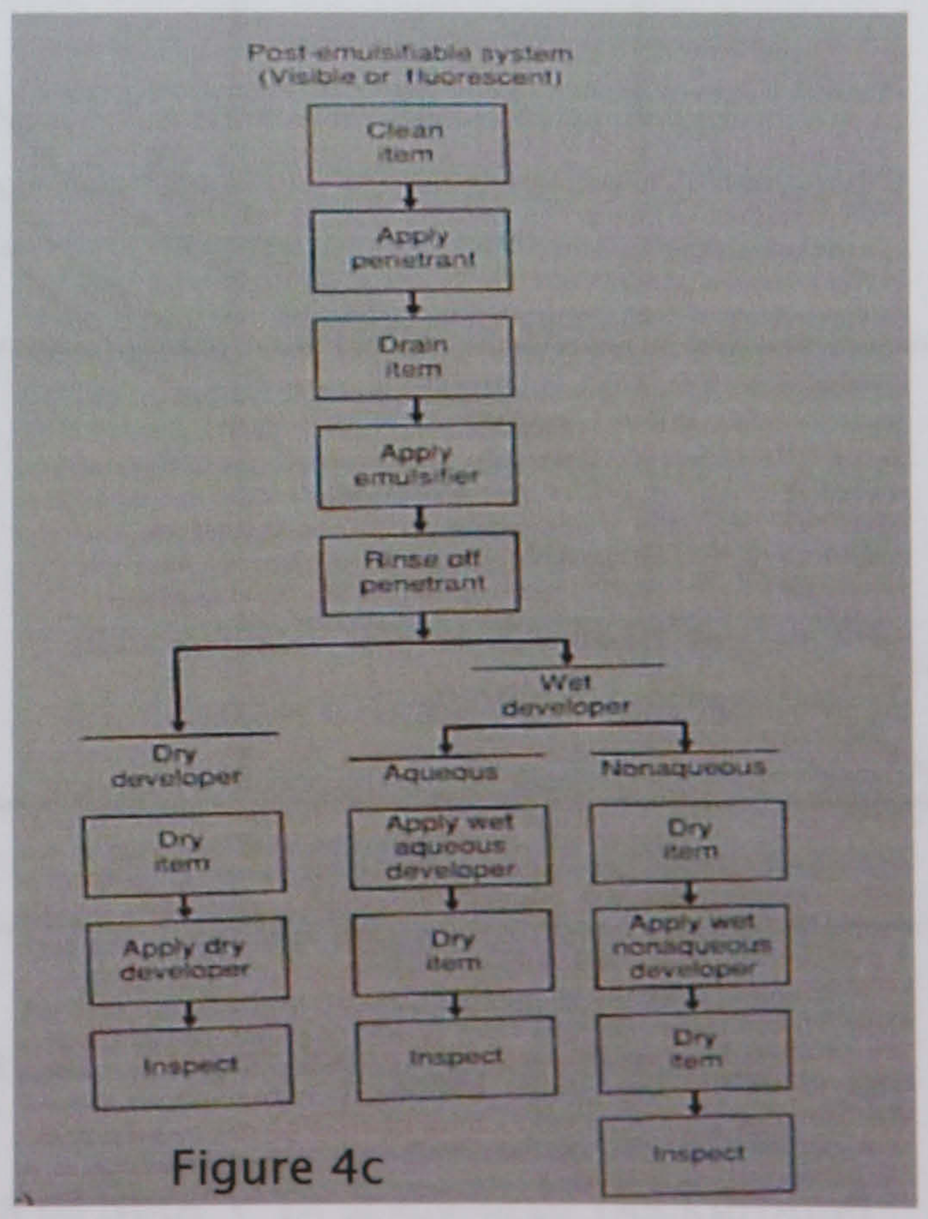

Figure 4c

Figure 4a – Procedure for Solvent removable penetrant process
Figure 4b – Procedure for Water Washable penetrant process
Figure 4c – Procedure for Post Emulsified penetrant process

The selection of a liquid penetrant system is not a straightforward task. There are a variety of penetrant systems and developer types that are available for use, and one set of penetrant materials will not work for all applications. Many factors must be considered when selecting the penetrant materials for a particular application. These factors include the sensitivity required, materials cost, number of parts and size of area requiring inspection, and portability.

When sensitivity is the primary consideration for choosing a penetrant system, the first decision that must be made is whether to use fluorescent dye penetrant or visible dye penetrant. Fluorescent penetrants are generally more capable of producing a detectable indication from a small defect because the human eye is more sensitive to a light indication on a dark background and the eye is naturally drawn to a fluorescent indication. The graph below (Figure 5) presents a series of curves that show the contrast ratio required for a spot of a certain diameter to be seen.

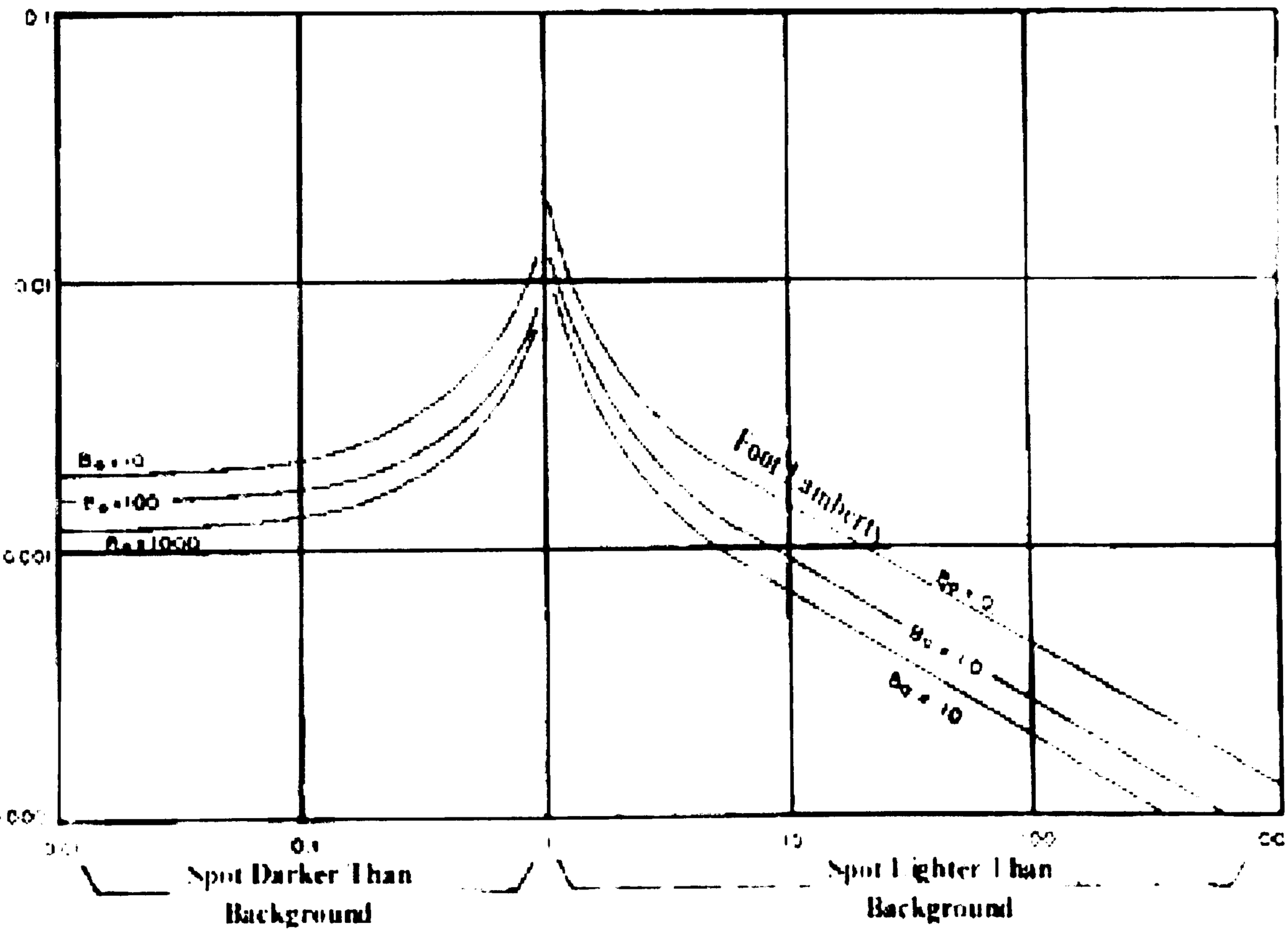

Figure 5 Contrast Ratios – Brightness of Spot V Brightness of Background

The curves show that for indications spots larger than 0.076 mm (0.003 inch) in diameter, it does not really matter if it is a dark spot on a light background or a light spot on a dark background. However, when a dark indication on a light background is further reduced in size, it is no longer detectable even though contrast is increased. Furthermore, with a light indication on a dark background, indications down to 0.003 mm (0.0001 inch) were detectable when the contrast between the flaw and the background was high enough.

From this data, it can be seen why a fluorescent penetrant offers an advantage over visible penetrant for finding very small defects. Data presented by De Graaf and De Rijk supports this statement. They inspected "Identical" fatigue cracked specimens using a red dye penetrant and a fluorescent dye penetrant. The fluorescent penetrant found 60 defects while the visible dye was only able to find 39 of the defects. [6]

Under certain conditions, the visible penetrant may be a better choice. When fairly large defects are the subject of the inspection, a high sensitivity system may not be warranted and may result in a large number of irrelevant indications. Visible dye penetrants have also been found to give better results when surface roughness is high or when flaws are located in areas such as weldments.

Since visible dye penetrants do not require a darkened area for the use of an ultraviolet light, visible systems are more easy to use in the field. Solvent removable penetrants, when properly applied can have the highest sensitivity and are very convenient to use but are usually not practical for large area inspection or in high-volume production settings.

Another consideration in the selection of a penetrant system is whether water washable, post-emulsifiable or solvent removable penetrants will be used. Post-emulsifiable systems are designed to reduce the possibility of over-washing, which is one of the factors known to reduce sensitivity. However, these systems add another step, and thus cost, to the inspection process.

Penetrants are evaluated by the US Air Force according to the requirements in MIL-I-25135 and each penetrant system is classified into one of five sensitivity levels. This procedure uses titanium and Inconel specimens with small surface cracks produced in low cycle fatigue bending to classify penetrant systems. The brightness of the indications produced after processing a set of specimens with a particular penetrant system is measured using a photometer. A procedure for producing and evaluating the penetrant qualification specimens was reported on by Moore and Larson at the 1997 ASNT Fall Conference. Most commercially available penetrant materials are listed in the Qualified Products List of MIL-I-25135 according to their type, method and sensitivity level. Visible dye and dual-purpose penetrants are not classified into sensitivity levels as fluorescent penetrants are. The sensitivity of a visible dye penetrant is regarded as level 1 and largely dependent on obtaining good contrast between the indication and the background.

2.3 Magnetic Particle Inspection

Magnetic Particle Inspection is a highly effective and sensitive method for revealing surface and near-surface discontinuities of castings made of ferromagnetic materials only.
The method is used to inspect a variety of product forms such as castings, forgings, and weldments. The only requirement from an inspectability standpoint is that the component being inspected must be made of a ferromagnetic material such iron, nickel or cobalt, or some of their alloys. Ferromagnetic materials are materials that can be magnetized to a level that will allow the inspection to be effective. Many different industries use magnetic particle inspection for determining a component's fitness-for-use

Some examples of industries that use magnetic particle inspection are the structural steel, automotive, petro-chemical, power generation and aerospace industries. Underwater inspection is another area where magnetic particle inspection may be used to test such things as offshore structures and underwater pipelines.

Magnetic particle testing uses magnetic fields and small magnetic particles, such as iron filings to detect flaws in components. In theory, it is a relatively simple concept. When a bar magnet is broken in the center of its length, two complete bar magnets with magnetic poles on each end of each magnet will result. If the magnet were cracked but not broken completely in two, a north and south pole will form at each edge of the crack, just as though the break had been completed. If iron particles were then sprinkled on this cracked magnet, these particles will be attracted not only to the ends of the magnets poles but also to the edges of the crack.

The Source of Magnetism

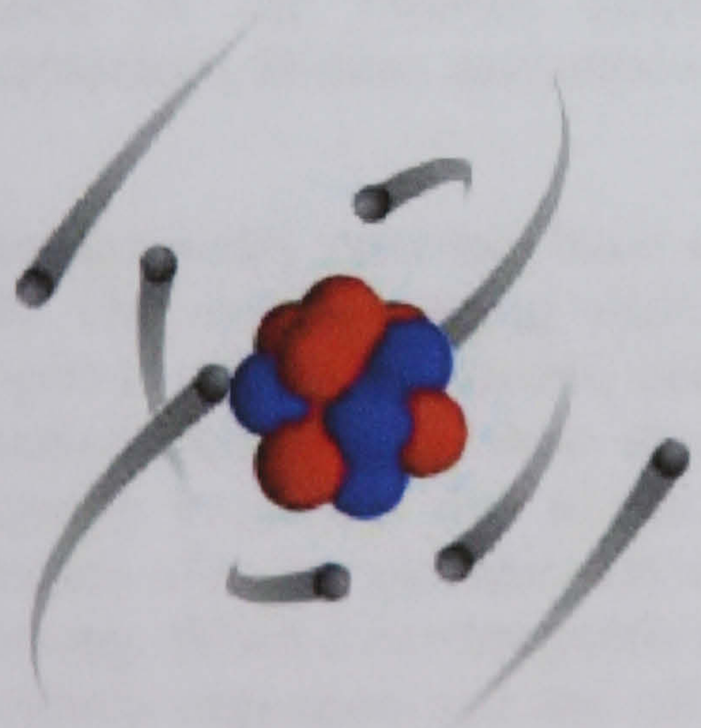

Figure 6 - Atom

All matter is composed of atoms (Figure 6), and atoms are composed of protons, neutrons and electrons.
The protons and neutrons are located in the atom's nucleus and the electrons are in constant motion around the nucleus. Electrons carry a negative electrical charge and produce a magnetic field as they move through space. A magnetic field is produced whenever an electrical charge is in motion. The strength of this field is called the **magnetic moment.**

This maybe hard to visualize on a subatomic scale but consider electric current flowing through a conductor. When the electrons (electric current) are flowing through a conductor, a magnetic field forms around the conductor. The magnetic field can be detected using a compass. The magnetic field will place a force on the compass needle, which is another example of a dipole. A bar magnet can be considered a dipole with a north pole at one end and south pole at the other

Since all matter is comprised of atoms, all materials are affected in some way by a magnetic field. However, not all materials react the same way.

When a material is placed within a magnetic field. the magnetic forces on the material's electrons will be affected. This effect is known as Faraday's Law of Magnetic Induction. However, materials can react quite differently to the presence of an external magnetic field. This reaction is dependent on a number of factors such as the atomic and molecular structure of the material, and the net magnetic field associated with the atoms. The magnetic moments associated with atoms have three origins. These are the electron orbital motion, the change in orbital motion caused by an external magnetic field. and the spin of the electrons

In most atoms, electrons occur in pairs. Each electron in a pair spins in the opposite direction. So when electrons are paired together, their opposite spins cause there magnetic fields to cancel each other. Therefore, no net magnetic field exists. Alternately, materials with some unpaired electrons will have a net magnetic field and will react more to an external field. Most materials can be classified as ferromagnetic, diamagnetic or paramagnetic

Diamagnetic metals have a very weak and negative susceptibility to magnetic fields. Diamagnetic materials are slightly repelled by a magnetic field and the material does not retain the magnetic properties when the external field is removed. Diamagnetic materials are solids with all paired electrons and, therefore, no permanent net magnetic moment per atom. Diamagnetic properties arise from the realignment of the electron orbits under the influence of an external magnetic field. Most elements in the periodic table, including copper, silver. and gold, are diamagnetic.

Paramagnetic metals have a small and positive susceptibility to magnetic fields. These materials are slightly attracted by a magnetic field and the material does not retain the magnetic properties when the external field is removed. Paramagnetic properties are due to the presence of some unpaired electrons and from the realignment of the electron orbits caused by the external magnetic field. Paramagnetic materials include Magnesium, molybdenum, lithium, and tantalum.

Ferromagnetic materials have a large and positive susceptibility to an external magnetic field. They exhibit a strong attraction to magnetic fields and are able to retain their magnetic properties after the external field has been removed. Ferromagnetic materials have some unpaired electrons so their atoms have a net magnetic moment. They get their strong magnetic properties due to the presence of magnetic domains. In these domains, large numbers of atoms moments are aligned parallel so that the magnetic force within the domain is strong. When a ferromagnetic material is in the unmagnetised state, the domains are nearly randomly organized and the net magnetic field for the part as a whole is zero. When a magnetizing force is applied, the domains become aligned to produce a strong magnetic field within the part. Iron, Nickel, and cobalt are examples of ferromagnetic materials. Components with these materials are commonly inspected using the magnetic particle method.

Magnetic Domains

Ferromagnetic materials get their magnetic properties not only because their atoms carry a magnetic moment but also because the material is made up of small regions known as magnetic domains. In each domain, all of the atomic dipoles are coupled together in a preferential direction. This alignment develops as the material develops its crystalline structure during solidification from the molten state. Magnetic domains can be detected using Magnetic Force Microscopy (MFM) and images of the domains like the one shown below can be constructed. [7]

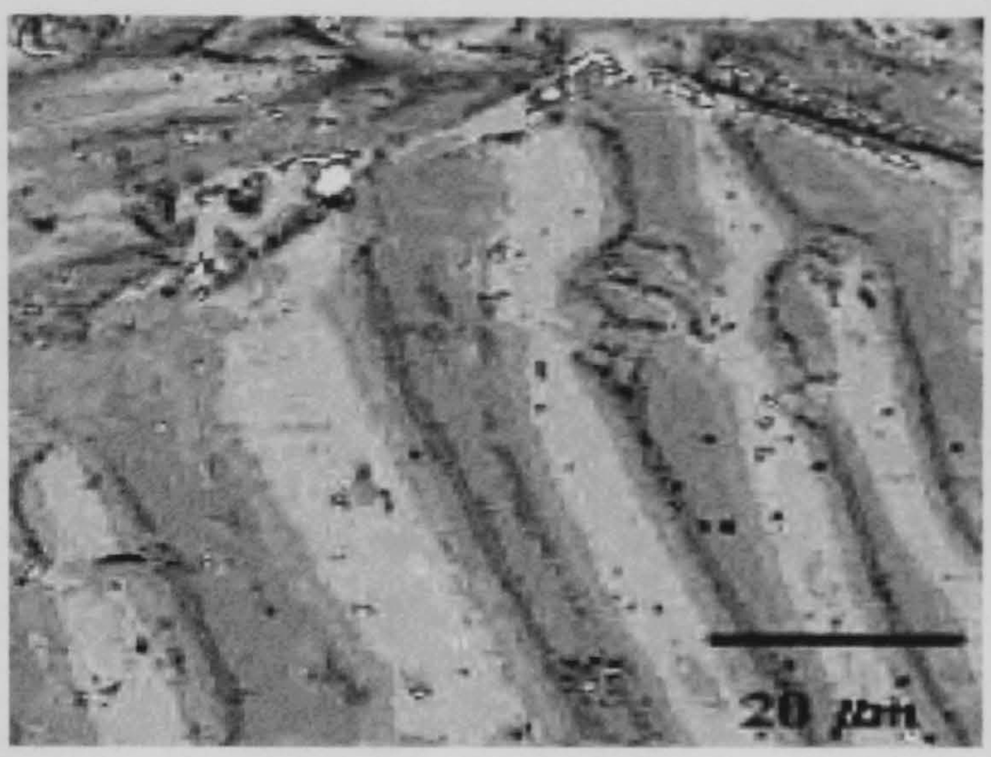

Figure 7 - Magnetic Force Microscopy (MFM) image showing the magnetic domains in a piece of heat treated carbon steel.

During solidification a trillion or more atom moments are aligned parallel so that the magnetic force within the domain is strong in one direction. Ferromagnetic materials are said to be characterized by "spontaneous magnetization" since they obtain saturation magnetization in each of the domains without an external magnetic field being applied. Even though the domains are magnetically saturated, the bulk material may not show any signs of magnetism because the domains develop themselves are randomly oriented relative to each other.
Ferromagnetic materials become magnetized when the magnetic domains within the material are aligned. This can be done my placing the material in a strong external magnetic field or by passing electrical current through the material. Some or all of the domains can become aligned. The more domains that are aligned, the stronger the magnetic field in the material. When all of the domains are aligned, the material is said to be magnetically saturated. When a material is magnetically saturated, no additional amount of external magnetization force will cause an increase in its internal level of magnetization.

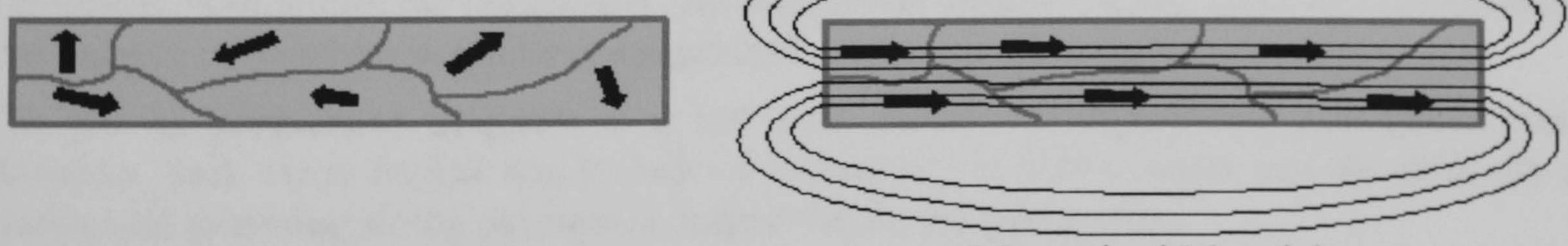

Unmagnetised Material Magnetised Material

Figure 8 – Magnetic domains in magnetized and unmagnetised material

Methods used to establish a magnetic field for Inspection

There are a variety of methods that can be used to establish a magnetic field in a component for evaluation using magnetic particle inspection. It is common to classify the magnetizing methods as either direct or indirect.

Magnetization Using Direct Induction (Direct Magnetization)

With direct magnetization, current is passed directly through the component. Recall that whenever current flows a magnetic field is produced. The magnetic lines of flux form normal to the direction of the current and form a circular field in and around the conductor. When using the direct magnetization method, care must be taken to ensure that good electrical contact is established and maintained between the test equipment and the test component. Improper contact can result in arcing that may damage the component. It is also possible to overheat components in areas of high resistance such as the contact points and in areas of small cross-sectional area.

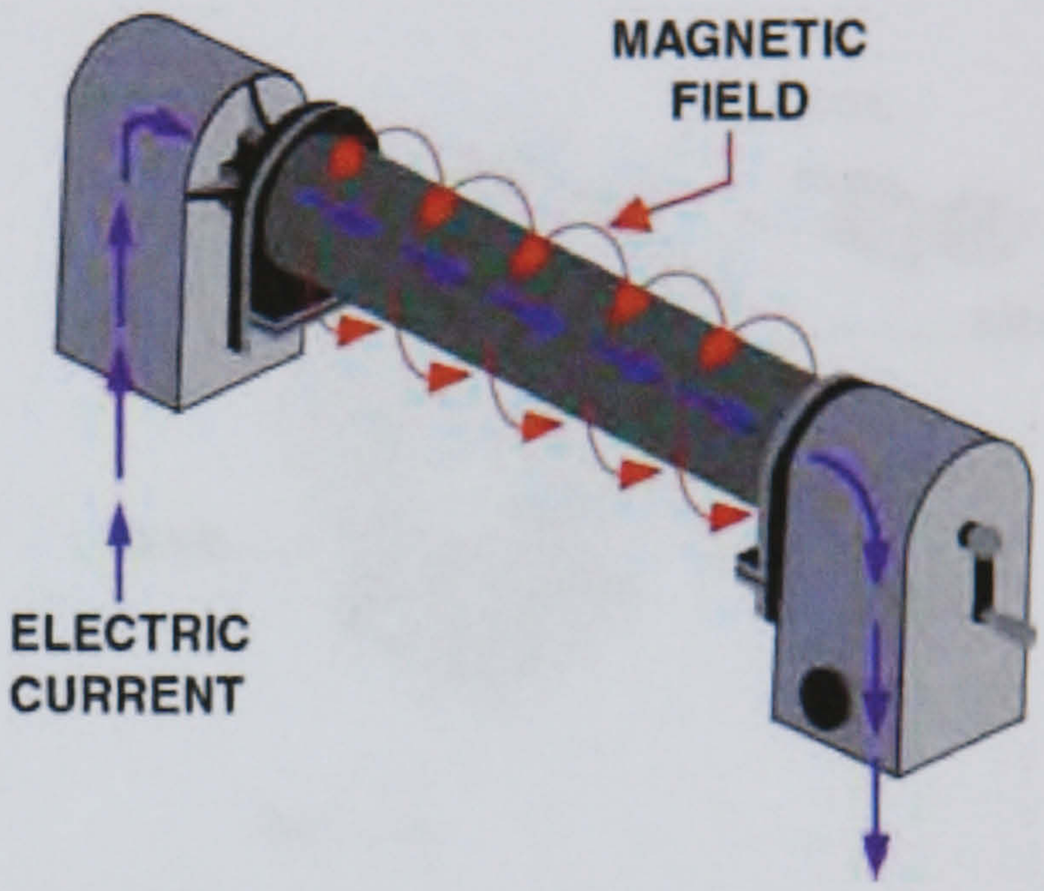

Figure 9 – Circular magnetization of a Bar

There are several ways that direct magnetization is commonly accomplished. One way involves clamping the component between two electrical contacts in a special piece of equipment. Current is passed through the component and a circular magnetic field is established in and around the component. When the magnetizing current is stopped, a residual magnetic field will remain within the component. The strength of the induced magnetic field is proportional to the amount of current passed through the component

A second technique involves using clamps or prods, which are attached or placed in contact with the component. Current is injected into the component as it flows from the contacts. The current sets up a circular magnetic field around the path of the current.

Magnetization Using Indirect Induction (Indirect Magnetization)

Indirect magnetization is accomplished by using a strong external magnetic field to establish a magnetic field within the component. As with direct magnetization, there are several ways that indirect magnetization can be accomplished.

The use of **permanent magnets** is a low cost method of establishing a magnetic field. However, their use is limited due to lack of control of the field strength and the difficulty of placing and removing strong permanent magnets from the component.

Electromagnets in the form of an adjustable horseshoe magnet (called a yoke) eliminate the problems associated with permanent magnets and are used extensively in industry. Electromagnets only exhibit a magnetic flux when electric current is flowing around the soft

iron core. When the magnet is placed on the component, a magnetic field is established between the north and south poles of the magnet.

The use of **coils** and **solenoids** is a second method of indirect magnetization. When the length of a component is several times larger than its diameter, a longitudinal magnetic field can be established in the component. The component is placed longitudinally in the concentrated magnetic field that fills the center of a coil or solenoid. This magnetization technique is often referred to as a "coil shot."

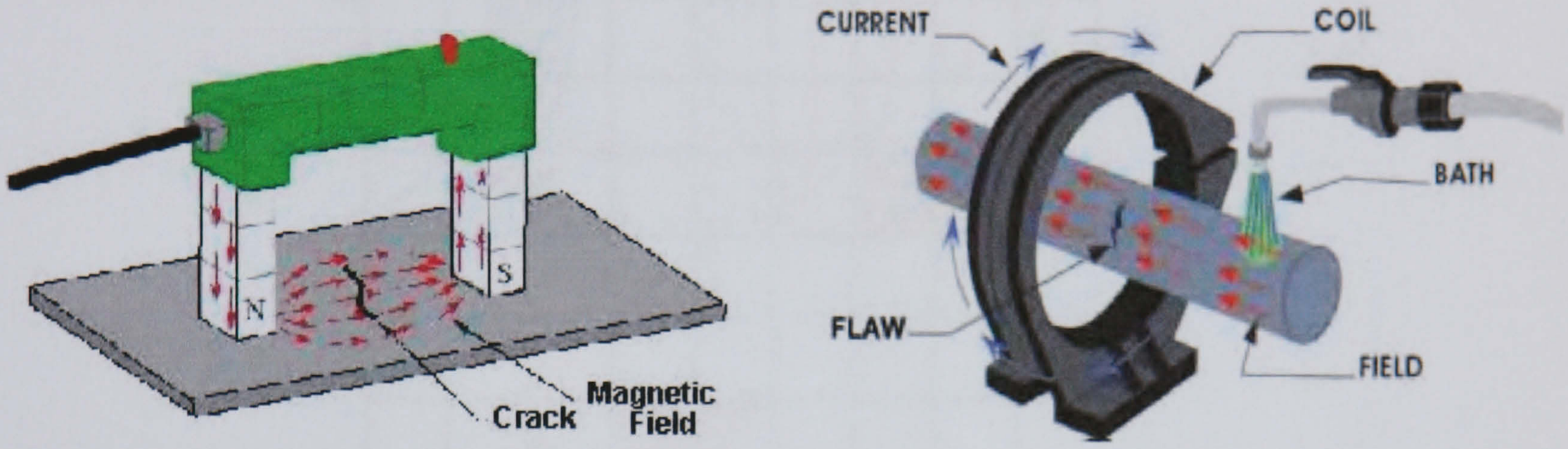

a) Electromagnet

b) Coils

Figure 10 – Two applications of longitudinal magnetisation

The magnetic particles are held in a suspension of either water or oil and are supplied by a pump and hose on the system. These particles are of either the visible type, which means that they can be seen in normal white light, or the fluorescent type. Fluorescent particles require the use of a blacklight, which causes the particle indications to illuminate. This is much the same as causing a blacklight poster to glow in the dark.

Demagnetisation

After conducting a magnetic particle inspection, it is usually necessary to demagnetize the component. Remanent magnetic fields can:

- affect machining by causing cuttings to cling to a component.
- interfere with electronic equipment such as a compass.
- can create a condition known as "arc blow" in the welding process. Arc blow may cause the weld arc to wander or filler metal to be repelled from the weld.
- cause abrasive particle to cling to bearing or faying surfaces and increase wear.

Removal of a field may be accomplished in several ways. This random orientation of the magnetic domains can be achieved most effectively by heating the material above its curie temperature. The curie temperature for low carbon steel is 770 degrees C or 1390 degrees F. When steel is heated above its curie temperature, it will become austenitic and loose its magnetic properties. When it is cooled back down it will go through a reverse transformation

and will contain no residual magnetic field. The material should also be placed with its long axis in an east-west orientation to avoid any influence of the Earth's magnetic field

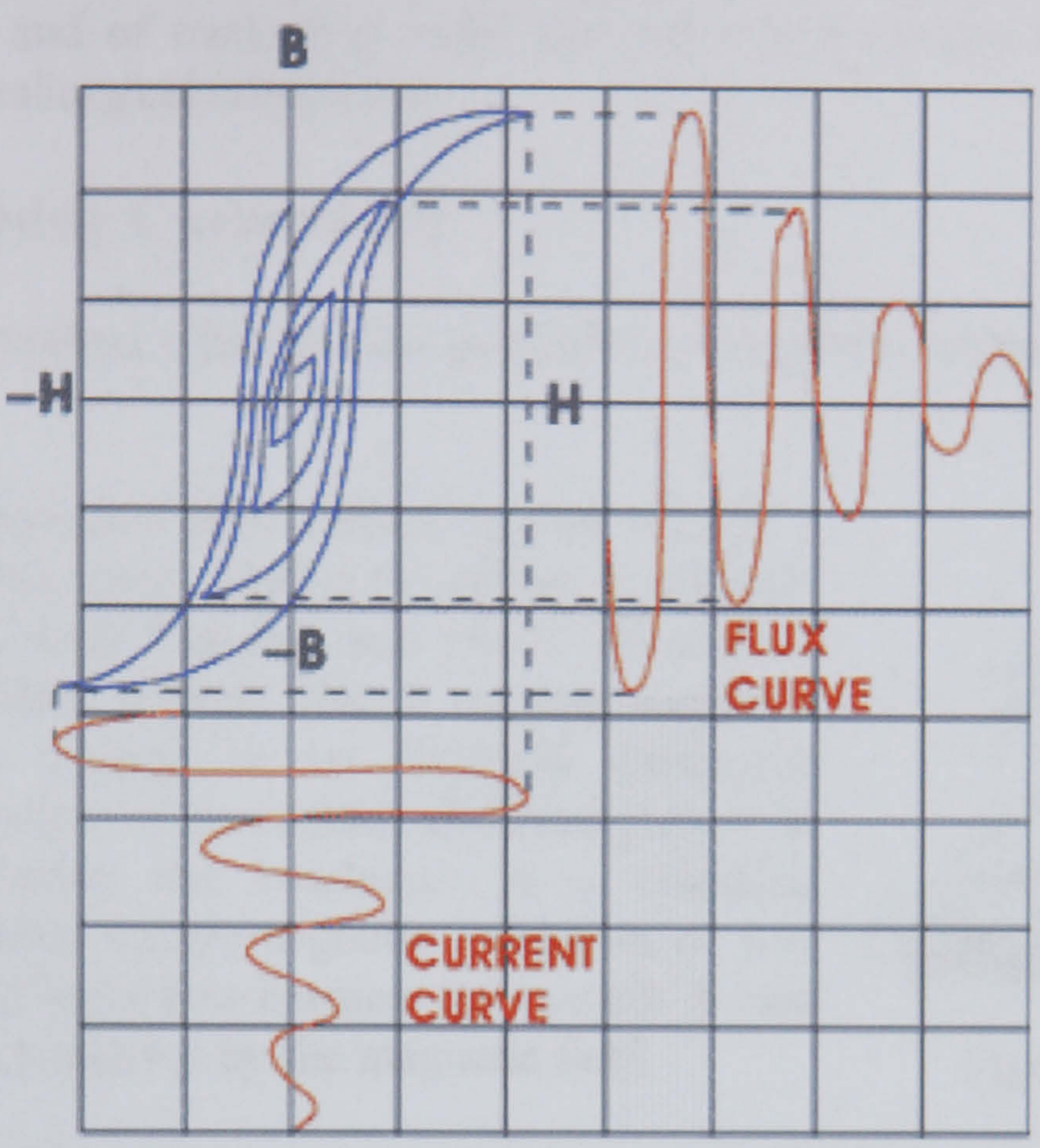

Figure 11- Flux & Current curve during demagnetization projected from hysteresis loop [8]

It is often inconvenient to heat a material above its Curie temperature to demagnetize it so another method that returns the material to a nearly unmagnetised state is commonly used. Subjecting the component to a reversing and decreasing magnetic field will return the dipoles to a nearly randomly oriented throughout the material. This can be accomplished by pulling a component out and away from a coil with AC passing through it. The same can also be accomplished using an electromagnetic yoke with AC selected. Also, many stationary magnetic particle inspection units come in a demagnetisation feature that slow reduce the AC in a coil in which that component is placed

A field meter is often used to verifying that the residual flux has been removed from a component. Industry standards usually require that the magnetic flux be reduced to less than 3 gauss after completing a magnetic particle inspection

2.4 Eddy Current Inspection

Eddy Current Inspection is a method of locating surface or sub-surface flaws in electrically conductive material and of evaluating small material characteristics such as heat treatment effects and other metallurgical conditions.

Introduction to eddy Currents [9]

The Eddy Current method relies on the principles of magnetic induction to interrogate the material under test.

In 1824 Oersted discovered that current passing though a coil created a magnetic field capable of shifting a compass needle. Seven years later Faraday and Henry discovered just the opposite. They noticed that a moving magnetic field would induce current in an electrical conductor (Figure 12). This process of generating electrical current in a conductor by placing the conductor in a changing magnetic field is called electromagnetic induction or just induction. It is called induction because the current is said to be induced in the conductor by the magnetic field.

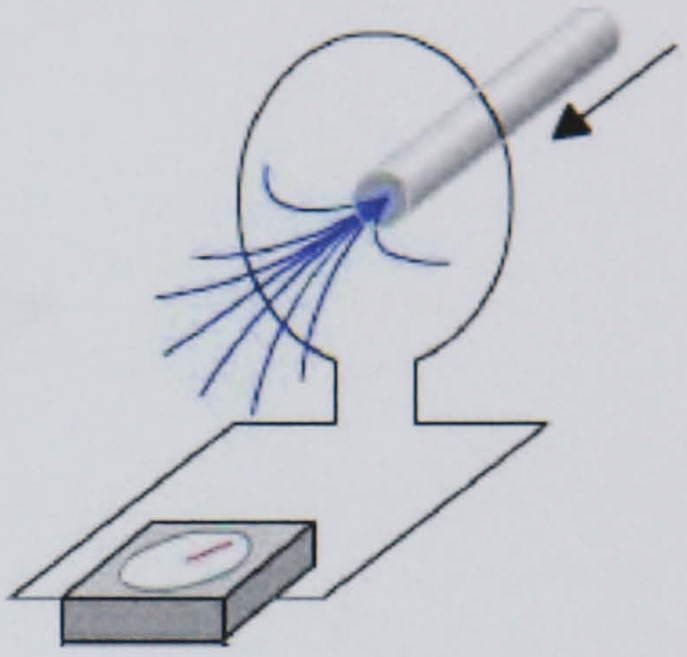

Figure 12- Induction

Faraday also noticed that the rate at which the magnetic field changed also had an effect on the amount of current or voltage that was induced. Faraday's Law for an uncoiled conductor states that the amount of induced voltage is proportional to the rate of change of flux lines cutting the conductor. Faraday's Law for a straight wire is shown below.

Where:

$$V_L = \frac{d\,\phi}{dt}$$

VL = the induced voltage in volts
dø/dt = the rate of change in magnetic flux in webers/second

Induction is measured in unit of Henries (H) which reflects this dependence on the rate of change of the magnetic field. One Henry is the amount of inductance that is required to generate one volt of induced voltage when the current is changing at the rate of one ampere per second. Note that current is used in the definition rather than magnetic field. This is because current can be used to generate the magnetic field and is easier to measure and control than magnetic flux.

Inductance

When induction occurs in an electrical circuit and affects the flow of electricity it is called inductance, L. Self-inductance, or simply inductance is the property of a circuit whereby a change in current causes a change in voltage in the same circuit. When one circuit induces current flow in a second nearby circuit, it is known as mutual-inductance [Figure 13]. The

image below shows an example of mutual-inductance. When an AC current is flowing through a piece of wire in a circuit, an electromagnetic field is produced that is constantly growing and shrinking and changing direction due to the constantly changing current in the wire. This changing magnetic field will induce electrical current in another wire or circuit that is brought close to the wire in the primary circuit. The current in the second wire will also be AC and in fact will look very similar to the current flowing in the first wire. An electrical transformer uses inductance to change the voltage of electricity into a more useful level. In nondestructive testing, inductance is used to generate eddy currents in the test piece.

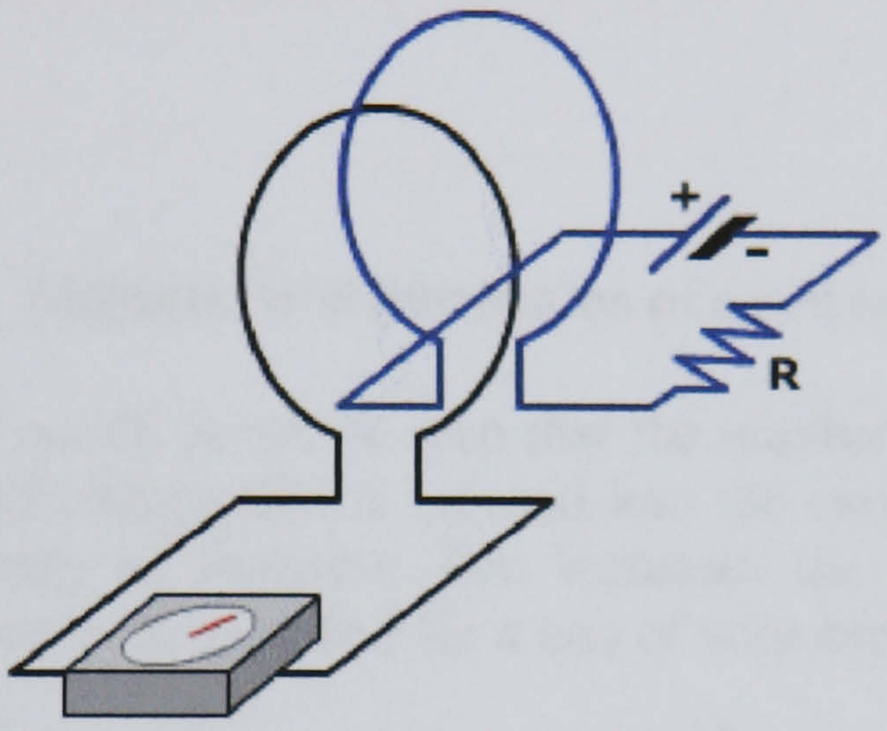

Figure 13 – Mutual inductance

It should be noted that since it is the changing magnetic field that is responsible for inductance, it is only present in AC circuits and that high frequency AC will result in greater inductive reactance since the magnetic field is changing more rapidly.

Self-Inductance and Inductive Reactance

The property of self-inductance is a particular form of electromagnetic induction. Self inductance is defined as the induction of a voltage in a current-carrying wire when the current in the wire itself is changing. In the case of self-inductance, the magnetic field created by a changing current in the circuit itself induces a voltage in the same circuit. Therefore, the voltage is self-induced.

The term inductor is used to describe a circuit element possessing the property of inductance and a coil of wire is a very common inductor. In circuit diagrams, a coil of wire is usually used to indicate an inductive component. Taking a closer look at a coil will help understand the reason that a voltage is induced in a wire carrying a changing current. The alternating current running through the coil creates a magnetic field in and around the coil that is increasing and decreasing as the current changes. The magnetic field forms concentric loops that surrounds the wire and joins up to form larger loops that surround the coil as shown in the image below. When the current increases in one loop the expanding magnetic field will

cut across some or all of the neighboring loops of wire, inducing a voltage in these loops. This causes a voltage to be induced in the coil when the current is changing.

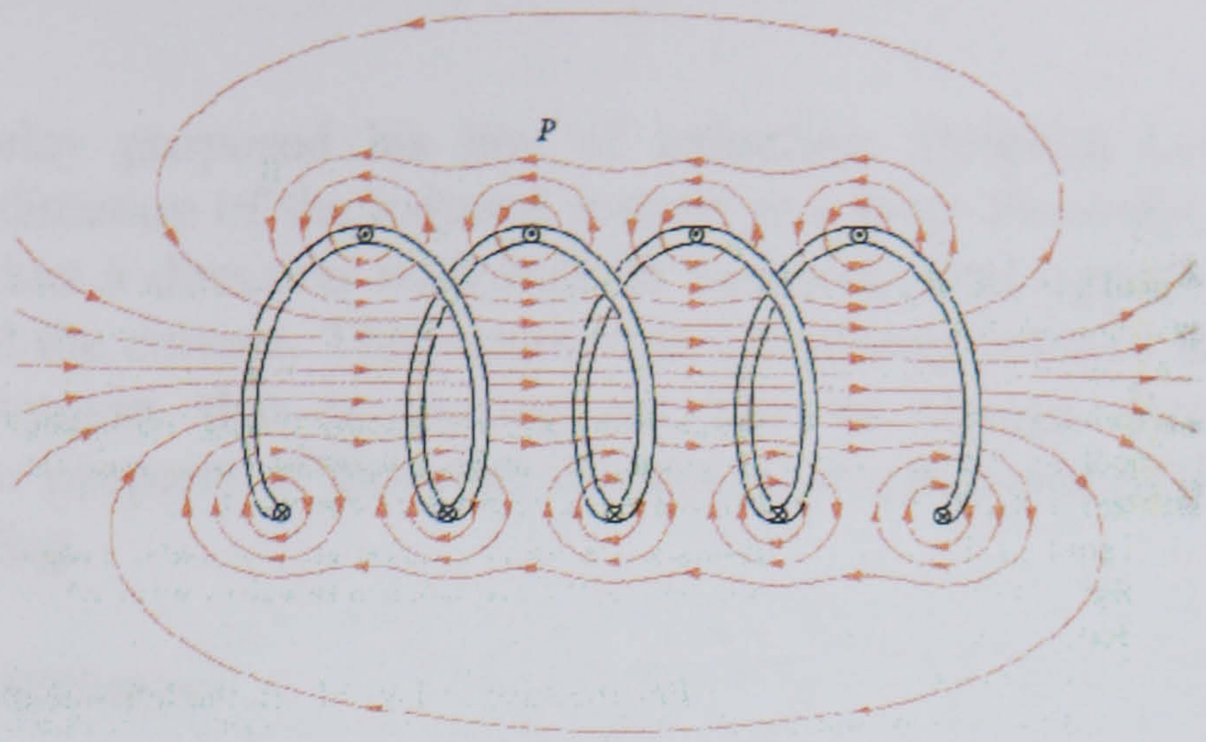

Figure 14 – Magnetic field distribution of a coil carrying a current

By studying this image of a coil, it can be seen that the number of turns in the coil will have an effect on the amount of voltage that is induced into the circuit. Increasing the number of turns or the rate of change of magnetic flux increases the amount of induced voltage. Therefore, Faraday's Law must be modified for a coil of wire and becomes the following

$$V_L = N\frac{d\phi}{dt}$$

Where:

V_L = the induced voltage in volts
N = the number of turns in the coil
$d\phi/dt$ = the rate of change in magnetic flux in webers per second

The equation simply states that the amount of induced voltage (V_L) is proportional to the number of turns in the coil and the rate of change of the magnetic flux ($d\phi/dt$). In other words, when the frequency of the flux is increased or the number of turns in the coil is increased, the amount of induced voltage will also increase.

In a circuit, it is much easier to measure current than it is to measure magnetic flux so the following equation can be used to determine the induced voltage if the inductance and frequency of the current are known. This equation can also be reorganized to allow the inductance to be calculated when the amount of inducted voltage can be determined and the current frequency is known.

Where:

$$V_L = L\frac{di}{dt}$$

V_L = the induced voltage in volts
L = the value of inductance in Henries
di/dt = the rate of change in current in amperes per second

Lenz's Law

Soon after Faraday proposed his law of induction, Heinrich Lenz developed a rule for determining the direction of the induced current in a loop. Basically, Lenz's law states that an induced current has a direction such that its magnetic field opposes the change in magnetic field that induced the current. This means that the current induced in a conductor will oppose the change in current that is causing the flux to change. Lenz's law is important in understanding the property of inductive reactance, which is one of the properties measured in eddy current testing.

Inductive Reactance

The reduction of current flow in a circuit due to induction is called inductive reactance. By taking a closer look at a coil of wire and applying Lenz's law [Figure 15], it can be seen how inductance reduces the flow of current in the circuit. In the image below, the direction of the primary current is shown in red, and the magnetic field generated by the current is shown in blue. The direction of the magnetic field can be determined by taking your right hand and pointing your thumb in the direction of the current. Your fingers will then point in the direction of the magnetic field. It can be seen that the magnetic field from one loop of the wire will cut across the other loops in the coil and this will induce current flow (shown in green) in the circuit. According to Lenz's law, the induced current must flow in the opposite direction of the primary current. The induced current working against the primary current results in a reduction of current flow in the circuit.

It should be noted that inductive reactance will increase if the number of windings in the coil is increased since the magnetic field from one coil will have more coils to interact with.

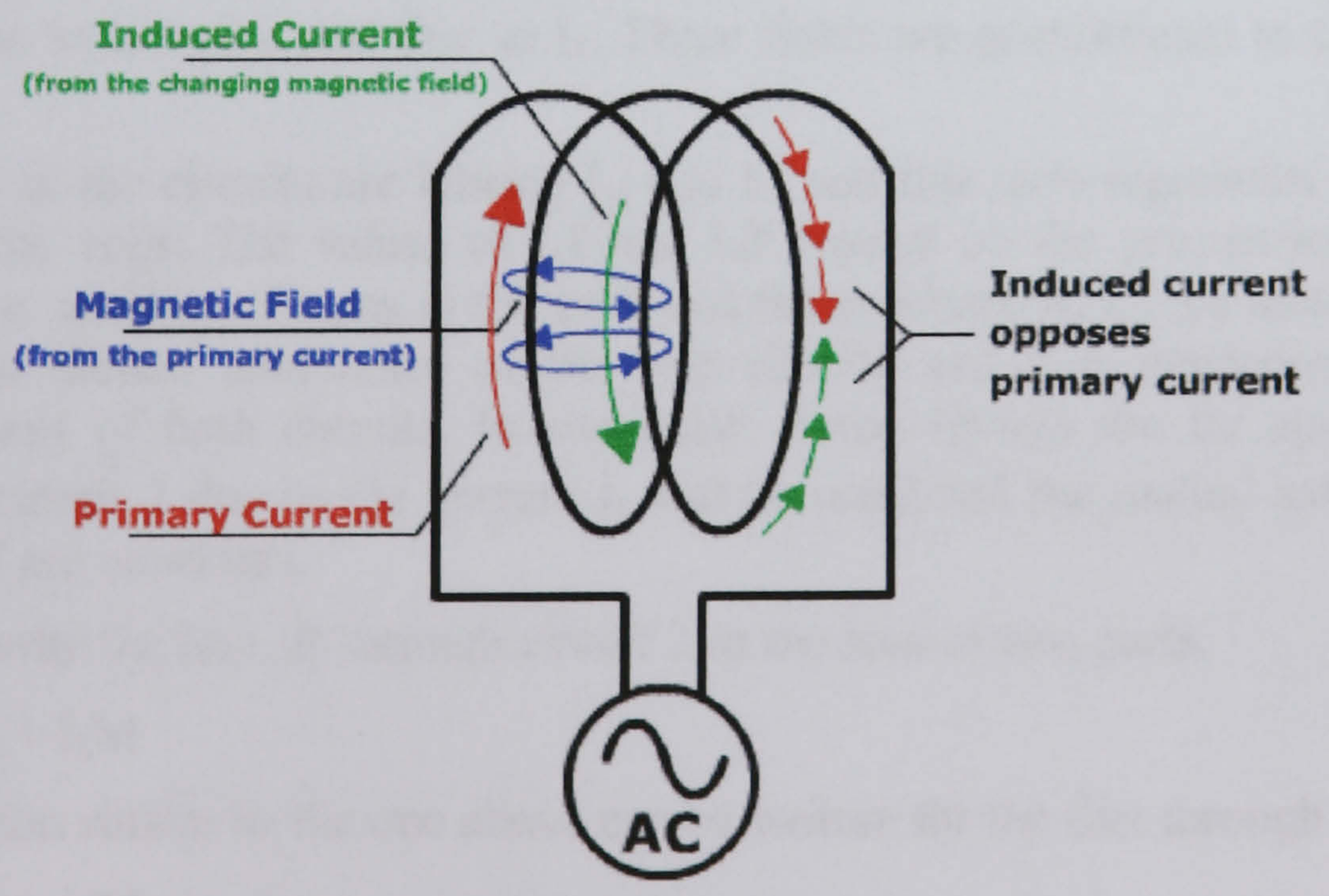

Figure 15 – Inductive reactance

Since inductive reactance reduces the flow of current in a circuit. it appears as an energy loss just like resistance. However, it is possible to distinguish between resistance and inductive reactance in a circuit by looking at the timing between the sine waves of the voltage and current of the alternating current. In an AC circuit that contains only resistive components. the voltage and the current will be in-phase, meaning that the peaks and valleys of their sine waves will occur at the same time. When there is inductive reactance present in the circuit. the phase of the current will be shifted so that its peaks and valleys do not occur at the same time as those of the voltage.

Mutual Inductance
(The Basis for Eddy Current Inspection)

The magnetic flux through a circuit can be related to the current in that circuit and the currents in other nearby circuits, assuming that there are no nearby permanent magnets. Consider the following two circuits.

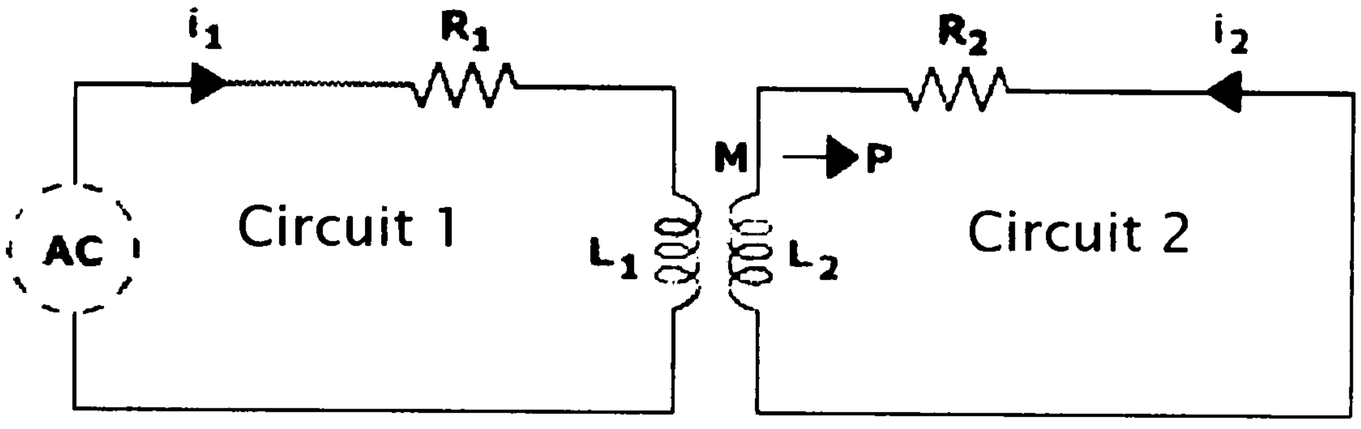

Figure 16 – Basic circuit for eddy current

The magnetic field produced by circuit 1 will intersect the wire in circuit 2 and create current flow. The induced current flow in circuit 2 will have its own magnetic field which will interact with the magnetic field of circuit 1. At some point P on the magnetic field consists of a part due to i_1 and a part due to i_2. These fields are proportional to the currents producing them.

The coils in the circuits are labeled L_1 and L_2 and this term represents the self inductance of each of the coils. The values of L1 and L2 depend on the geometrical arrangement of the circuit (i.e. number of turns in the coil) and the conductivity of the material. The constant M, called the mutual inductance of the two circuits and it is dependent on the geometrical arrangement of both circuits. In particular, if the circuits are far apart, the magnetic flux through circuit 2 due to the current i_1 will be small and the mutual inductance will be small. L_2 and M are constants.

We can write the flux, B through circuit 2 as the sum of two parts.

$$B_2 = L_2 i_2 + i_1 M$$

An equation similar to the one above can be written for the flux through circuit 1.

$$B_1 = L_1 i_1 + i_2 M$$

Though it is certainly not obvious, it can be shown that the mutual inductance is the same for both circuits. Therefore, it can be written as follows:

$M_{1,2} = M_{2,1}$

How is mutual induction used in eddy current inspection?

In eddy current inspection, the eddy currents are generated in the test material due to mutual induction. The test probe is basically a coil of wire through which alternating current is passed. Therefore, when the probe is connected to an eddy current **instrument**, it is basically represented by circuit one below (Figure 17A). The second circuit can be any piece of conductive material.

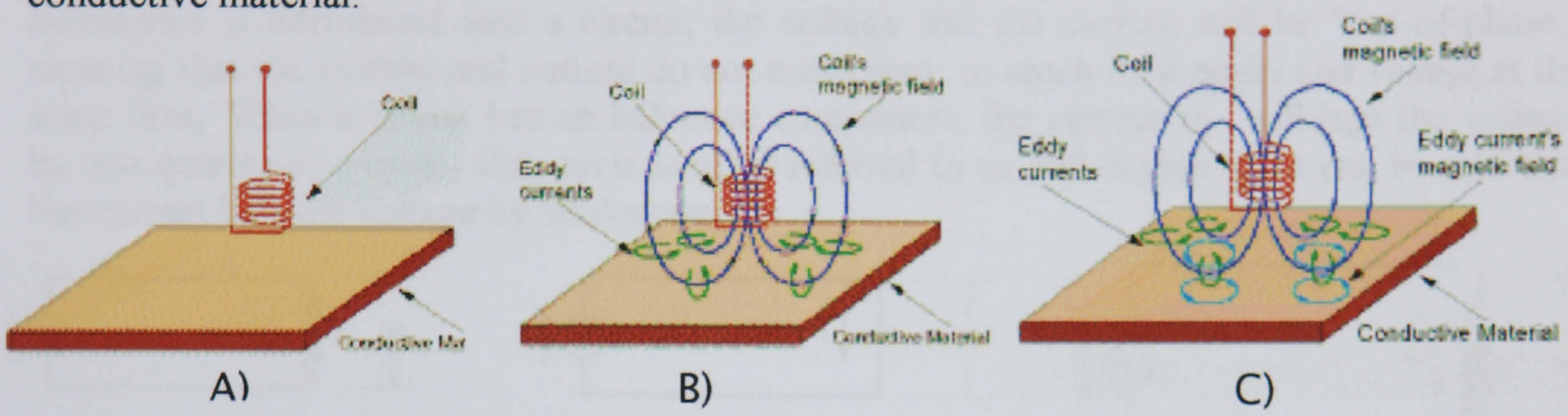

Figure 17 – Shows various stages to mutual induction in eddy current inspection

When alternating current is passed through the coil, a magnetic field is generated in and around the coil. When the probe is brought in close proximity to a conductive material, such as aluminum, the probes changing magnetic field generates current flow in the material (Figure 17B). The induced current flows in closed loops in planes perpendicular to the magnetic flux. They are named eddy currents because they are thought to resemble the eddy currents that can be seen swirling in streams

The eddy currents produce their own magnetic fields (Figure 17C) that interact with the primary magnetic field of the coil. By measuring changes in the resistance and inductive reactance of the coil, information can be gathered about the test material. This information includes the electrical conductivity and magnetic permeability of the material, the amount of material cutting through the coils magnetic field, and the condition of the material (i.e. whether it contains cracks or other defects.)

The distance that the coil is from the conductive material is called **liftoff,** and this distance affects the mutual-inductance of the circuits.

Liftoff can be used to make measurements of the thickness of nonconductive coatings such as paint that hold the probe a certain distance from the surface of the conductive material

It should be noted that if a sample is ferromagnetic, the magnetic flux is concentrated and strengthened despite opposing eddy current affects. The increase inductive reactance due to the magnetic permeability of ferromagnetic materials makes it easy to distinguish these materials from non-ferromagnetic materials.

Circuits and Phase

A circuit can be thought of as a closed path in which current flows through the components that make up the circuit. The current (i) obeys Ohm's Law. The simple circuit below consists of a voltage source (in this case an alternating current voltage source) and a resistor. The graph below the circuit diagram shows the value of the voltage and the current for this circuit over a period of time. This graph shows one complete cycle of an alternating current source. From the graph, it can be seen that as the voltage increases so does the current. The voltage and the current are said to be "in-phase" since the zero, peak, and valley points occur at the same time. They are also directly proportional to each other.

In the circuit below, the resistive component has been replaced with an inductor. When inductance is introduced into a circuit, the voltage and the current will be "out-of-phase," meaning that the voltage and current do not cross zero, or reach their peaks and valleys at the same time. When a circuit has an inductive component, the current (i_L) will lags the voltage by one quarter of a cycle. One cycle is often referred to as 360 degree, so it can be said that the current lags the voltage by 90 degrees.

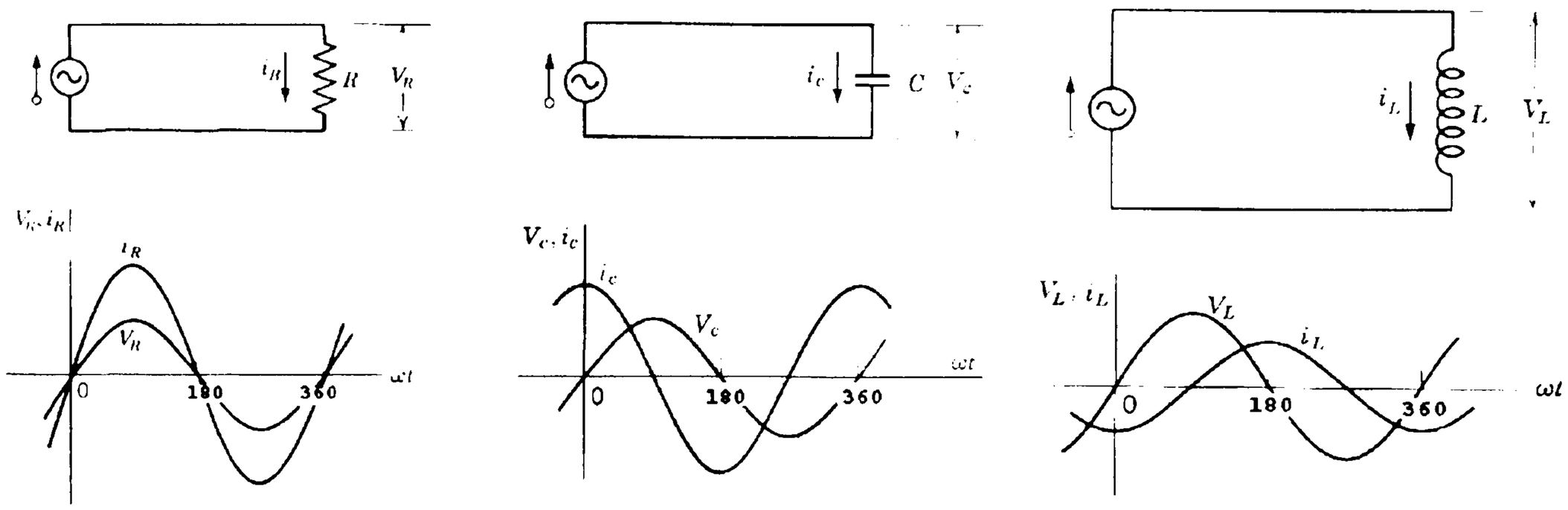

a) b) c)

Figure 18 - a) – Resistive circuit; b) – Capacitive circuit; c) – Inductive circuit

The resistive and inductive components are of primary interest in eddy current testing since the test probe is basically a coil of wire, which will have both resistance and inductive reactance. However, for the sake of completeness, capacitance also needs to be mentioned. This simple circuit below consists of an alternating current voltage source and a capacitor. Capacitance in a circuit caused the current (i_c) to lead the voltage by one quarter of a cycle (90 degrees current lag).

When there is both resistance and inductive reactance (and/or capacitance) in a circuit, the combined opposition to current flow is known as impedance.

Impedance

Electrical Impedance (Z) is the total opposition that a circuit presents to alternating current. Impedance is measured in ohms and may include resistance (R), inductive reactance (XL), and capacitive reactance (XC). However, the total impedance is not simply the algebraic sum of resistance, inductive reactance, and capacitive reactance. Since the inductive reactance and capacitive reactance are 90 degrees out of phase with the resistance and, therefore, their

maximum values occur at different times. vector addition must be used to calculate impedance.

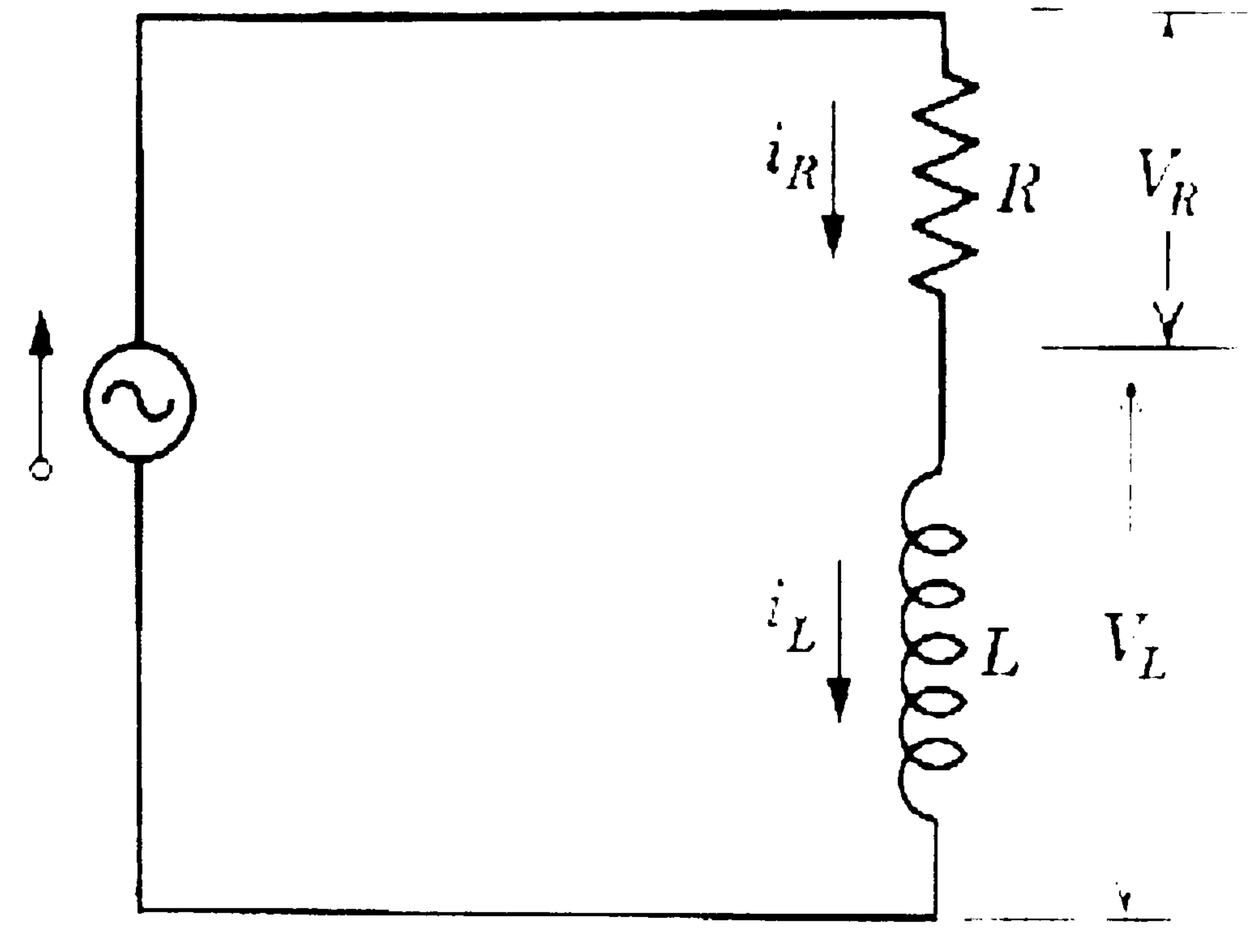

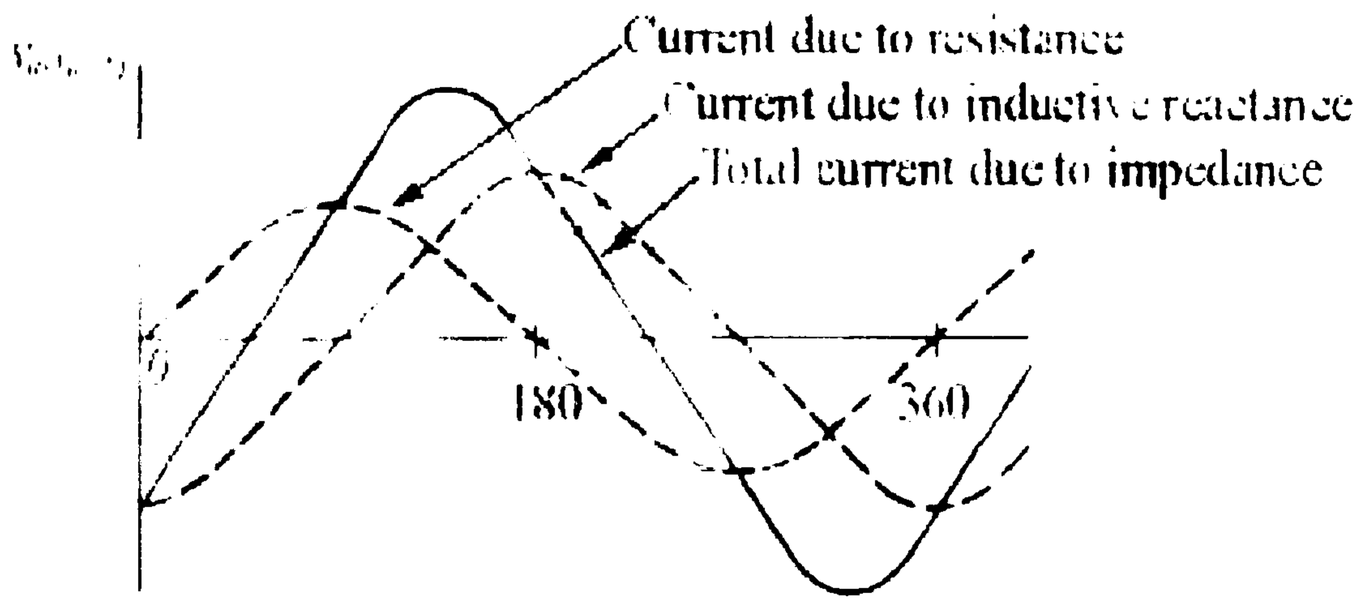

Figure 19 – Impedance circuit

In the image above, a circuit diagram is shown that represents an eddy current inspection system. The eddy current probe is a coil of wire so it contains resistance and inductive reactance when driven by alternating current. The capacitive reactance (XC) can be dropped as most eddy current probes have little or no capacitive reactance. The solid line in the graph above shows the circuit's total current, which is affected by the total impedance of the circuit. The two dashed lines represent the portion of the current that is affected by the resistance and the inductive reactance components individually. It can be seen that the resistance and the inductive reactance lines are 90 degrees out of phase, so when combined to produce the impedance line, the phase shift is somewhere between zero and 90 degrees. The phase shift is always relative to the resistance line since the resistance line is always in-phase with the voltage. If more resistance than inductive reactance is present in the circuit then the impedance line will move toward the resistance line and the phase shift will decrease. If more

inductive reactance is present in the circuit then the impedance line will shift toward the inductive reactance line and the phase shift will increase.

The relationship between impedance and its individual components (resistance and inductive reactance) can be represented using vector as shown above. The amplitude of the resistance component is shown by a vector along the x-axis and the amplitude of the inductive reactance is shown by a vector along the y-axis. The amplitude of the impedance is shown by a vector that stretches from zero to a point that represents both the resistance value in the x-direction and the inductive reactance in the y-direction. Eddy current instruments with impedance plane displays present information in this format.

The impedance in a circuit with resistance and inductive reactance can be calculated using the following equation.

Impedance without capacitive reactance $$Z = \sqrt{R^2 + X_L^2}$$

If capacitive reactance is present in the circuit, its value would be subtracted from the inductance term before squaring and calculated using the following equation:

Impedance with capacitive reactance $$Z = \sqrt{R^2 + (X_L - X_C)^2}$$

The phase angle of the circuit of the circuit can be calculated using the equation below.

$$\Theta = \tan^{-1} \frac{X_L}{R}$$

Depth of Penetration & Current Density

Eddy currents are closed loops of induced current circulating in planes perpendicular to the magnetic flux. They normally travel parallel to the coil's winding and flow is limited to the area of the inducing magnetic field. Eddy currents concentrate near the surface adjacent to an excitation coil and their strength decreases with distance from the coil as shown in the image [Figure 20]. Eddy current density decreases exponentially with depth. This phenomenon is known as the skin effect.

Skin effect arises when the eddy currents flowing in the test object at any depth produce magnetic fields which oppose the primary field, thus reducing net magnetic flux and causing a decrease in current flow as depth increases. Alternatively, eddy currents near the surface can be viewed as shielding the coil's magnetic field, thereby weakening the magnetic field at greater depths and reducing induced currents.

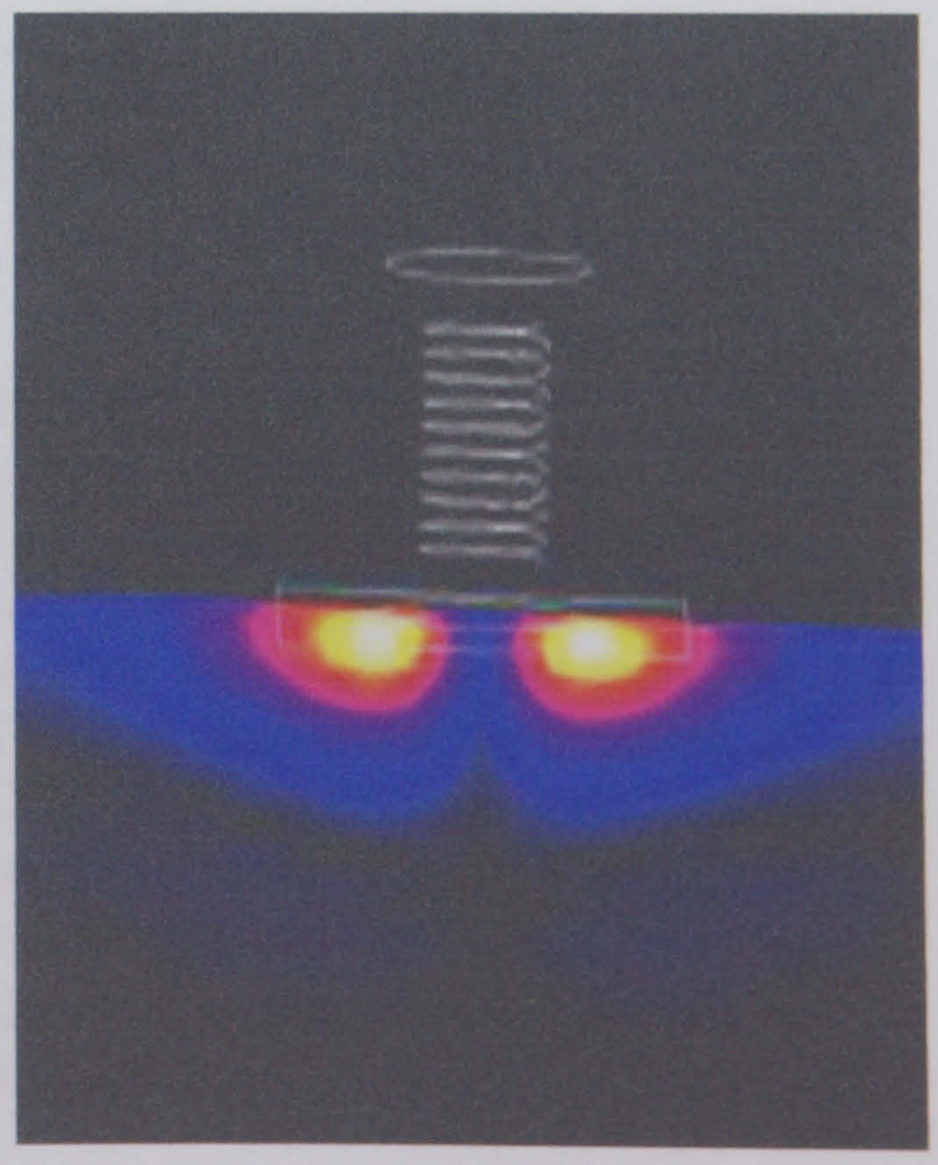

Figure 20 – Penetration of eddy currents

The depth that eddy currents penetrate into a material is affected by the frequency of the excitation current and the electrical conductivity and magnetic permeability of the specimen. The depth of penetration decreases with increase in frequency, conductivity and magnetic permeability [Figure 21]. The depth, at which eddy current density has decreased to 1/e, or about 37% of the surface density, is called the standard depth of penetration. The word 'standard' denotes plane wave electromagnetic field excitation within the test sample (conditions which are rarely achieved in practice). Although eddy currents penetrate deeper than one standard depth of penetration they decrease rapidly with depth. At two standard depths of penetration (2), eddy current density has decreased to 1/e squared or 13.5% of the surface density. At three depths (3) the eddy current density is down to only 5% of the surface density.

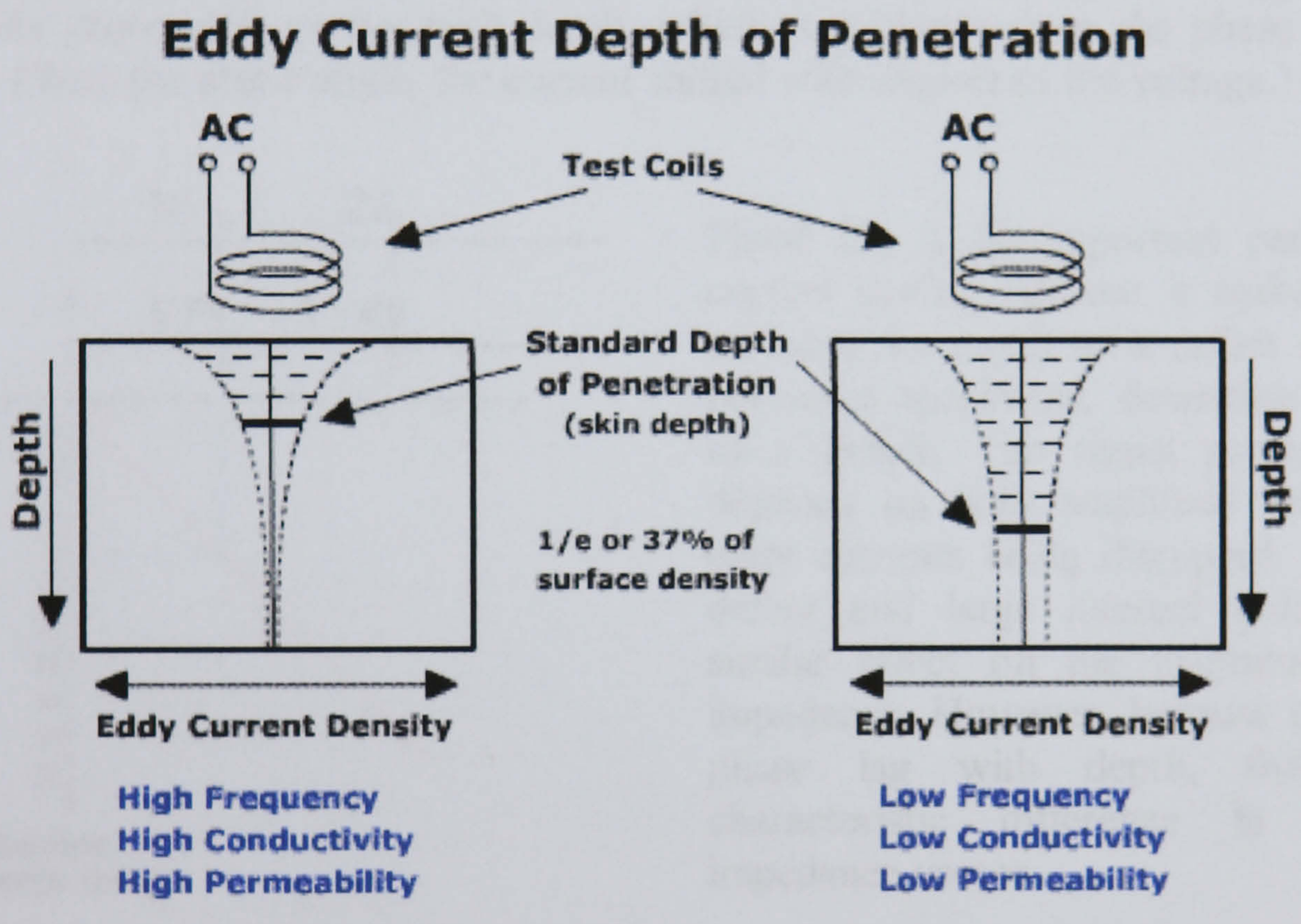

Figure 21 – Factors affecting eddy current depth of penetration

Since the sensitivity of an eddy current inspection depends on the eddy current density at the defect location, it is important to know the strength of the eddy currents at this location. When attempting to locate flaws, a frequency is often selected which places the expected flaw depth within one standard depth of penetration. This helps to assure that the strength of the eddy currents will be sufficient to produce a flaw indication. Alternately, when using eddy currents to measure the electrical conductivity of a material, the frequency is often set so that it produces three standard depths of penetration within the material. This helps to assure that the eddy currents will be so weak at the back side of the material that changes in the material thickness will not affect the eddy current measurements

One should also note that although the currents are restricted to flow within specimen boundaries, the magnetic field extends into the air space beyond. This allows the inspection of multilayer components separated by an air space

Phase Lag

Phase lag is a parameter of the eddy current signal that makes it possible to obtain information about the depth of a defect within a material. Phase lag is the shift in time between the eddy current response from a disruption on the surface and a disruption at some distance below the surface. The generation of eddy currents can be thought of as a diffusion process meaning that the eddy currents below the surface take a little longer to form than those at the surface. Therefore, subsurface defects will be detected by the eddy current instrument a little later in time than surface defects. Both the signal voltage and current will have this phase shift or lag with depth, which is different from the phase angle discussed earlier. (With the phase angle, the current shifted with respect to the voltage.)

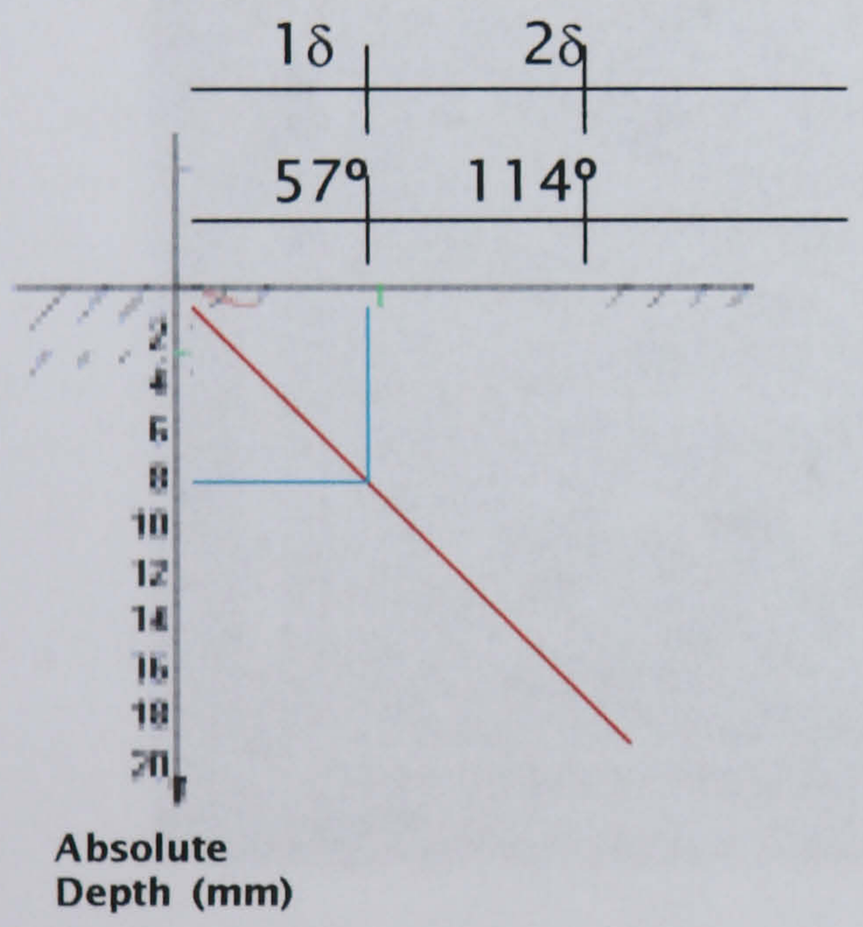

Phase lag is an important parameter in eddy current testing because it makes it possible to estimate the depth of a defect and with proper reference specimens, determine the rough size of a defect. The signal produced by a flaw depends on both amplitude and phase of the eddy currents being disrupted. A small surface defect and large internal defect can have a similar effect on the magnitude of test coil impedance. However, because of the increasing phase lag with depth, there will be a characteristic difference in the test coil impedance vector.

Figure 22 – Eddy current phase lag

At one standard depth of penetration[Figure 22], the phase lag is 57 degrees or one radian. This means that the eddy currents flowing at one standard depth of penetration (1δ) below the surface, lag the surface currents by 57 degrees. At two standard depths of penetration (2δ) they lag the surface currents by 114 degrees. Therefore by measuring the phase lag of a signal, the depth of a defect can be estimated.

Applications of Eddy Current

Eddy Current methods of inspection are effective with both ferromagnetic and non-ferromagnetic metals. They are not quite as sensitive to small, open defects as are liquid penetrant or magnetic particle methods. Because of the skin effect, Eddy Current inspection is generally restricted to depths less than 6 mm. The results of inspecting ferromagnetic materials can be obscured by changes in the magnetic permeability of the test piece. If electrical conductivity or other properties including metallurgical properties are being determined, changes in temperature must be avoided to prevent erroneous results.

The impedance plane diagram [Figure 23] is a very useful way of displaying eddy current data. As shown in the figure below, the strength of the eddy currents and the magnetic permeability of the test material cause the eddy current signal on the impedance plane to react in a variety of different ways.

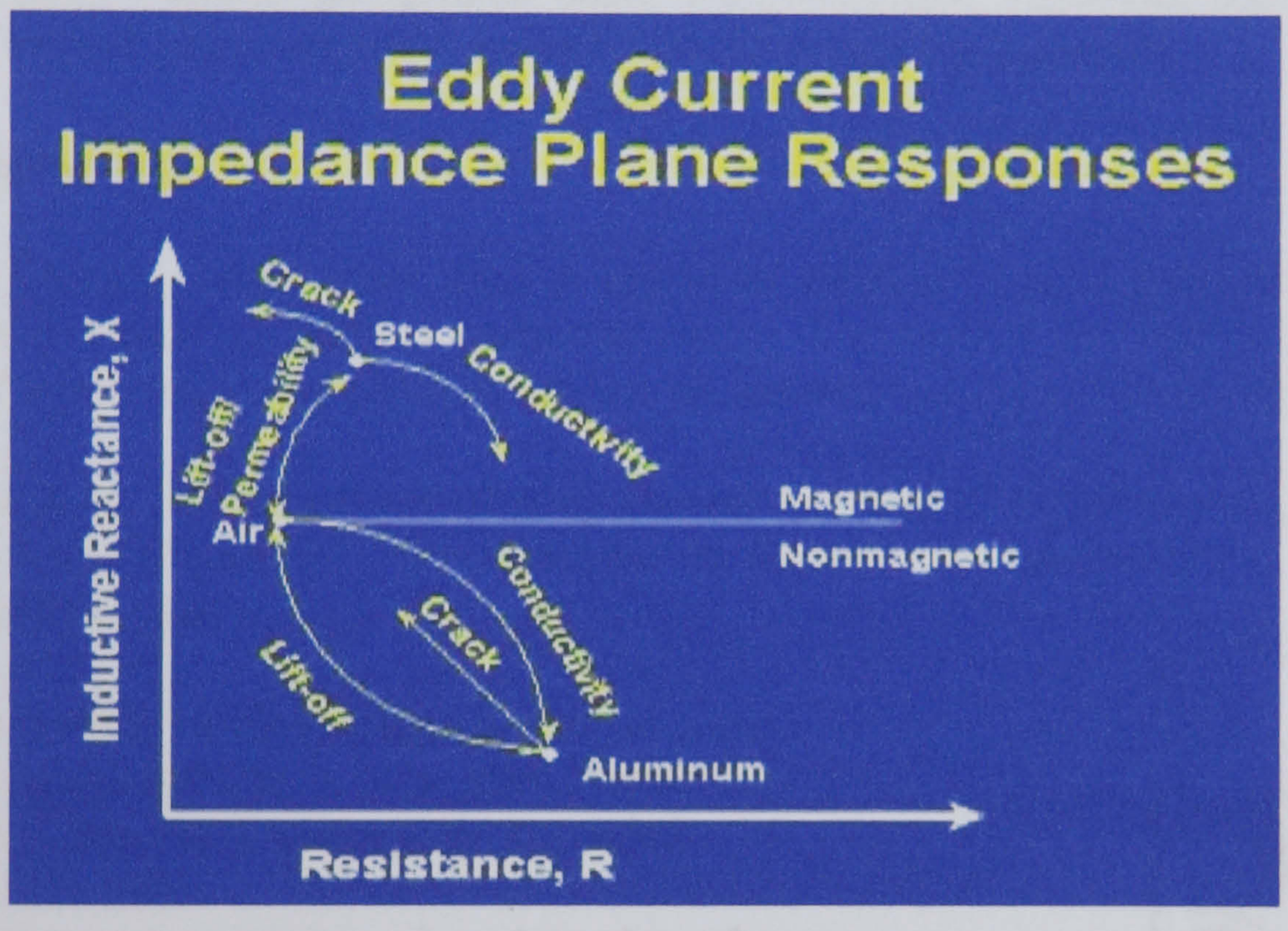

Figure 23 – Impedance Plane Diagram [10]

If the eddy current circuit is balanced in air and then placed on a piece of aluminum, the resistance component will increase (eddy currents are being generated in the aluminum and this takes energy away from the coil and this energy loss shows up as resistance) and the inductive reactance of the coil decreases (the magnetic field created by the eddy currents opposes the coil's magnetic field and the net effect is a weaker magnetic field to produce inductance). If a crack is present in the material, fewer eddy currents will be able to form and the resistance will go back down and the inductive reactance will go back up. Changes in conductivity will cause the eddy current signal to change in a different way.

When a probe is placed on a magnetic material such as steel, something different happens. Just like with aluminum (conductive but not magnetic) eddy currents form, which takes energy away from the coil and this shows up as an increase in the coils resistance. As with aluminum, the eddy currents generate their own magnetic field that opposes the coils

magnetic field. However, you will note for the diagram that the reactance increases. This is because the magnetic permeability of the steel concentrates the coil's magnetic field this increase in the magnetic field strength completely overshadows the magnetic field of the eddy currents. The presence of a crack or a change in the conductivity will produce a change in the eddy current signal similar to that seen with aluminum.

Applications of Eddy Current and electromagnetic methods of inspection to castings can be divided into the following categories.

1) Detecting near-surface flaws such as cracks, voids, inclusions, blowholes and pinholes.
2) Sorting according to alloy, temper, electric conductivity, hardness and other metallurgical factors.
3) Gauging according to size, shape, plating thickness or insulation thickness.

Because Eddy Currents are created using electromagnetic induction, the inspection method does not require direct electrical contact with the part being inspected.

Test Equipment

In Eddy Current testing more than in any other method of non-destructive testing, the test system is designed to fulfill a particular need. The testing parameters which, dictate the choice of one system over another, are just as important as the test system itself.

There are many different types of eddy current instrument on the market, but all are similar in many ways [Figure 24] while varying in function and accessories. All Eddy Current instruments contain:

a) A source of alternating current; in some instruments this is of a fixed frequency, in others the frequency can be varied.
b) A test coil.
c) Electronic circuitry for detecting the impedance or change of impedance in the test coil. (It is in the circuitry that there is the greatest variation between instruments).

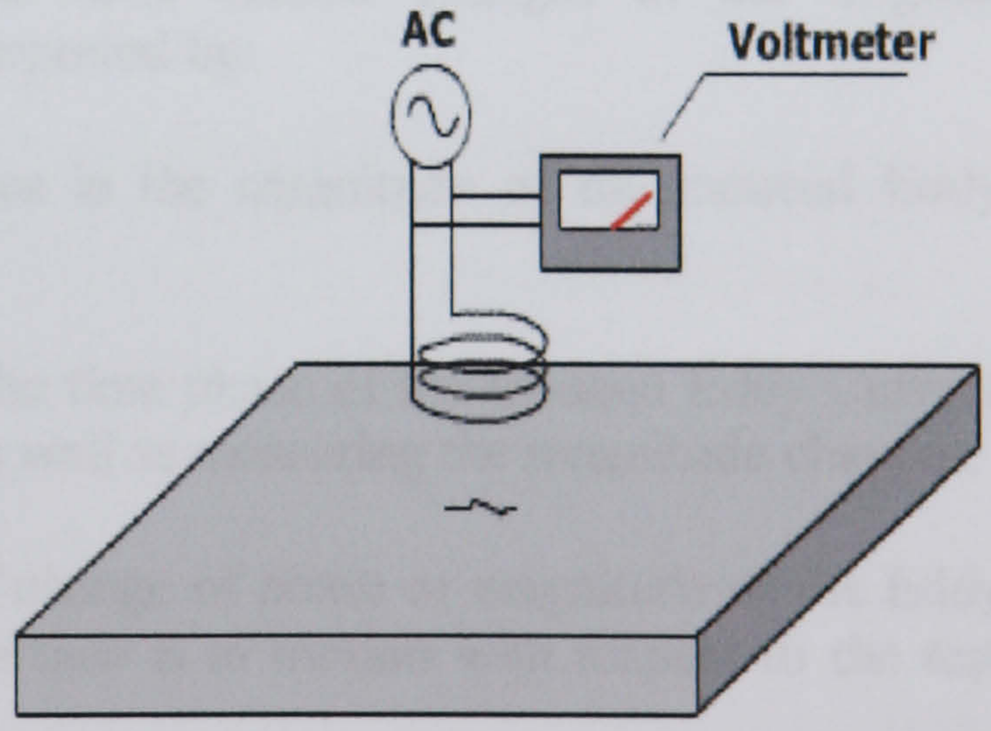

Figure 24- Typical instrument set-up

Very few Eddy Current instruments are direct reading; most are indicating a change that is proportional in some way to the change in impedance in the test circuit. The test equipment has therefore to be calibrated, using standards that have known qualities, before the readings have any meaning for the operator.

The test or inspection coils can take a variety of forms and can be arranged in a variety of ways.

Basically, however, there are three types of test coils used in Eddy current testing:

1) Surface coils (Figure 25a). These can be used for surface flaw detection, conductivity measurement and coating thickness measurement.
2) Encircling coils (Figure 25b) used for flaw detection, e.g. in tubes and bars, material evaluation, or bulk effects.
3) Internal (bobbin type) coils (Figure 25c). Mainly used for flaw detection of inner circumference of tubes.

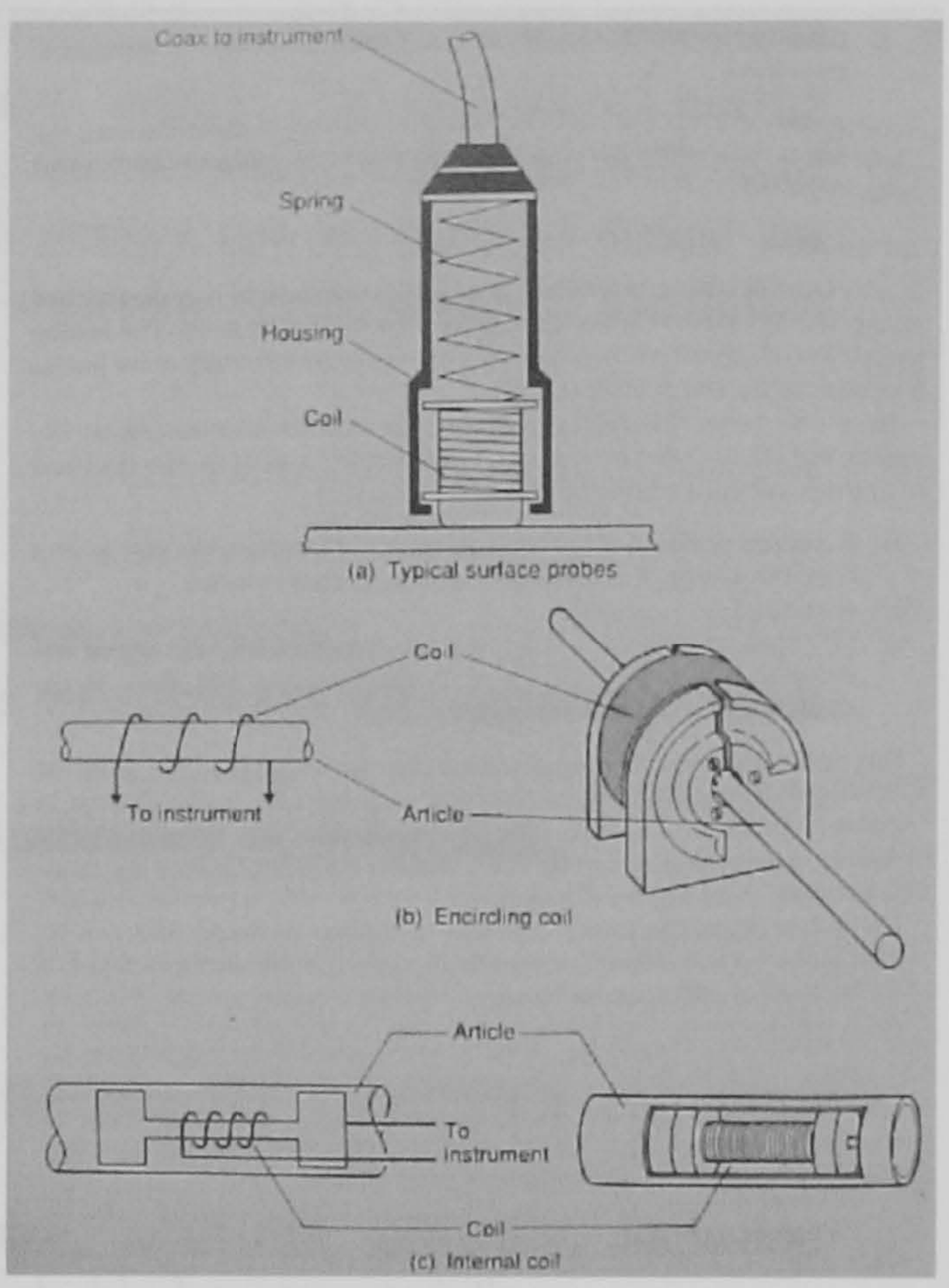

Figure 25 – Typical eddy current inspection coils [11]

Once Eddy Currents have been generated and have caused changes in the original magnetising field, the changes detected may be interpreted by:

1) Impedance analysis: measuring net changes in the magnitude of the induced Eddy Current field.

2) Phase analysis: measuring net changes in the time phase of the induced Eddy Current field with respect to the test coil voltage, as well as measuring the magnitude changes.

3) Modulation analysis: measuring the rate of change of phase or magnitude of the Eddy Current field, in instances where the test article is in motion with respect to the test coil.

2.5 Ultrasonic Inspection

Ultrasonic inspection is a non-destructive method in which beams of high-frequency acoustic energy are introduced into the test material to detect surface and sub-surface flaws and to measure the thickness of the material or distance to a flaw. An ultrasonic beam will travel through a material until it strikes an interface or defect, which interrupts the beam and reflects a portion of the incident acoustic energy. The amount of energy reflected is a function of the nature and orientation of the interface or flaw as well as of the acoustic impedance of such a reflector. Reflected energy can be used to define the presence and locations of defects, the thickness of the material, or the depth of the defect beneath a surface.

The advantages of ultrasonic tests are:

1) High sensitivity, which permits the detection of minute cracks.
2) Great penetrating power, which allows the examination of extremely thick sections. e.g. Industrial shafts up to 3m length
3) Accuracy in measurement of flaw position and estimation of defect size.

Ultrasonic tests have the following limitations:

1) Size-contour complexity and unfavourable discontinuity orientation can pose problems in interpreting the echo pattern.
2) Undesirable internal structures, e.g. grain size, structure, porosity, inclusion content or fine dispersed precipitates, can similarly hinder interpretation.

Effect of casting shape

Because castings are rarely simple flat shapes, they are not so easy to inspect as are such products as rolled rectangular bars. The reflections of a sound beam have been used for automated defect characterisation systems, in which porosity, cracks and dross have been distinguished.
However, because of the requirement to scan the probe over the surface, the application of B-Scan and C-Scan methods has generally been limited to simple geometric shapes having good surface finish, such as welded plate structures. Application of B and C Scans to castings is currently restricted, although greater use is likely with either improved scanning systems or arrays of ultrasonic probes.

Structure Evaluation

This is an area of growing importance for foundry engineers. Ultrasonic velocity measurements are already widely used as a means of guaranteeing the modularity of graphite structure and, if the matrix structure is known to be consistent, of guaranteeing the principal material properties of ductile irons. Velocity measurements have been used to evaluate compacted graphite-iron structures to ensure that the desired properties have been consistently obtained.

2.6 Radiography

Radiography is a general term given to material inspection methods based on the differential absorption of penetrating radiation. The principles are thus based on three basic elements; a radiation source or probing medium, the test piece or object being evaluated, and a recording medium.

A radiograph is basically a two-dimensional picture of intensity distribution of penetrating radiation, projected from the source (ideally a point source), which has passed through the object.

Three forms of penetrating radiation are currently used in radiography: X-rays, gamma rays and neutrons.

Industrial radiographic inspection of castings is based on exposure to short wavelength radiation in the form of X-rays or gamma rays from a suitable source. The amount of radiation absorbed by a particular part is a direct function of its effective thickness and the radiographic density of the material. Radiation intensity is thus influenced by internal cavities or by inclusions of substances possessing different radiographic density from that of the base metal. The resulting local variations in intensity of the emergent radiation (or shadow effects) can be detected with the aid of imaging media such as photographic films, fluorescent screens or electronic devices.

Film radiography is the technique most commonly applied to castings, although the less sensitive fluorescent screen offers a convenient method for the rapid inspection of light alloys in thin section. Recent advances in image intensifiers and low level television cameras have provided radiographic capabilities for both light and dense metal alloy inspection, with good sensitivities routinely being achieved in production applications.

Various types of image conversion technique allow the viewing of radiographic images while the test piece is being irradiated and moved relative to the radiation source and detector. These techniques are described as "real-time radiography" and near-real-time radiography", the difference being that the formation of near-real-time images occurs after a time delay, thus requiring limitation of the test object motion.

On radiographic film, the image of a discontinuity or void appears in most instances as a dark shadow, representing the local increase in the transmission of radiation because of the effective reduction in metal thickness in the path of the beam. Some inclusions found in light alloys (notably aluminium oxide and tungsten) reduce transmission; their images therefore appear lighter than the matrix. For high sensitivity of discontinuity detection, therefore, the conditions for the production of a radiograph must be carefully selected to secure the required degree of contrast in the image. Sensitivity and exposure time must be considered together, in other to obtain high quality radiographs at a reasonable cost.

Image quality and radiographic sensitivity [12]

The quality of radiographs is affected by many variables and image quality is measured with indicators (IQI's), sometimes referred to as penetrameters. There are many types of IQI (usually made of the same material as the test piece) and when used during radiographic inspection they measure image contrast and, to a limited extent, resolution.

Detail resolution is not directly measured with IQI's because flaw detection depends on the nature of the flaw and its shape and orientation relative to the radiation beam. Image quality is governed by image contrast (radiographic contrast) and resolution (radiographic definition). These two characteristics are interrelated in a complex way and are affected by several factors. Many variables affecting radiographic contrast and definition are summarized below and briefly addressed in following sections.

Radiographic Contrast

Subject contrast is determined by the following variables:
- Absorption differences in the specimen
- Wavelength of the primary radiation
- Scatter or secondary radiation

Film contrast is determined by the following:
- Grain size or type of film
- Chemistry
- Concentration
- Time of development
- Temperature
- Degree of mechanical agitation (physical motion)

Density of the radiograph

- Higher density will provide greater contrast.
- Lead screens in the thickness range of 0.004 to 0.015 inch typically will reduce scatter radiation at energy levels below 150, 000 volts. Above this point they will emit electrons to provide more exposure of the film to ionizing radiation thus increasing the density of the radiograph.
- Fluorescent screens provide no filtering. When exposed to radiation they produce visible light exposing the film.

Definition

Geometric factors include the following:
- Focal spot size, which is the point of origin of the radiation, should be nearly a point source as possible.
- Source to film distance, which is the distance from the source to the part, should be held at a minimum.
- Specimen to part distance. The specimen and film should be in intimate contact.
- Abrupt changes in specimen thickness may cause distortion on the radiograph.
- Movement of the specimen during the exposure will produce distortion on the radiograph.

Film graininess, and screen mottling
- The speed of film will dictate the definition of the radiograph.
- Wavelength of the radiation will influence apparent graininess. As the wavelength shortens and penetration increases, the apparent graininess of the film will increase.
- Increased development of the film will increase the apparent graininess of the radiograph

Radiographic sensitivity, which should be distinguished from image quality, generally refers to the size of the smallest detail that can be detected. Although radiographic

sensitivity is often synonymous with image quality in applications requiring the detection of small details, a distinction should be made between radiographic sensitivity and radiographic quality. Radiographic sensitivity refers more to detail resolvability, as distinct from spatial and contrast resolution.

Controlling Radiographic Quality

One of the methods of controlling the quality of a radiograph is through the use of image quality indicators (IQI). IQI's provide a means of visually informing the film interpreter of the contrast sensitivity and definition of the radiograph. The IQI indicates that a specified amount of material thickness change will be detectable in the radiograph, and that the radiograph has a certain level of definition so that the density changes are not lost due to unsharpness. Without such a reference point, consistency and quality could not be maintained and defects could go undetected.

Image quality indicators take many shapes and forms due to the various codes or standards that invoke their use. In the main two IQI styles are prevalent [Figure 26]; the placard, or hole-type and the wire IQI. IQI's come in a variety of material types so that one with radiation absorption characteristics to the material being radiographed can be used.

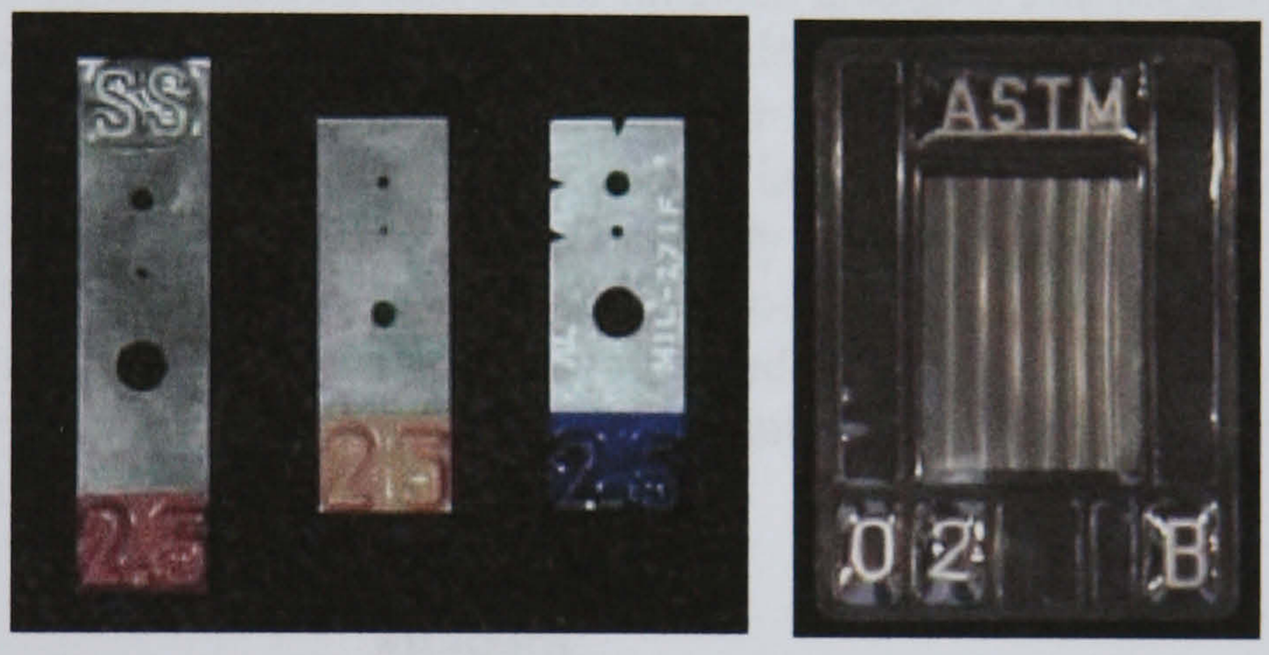

Figure 26 – Types of Image Quality Indicators (IQI's)

Placement of IQI's

IQI's (penetrameter) should be placed on the source side of the part over a section with a material thickness equivalent to the region of interest [Figure 27]. If this is not possible, the IQI may be placed on a block of similar material and thickness to the region of interest. When a block is used, the IQI should the same distance from the film as it would be if placed directly on the part in the region of interest. The IQI should also be placed slightly away from the edge of the part so that at least three of its edges are visible in the radiograph.

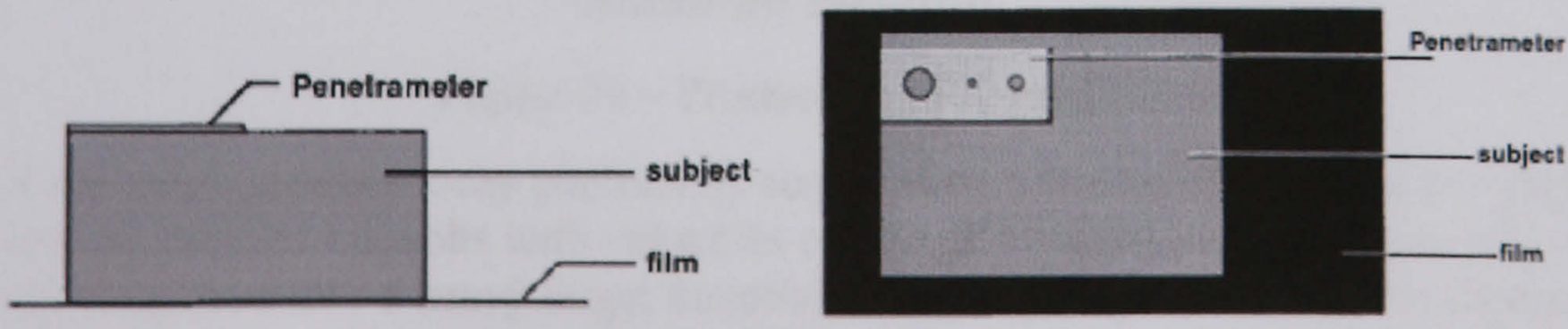

Figure 27.- Placement of IQI's

X-RAY Equipment

X-rays are just like any other kind of electromagnetic radiation. They can be produced in parcels of energy called photons, just like light. There are two different atomic processes that can produce X-ray photons. One is called Bremsstrahlung and is a German term meaning "braking radiation." The other is called K-shell emission. They can both occur in the heavy atoms of tungsten. Tungsten is often the material chosen for the target or anode of the x-ray tube. Figure 28 illustrates the generation of X-rays where the electrons from the heated coil are accelerated across to strike the tungsten target.

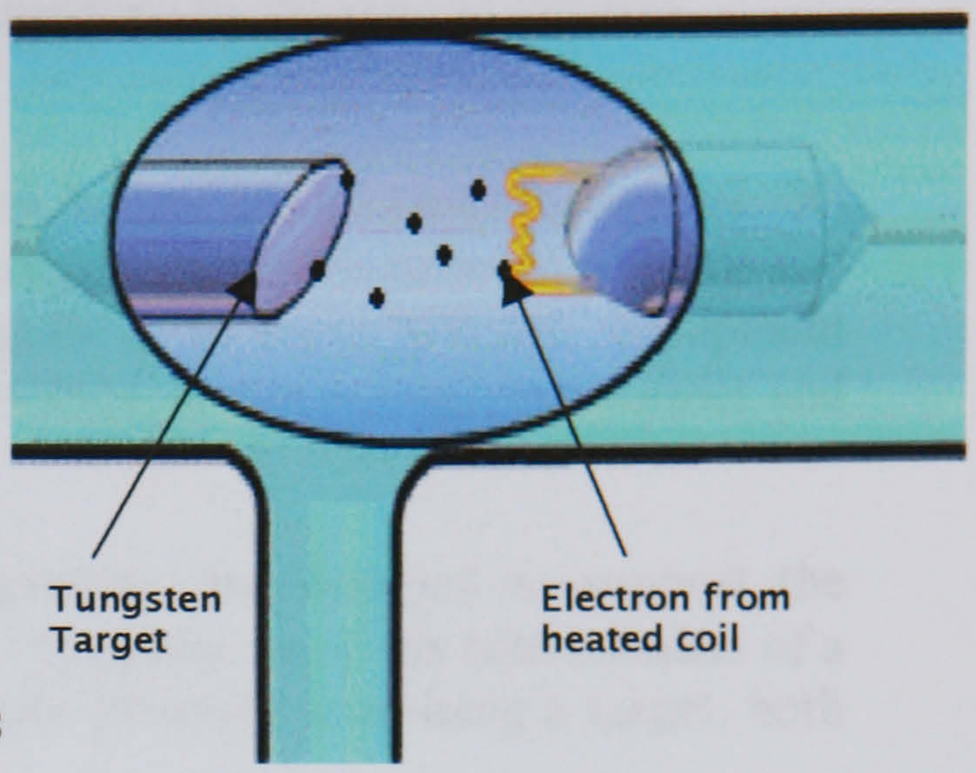

Figure 28 – Construction of X-ray tube head

Both ways of making X-rays involve a change in the state of electrons. However, Bremsstrahlung is easier to understand using the classical idea that radiation is emitted when the velocity of the electron shot at the tungsten changes. The negativity charged electron slows down after swinging around the nucleus of a positively charged tungsten atom. This energy loss produces X-radiation. Electrons are scattered elastically and inelastically by the positively charged nucleus. The inelastically scattered electron loses energy, which appears as bremsstrahlung. Elastically scattered electrons (which include backscattered electrons) are generally scattered through larger angles. In the interaction, many photons of different wavelengths are produced, but none of the photons have more energy than the electron had to begin with. After emitting the spectrum of X-ray radiation the original electron is slowed down or stopped.

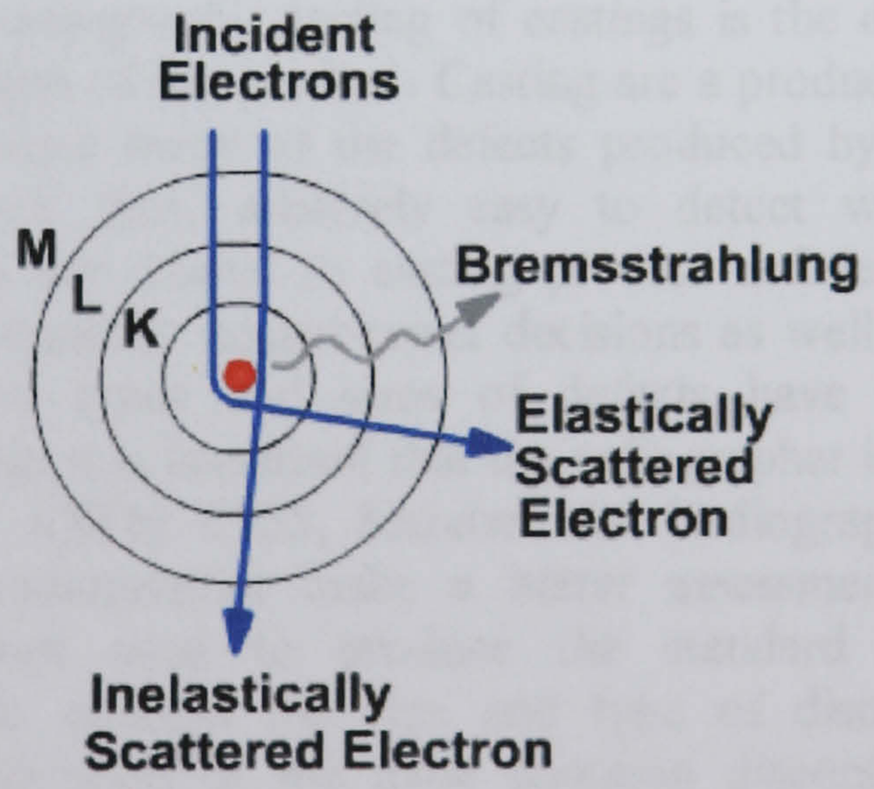

Figure 29 – Production of X-ray Photons

X-ray tubes produce x-ray photons by accelerating a stream of electrons to energies of several hundred kilovolts with velocities of several hundred kilometers per hour and colliding them into a heavy target material. The abrupt acceleration of the charged particles (electrons) produces Bremsstrahlung photons [Figure29]. X-ray radiation with a continuous spectrum of energies is produced ranging from a few KeV to a maximum of energy of the electron beam. Target materials for industrial tubes are typically tungsten,

which means that the wave functions of the bound tungsten electrons are required. The inherent filtration of an X-ray tube must be computed, this is controlled by the amount that the electron penetrates into the surface of the target and by the type of vacuum window present.

Radiation in the inspection of castings is usually from X-rays and gamma ray sources. X-ray equipment varies in size and output, and the conventional design of an X-ray tube and its high voltage iron-core transformer provides outputs up to about 500 Kv. Equipment providing these levels of output consists of an X-ray tube, a high voltage transformer and a control panel

The tube is the production unit; the other components are designed to support the function of the tube or to meet safety requirements. Typically, an X-ray tube consists of a cathode structure containing a filament, and an anode structure containing a target, both within an evacuated chamber or envelope (Figure 4).

Depending on the size of focal spot achieved, X-ray tubes are sometimes classified as:

Conventional tubes, with focal spot sizes between 0.4 x 0.4 mm and 5 x 5 mm.

Micro-focus tubes, with focal spot sizes down to 0.005 mm.

For higher energy X-rays other designs are used, providing energy levels up to 30 MeV. These include linear accelerators and betatrons. Linear accelerators, which produce high velocity electrons by means of radio-frequency energy coupled to a wave-guide, have extended industrial applications.

RADIOGRAPH INTERPRETATION - CASTINGS

The major objective of radiographic testing of castings is the disclosure of defects that adversely affect the strength of the product. Casting are a product form that often receive radiographic inspection since many of the defects produced by the casting process are volumetric in nature and, thus, relatively easy to detect with this method. These discontinuities of course, are related to casting process deficiencies, which, if properly understood, can lead to accurate accept-reject decisions as well as to suitable corrective measures. Since different types and sizes of defects have different effects of the performance of the casting, it is important that the radiographer is able to identify the type and size of the defects. ASTM E155, Standard for Radiographs of castings has been produced to help the radiographer make a better assessment of the defects found components. The castings used to produce the standard radiographs have been destructively analyzed to confirm the size and type of discontinuities present. The following is a brief description of the most common discontinuity types included in existing reference radiograph documents (in graded types or as single illustrations).

3.0 STUDY 1 - INSPECTION OF CNC MATERIAL Cu-Ni-Cr [1.6%CR] TO FIND OXIDE ENTRAPMENTS

3.1 Background

Some years ago the marine industry began a research programme to identify an alloy to replace the traditional Nickel Aluminium Bronze (NAB) whose corrosion resistance was significantly improved so reducing maintenance and repair costs. Of the candidate materials an alloy of 70/30 Copper Nickel with addition of 1.6% Chromium (CuNiCr) was selected and the comparative properties of these two alloys is listed in table 1.

TABLE 1. COMPARATIVE PROPERTIES OF NICKEL ALUMINIUM BRONZE AND COPPER/NICKEL/CHROMIUM [13]

Property	**NAB**	**CuNiCr**
0.2% Proof test [MNm^3]	270	300 - 320
Elongation [%]	15	18 - 25
Fracture toughness Izod Impact J	17	45 - 60
Corrosion [mm. $yr.^{-1}$]	0.07	0.02
Crevice Corrosion [mm. $yr.^{-1}$]	0.5	<0.2
Melting Range [°C]	1050-1080	1180-1230
Density [g/cm^3]	7.6	8.8
Thermal Conductivity [WK^{-1}]	40	23
Electrical Resistivity [μ ohm m]	0.2	0.35
Magnetic Permeability [μ]	1.4	1.01

After much experimentation and industrial trials a naval engineering standard NES 824 was raised to detail production requirements for Copper Nickel Chromium alloy sand castings and ingots. This NES specifies the requirements for manufacture, inspection and testing of sand castings and ingots in Copper Nickel Chromium.

The chemical composition of castings is given in Table2 [13]. The chemical composition of ingots is to be agreed between the ingot manufacturer and purchaser to ensure that due allowance is made for impurity pick-up during the casting processes.

Microstructures have a significant effect on the mechanical and physical properties of materials and there suitability for end use application. As with other copper nickel alloys, copper nickel chromium has single-phase structures. In the as cast condition, the wide freezing range gives rise to heavily cored dendrites. The addition of chromium which has a high affinity for the oxygen and carbon frequently present during industrial melting and casting processes, microstructures can therefore appear to be more complex than would be expected from the binary equilibrium diagrams.

The rectification of casting defects by welding requires the successful completion of weldability tests. Weldability is adversely affected by impurities at the grain boundaries of the 'as cast' material. In order to increase the probability of producing castings, which are, easy to weld repair it is recommended that the impurities are not exceeding those specified in table 3.

It is important also that the carbon content be kept to an absolute minimum and the Titanium content is to be aimed towards the upper limit of that specified.

TABLE 2. CHEMICAL COMPOSITION OF COPPER NICKEL CHROMIUM CASTINGS [13].

ELEMENT	Percentage by Weight	
	Min.	**Max.**
Nickel	29.00	32.00
Chromium	1.6	2.0
Iron	0.5	1.0
Manganese	0.5	1.0
Silicon	0.20	0.40
Zirconium	0.05	0.15
Titanium	0.10	0.20
Copper	REMAINDER	

TABLE 3. IMPURITY LEVELS

IMPURITY	Percentage by Weight Not more than
Lead	0.0015
Bismuth	0.0005
Sulphur	0.0030
Carbon	0.0060
Selenium	0.0005
Tellurium	0.0010
Zinc	0.0030

For quality assurance purposes the castings produced in accordance with NES 824 are classified as follows:

Class I
A casting whose failure would lead to uncontrollable flooding, the total immobilization of the ship, or serious hazard to personnel.
Note; This class of casting has very high standards of inspection and acceptance and is intended to be used in critical parts of ships and submarines.

Class II
A casting whose failure would lead to severe but controllable flooding, the serious disruption of weapon systems, main propulsion machinery. or its attendant auxiliaries including generators.

Class III
All other castings.

3.2 Quality Assurance of CuNiCr Castings

The quality assurance requirements stipulates test methods both Destructive and Non-Destructive. Note: as this study examines the problem of oxide network entrapment for quality assessment of each casting, similar effects on mechanical properties are therefore considered to be outside the scope of this work.

In NES 824 Non-destructive tests other than Visual/Optical are applicable to all Class I and Class II castings with particular regard for areas identified as critical test regions (**ctr**) and test regions (**tr**). Visual/Optical inspections, at X5 magnification if necessary are applicable 100% to all castings.

The Non- destructive methods applied in accordance with NES 824 for Copper Nickel Chromium castings are these which had been established for similar castings in Nickel Aluminium Bronze are:

3.2.1 Dye Penetrant
[Colour Contrast Method]
All internal and external surfaces of Class I and Class II castings, which will remain in the as-cast treated state, in the finished component, are subject to 100% liquid penetrant examination. Surfaces, which will be machined for the finished component, are to be subjected to 100% penetrant examination after machining.

3.2.2 Acceptance criteria for penetrant inspection.
Indications of cracks, hot tears or chain-like porosity are not acceptable. Isolated pin-point porosity is acceptable except in areas where sealing of a housing against a running shaft is required, e.g. pump glands, propeller shaft seals etc. Where pinhole porosity is present in critical test and test regions, indications which are larger than pinpoint are limited as follows:

1. The maximum size of indication must not exceed 3mm diameter bleed out.
2. The sum of the diameter of indications in an area of 5000mm^2 must not exceed 24mm.

3.2.3 Radiography

Critical test regions (**ctr**) and test regions (**tr**) to be subjected to 100% radiographic examination. All sub-surface imperfections are to be identified for subsequent assessment in accordance with the acceptance standards.

3.2.4 Acceptance criteria for radiographic inspection.

Cracks, hot tears or cold shuts are not acceptable in any area of the castings. Internal porosity and shrinkage are acceptable where:

1. The local reduction in wall thickness does not exceed 5% of the design wall thickness in critical test regions and 10% of the design wall thickness in test regions.
2. The total defective area does not exceed 10% of each critical test region and 20% of each test region containing the defect

From discussions with the Ministry of Defence it appears that considerable tonnage and range of castings had been manufactured from this alloy to the requirements of NES 824 prior to this problem being recognized. All the cast material having been subjected to the standard Non Destructive Testing programme of visual inspection, colour contrast penetrant testing [commonly referred to as Dye Penetrants] and radiography and assessed to the acceptance criteria specified above.

Subsequent machining of the certified material, however, identified discontinuities not reported during casting acceptance tests. For example, an adapter cover had been produced by Rosyth Royal Dockyard foundry, based near Edinburgh, Scotland, revealing no unacceptable defects by both Penetrant and Radiographic examination in the as cast condition. Subsequent machining revealed "linear" type discontinuities, of which, some could be seen visually and later other by dye penetrant examination of the machined surface. Similar experiences were reported, we understand, by V.S.E.L. based in Barrow-In-Furness however the discontinuities they found were more non-linear.

3.3 Metallurgical Examination of Oxide Network Discontinuities

Laboratory examinations of the initial samples containing the "linear" oxide indications showed the discontinuity to be predominantly interdendritic (V.S.E.L reported some intergranular) in nature with an associated band of particulate [14].

A section enclosing the longest of the linear type defects was removed from the casting and this was subsequently machined back to the defect. The resulting section

perpendicular to the defect was then, after polishing, examined using an optical scanning electron microscope.
Examination by optical microscopy showed that the linear type defect extended into the casting to a depth of approximately 5mm from the machined surface [Figure 30].

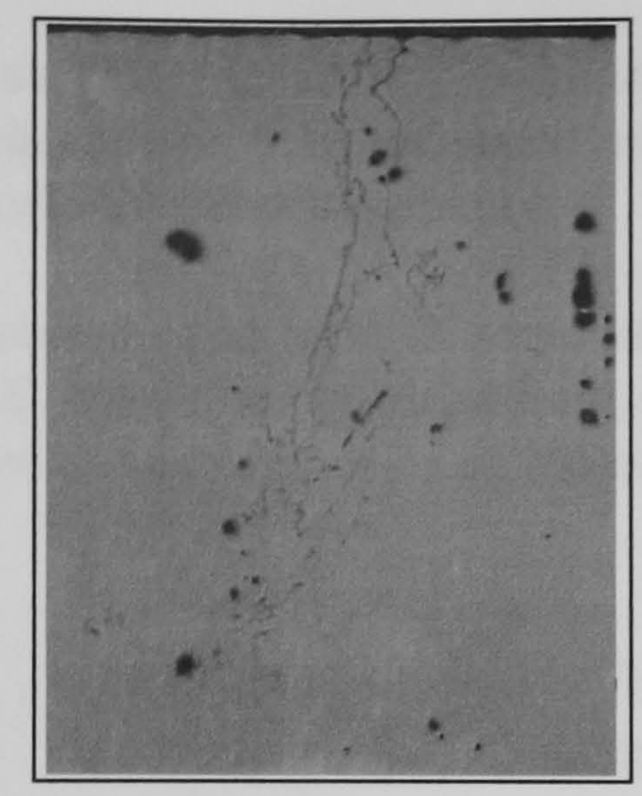

Figure 30. Linear Oxide Type Defect
X 20

Figure 31. Interdendritic oxide network of
defects with band of particulate. X50

Particulate material was present along much of the network of the defect and more substantial amounts of particulate of similar appearance were present in a band close to the defect [Figure 31]. Etching with dilute acid alcohol ferric chloride revealed that the defect and the adjacent band of particulate were predominantly of an interdendritic nature.

Element analysis using the scanning electron microscope revealed that the particles in the band formation were strongly rich in Zirconium with only minor amounts of the matrix elements being detectable [Figure 32]. The particulate material contained within the linear type defects was also strongly Zirconium rich and some cases significant amounts of Titanium were also detectable.

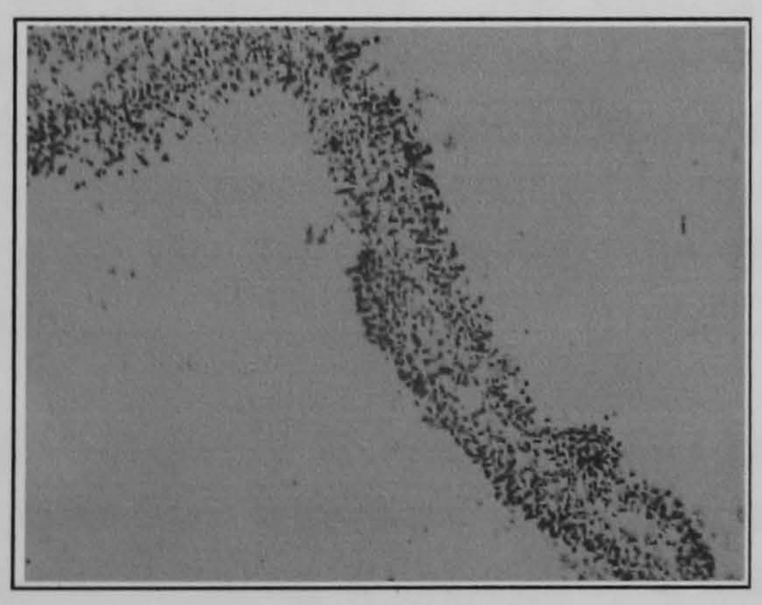

Figure 32. Zirconium Rich
Particulate X200

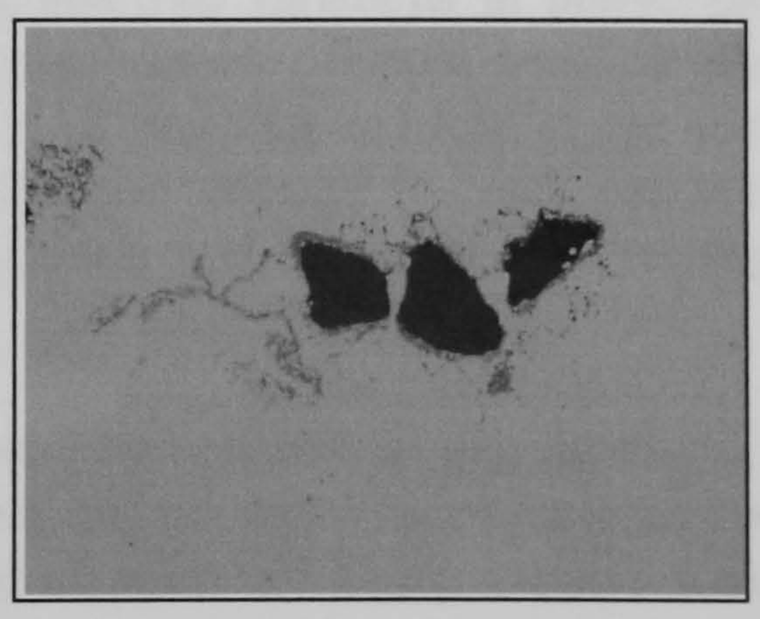

Figure 33. Silicon Inclusion removed by polishing
+associated particulates. X75

The discontinuity itself is reported to be an oxide of zirconium, titanium and silicon with the particulate band formations rich in zirconium.

The oxides of silicon were significantly large in size and it was these. which were dragged out or fragmented on machining, and this is responsible for the dye penetrant indications [Figure 33]. The regions of zirconium and titanium being considerably finer and coherent with the matrix produce no dye indication, but are visually detectable.

The surface "linear" type indications on sectioning show the discontinuity to be associated with a compounded inclusion penetrating the matrix and having an oxide network towards its extremity.

The severity and form of some of these oxide discontinuities caused concern and the M.O.D started an investigation to find a possible NDT method for discovering both surface and subsurface oxide inclusion networks in cast CuNiCr material.

3.4 Investigations of Heat Affected Zone Cracking in High Strength Cupro Nickel Chromium NES 824

3.4.1 Introduction

Some casting produced from High strength Cupro-Nickel alloys are subject to weld repairs. Unfortunately irrespective of strengthening additions of (Cr + Si) or (Nb + Si), these alloys exhibit sensitivity to heat affected zone (HAZ) cracking. This problem, which is attributed to a phenomenon called ductility dip exhibited by this class of alloys, has been recognised for many years. As part of the demonstrator programme a low welding success rate (approx. 15%) was experienced with the Cu-Ni-Cr alloy, NES 824.

Following a brief series of welding trials on cast plate and on a demonstrator 4-way casting, it was shown that the heat affected zone cracking was attributed to parent material condition and unless this could be modified to an acceptable state the problem could not be eliminated. The welding trial involved variations in pre-welding heat treatment and use of MIG and TIG welding processes. Simple bead on plate runs without using any filler material resulted in HAZ cracking and lead to the conclusion that this was a parent material problem and that the tendency to crack was probably a function of the known ductility dip phenomenon and levels of low melting point impurities.

The work reported is based on casts produced by commercial organizations and the work undertaken was based on a practical basis and not one of pure research due to the urgency in acquiring a solution to a material of poor and highly variable weldability. There were additional constraints in that major changes to the prime alloying elements were not permissible.

3.4.2 Chemical Analysis

Initially chemical analysis was undertaken but in order to obtain more detailed results of the impurity level in the alloys the use of Glow Discharge Mass Spectrometry (GDMS)[15] was employed, providing analysis of over 40 elements in each cast. Only selections of those elements analyzed are considered for discussion and principally consist of these elements;

a) known to be prime contributors to intergranular cracking (Bi, Pb, Se. Te).
b) impurities which have shown cast to cast variations (Zn, Mg, Al, C).
c) Zr and Ti

Zirconium is intended to act as a getter for oxygen and nitrogen, whilst titanium is intended as a grain refining agent. Also included in table is the Bismuth Equivalent proposed by GAVIN [16] and subsequently used at Cranfield to describe the cumulative effect of low melting point impurities on the ductility dip phenomenon in 90/10 Cupro-Nickel. No known comparable exercise has been undertaken for the strengthened 70-30 Cupro-Nickel alloys.

Although not reported here in detail it was noted that there were marked variations in prime elements of the casts reported by GDMS in comparison to those reported by foundries. This clearly cast doubt on the accuracy of impurity levels reported. Subsequently repeat analyses were undertaken by another laboratory using differing techniques. In essence analysis of prime elements was found to be insufficiently accurate using GDMS but that there was very good comparison between impurity levels. GDMS is a surface analysis technique covering a relatively small area and the cupro-nickel-chromium casts were of variable grain size with marked segregation of the element in the cast state.

Examination of the results failed to show that any one element or group of elements was responsible for poor weldability. However the general trend of reducing impurity levels did result in improved weldability. This was complicated by the high grain size present but the general the trend was that as the % Ti increased, the grain size reduced. However the levels of Ti even when approaching 0.2% Ti were insufficient to result in a massive reduction in grain size. This is because grain size in this alloy will be controlled by degree of superheat when casting and cast section thickness i.e. a higher degree of superheat will be necessary to fully fill a large, complex, thick walled casting and the inevitably lower cooling rate will produce a larger grain (or more correctly, dendrite) size.

In essence this means that where a large grain /dendrite size material is present the grain boundary network through the casting section is reduced and thus impurity levels will be more concentrated, thereby weakening the grain boundary cohesive strength. This. combined with the weld thermal cycle induced ductility dip would inevitably result in the heat affected zone cracking.

The solution is clearly both a reduction in impurity content and grain size. The first can be achieved by using high purity stock material and has in fact been demonstrated in several casts. Reducing grain size is more problematic as indicated above. However, increased levels of Ti above that currently permissible would probably be beneficial but the effect on other material properties would need to be examined.

3.4.3 Mechanical Properties and Hot Ductility Testing

Tensile tests carried out at temperatures of 650 - 700°C were undertaken. Again the trend of reduced impurity resulted in increased hot ductility. There are problems associated with using this as an acceptance standard from not only the actual test but also the effect of the variable grain size and this still has to be satisfactorily resolved.

A series of specimens have been produced for testing to enable full ductility dip curves for some five different casts of variable chemical analysis to be produced. Of the results available to date the ductility dip trough occurs at 700°C and the lower hot ductility values at this temperature (typically 0-2%) were for alloys of comparatively high impurity content. Alloys of low impurity levels produced hot ductilities at 650 - 700°C of approaching 6%.

The tensile properties of the weld metal specimens were far in excess of those of the parent material and in particular, the heat affected zone.

3.4.4 Welding

The weldability of the alloy has been generally assessed by the severity of cracking observed both at the surface of the welded surface and on weldment sectioning. All cracking was found to occur only within the heat affected zone although cracks did on occasion penetrate the parent material. In order to obtain some degree of conformity only synergic pulsed MIG (resulting in low heat input) was used with a standard weld preparation of approximately 20mm depth. All welding was carried out under high restraint for the simple reason that the majority of weld repair will be required in the thicker sectioned, more complex castings where high restraint will always be present.

Additional work has been undertaken at The Welding Institute using MMA electrodes produced commercially. A closely matching consumable tested by TW1 resulted in extensive re-heat cracking within the weldments whilst a differing consumable based upon a 70-30 cupro-nickel with additions of chromium in the coating resulted in a crack free weld. Welding was undertaken on 25mm plate and was reported crack free. Subsequent examination again showed the presence of HAZ cracking.

3.4.5 General Discussion

From the first analyses there appeared to be a clear-cut trend of improved hot ductility and weldability with lower Bi equivalent (i.e. reduced, low melting point impurity levels), and reducing grain size with increasing Ti and Ti/C. Subsequent examination of thicker plate followed the same trend but suggested that greater control was necessary

particularly as regards grain size. With thicker walled casting grain size was inevitably larger and grain size of the order of 10mm was not uncommon. A fine grain size material results in a much longer grain boundary network and potentially a lower concentration of impurities.
Thus, two factors need to be controlled: -

a. Low melting points impurities

These can only be reduced by the use of high purity virgin material and good husbandry during manufacture i.e. ensure minimum contamination

b. Grain/Dendrite Size

Keeping grain size small reduces the affect of low melting point impurities but grain size is controlled by several processing related factors: -

i degree of melt superheat

ii casting section thickness

iii Cooling rate

Titanium is known to act as a grain-refining agent but for given casting parameters the level of titanium content to produce a specific grain size is not known. In addition, lengthy melting cycles can reduce Ti content in the melt.

3.4.6 Conclusions

HAZ cracking in the Cu-Ni-Cr alloy following welding operations is a function of the ductility dip phenomenon and the severity of cracking a function of the cumulative quantity of low melting point impurities (i.e. Bi, Pb, Se, Te etc.). If these levels are kept to below the maxima currently required a marked improvement in weldability is expected (and judged to be >70%).

The effect of increasing Ti level in order to further reduce grain size will result in an increase in grain boundary length, which will further reduce impurity concentrations in these areas.

Synergic MIG welding of low impurity alloys gave excellent response even under high restraint, whereas alloys of high impurity level suffered extensive cracking.

The larger section thickness casting will remain problematic. The need for weld repair will almost always be present and can only be successfully achieved by control of impurity levels although effects to reduce grain size will remain useful.

Thinner wall castings are likely to be less of a problem due to the smaller grain size. However, it should be noted that acceptance of higher impurity levels in the original cast shape may result in the shape being unweldable at some future date.

The need for finding HAZ cracking remains and is as important as detection and evaluation of linear oxide network in the body of the casting.

4.0 INVESTIGATION FOR SUITABLE NDT METHODS

To date non-destructive testing of castings produced from CuNiCr material has been the same as that for N.A.B. material, namely, Radiography for internal volumetric discontinuities and Dye Penetrant inspection for surface discontinuities in both the as cast condition and that of machined surface.

Investigations of Dye Penetrant indications present on the machined surface of several CuNiCr casting revealed the presence of extraneous material in the form of "washed-in" dross networks. Subsequently, the dross was identified as being oxides of silicon, titanium and zirconium. The oxides of silicon were significantly larger in size than others and it was these, which were either dragged out or fragmented on machining, and these were responsible for the Dye Penetrant indications [Figure 33]. The titanium and zirconium oxides being considerably finer and coherent with the matrix, did not initially produce indications. However, their presence could easily be detected visually.

Some CuNiCr castings are in service having passed all the NDT acceptance tests specified in NES 824 Part 1 issue1. The severity of some of these oxide discontinuities [see Figure34] that may be present in these castings could cause premature failure. This prompted an urgent investigation to find, by consultation as necessary with NDT agencies, a possible NDT method of discovering oxide discontinuities in cast CuNiCr material.

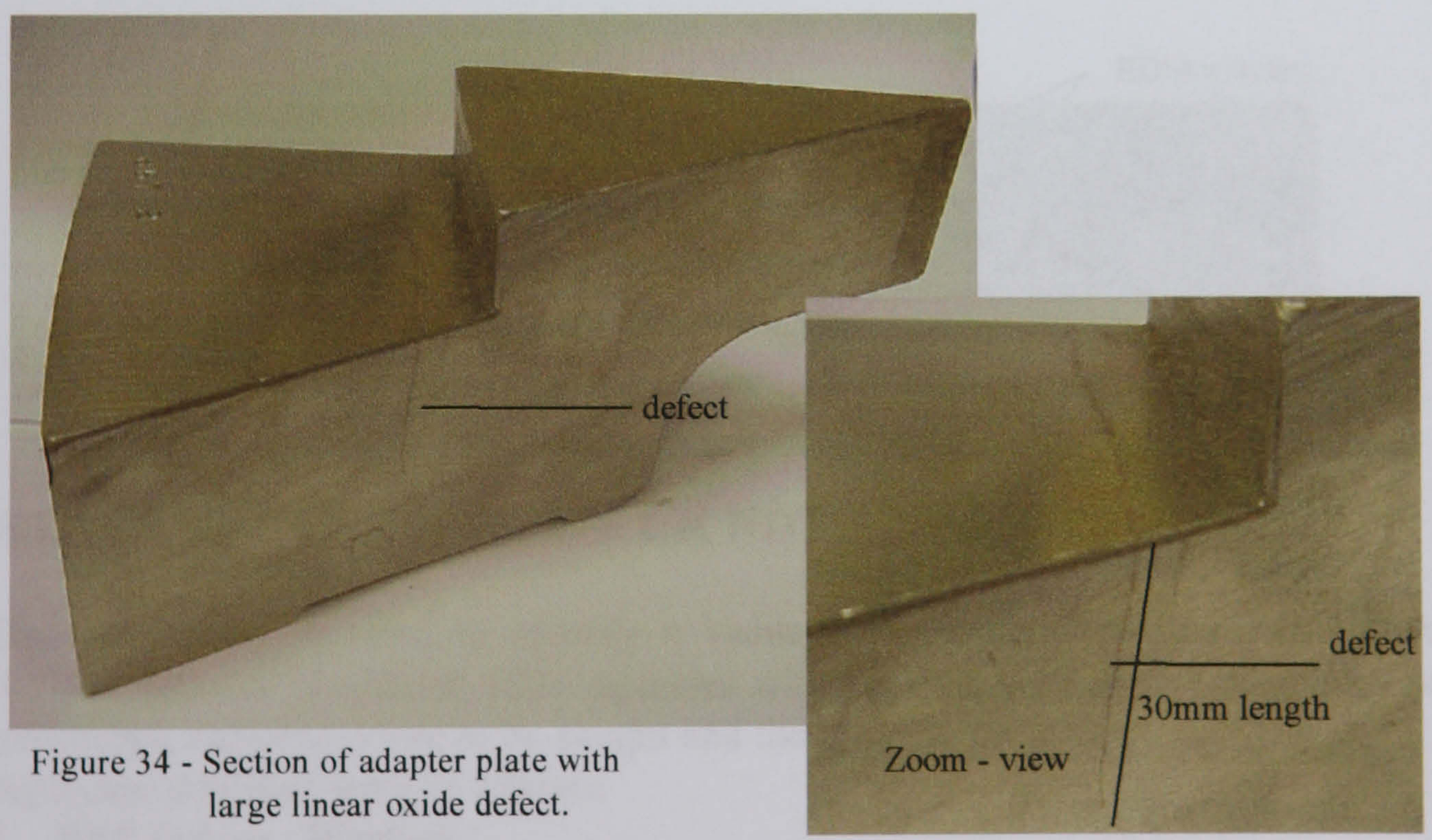

Figure 34 - Section of adapter plate with large linear oxide defect.

Investigations by the MOD agencies to date had demonstrated that cast CuNiCr is very difficult material to examine ultrasonically.

The coarse anisotropic structure [see Figure 35, 36 & 37], results in high attenuation, scattering and low signal to noise ratios and in some cases giving total loss of backwall and high levels of unwanted signals. Macro examination showed that the grain structure varied considerably from one section of cast material to another. Grain size of 2.0 to 3.0mm equi-axed to 12.0mm columnar structures were present in the same casting was not uncommon, see Figure 37.

Radiographic evaluations to date have only dealt with normal volumetric discontinuities. No effect or techniques have been devised to locate these particular oxide inclusions.

Figure 35 - Coarse grain structure - section of adapter plate.(X1.5)

Figure 36 - Coarse grain structure - section of adapter plate adjacent . (X1.5)

Figure 37 - Anisotropic grain structure (X 1)

4.1 Consultation with Various UK NDT Agencies

Due to the urgent need to identify a viable inspection system for examining this difficult material prominent NDT agencies with experience or involvement with such anisotropic material where to be sought and the problem presented.
Agencies identified were as follows:

1. BNF Fulmer : Wantage
2. AEA Harwell : Didcot
3. Rolls Royce & Associates : Derby
4. Babcock Energy Ltd. : Renfrew

5. Sonomatic : Warrington
6. Wells Krautkramer : Coventry
7. R.T.D. (UK) Ltd. : Bristol

All but two companies agreed to look at the samples.
Sonomatic and Rolls Royce Associates were unable to assist due to lack of experience with such cast materials or materials of similar characteristics. Two additional companies Rolls Royce, Bristol and V.S.E.L. were contacted to replace the ones that declined.

From the visits, discussions and brief experimentation with the samples provided, it was evident that no NDT method, technique or equipment is currently available for the detection of oxide network type discontinuities in cast CuNiCr material covering the thickness range of 15mm to 100mm. The agencies in the main for subsurface defects favoured the use of ultrasonics and application of derivative UT techniques already available, and if possible further development of this NDT discipline.
Eddy Current examination for surface flaw detection was briefly discussed by some agencies, but no concrete Eddy Current technique or proposal was put forward. Low frequency Eddy Current inspection for 10-12 mm below the surface was put forward by N.N.D.T.C. Harwell as possible development projects. Other ultrasonic methods offered for development were as follows:

1. Scanning Acoustic Microscope
2. Split Spectrum Processing Method
3. Signal Averaging for Ultrasonics
4. Spatial Averaging Technique
5. T.O.F.D.

It was clear the approach by all the agencies was not going to produce a suitable and practical solution to this now serious problem without significant research and development and even then the method developed may not be practical.

Using the samples provided to the agencies the author independently evaluated the application of Eddy Current, using readily available equipment and probes. From our experience with difficult materials and knowing the nature of the discontinuities sought that two areas need separate consideration;

1. Surface Flaw Detection

2. Sub-surface Flaw detection

4.2 Surface Flaw Detection

The importance of surface flaw detection is recognized by the M.O.D., thus the requirements in NES 824 for dye penetrant examination of as cast and machined surfaces. Since the detection of oxide inclusion networks was reported to be difficult, if not impossible, by dye penetrant inspection, it was important to establish another

NDT method for reliable surface flaw detection. As the material is non-ferromagnetic then Eddy Current inspection should meet the requirements.

Initial trials demonstrated ease of oxide discontinuity detectability even on rough surfaces. A good separation of signals were obtained from the discontinuities and other parameters effecting Eddy Current inspection in such materials. With some additional work, Eddy Current inspection can be developed to satisfy the requirements of NES 824 for surface flaw detection.

4.3 Sub-surface Flaw Detection

Low frequency Eddy Current work could possibly yield useful results for limited sub-surface inspection. Initial trials showed some promise with detections at 4mm below the inspection surface. It was considered that with suitable development of probes and specific techniques greater penetration could be achieved and sensible results for oxide network detection could be obtained.

Sub-surface inspection beyond the capabilities of eddy current inspection will still need to be addressed. Here two avenues would be worthy of consideration, representing the most cost affective means of determining the feasibility of such inspections:

4.3.1 Radiography

It is the author's opinion that further trials with radiography should be considered, optimizing existing radiographic techniques for thicker castings and evaluating the use of x-ray radiography instead of Gamma Ray radiography for casting thickness up to 60mm.

Considering the linear attenuation coefficient and mass attenuation coefficient for the CuNiCr material and those for the discontinuity sought and all other things being equal, our brief calculations indicate a linear oxide inclusion of length 10% or more of the casting thickness at point of testing, using a good technique, should be detectable.

X-ray or Gamma Ray Absorption Calculations [17]

The absorption of an X-ray or Gamma Ray beam passing through matter (and the beam's resulting attenuation) is the consequence of a series of single events; during each event a photon is removed from the beam after interaction with a nucleus or an orbital electron in the absorbing elements. The total probability (per atom) for scattering or absorption of a photon of the original energy is given by a proportionality constant,σ. This is often referred to as the cross-section because it has the dimensions of an area.

The total attenuation coefficient is the sum of the attenuation coefficient due to scattering, the photoelectric effect, and pair production. The photoelectric effect is that process in which a photon transfers its total energy to an electron in some shell of an atom. It is most significant at lower photon energies. As photon energy increases,

scattering becomes the main process contributing to attenuation. Very high energy photons are absorbed by pair production, in which a photon is converted into an electron and a positron. This process occurs in the electrical field of a nucleus and requires a minimum photon energy of 1.02 MeV.

The total attenuation coefficient can be expressed in three different forms:

The ***atomic attenuation coefficient*** measures the probability of absorption, per atom of absorbing material, in barns [one barn is equivalent to 10^{-28} m^2 or 10^{-24} cm^2 .]

The ***mass attenuation coefficient*** measures the probability of absorption per gram of absorbing material in a square centimeter of the beam.

The ***linear attenuation coefficient*** measures the probability of absorption per centimeter of the absorbing material's thickness.

Linear Attenuation Coefficient

The linear attenuation coefficient μ, can be expressed as:

$$\mu = (\mu / \rho) \times \rho$$

where (μ / ρ) is the mass attenuation coefficient, and ρ is the density of the absorbing material. The linear attenuation coefficient has a dimension of cm^{-1}

E.G. The linear attenuation coefficient of water, for example, is:

$0.0705 \text{ X } 1 = 0.0705 \text{ cm}^{-1}$

Where; 1 is the density (ρ), in grams per cubic centimeter at standard temperature and pressure; 0.0705 is the mass attenuation coefficient (μ / ρ) for water.

Mass Attenuation Coefficient

The mass attenuation coefficient (μ / ρ) of a compound or mixture is the sum of the mass attenuation coefficient of the constituent elements, weighted in proportion to their relative abundance (R).

$$(\mu / \rho)_{total} = (\mu / \rho_a)R_a + (\mu / \rho_b)R_b + \ldots\ldots$$

e.g. the mass attenuation coefficient at say 0.02 MeV for air (a mixture), which consists in percentage [by weight] primarily of N_2 (75.6%), O_2 (23.1%) and A (1.3%). The mass attenuation coefficient are: Nitrogen, 0.598 g/cm^2; oxygen, 0.840 g/cm^2; and argon, 8,87 g/cm^2. Therefore the total mass attenuation coefficient for air at 0.02 MeV is:

$\mu / \rho_{air} = (0.598 \text{ X } 0.756) + (0.840 \text{ X } 0.231) + (8.87 \text{ X } 0.013) = 0.761 \text{ g/cm}^2$

The *linear attenuation coefficient* for CuNiCr material to NES 824 is calculated as follows:

The linear attention coefficient μ_{CuNiCr}, can be expressed as:

$$\mu_{CuNiCr} = (\mu/\rho)_{CuNiCr} \times \rho_{CuNiCr}$$

First we calculate the mass attenuation coefficient for the alloy;

$$(\mu/\rho)_{CuNiCr} = (\mu/\rho_{Cu})\,R_{Cu} + (\mu/\rho_{Ni})\,R_{Ni} + (\mu/\rho_{Cr})\,R_{Cr} + (\mu/\rho_{Fe})\,R_{Fe} + (\mu/\rho_{Ti})\,R_{Ti} + (\mu/\rho_{Zr})\,R_{Zr} + (\mu/\rho_{Mn})\,R_{Mn} + (\mu/\rho_{Si})\,R_{Si}$$

Mass attenuation coefficient (μ/ρ) for the various main elements for the CuNiCr alloy at a specific photon energy [0.5 MeV] are as follow;

Copper (atomic wt.63.54) = 0.0834
Nickel (atomic wt.58.69) = 0.0869
Chromium (atomic wt.52.01) = 0.0827
Iron (atomic wt.55.85) = 0.0841
Titanium (atomic wt.47.90) = 0.0818
Manganese (atomic wt.54.93) = 0.0818
Zirconium (atomic wt.91.22) = 0.0859
Silicon (atomic wt.28.09) = 0.0873

$$(\mu/\rho)_{CuNiCr} = 0.0834 \times 0.656 + 0.0869 \times 0.305 + 0.0827 \times 0.018 + 0.0841 \times 0.0075 + 0.0818 \times 0.0020 + 0.0859 \times 0.0010 + 0.0818 \times 0.0075 + 0.0873 \times 0.0030$$

$(\mu/\rho)_{CuNiCr}$ = 0 0844 gms/cm^2

ρ_{CuNiCr} = 8.8 gms/cm^3

Linear Attenuation Coefficient = μ_{CuNiCr} = **0.0844 X 8.8 = <u>0.743 cm^{-1}</u>**

The oxide networks have been analysed as predominantly being Zi [Zirconium]. Ti [Titanium] or Si [Silicon]

Linear attenuation coefficients for the Oxide networks based at 0.5MeV are as follows:

Zirconium oxide =0.561 **cm^{-1}**
Titanium oxide =0.371 **cm^{-1}**
Silicon oxide =0.205 **cm^{-1}**

The linear attenuation coefficient for the major constituents for the oxide networks to that of the alloy differ sufficiently to give a radiographic image of the defect sought when radiographic inspection techniques are used. However this only applies if the main beam of radiation is parallel to the defect direction.

4.3.2 Ultrasonics

As already discussed, ultrasonic inspection is difficult if not impossible. The material not only contains coarse grain and anisotropic structure giving high attenuation, scatter and low signal to noise ratio, it is also possible that as the large grains exhibit a substantial degree of grain alignment, which can cause an anomalous form of refraction which has become known as "skewing"

For ultrasonic inspection of such a difficult material, a number of technique development have been proposed to possibly alleviate the inspection problems.

Before the merits of each proposal should be considered, it is my view that a systematic investigation into the ultrasonic properties of cast CuNiCr material be carried out.

The inspection problems of CuNiCr material appear consistent with those exhibited by austenitic welds and casting, which originally were considered generally to be uninspectable by ultrasonics. These materials also contain coarse, anisotropic grain structure with high effective attenuation and poor inspectability, an area in which Babcock Technology Centre have extensive experience. Babcock were therefore requested to undertake a systematic investigation of the attenuation, noise and beam skewing levels within the material and to correlate these effects to the microstructure. This was considered the most effective way of determining whether improvements in ultrasonic capability was a realistic proposition and if so what the basis of improved ultrasonic technique might be.

Past studies on austenitic materials have been successful in leading to a greatly improved understanding of how ultrasonic properties are related to the micro - structure and how to minimize the various adverse effects by appropriate choice of technique and equipment.

The study by Babcock on Cu-Ni-Cr materials concluded that the microstructure in the main from the three test specimen examined was generally equiaxed grains of uniform size interspersed with areas of columnar grain structure. The Cu-Ni-Cr alloy has locally highly variable attenuation for 2MHz frequency ultrasonic beams. This variability is lessened by the use of 1MHz frequency beams. The material structure is such that the ultrasonic beams are diverted from their true angle, which apparently increases with increasing range for the 45° 2Mhz probe and decreases for the 45° 1 MHz probe. The 2 MHz 60° probe did not conclusively show any consistent distortion.
The optimised probes for austenitic weld and casting inspection were anticipated to be best. However, the overall sensitivity using these existing probes was considered likely to fall some way short of that required, even for fully optimised procedures

Summary of the report issued by Babcock Technology Centre [E/92/043] on measurements made to assess attenuation, scattering, and beam distortion is attached in appendix 1.

4.4 Conclusions

From the visits, discussions and appropriate experimentation with the samples provided, it is evident that no NDT method, technique or equipment is currently available for the detection of oxide inclusion network type discontinuities in cast CuNiCr material, covering the thickness range of 15mm to 105mm.

In light of the initial success of the Eddy Currents for both surface and limited sub-surface detection it was appropriate that steps be taken to:

1. Develop a reliable Eddy Current inspection method of surface breaking oxide discontinuities on both machined and as cast surface conditions.
2. Develop a reliable Eddy Current inspection method for detection and if possible identification of Sub-surface oxide networks. Reliability trials with sectioning and defect confirmation to form part of this work. It was agreed also that sub-surface detection technique should provide at least 10mm of inspectable depth.

Radiographic techniques for sub-surface inspection would provide good results provided the linear oxide networks were in the same direction as the radiation beam impinging on the sample. As the direction and orientation of the oxide defects is unknown then the feasibility of Radiography being an effective and practical method of inspection becomes unreliable.

Ultrasonic inspection of this material is known to be problematic, with high effective attenuation and after the extensive study by Babcock Technology Centre for material characterization and probe optimisation the method still appears to be poor for defect detection capability.

5.0 DEVELOPMENT OF SURFACE AND SUB-SURFACE EDDY CURRENT TECHNIQUES

A number of esoteric techniques such as scanning acoustic microscopy were considered but reserved for further investigation only if no more accessible method was developed. The approach used was to separate the problems of detecting surface defects and sub-surface defects separately. While both penetrant testing and radiography had been used with disappointing results they were re-investigated and some trials were made with ultrasonic techniques. None of these offered a reliable or practical solution to the problem.

While the nature of cast materials does not generally favour the use of eddy current testing this was found to give excellent results in the present case. The favourable initial results lead to the development of two specific procedures, the one for detecting surface defects and the other for indicating sub-surface problems.

5.1 Experimental Procedures

PROCEDURE FOR DETECTING SURFACE DISCONTINUITIES

An impedance eddy current flaw detector with selectable frequencies of 2 MHz and 4 MHz. was used in conjunction with shielded austenitic probes. A pencil type and angle tip probe, were sufficient to cover the verity of curvatures presented by casting to be inspected. See appendix 2 for details on equipment

Prior to manual scanning the instrument was calibrated on a test block of the CuNiCr alloy with slots of 1, 2, 3, and 4-6 mm. depth; the slots are nominally 0.25 mm. wide. Part of the block's surface was in the "as cast" state and part machined in order to allow appropriate calibration. Calibration was to 0.1 of the thickness of the component to be tested; this was achieved by selection of the appropriate slot in the block.

All surfaces examined were clean, dry, and free of loose scale or other debris.

Manual scanning was carried out after zero compensation at several positions with a scan pitch of 2 mm, and the, entire area under investigation subjected to at least two scans at 90° to each other. All edges were scanned individually with the help of an edge support to maintain the angle of the probe with respect to the surface after zero compensation with the probe placed at the edge.
The procedure that was produced is shown in Appendix 3

PROCEDURE FOR TESTING FOR SUB-SURFACE DISCONTINUITIES (To a Depth of 10 mm)

A phase analysis eddy current flaw detector with the capability to work at a frequency of 2 KHz was used with a specific probe having a working frequency range of 100Hz to 100 KHz.

The choice and characteristics of the probe were crucial in that subsurface eddy current densities had to be sufficient to give detections at depths of 10mm. Probe design and selection is a blend of theory and experience and after much experimentation a probe

with low frequency characteristic having separate sensing (pick-up) and excitation (driver) coils was observed to give the best results. The sensing coil near the test piece detects the eddy current field reflected from it, whilst the eddy currents are created by a driver coil situated around or near the sensing coil [Figure 38]. The performance of this type of low frequency probe was further enhanced by utilising a ferrite core material to provide a focused magnetic field, thus improving the penetration characteristics through the material. The probe is absolute in effect but has built-in balance coils and can be connected directly to differential input instruments.

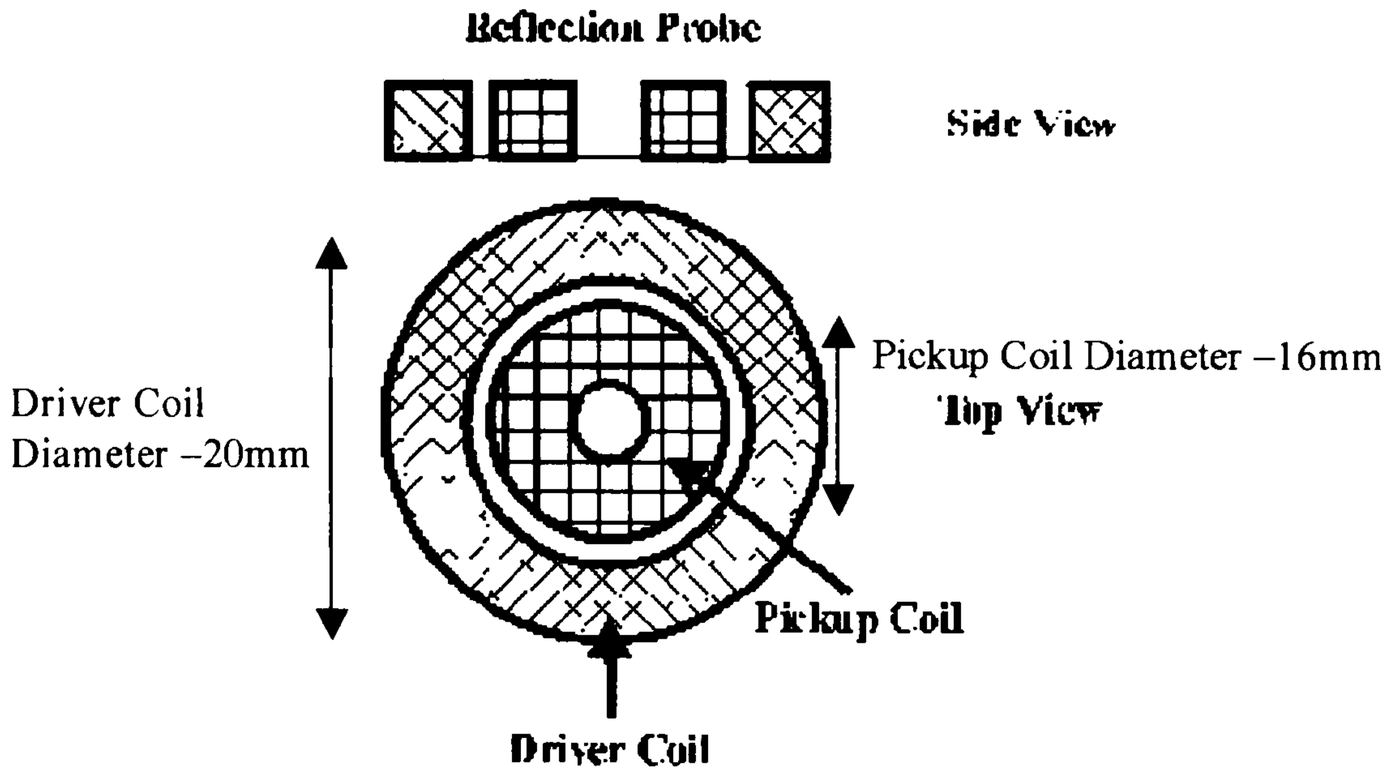

Figure 38 – Typical coil arrangement for reflection probe

A typical reflection probes arrangement used contained one set of coils [150 turns, each of SWG42 copper wire 20mm diameter], which generates the primary field and a second set [150 turns, each of SWG42 copper wire 16mm diameter], which senses the response in the test piece. The exact design details are contained in the Ministry of Defence report " Surface and Sub-Surface Eddy Current Examination of NES 824 material" report: BAeSema M1247/93/C3404/2.

Scanning speeds for both calibration and inspection must remain essentially the same in order to avoid variation in the signal amplitudes. Prior to manual scanning the equipment was calibrated on a suitable test block manufactured from the copper/nickel/chromium alloy away from any edges so that the zero position was in the centre of the screen, the phase was adjusted so that the spot moved horizontally to the left and eventually off the screen on lift off. The equipment was calibrated separately for testing edges.

100% of all areas of interest were scanned with two passes the one being at 90° to the other away from edges; edges were scanned smoothly using an edge support in order to maintain constant angle and distance.

The procedure produced is shown in Appendix 4

5.2 Results

Fifty five castings of variable size and complexity of shape were inspected for both surface and sub-surface defects in four stages which were considered to be in increasing practical difficulty. The masses of the castings ranged from between 1 and 2 kilogram to approximately 1000 kilogram. Figure 39 shows two typical casting subjected to eddy current inspection.

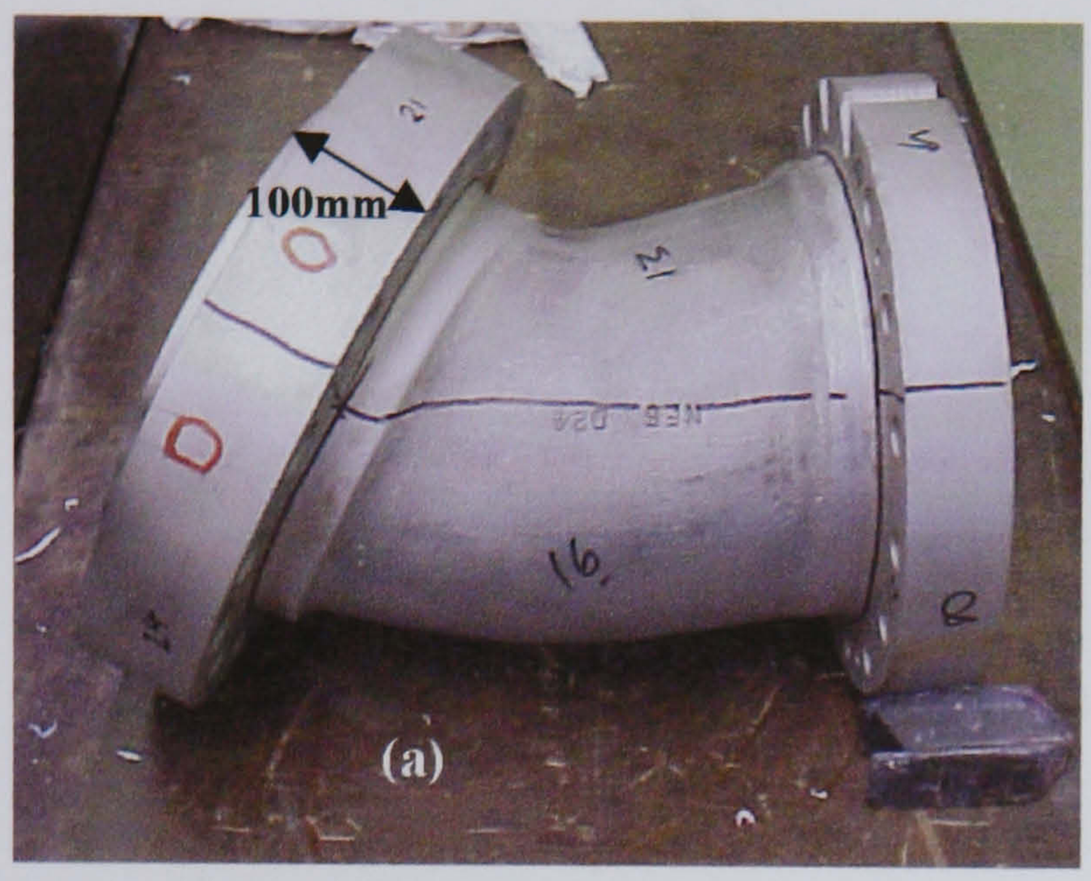

Figure 39 (a) – Large Cast Bend (b) Smaller Cast Elbow

In total 305 defect indications were reported, 156 being surface indications and 149 sub-surfaces. The number of indications per test component ranged from none to twenty for surface indications and from none to sixteen for the sub-surface problems. The extent of the indications ranged from 1 to 340mm. length for surface indications and areas from 2 x 2 mm to 98 x 300 mm. for sub-surface effects. Some sub-surface indications were found to be present over the entire surface inspected. These results are summarised in table 4.

TABLE 4. SUMMARY OF THE RESULTS OF SCANNING 55 CAST COMPONENTS IN COPPER/NICKEL/CHROMIUM ALLOY

	Surface indications	**Sub-surface indications**
Total number	156	149
Range of number of defects per casting.	0 to 20	0 to 16
Extent of indications	0 to 30 mm.	2 x 2 mm. to 98 x 300 mm

Nine castings were further investigated destructively and some of the discontinuities detected identified; these were found to be either shrinkage/micro-shrinkage or oxide networks which ranged from being very fine to extensive and coarse.

The characteristics of the plots for sub-surface discontinuities were found to follow a clear pattern; indications of shrinkage and micro-shrinkage were seen to be regular with high amplitude resembling a classical Lissajous diagram as is shown in figure 40.

Where oxide networks existed the plot was seen to be irregular with much reduced amplitude as is seen in figure 41.

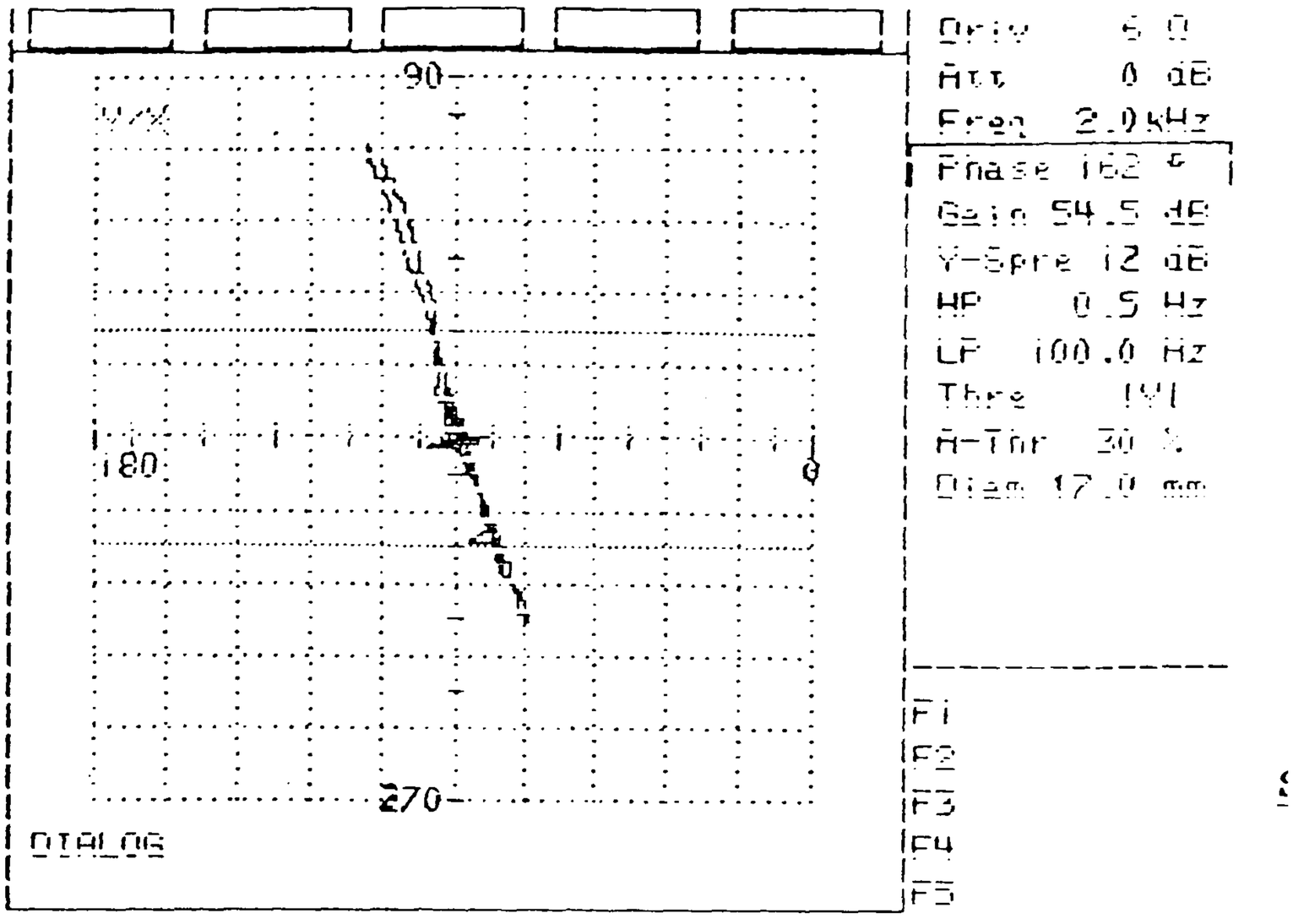

Figure 40 – Eddy current signature[X/Y] from shrinkage defect in the casting

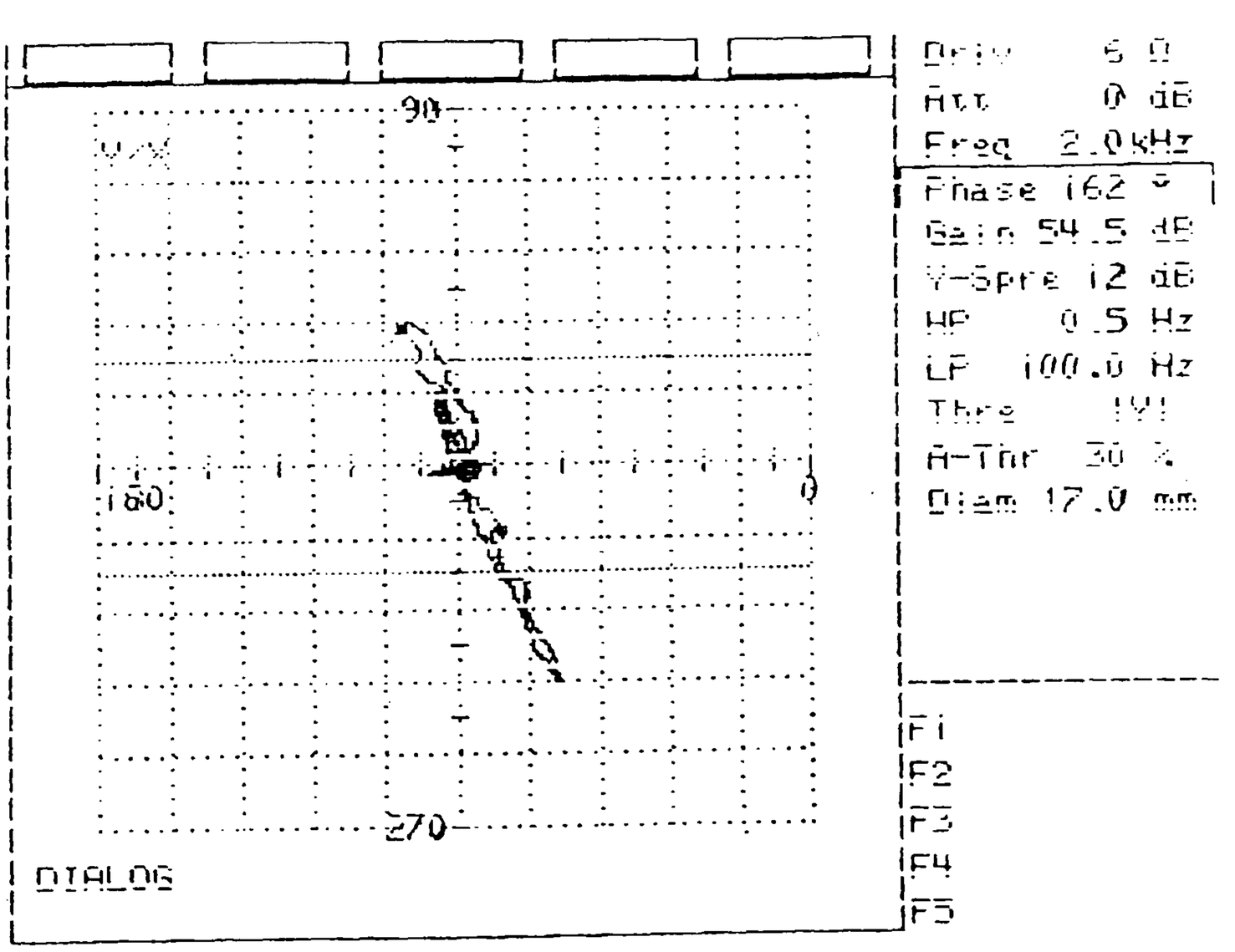

Figure 41 – Eddy current signature[X/Y] from oxide network present in the casting

Figure 42.shows a further plot with a different characteristic shape from either of the previous cases and this was ascribed to the presence of traces of material having very high magnetic susceptibility.

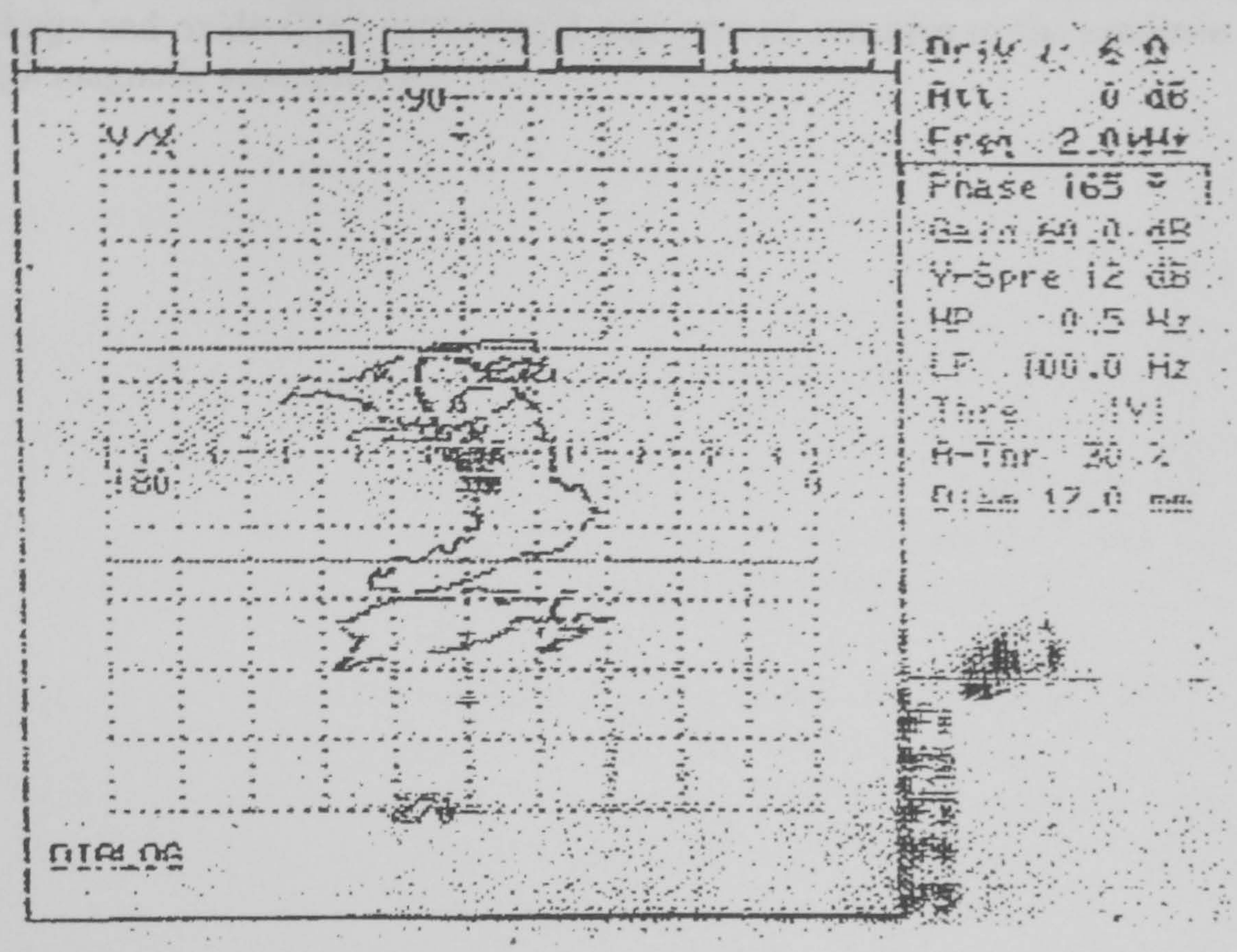

Figure 42 – Eddy current signature[X/Y] indicating the presence of a contaminant having magnetic permeability

These results were obtained by reporting all indications from both procedures, surface and sub- surface indications. If the eventual quality acceptance standard were to use this as its acceptance level only 23.6% of the sample of 55 castings would be acceptable with 50% showing surface discontinuities and 59.2% sub-surface discontinuities.

Discontinuities occur in castings normally and the presence of some must be accepted and levels of acceptance must be set and applied. The tests were repeated after setting the gates of the equipment to ignore discontinuities typified by first a slot of 0.5 mm. depth for the surface detection and 12 x 0.25mm area and 5.00 mm deep artificial defect through a 6 mm. coupon for the sub-surface examination. This improved the acceptance level to 29.1 % overall with 61.2% passing the test for surface discontinuities and 50% the subsurface limit for size of discontinuities. By increasing the thresholds to a 1.0 mm. depth for surface discontinuities and calibrating through a 12 mm. coupon for sub-surface discontinuities the overall acceptance level rose sharply to 71.7% with the acceptance levels for surface detection rising to 89.8% and to 73.9% for the sub-surface testing.

5.3 Conclusion

A reliable, if unusual, method was achieved for the testing of cast components in the alloy of CuNiCr by use of established equipment, which is widely available with specifically enhanced probes. The method was shown to allow discrimination between shrinkage and oxide filled networks; it also proved sensitive to the presence of material of high magnetic susceptibility.

6.0 STUDY 2 - INSPECTION OF PHASE SELECTIVE CORROSION IN NICKEL ALUMINIUM BRONZE

6.1 Introduction

Nickel aluminium bronze (NAB) castings are extensively used in submarine sea water systems and as they are subjected to full diving pressure a high standard of integrity is required. After about six years operational use it became evident that these castings were prone to preferential corrosion propagating at about 1 mm/year, the attack initiating at crevices and weld heat affected zones. The first most serious case occurred in large castings exhibiting dealloying to a depth of approximately 6mm (1/4 in.).

Originally such castings were manufactured to DGS Specification 8520. In view of the problem a modified specification DGS 348 was issued in July 1975 to conform to US Navy practice which was thought to provide immunity to preferential phase corrosion. After number of years of service, metallurgical examination of castings manufactured to DGS 348 indicated that this material would still be susceptible to some degree of preferential phase corrosion. The corrosion resistance of cast nickel-aluminium bronze in seawater thus became suspect and the Navy initiated an extensive investigation into causes and detection of selective phase corrosion of nickel-aluminum bronze castings.

Numerous nickel-aluminum bronze castings having varying lengths of seawater service were destructively examined to assess the magnitude of the corrosion problem. Nearly all the cast nickel-aluminum bronze castings exhibited selective phase corrosion to some degree as shown in figure 43 [photo 1, 2 &3]. The corrosion performance of the cast material varies depending upon the chemical composition of the individual phase present.

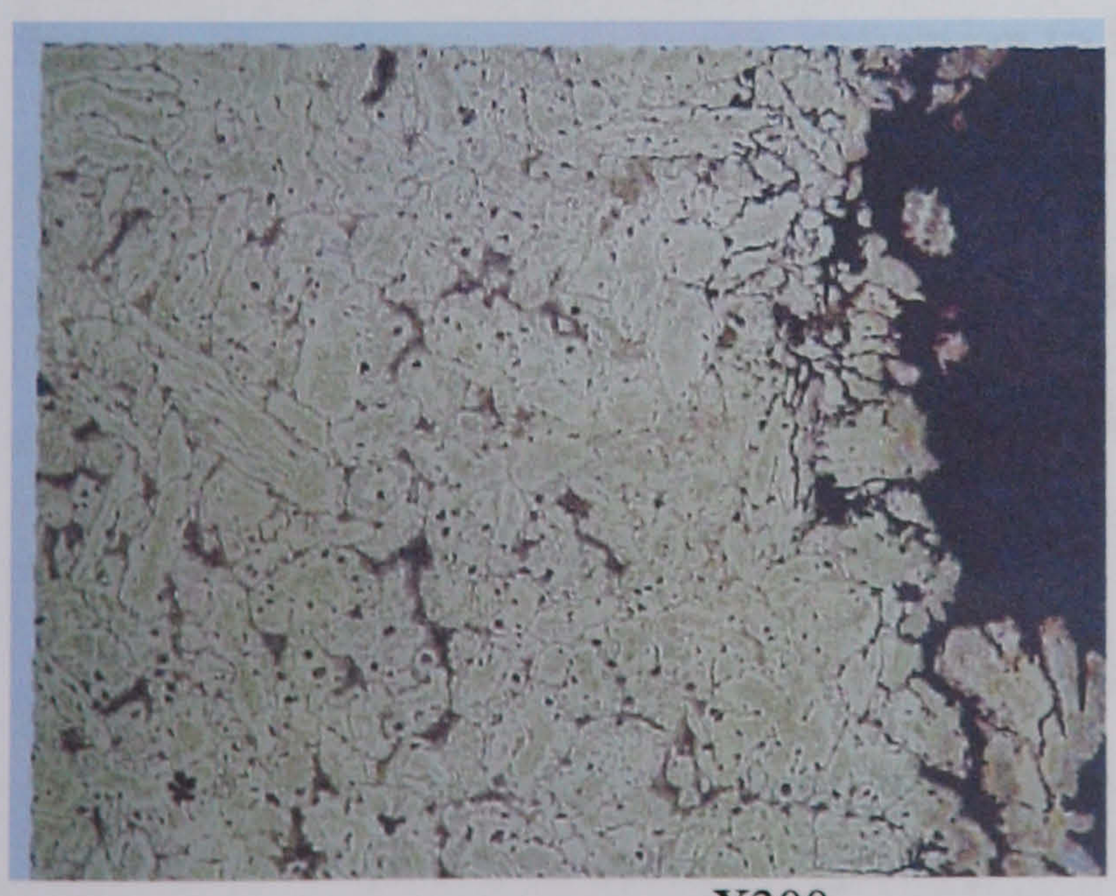

X300

Photo No.1

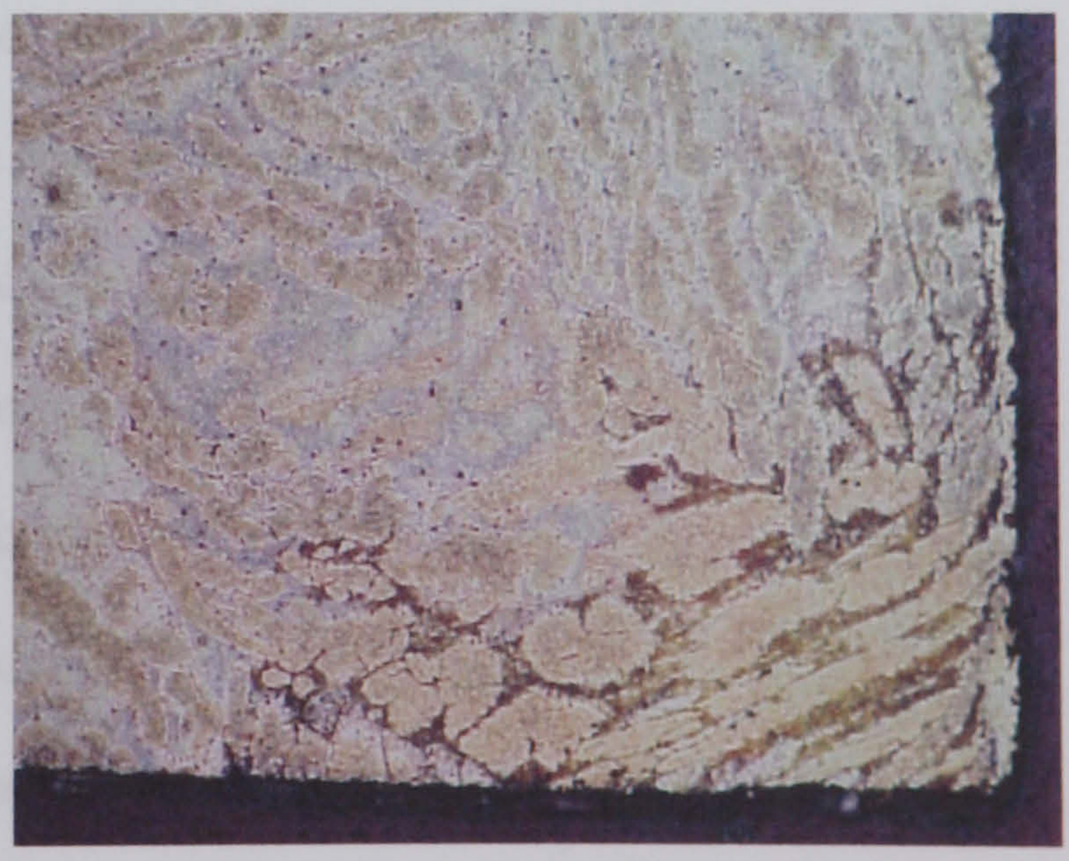

X 200

Photo No.2

Figure 43

X 50

Photo No.3

Figure 43 – Photo's 1, 2 & 3show various aspects of Phase Selective Corrosion in κ_{III}

Consequently there is a need for a non-destructive inspection (NDI) technique to validate in-service Nickel-Aluminium Bronze castings.

6.2 Objective

To investigate and experiment with new eddy current and flux-leakage detection techniques for the detection of phase selective corrosion with the ultimate aim for revalidation of NAB castings. The primary task being the ability to inspect from the remote side, thus enabling in-situ inspection to be performed

From a substantive list of work detailed the project focused on the following:

1) Preliminary evaluation by using Eddy Flux Technology

2) Magnetic property determinations and magnetic mapping

3) Design and develop probe/sensor for sub-surface detections

4) Experimentation with Maxwell equipment

5) Carry out extensive evaluation of test sample pieces as provided by DRA [Defence research agency]

The essential aim was to enable identification of corroded areas and to measure the depth of corrosion.

6.3 Nickel Aluminium Bronze

Copper and its alloys have been associated with the sea on account of their excellent corrosion-resistance and ability to with stand marine fouling. Copper-sheathed wooden ships and gunmetals for corrosion resistant castings are part of history but increased mechanization of naval ships has progressively led to demands for material of higher strength and greater resistance to higher water speeds and corrosion.
Aluminium Bronze [Cu-Al, and Cu-Al-Fe] alloys were developed in the 1950's for naval use to provide the physical properties, corrosion resistance, and the ability to be joined by fabrication processes without detriment to their corrosion properties. Seawater trials conducted in the early and mid sixties of these primarily "duplex phase" alloys identified the potentially serious corrosion problem of "de-aluminisation" or "selective phase corrosion" in cast and wrought aluminum bronze alloys being used for seawater service [18]. Dealloying was viewed as an "insidious" form of corrosion since it is primarily a sub-surface phenomena and there is usually no visible evidence of corrosion on the metal surface. Since aluminum bronze castings were being used for a variety of components in ships seawater systems including valve bodies, pump casings and rotors, the corrosion behavior of the cast alloys became of primary interest to the Royal Navy.

The tensile strength and ductility of dealloyed aluminum bronze are significantly lower than that of sound metal. Tensile tests of completely dealloyed samples of Class-2 cast aluminum bronze showed a 60 percent reduction in tensile strength and almost zero ductility [18]. Other tensile tests conducted on completely dealloyed metal of Class-3 cast aluminum bronze using sub-size flat tensile specimens showed an average reduction in tensile strength of 79 percent and less than 1 percent ductility [18].

Investigations were conducted on the effects of composition, microstructure, heat treatment and welding on the seawater corrosion behavior of cast aluminum bronze alloys [19]. While carefully controlled heat treatment of aluminum bronze alloys was shown to improve their resistance to dealloying, the variable compositions and metallurgical complexity of the cast alloys complicates the heat treatment option. Welding also negates any advantages acquired through heat treatment and leaves the weld and HAZ regions highly susceptible to dealloying. Post weld heat treatment is then required to once again restore adequate corrosion resistance.

Growing recognition during the 1960's of the benefits available through compositional adjustments that could minimize or eliminate dealloying in the duplex phase aluminum bronze alloys lead to the use of nickel-aluminum bronze (Cu-Al-Ni-Fe) alloys.

The improved dealloying resistance of nickel-aluminium bronze was observed to be strongly influenced by the nickel content. Results of two-year seawater tests indicated that

cast nickel-aluminum bronze alloys with less than 10% aluminium and containing a minimum of 4 % nickel exhibit high resistance to dealloying.

This work resulted in a shift by the Navy to the use of the more corrosion resistant nickel-aluminum bronze alloys containing a minimum of 4% nickel. While cast nickel-aluminum bronze containing a minimum of 4 % nickel offered superior dealloying resistance than cast aluminum bronze alloys, nickel-aluminum bronze as cast, still exhibited some susceptibility to dealloying especially at the high end of the permissible range for aluminum. In addition, as-welded cast nickel-aluminum bronze containing 4 percent nickel exhibited susceptibility to dealloying in the cast metal heat-affected zone (HAZ). Post-weld heat treatment of the welded nickel-aluminum bronze castings restored dealloying resistance in the cast metal HAZ.

The Nickel aluminium Bronze composition considered most was that of:

8.8 –10% Aluminium (Al)

4 –5.5% Iron (Fe)

4 –5.5% Nickel (Ni)

1.5% Maximum Manganese (Mn), [Remainder – Copper (Cu)]

The copper can be considered as the solvent, which takes up into solution a certain proportion of the other elements and this contributes to the strength of the copper.

The optimum mechanical properties of the cast Nickel-Aluminium Bronze are:

Tensile Strength = 587 N/mm^2 minimum,

0.2% proof stress = 230 N/mm^2 minimum,

Elongation = 15% as minimum

It is not intended to deal with the complexity of the metallurgy that is associated with this alloy suffice to say that up to seven separate phases based on morphology have been observed in the as cast structure.

The morphology of the microstructure identified and the nomenclature given to the various forms of precipitates of κ [Kappa] phase [See Figure 44] are as follows:

κ_I -a rosette form

κ_{II} -a spheriodised precipitate at the grain boundary

κ_{III} -a lath shaped phase

κ_{IV} -a fine precipitate within the α- grains.

The temperature for the formation of the κ phases was dependent on the composition of the alloy as indicated by the equilibrium diagrams –see figure 45. Under equilibrium conditions for the 5.0% Ni plus 5.0% Fe alloy, the κ phases nucleated at temperatures about 950°C. From electron optical microscope examination of the as-cast material the κ_{III} was based on FeAl/NiAl.

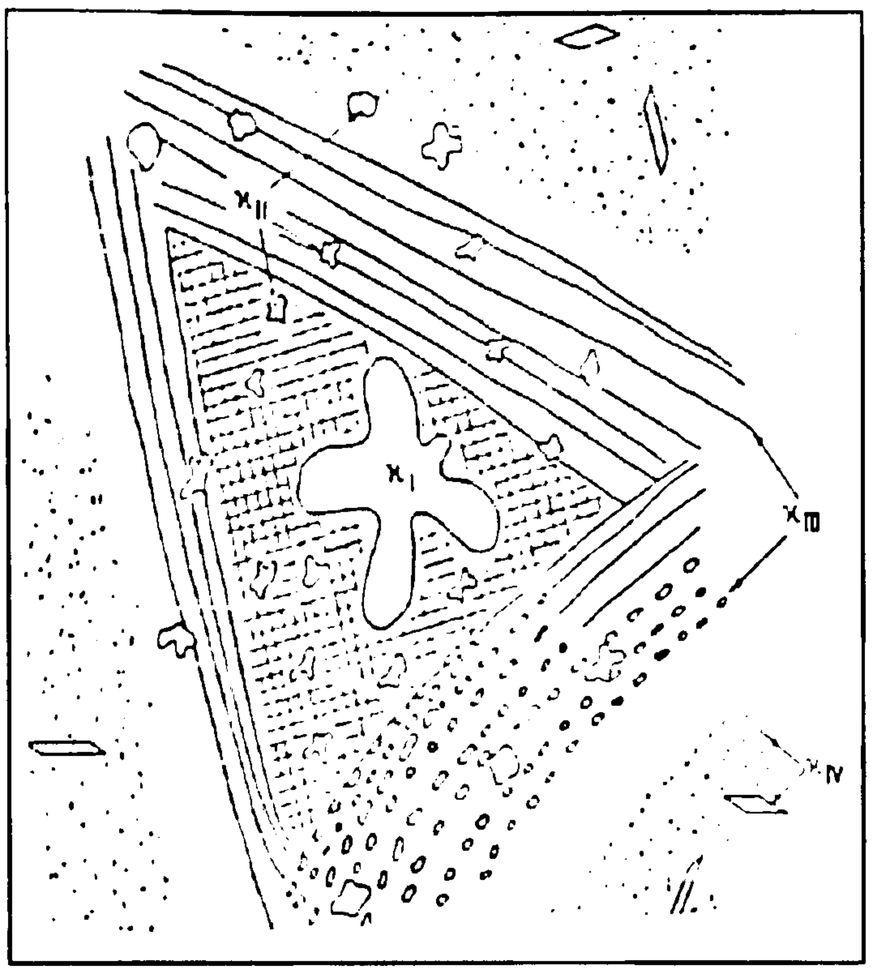

Figure 44- Different precipitate microstructures

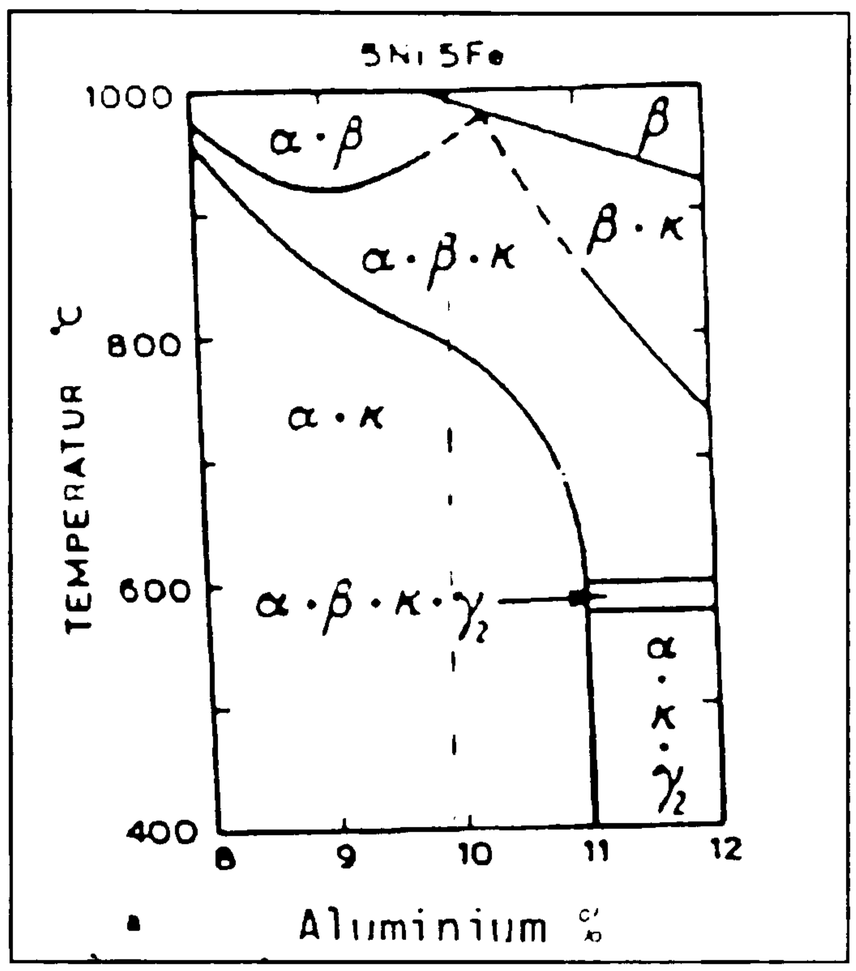

Figure 45 - Binary phase diagram of NAB

6.4 The Form and Shape of the Corrosion Defects

The problem with nickel-aluminium bronze castings is preferential phase corrosion associated with κ_{III} phase in a complex microstructure. The κ_{III} phase, which is based on a NiAl structure with copper and nickel in solution, behaves like stainless steel. In seawater under well-aerated conditions it forms a passive film and is electro-chemically nobler than the surrounding α phase, and consequently the α phase in the vicinity of the κ_{III} phase corrodes. However when there is limited availability of oxygen to passivate the κ_{III} such as in a crevice the κ_{III} becomes active and corrodes very rapidly. As the corrosion is accompanied by a re-deposition of copper the grains surrounding the corroded κ_{III} are retained in position as a spongy porous mass with little deformation or discolouration of the surface to indicate visually that corrosion has occurred. Such corrosion occurs in two forms (a) plug corrosion in the parent metal of the cast nickel-aluminium bronze and, (b) in the parent metal heat affected zone (HAZ) of a weld. The plug corrosion in parent metal nickel-aluminium bronze takes the form of a hemispherical plug around the surface of a crevice formed by debris, biofouling, or seawater filled in close fit conditions between

components. With HAZ corrosion the attack initiates in a zone 1 to 3 mm from the weld metal which, may propagate either as a wedge into the parent metal or as a narrow 2-3 mm wide plug in the parent metal running parallel to the weld. The HAZ corrosion is potentially more dangerous than parent metal plug corrosion as the former occurs around a weld, which could result in the weld metal falling out whereas the plug corrosion is more likely to be in small isolated areas. This description of the corrosion is a generalisation as many variants occur due to the complexity of the microstructure, the in-service operating conditions and component shapes.

Practically, Nickel-Aluminium Bronze castings with the required mechanical properties cannot be made without the formation of the κ_{III} phase. This phase takes the form of interwoven rods of typical dimensions 0.01 mm long and 0.0005 mm diameter. Zones of $\alpha + \kappa_{III}$ structure are randomly dispersed through the microstructure occupying about 1% of the volume.

Analysis of κ_{III} phase was obtained using an Analytical Electron Microscope on various samples from a study carried out many years ago. A series of specimens was prepared from several batches of as cast NAB. Polished cross sections were prepared by conventional metallographic techniques for examination. The results obtained were as per Table 5 below.

Table 5 **ANALYSES OF k III PHASE (WT %) using an Analytical Electron Microscope** [19]

ANALYSIS No.	Al	Si	Mn	Fe	Ni	Cu
1	7.74	0.59	2.21	26.56	33.31	29.59
2	7.73	0.29	2.35	25.96	6.38	27.29
3	9.03	0.54	2.40	20.87	40.96	26.20
4	9.06	0.71	2.31	16.73	44.19	27.00
5	7.86	0.94	2.04	22.34	36.75	30.08
6	9.19	0.69	2.27	25.52	40.39	21.94
7	8.73	0.50	2.35	28.19	41.02	19.22
8	7.72	0.39	2.21	25.47	39.13	25.08
9	3.63	2.63	3.07	72.85	7.40	10.42

10	7.52	0.35	2.49	20.64	42.89	26.12
11	7.75	0.00	2.38	19.89	39.77	30.21

The results obtained during this investigation differ significantly but the measured mean chemical composition (wt %) of the κ_{III} phase in cast nickel aluminium bronze was determined as:

Cu = 26.3 $\pm$ 3.5, Ni = 39.5 $\pm$ 3.2, Fe = 23.2 $\pm$ 3.7.
Mn = 2.3 $\pm$ 0.1, Si = 0.6 $\pm$ 0.2, Al = 8.2 $\pm$ 0.7.

A further complication for the NDT of NAB can be the presence of aluminium bronze welds used for the repair of most of the older NAB castings. Using 90/10 CuAl the welds become very susceptible to selective phase corrosion but of the $\gamma 2$ phase, which is likely to be present in the microstructure.

7.0 EVALUATIONS USING EDDY FLUX TECHNOLOGY

7.1 The Method

EDDY FLUX [Figure 46] is new Non Destructive Testing equipment supplied by Ixtrem, a company based in the heart of France working in the magnetic and electromagnetic field, using traditional magnetic examination techniques and those based on electromagnetic using the technology of multifunction probes.

In one single probe, it is possible to combine the following techniques:

- Traditional Eddy current by impedance variation.
- Eddy currents detected by magnetic field distortion.
- Flux Leakage (analysis of magnetic flux created by defects).

Figure 46 – Eddy Flux Computer based equipment

This new technology is used for both ferro-magnetic and electricity-conductive materials. Unlike standard Eddy Currents it is possible with this equipment to detect defects up to a depth of 30mm. with a signal to noise ratio better than five.

This multifunction measurement equipment provides NDT specialists with a powerful analysis capability, thus being able to perform many different types of evaluations such as; defect detection, material sorting, coating thickness, and hardness measurements.

EDDY FLUX is able to perform fine analysis of magnetic field (intensity and visualization of wave forms) and field variations in the air or at the surface of the material since its sensitivity can reach 10^{-7} Tesla.

7.2 Equipment Description

The Eddy Flux equipment consists of an industrial computer containing the necessary software, a current generator, and a series of probes, which are designed for different applications and sensitivity levels.

This equipment opens up new prospects by use of systems and software compatible with the use of a Hall type magnetic probe (probes using the Flux Leakage technique) and *or* impedance variation (probes used by Eddy Current testing). The software system allows the non-disturbance of signals by low magnetic permeability variations when using filters adapted to the speed of testing.

This unique combination of hardware, software and newly developed magnetic field measurement probes allows the test apparatus to provide a multiplicity of information

Equipment features:

1. The equipment provides two acquisition/testing modes:

- a classic mode: *without a signal demodulation, used by Leak Testing (also-called magnetography or flux leakage).*

-a demodulated mode: *a signal demodulation may be operated, which is helpful in assessing Eddy Current results.*

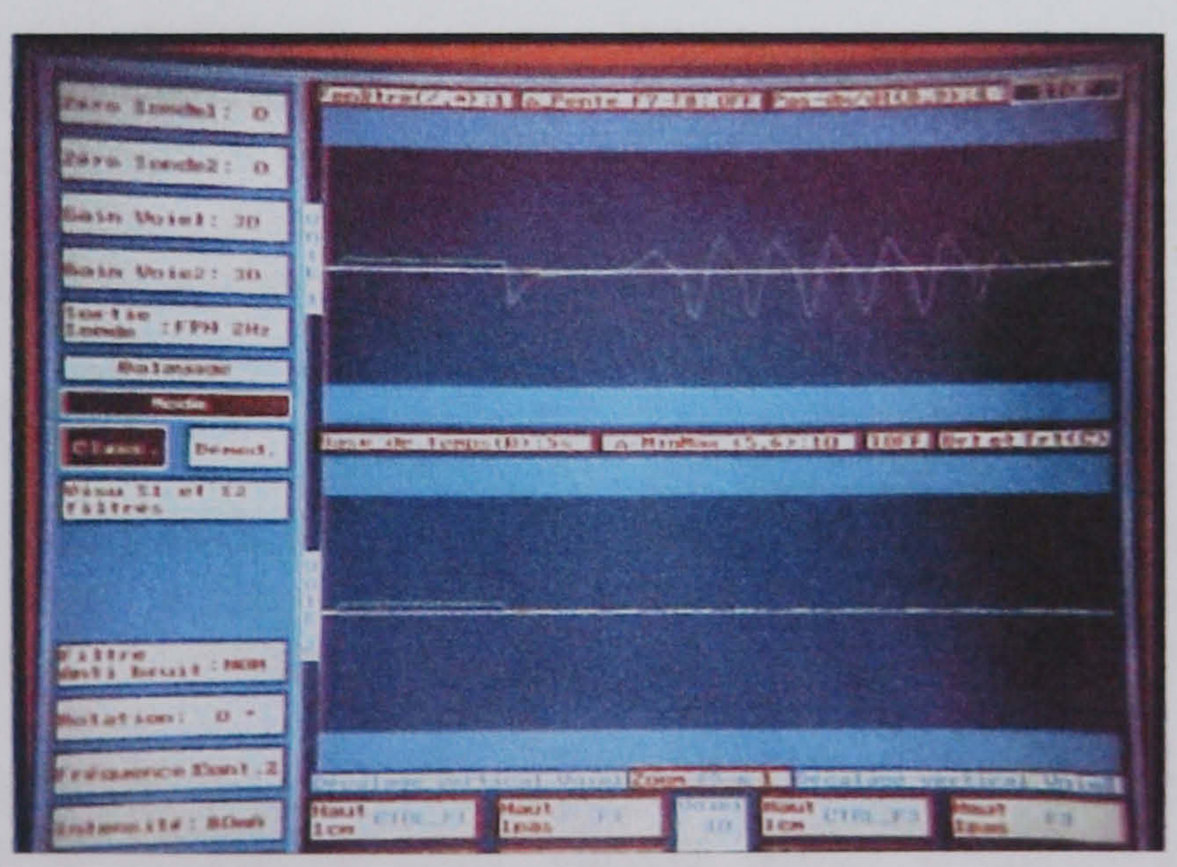

Figure 47 – Equipment -typical screen display

Several modes of signal representation are possible; be it in absolute or differential mode. with the possibility to demodulate when using a reference probe.

2. Scanning analysis according to time and the impedance plane.

3. A variable range of frequency from 25 Hz to 100 KHz.

A magnetic field measurement probe has been developed which provides high resolution and sensitivity with semi- conductive technology with a very low noise level, thus allowing magnetic field measurement down to $\mathbf{10}^{-7}$ Tesla.

7.3 Testing Modes

Flux Leakage

a) Traditional Testing –(tangential magnetic field on the test surface)
In this case, an external magnetizing source is used (not integrated in the probe), and it generally requires coils, electro-magnets, or permanent magnets. An advantage lies in having high sensitivity probes, which allow the dimensions and intensity of magnetizing sources to be consequently reduced.

b) Testing with an external magnetizing source with a magnetic field being oriented perpendicularly to the surface under test.

c) Testing with a magnetizing source integrated in the probe, with the magnetic field direction perpendicular or tangential to the testing surface.

d) Testing in Remanence
In view of the very high probe sensitivity it is possible to test using the remanent field. In this case lift-off and other interfering effects are reduced and it becomes possible for defects to be detected up to a 30 mm. depth with a signal to noise ratio better than five.

Traditional Eddy Current

The information concerning traditional Eddy current is obtained when working either with a probe that uses the same inductive coil for both detecting/excitation or where separate excitation and detection coils are present in the same sensor.

The main advantage of using the EddyFlux equipment compared to standard eddy current apparatus is the use of traditional eddy current probe configurations but with the advantage of being able to adjust the excitation current to levels much higher than normally used. The higher currents allow for greater magnetic field strength that provides

means of using the higher flux density to detect small field compression caused by discontinuities deeper in the material.

Eddy Current Detected by Magnetic Measurement Probe (MEC)

The use of magneto-resistive sensors for electromagnetic nondestructive evaluation has grown considerably in the past 10 years. Technological advances in the research and development of magneto-resistive materials has led to commercially available sensors with many qualities well suited for electromagnetic NDE. Incorporation of these sensors into electromagnetic NDE probes has widened the application range of the field. In particular, the low frequency sensitivity of the devices provides a practical means to perform electromagnetic inspections on thick-layered conducting structures.

Electromagnetic inspection of thick conducting materials requires a low frequency excitation, due to the skin depth relationship [20,21], which is given in CGS units by

$$B_z = B_o \exp(-Z/\delta),$$

$$\delta = \mathbf{c} / \sqrt{2\pi\mu_p\omega\sigma}$$

Where B_z is the magnetic field at depth z into the material under test, B_0 is the magnetic field at the surface, c is the speed of light, μ_p is the permeability, ω is the angular frequency, σ is the conductivity, and δ is the skin depth. The skin depth of a highly conducting material will be quite small unless the frequency of operation is also lowered.

An eddy current device designed for deep inspections must be sensitive to low frequency magnetic fields. Pickup coil type sensors, however, become ineffective in this frequency range due to Faraday's law of electromagnetic induction, which states;

$$\varepsilon = -\frac{A}{c}\frac{dB}{dt}\cos(\theta),$$

The electromotive force, ε, induced around a circuit is proportional to area enclosed, A, multiplied by the time rate of change of the magnetic field through the circuit. Since the output of the coil is proportional to the time rate of change of the magnetic field the effectiveness of the inspection decreases with decreasing frequency.

Magneto-resistive sensors respond to the magnitude of the external field instead of the time rate of change of the field and therefore do not lose sensitivity at low frequencies. In the absence of an applied field, the resistivity of the magneto-resistive element is high due to scattering between oppositely polarized electrons in the antiferro-magnetically coupled multi-layers of the device. An external field aligns the magnetic moments of the

ferromagnetic layers, eliminating this scattering mechanism and thereby reducing the resistivity of the material [22].

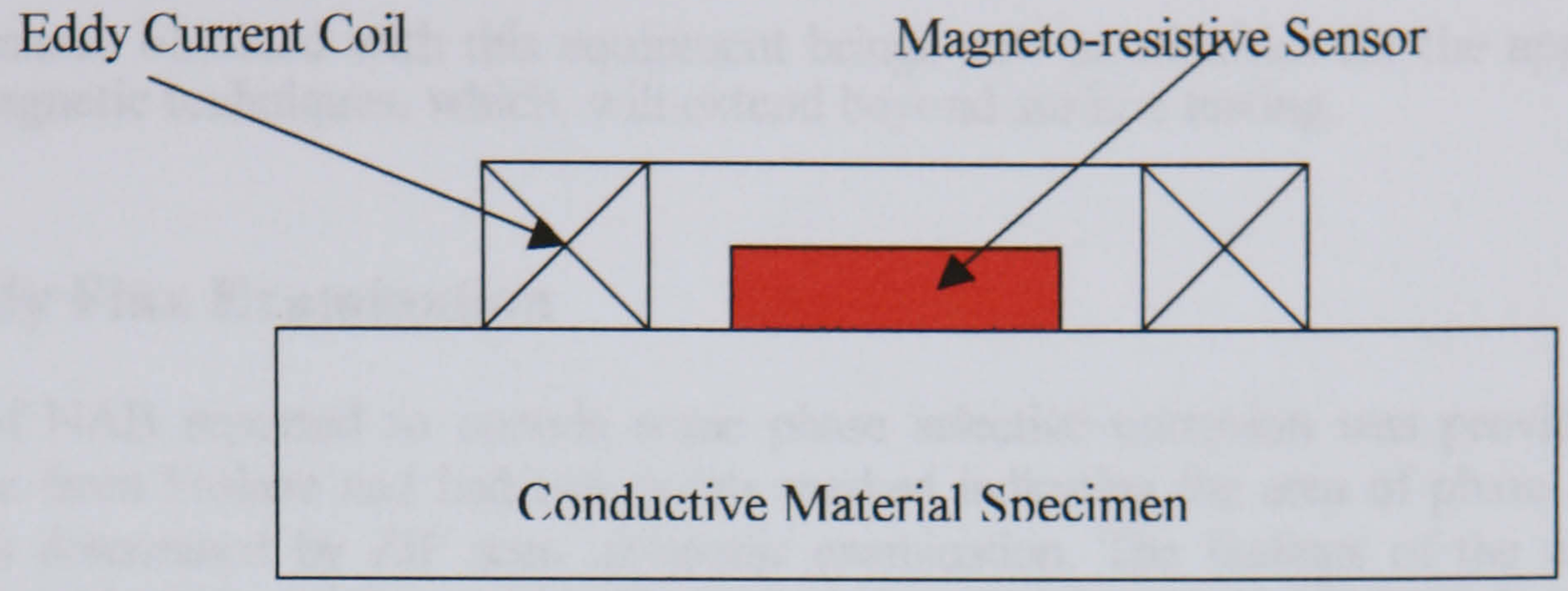

Figure 48 – A schematic of eddy current coil with magneto-resistive sensor

Most of the study focused on the use of these special sensors as the measurement of the magnetic field associated with eddy current disturbance offers various advantages in comparison with traditional Eddy Current or flux leakage techniques. The advantages offered are:

-The information given by the eddy current coil and magnetic probe are different but complementary.

-Possibility to work at a very low frequency with small magnetic probes while keeping the same signal to noise ratio (this is not the case with Eddy currents).

-The size of the probes used in MEC, that is Eddy Current with a magnetic probe as a detection means, is smaller than the size of standard coil type probes which results in better resolution.

-Whatever frequency is used, the reaction to the magnetic probe is the same (application of pulsed Eddy Current).

-Unlike traditional Eddy current, MEC method is easy to use on the surfaces of work pieces directly from a foundry or a rolling mill with little noise being generated.

The EDDY FLUX equipment opens up new prospects for the testing and examination of:

--Ferro-magnetic material by NFL or TFL independently or combined with MEC and traditional Eddy Current.

-Electrically conductive magnetic materials by MEC or pulsed MEC independently or combined with traditional Eddy Current.

The performance obtained with this equipment brings new possibilities for the application of electromagnetic techniques, which, will extend beyond surface testing.

7.4 Eddy Flux Examination

A sample of NAB reported to contain some phase selective corrosion was provided. The sample came from Faslane and had two points marked indicating the area of phase selective corrosion as determined by ZIP scan ultrasonic examination. The findings of the ultrasonic work conducted by Babcock is report " Ultrasonic scans of NAB Sample NABPC for Babcock Rosyth / MOD " are presented in Appendix 5.

The availability of this sample with "known" phase selective corrosion was only two days thus only some probe/equipment parameter changes could be evaluated.

Sample NABPC: Sample thickness 17.7mm Area of scanning 128 x 80mm

It was noted that a large weld repair was present and the reported corrosion was in close proximity to this repair. Figure 49 shows the underside of the sample [side exposed to the working fluids] and again evidence of weld repair is evident.

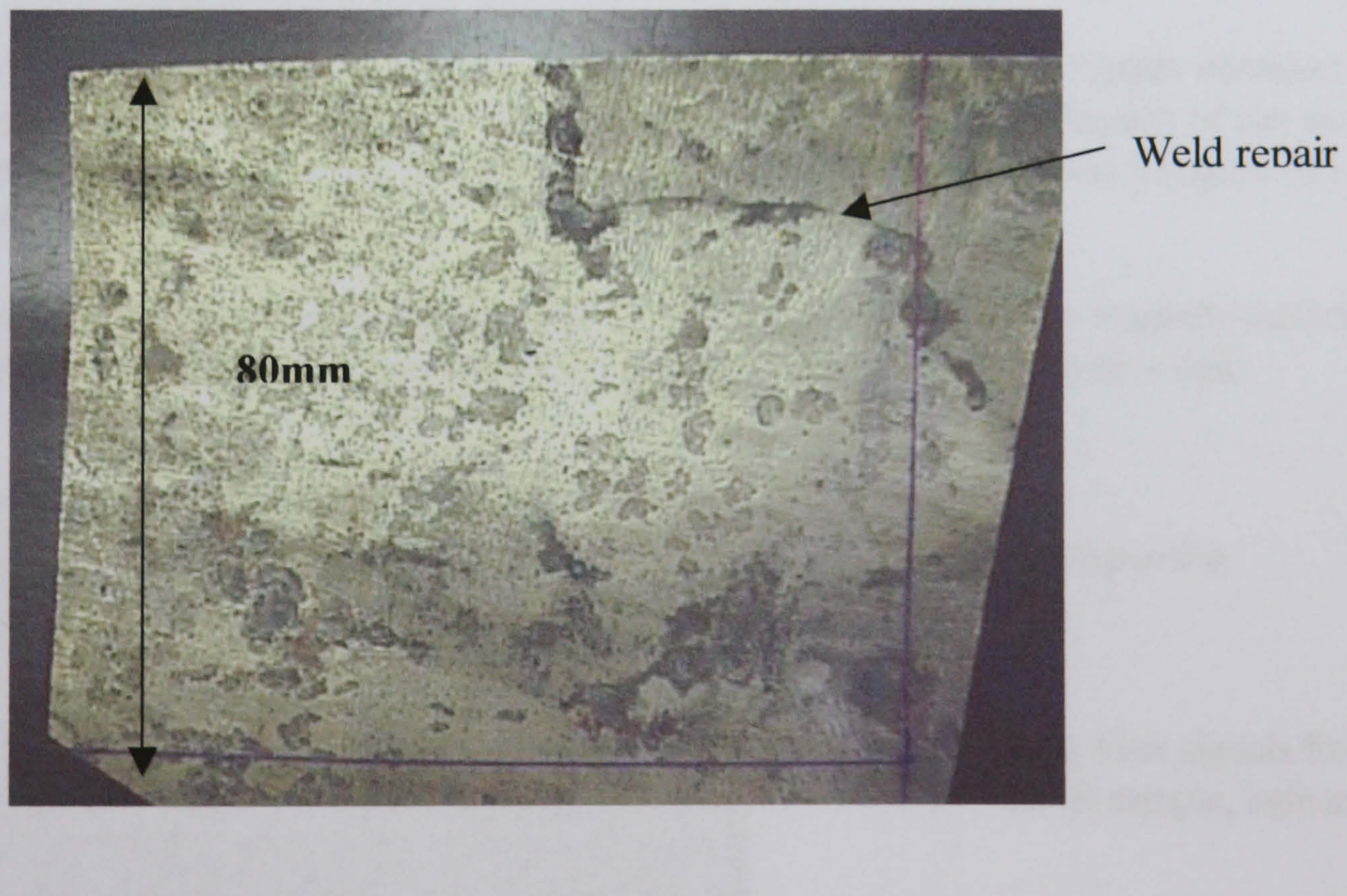

Figure 49 – Nickel-Aluminium Bronze Faslane Test Block NABPC

The first trial was conducted on the NABPC sample using the Eddy Flux equipment and a magneto-resistive probe, designation **3C001,** with what is termed as normal sensitivity of detection. The probe sensitivity is an inherent feature of the probe and influenced by its design. The**3C001** probe is of the MEC family. The complete surface of this sample was scanned using the same scanning pattern as for the ultrasonic examination.

Three areas were observed to give positive indications as illustrated follow:

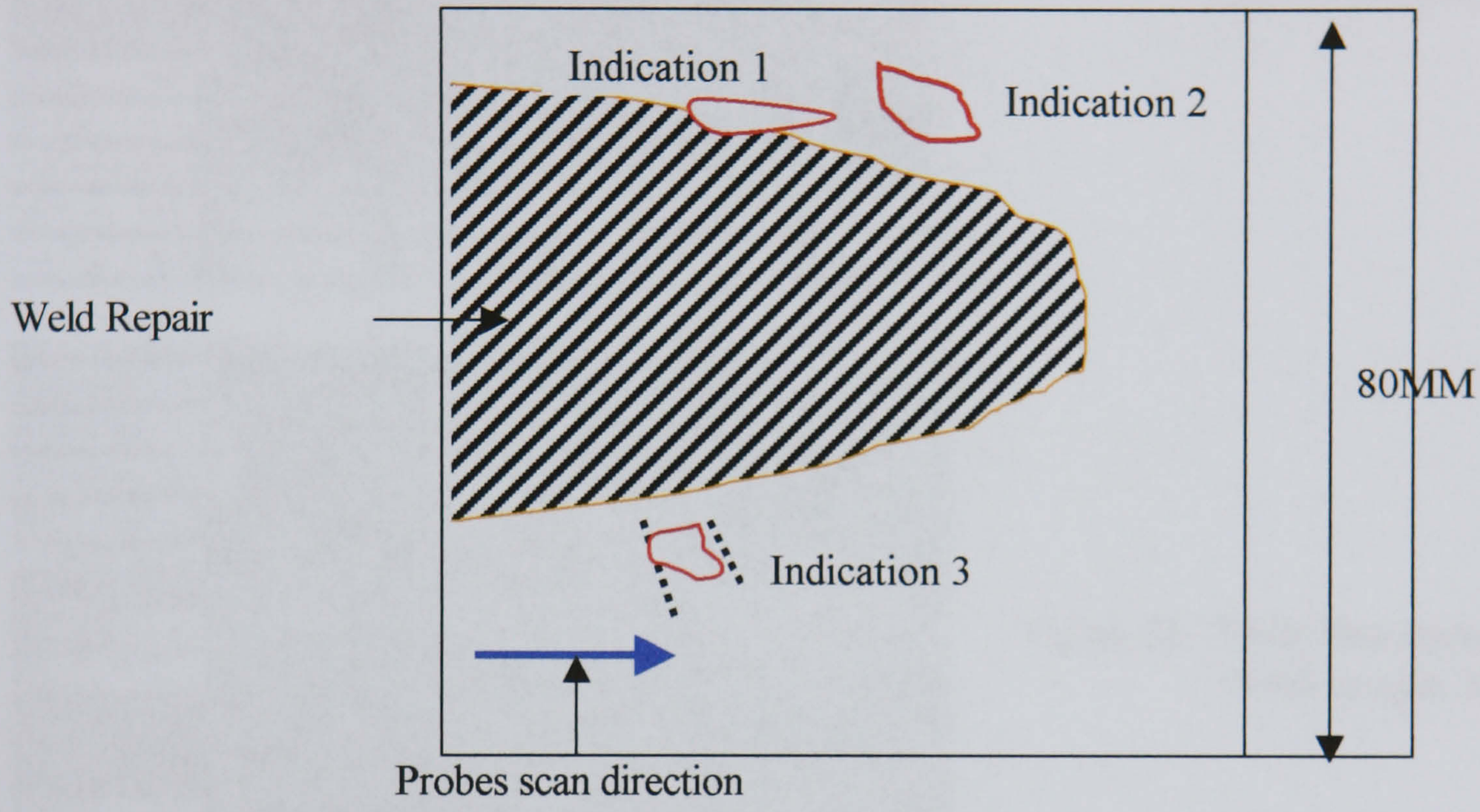

As shown Eddy Flux examination located three positions of interest. The signals obtained at each indicated area are shown in figures 50, 51 & 52. The ultrasonic examination of the same block reported positions of selective position corrosion correlating to indication 3 (figure 52) of the Eddy Flux scan.

Figure 50 shows signals from both the magnetic flux leakage detected by the magneto-resistive sensor and also the eddy current signal from the impedance change in the inductive coil.

Figure 50 –Eddy Flux signals from NAB sample, indication 1

Figure 51 –Eddy Flux signals from NAB sample, indication 2

Figure 52 – Eddy Flux signals from NAB sample, indication 3

Figure 51 shows a higher amplitude from the impedance change than a signal for flux dispersion. This could result from the presence of material conductivity change rather than, say, a discontinuity. Figure 52 shows the converse in that the impedance change signal has small amplitude compared to the flux dispersion. This is indicative of magnetic flux change from sources deep in the material. This signal seen at this location may correspond to the ultrasonic zip-scan signals form the same indications. This could only be confirmed if the sample could be cut.

Clearly Eddy Flux has identified sources of signal generation and the reasons or explanation of such changes needs to be investigated and established.

Whilst the selective corrosion on sample NABPC was not readily evident, in the second sample supplied, however, there was clear visual evidence of significant levels of selective phase corrosion having taken place, but the physical size of the sample prohibited scanning to do any exploratory work. Since the corrosion levels present in this sample were significant, the opportunity to gain even limited data, reaction to applied fields and measurement of any

remanent effects was taken, even though the active area carrying the test was limited, in the hope that it could lead to ideas of probe design or adaptation. Figure 53 shows the small sample piece [75mm x 35mm x 8mm] with the probe in position to carry out the restricted scan.

The first test was conducted with medium sensitivity sensor, which is affected by remanent fields only. This means that no active field [magnetic energy] external or from the sensor was applied to the sample before or during the test. The scans from the both the corroded and surface remote to the corrosion were carried out with this set up. Figure 53 illustrates the testing from the remote side to corrosion and figure 54 shows the Eddy flux signals form the remanent field within the sample.

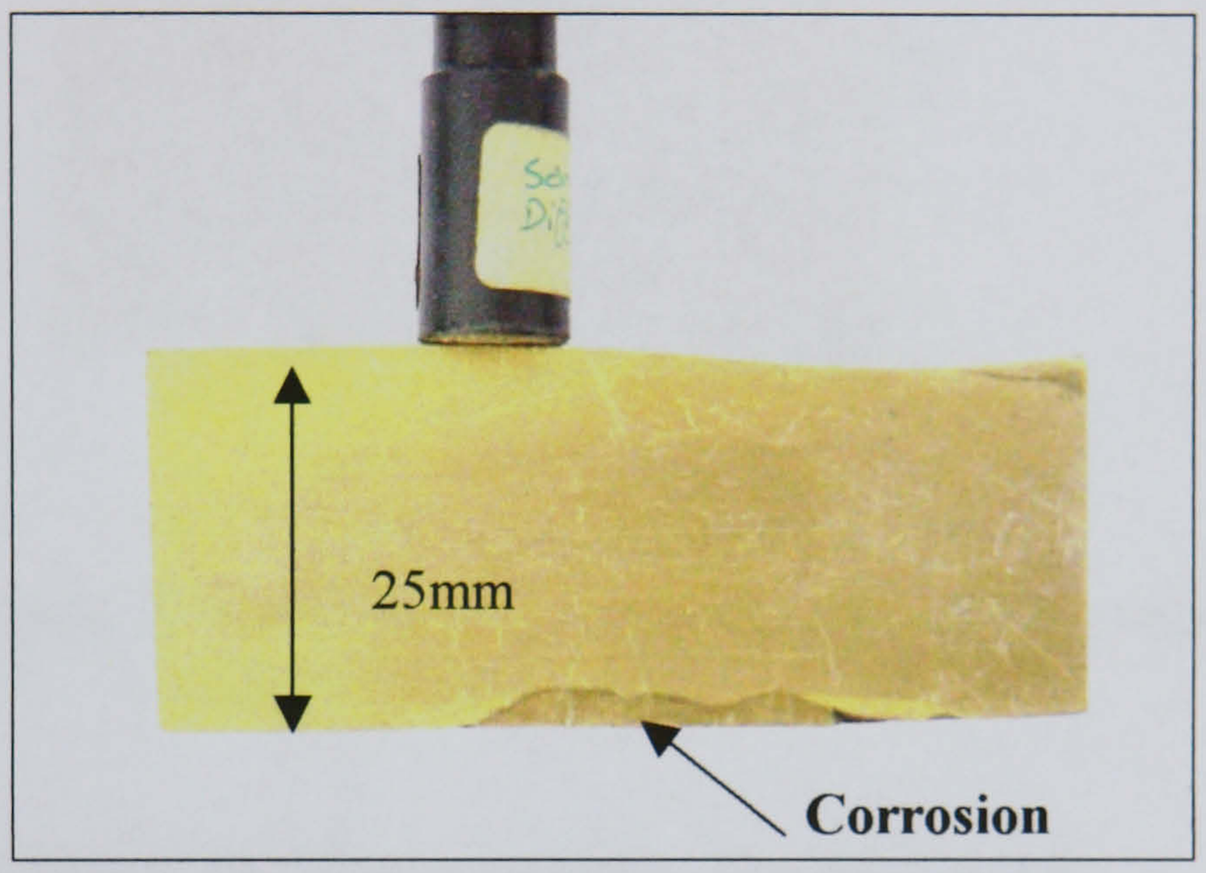

Figure 53 – Shows the small sample with sensor positioned remote to the corrosion surface.

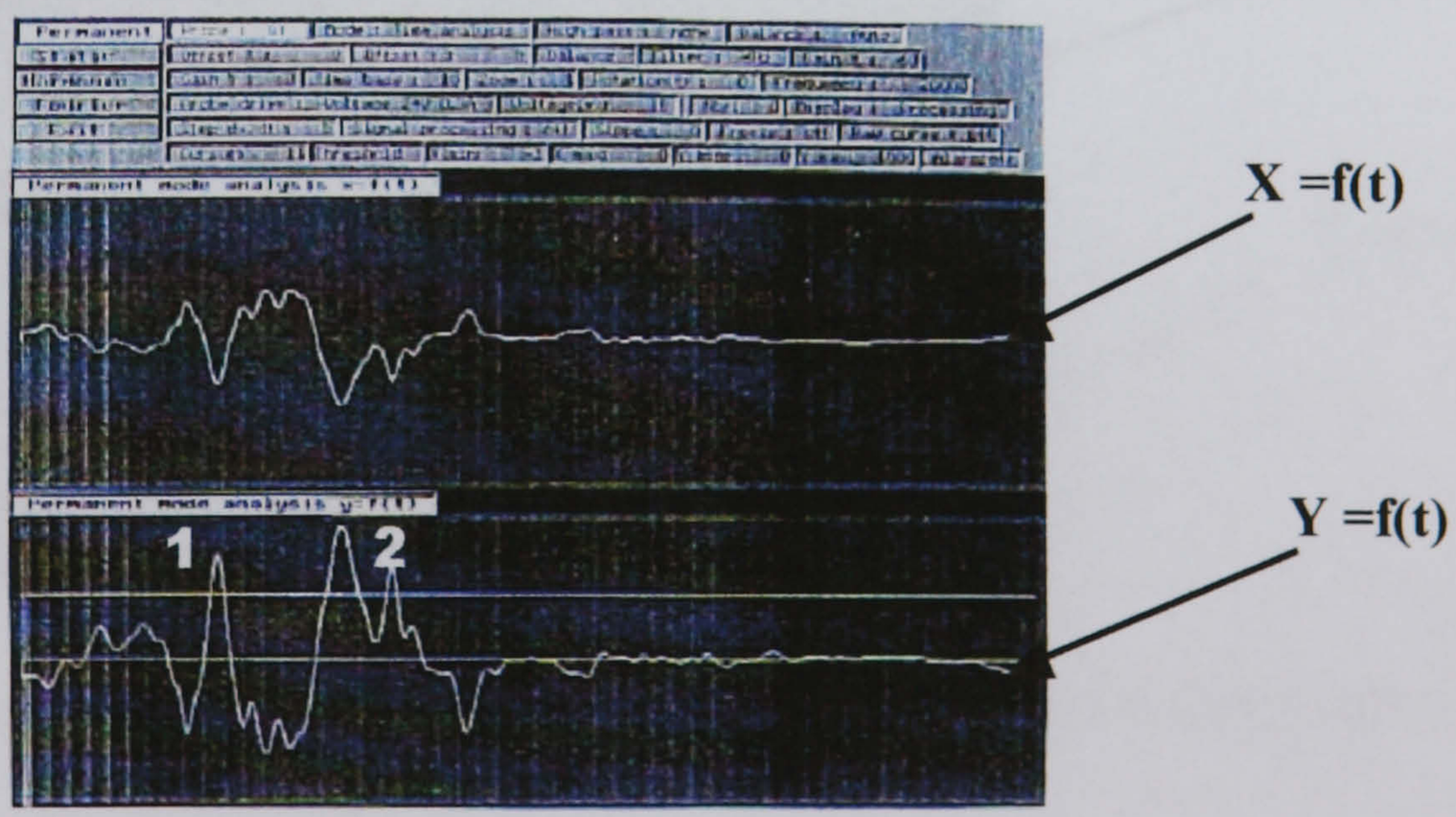

Figure 54 – Shows the Eddy Flux signal form the remanent field when testing from the remote side of corroded surface.

The start of corrosion is indicated by signal (1) and the finish by signal (2)

Figures 55and 56 show probe positioning and the Eddy Flux signals respectively when testing from the corroded face. It should be noted that the signal amplitude was reduced by some 30db to show the complete signal on the display screen.

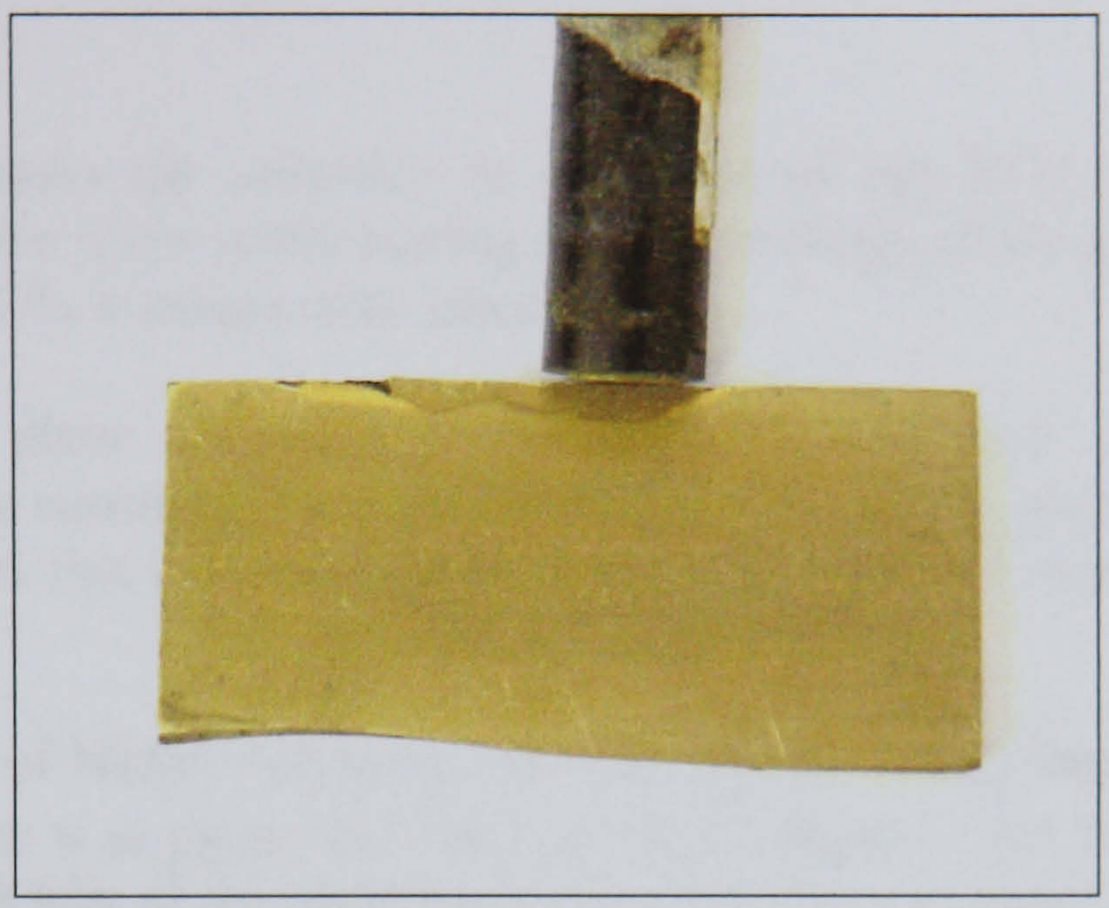

Figure 55 – Shows the small sample with sensor positioned on the corroded surface.

Figure 56 – Shows the Eddy Flux signal form the remanent field when testing on the corroded surface.

The signal obtained indicates that magnetic effects present may be associated with the high iron (Fe) content of the corroded area. Clearly the composition and magnetic susceptibility of the selective phase corrosion needs to be assessed for this type of detection technique to have any opportunity of working.

8.0 MAGNETIC PROPERTY DETERMINATION AND MAGNETIC MAPPING

In order to assess the suitability or otherwise of any NDT technique available it is first necessary to have some understanding of the metallurgy of the alloy, the corrosion mechanism and the form of the corrosion that takes place.

The selective phase corrosion results in the re-deposition of copper and the α grains surrounding the corroded phase are retained in position as a spongy porous mass. There is little visual indication that the corrosion has taken place with no means of determining the severity of the attack

The corrosion of Nickel Aluminium Bronze (NAB) castings takes the form of selective phase corrosion of the κ_{III} phase and evidence so far suggests that it is particularly severe when it occurs in the vicinity of the heat-affected zones of the weld repair areas.

The non-destructive examination problem is to locate and measure agglomerations of tiny defects filled with porous copper and more specifically corrosion occurring in an alloy of widely varying grain structure. In the worst case these agglomerations may be in the form of a narrow 2-3 mm band adjacent to weld repairs.

The results in section 6.4 show the mean chemical composition (wt %) of the κ_{III} phase in cast nickel aluminium bronze as:

Cu = 26.3 $\pm$ 3.5, Ni = 39.5 $\pm$ 3.2, Fe = 23.2 $\pm$ 3.7, Mn = 2.3 $\pm$ 0.1,
Si = 0.6 $\pm$ 0.2, Al = 8.2 $\pm$ 0.7.

As the most serious form of corrosion is that of selective phase corrosion, which results in the dissolution of the κ_{III}, and as this phase contains approximately 26% copper and some, if not all of this, is re-deposited during the dissolution process then clearly a change in magnetic properties must also have taken place. Highly permeable elements, Fe and Ni, are lost during the dissolution process.

Magnetic mapping of the sample was investigated with remnant fields, as the sample was not large enough for active magnetic evaluation.

Equipment:

X-Y scanner

Auto c-scan drive and data acquisition

Ed-scan software [a specific software for displaying voltage fluctuations]

Magnetometer and probe

The NAB test block was demagnetised to remove any residual field after Eddy Flux examination. Scanning was carried out at a 2mm pitch on the area as defined by the ultrasonic examination (refer to section 7.4.).

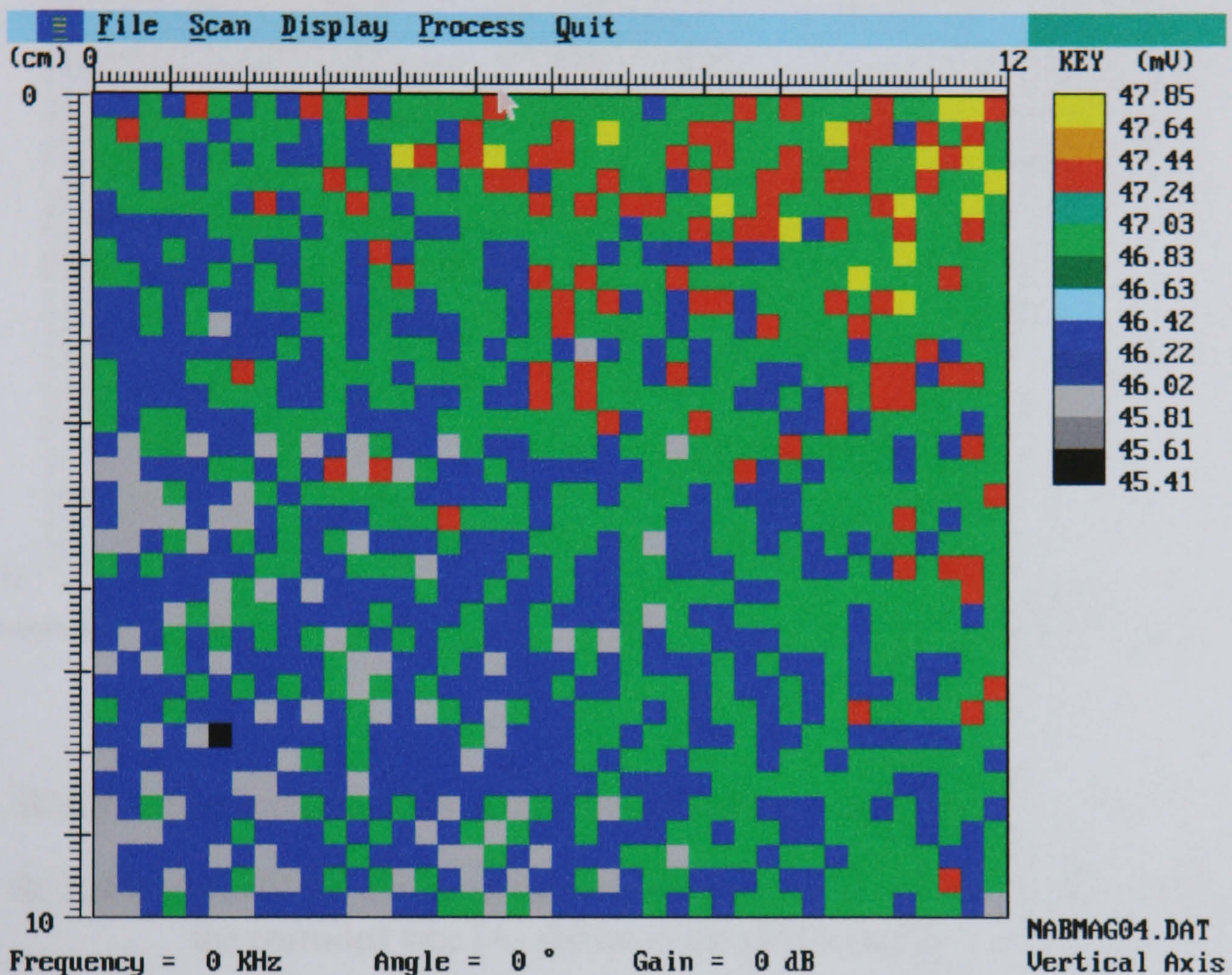

SCAN 1

SCAN 2

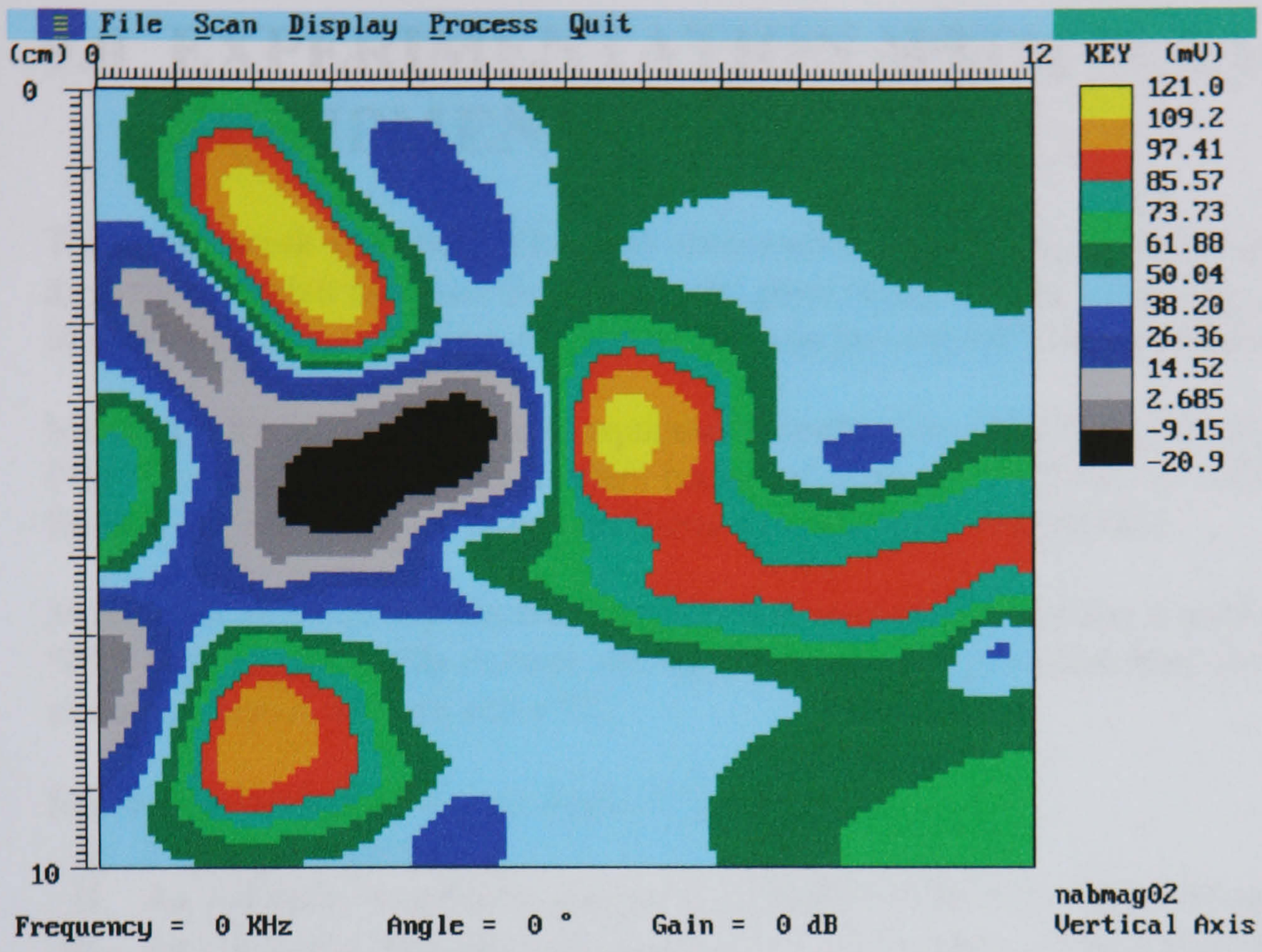

SCAN 3

SCAN 1- is of ambient fields in the area or location of scans for scans 2 and 3

SCAN 2 – Is of NAB test block as shown in figure 49 in section 7 with scanning on the corroded face [As shown in the photograph]

SCAN 3 – Is of NAB test block from the remote surface to that of corrosion

The reading from the above scans can be converted to magnetic field as follows:

$10mV \approx 1\mu T$

The scan of ambient field measured varies between 45 to 47 mV i.e. 4.5 to 4.7 microtesla. The scan of corroded face shows a variation – 17.5μT to + 16.7μT. The position of the highest field follows the weld repair profile to some degree.

The scan for the face opposite the corrosion, shows number of poles to be present, the relevance of which can only be determined by sectioning the test block for material and microstructure evaluation.

Magnetic mapping gives information but this would need to be investigated, by sectioning the sample, for the source of magnetic deviation. Active magnetisation would yield more information on sub-surface magnetic variations. Sample section was not permitted.

9.0 EXPERIMENTATION WITH MAXWELL EQUIPMENT

The earlier work with Eddy Flux was encouraging in that phase selective corrosion detection form the corroded face was detectable with good signal to noise ratio. The detection, however from the remote face to the corroded surface was proving not to be so conclusive.

Maxwell is the next generation of equipment produced by IXTREM of France. It differs for the Eddy Flux equipment in that it offers better software and hardware as well as new additional features and techniques of Magnetic Harmonics and Static Examination.

Maxwell is an advanced electromagnetic measurement and testing system dedicated to NDT applications (Eddy current and flux leakage). The actual product is composed of electronic cards, sensors and a PC.

Maxwell is composed of (see figure 57):

I. 2 ISA bus boards:
II. An Arbitrary wave form and pulse generator 0-10 MHz, 20 V 300mA
III. An Ultra-fast data acquisition and signal processing card with demodulation module and hardware.
IV. High pass and low pass filters.

Figure 57. - Maxwell equipment

The new Magnetic Harmonics technique offered is an Exotic electromagnetic NDT technique using low frequency sinusoidal magnetic field (50 Hz generally) to saturate the material to be tested for detecting defects in ferrous material. During alternating magnetisation a non-sinusoidal magnetic field strength is obtained. Because of the influence of hysteresis only the odd upper harmonics are generated beside the exciting frequency and analysed.

Static Examination is means of applying a spectrum of frequencies to interrogate the same portion of the material under evaluation via the same sensor.

The electromagnetic techniques used from the Maxwell equipment to find Selective Phase Corrosion was:

1) Magnetic Flux Leakage

2) Combined Flux Leakage and Eddy Currents

9.1 Principles of Techniques Applied

a) Magnetic Flux Leakage

The technique of magnetic flux leakage (MFL) testing is a commonly used inspection method. While some forms of MFL may not be as sophisticated as other methods of inspection. it is probable that more ferromagnetic material is inspected by MFL than any other method.

Magnetic flux leakage methods consist primarily of two steps. The first is a method of magnetising the part, and the second is the use of a magnetic flux sensitive detector to scan flux diverted by discontinuities. See figure 58.

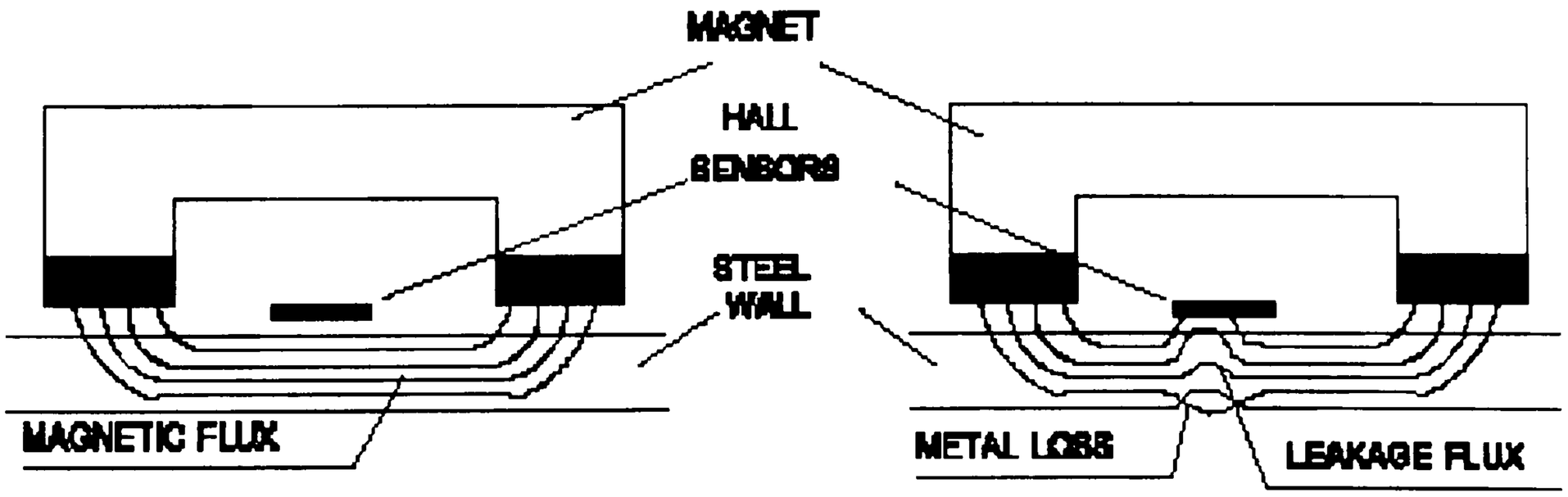

Figure 58 – Simple magnetic flux detection set up with indirect magnetisation.

In magnetising the part consideration must be given to suitability of the magnetic field generated within the material. In some ferromagnetic materials, the residual field [the field that remains after removal of an external magnetising field] is often adequate for surface flaw detection. In practice, however, residual magnetisation is rarely used because use of an applied

magnetising field ensures that the material is in a desired magnetic state and because an applied field provides more flexibility: that is, one can produce a high or low flux density in specimen as desired. The control of the strength and direction of the magnetisation can be useful in improving flaw detectability and in discriminating among different types of flaws. In general the magnitude of the magnetisation should be chosen to maximise the flaw leakage field with respect to other field sources that might interfere with flaw detection. The direction of the field should be perpendicular to the largest flaw dimension to maximise the effect of the flaw on the leakage field.

It is possible to generate magnetic field in a specimen either directly or indirectly. In direct magnetisation, current is passed directly through the part. With the indirect approach, placing the part in a magnetic field that is generated by an adjacent current conductor or a permanent magnet is suitable to induce the desired magnetisation.

MFL method being considered for these experiments is not being applied directly to the part. Thus design considerations for magnetisation of parts often requires minimising the magnetic reluctance of the magnetic circuit, consisting of:

1) The part,

2) The magnetising system,

3) Any air gap which, might be present.

In this MFL method a DC magnetic field is set up perpendicular to the direction of the defect. The magnetic flux, which is bent round the defect, emerges above the surface, thus producing a Magnetic flux leakage in the part being inspected which can be detected by a variety of sensors, which include pickup coils, Hall elements, Magneto-diodes, Forster microprobes (ferro-probes) and Magneto-resistive elements. Signals from the probes are processed electronically and presented in a manner that indicated the presence of the discontinuities.

Previous findings report that Non-Destructive inspection of defects using the Magnetic Flux Leakage method presents several experimental and theoretical difficulties. It is shown that the leakage field strength around a defect is linked linearly with the field strength inside it. Thus, a prerequisite to a better understanding of the phenomenon is the determination of the magnetic field strength inside the defect as a function of defect geometry, magnetic properties of the material and applied field strength. Equations are presented [23&24] which enable computation of this quantity for both the linear and non-linear cases. Discrepancies between measurement and calculations using the method of finite elements emphasise the need for accurate knowledge of the magnetic field strength inside the defect.

Discussed also in various publications are the practical significance of the different sections of the magnetisation curve and Hysteresis loop to the magnetic leakage flux method for Non-Destructive material testing.

b) Combined Flux leakage and Eddy Currents

In conventional Eddy Current a coil supplied with an alternating current at a known frequency provides the mechanism by which the eddy currents are created in the metal surface. The data from field variations associated with interactions of the eddy currents and the defects are obtained by incorporating a separate detection coil into the same probe head as that producing the eddy current.

Introducing a magnetic sensor in the coil allows us to have an 'image' of the eddy current compared with that normally obtained with a coil. Figure 59 shows a schematic diagram of the probe that was used, manufactured to a design based upon the NASA developed Self-Nulling Eddy Current Probe for surface and near surface flaw detection [25].
The new probe has two main design changes from the original Self-Nulling Eddy Current Probe. A GMR sensor is used in place of a pickup coil as the field sensor and a second current source is added to provide active feedback to the GMR sensor location.

The probe was constructed by Ixtrem of France by winding 40 turns SWG24 copper wire around a ferrite tube (8.0mm ID x 20mm OD x 25mm high) to produce the eddy current/magnetisation coil and then placing a specific magnetoresistive sensor with feed back circuit placed in side the ferrite tube as the detection sensor.

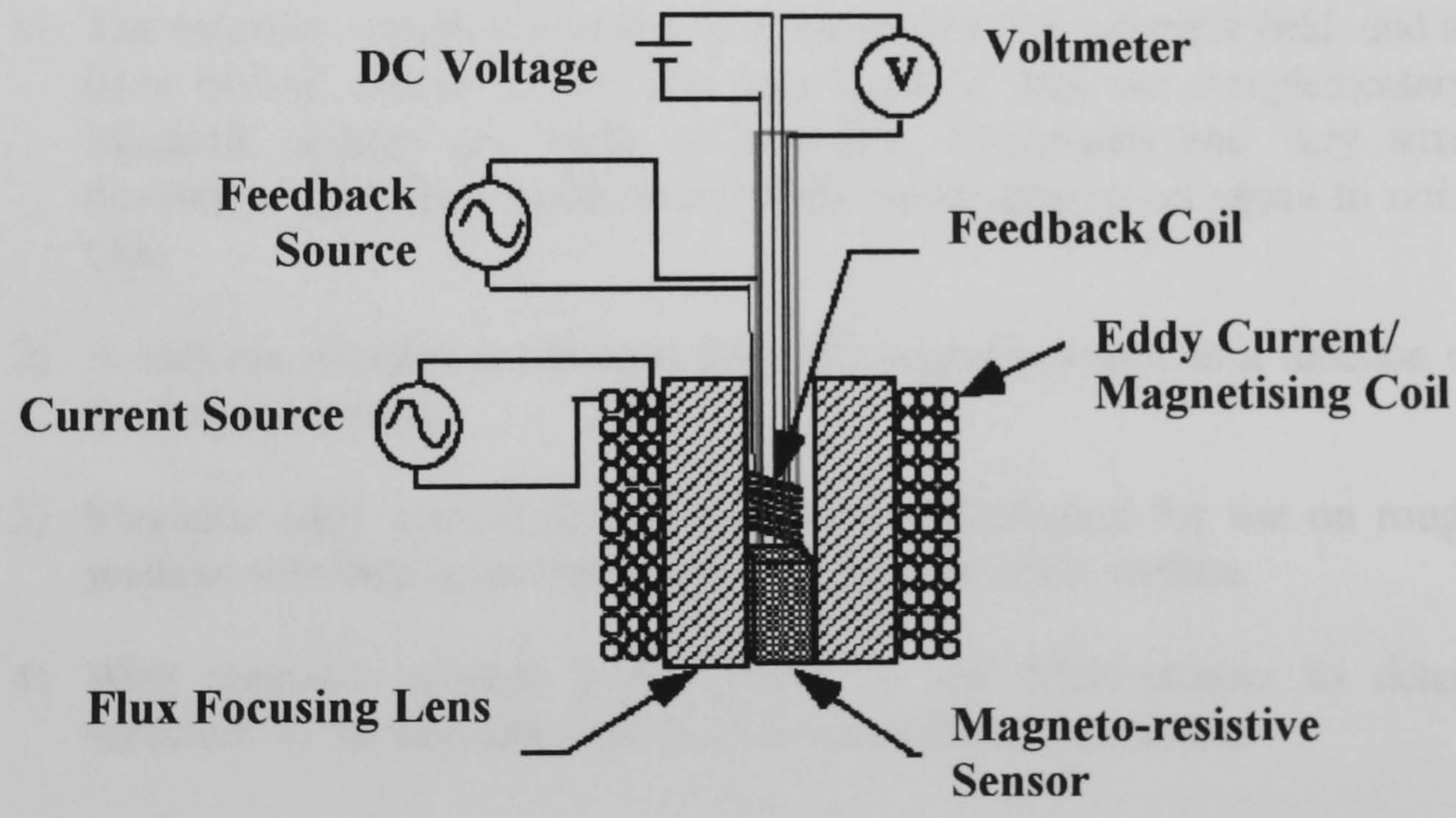

Figure 59. - Schematic diagram of a new Magneto-resistive Probe.

Coil transducers respond to the time rate of change of the magnetic field for the entire pattern of eddy currents or to flux leakage induced in the test object by the exciting coil field, at least those magnetic reaction flux lines created by the eddy currents which actually couple with the coil. Generally response is greatest to those areas within the circumference of the test coil, and to test-object conditions that change the total magnitude of flux linked with the pickup coil. Sensitivity to test object variations diminishes with distance from the exciting coil and coaxial

pickup coil winding. Use of very large-area test coils generally results in loss of sensitivity to small discontinuities even at short distances from the coil winding.

On the other hand, magnetic detectors respond most sensitively to small areas of the test object close to the detector, and these can be quite remote from the exciting coil. In fact, semiconductors can sometimes advantageously be placed in certain locations and orientations where there is no sensitivity to normal field distribution of the exciting coil, but where unique response to distortions in eddy current flow paths can be obtained.

With coil detectors it is often necessary to utilise higher test frequency ratios and to accept correspondingly lower depths of eddy current penetration within the test material.

Magnetic detector signals are directly proportional to the actual magnitudes of the magnetic flux density B and have uniform sensitivity over a wide range, including the lowest possible test frequency (DC). This is why magnetic elements are also used as detectors in diverted flux test systems. In addition, sensitive measurements can be made of relatively low eddy current reaction fields and flux leakage fields, corresponding to very low-test frequencies with great depths of penetration

This method of measuring the disturbance of the eddy currents shows a number of advantages over the conventional eddy current measurement: -

1) The magnetic sensor is sensitive to a variation in the magnetic field, and an eddy current coil to dØ/dt. The two types of data are complementary. Magnetic sensors can work at very low frequencies and very small dimensions [less than a millimeter] while maintaining good signal to noise ratio.

2) A uniform response is obtained from the magnetic sensor as a function of the frequency used.

3) Magnetic eddy current sensors can be readily adapted for use on rough surfaces with little noise being generated by state of the surface.

4) With magnetic sensors it is possible to use Multi-sensors to detect variations in the magnetic field in three axes without interaction.

9.2 Maxwell Examination

9.2.1 Special probe manufacture was commissioned:

1) Very high sensitivity Magneto-restrictive probes for detection of small-diverted field applied in remanent mode. - Probe diameter 20mm

2) Combined Flux leakage and eddy current probe – with low frequency and adapted for rough surface application, See figure 59 – Probe diameter 25mm.

9.2.2 Test Samples Supplied by DRA

Two samples were provided by DRA [Defence Research Agency] each containing some degree of phase selective corrosion as illustrated below.

Sample 1(fig. 60) wall thickness varies between 30 - 35mm

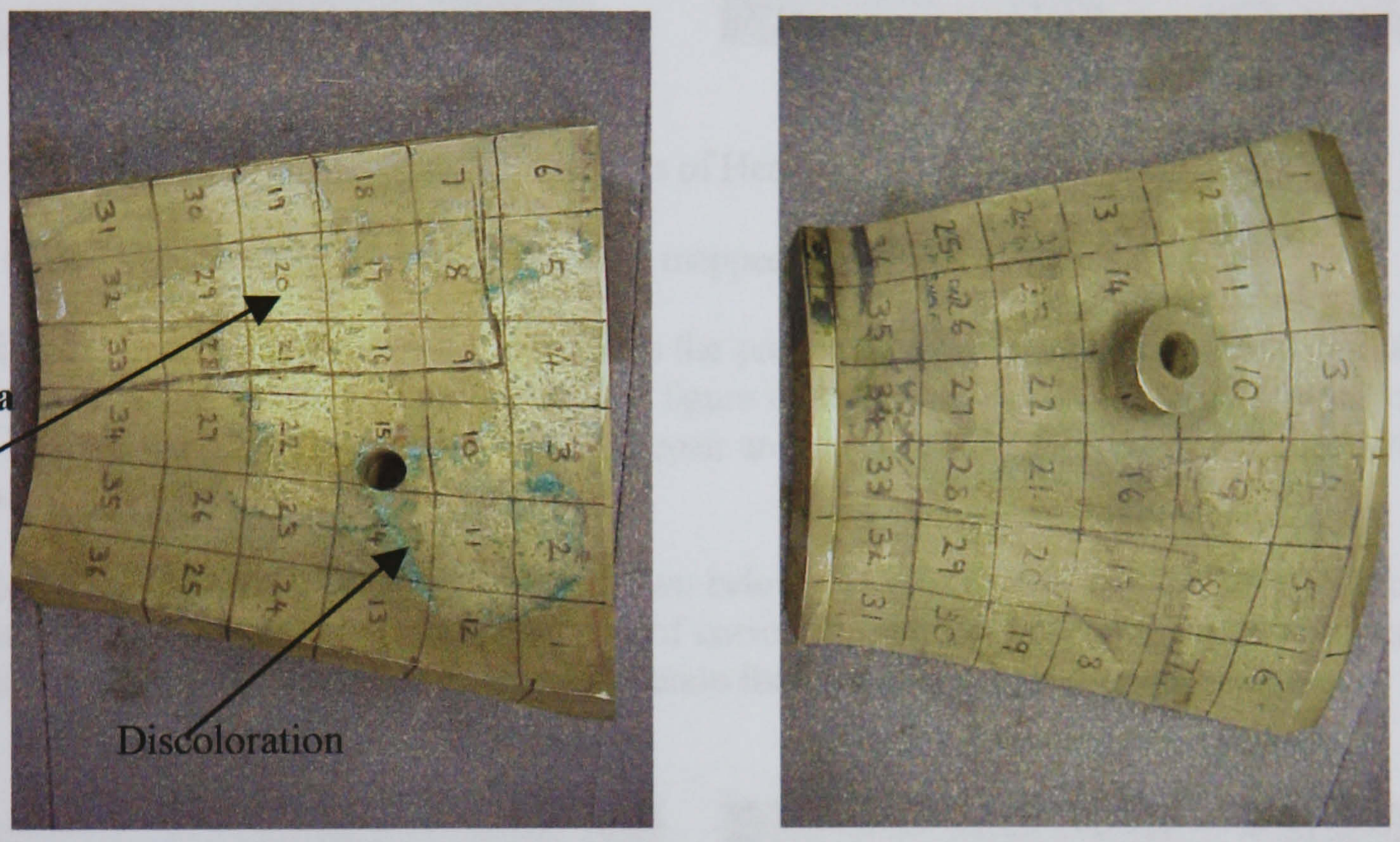

Corroded **Face remote to corrosion**

Figure 60 – shows sample 1 mapped for investigation

Sample 2 (figure 61)– Sections of header with wall thickness varying between 30 – 40mm

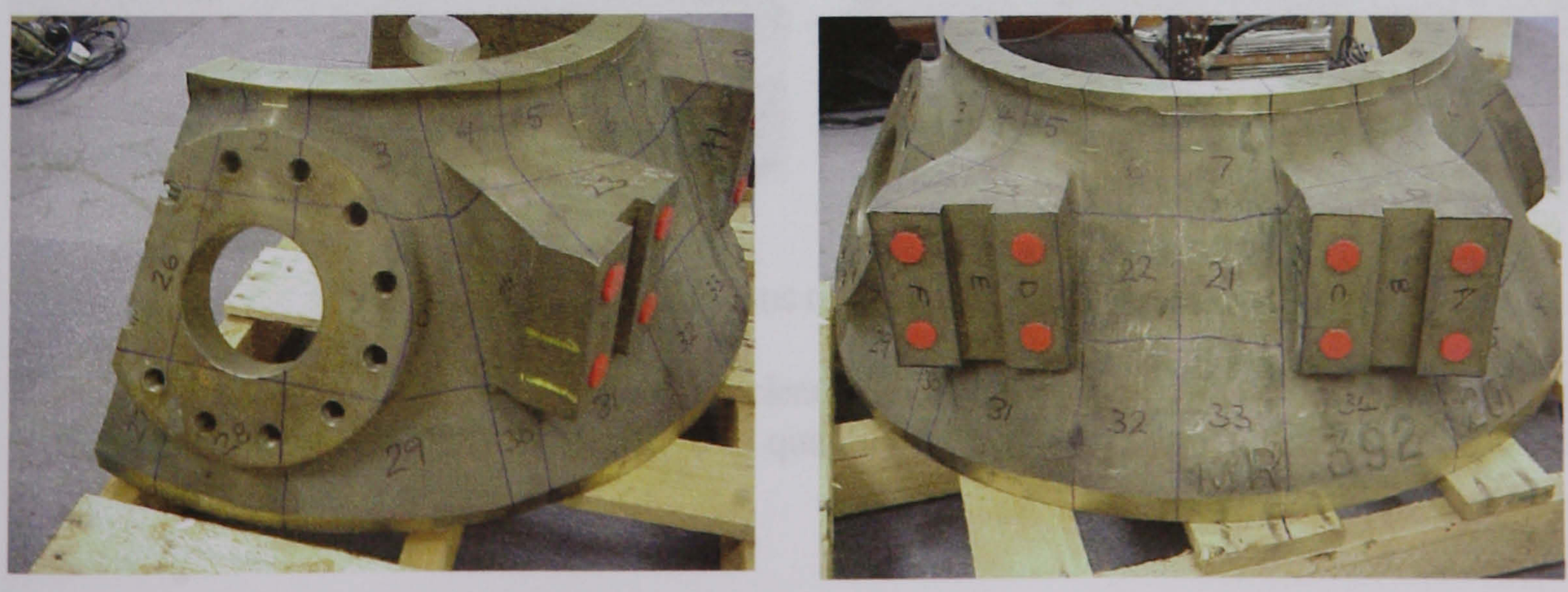

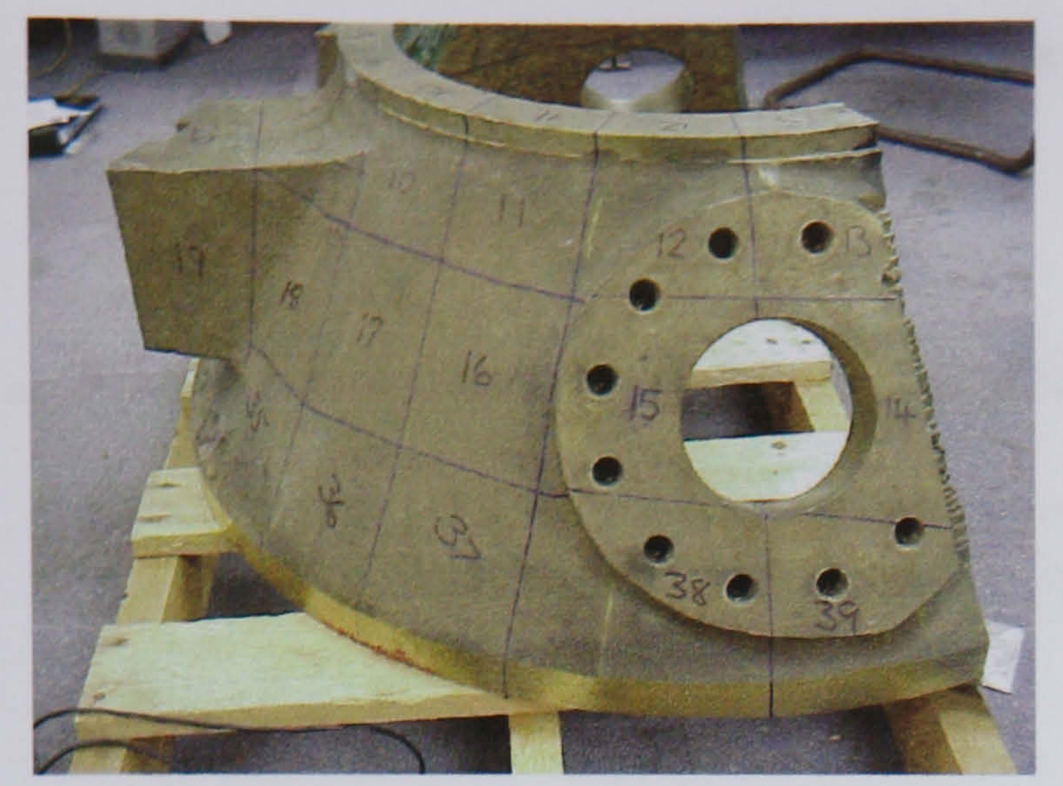

Sections of Header

Figure 61 – Sample 2, sections of header mapped for investigation

Chemical etching process was used to confirm the presence of phase selective corrosion in all the samples. For sample 1 and as illustrated in figure 60 the corroded face shows discoloration at the heat affected zone and edge of a weld repair area as corrosion, however two other weld repairs show no discolouration effects.

Sample 2 exhibited more discoloration as shown below and again some areas of discoloration are associated with weld repairs. Association of corrosion with weld repaired is easily evident from these photographs but with closer examination the weld patches are identifiable.

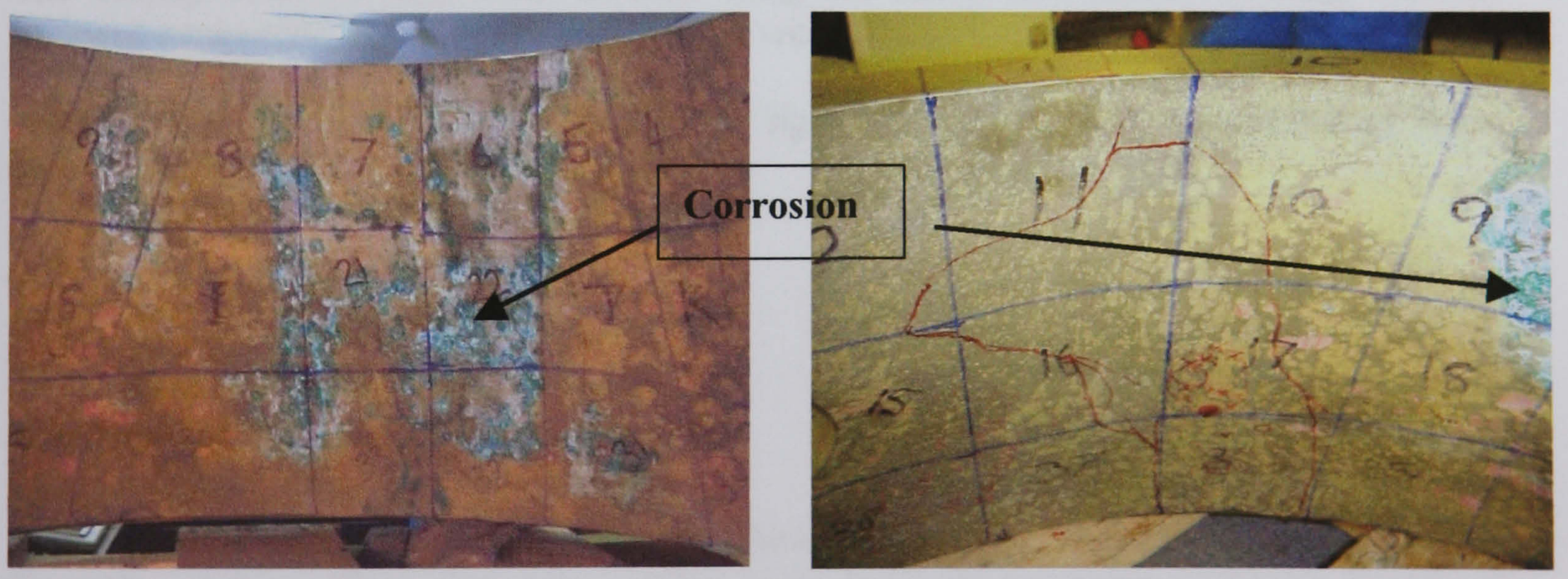

Portions of sample 2

Whilst the surface area of the corrosion was clearly evident, the extent of corrosion through the section was not defined. DRA was unable to quantify the selective phase corrosion in terms of its depth.

Sectioning or grinding of the samples was not permitted, this being the only sure way of knowing how much corrosion truly exists.

9.2.3 Examination of Test Samples Supplied by DRA

It must be emphasised that the examination of the two test samples was carried out from the outer surface this being the surface remote from the corrosion face.

PREPARATION

Firstly the casting examination surface was cleaned. Secondly, the castings were mapped into areas that corresponded with the inner and outer surfaces. Those areas that did not correspond with the inner and outer surfaces, due to dimensional changes, were designated by a letter [see header section photographs above].

METHOD

Equipment: Maxwell – Permanent Mode [Eddy Current/Flux leakage mode]

Probes: 1 - **3C03** –Special high sensitivity Flux leakage detection probe. [Remanent]

2 - **AD01** – Eddy current /Magneto-resistive probe [Active]. See figure 59

The casting outer surfaces were scanned using the above two probes working with the Maxwell equipment. The scanning was by hand with 10% surface overlap for each scan.

Any significant indications were recorded. The significant indications were those having signal amplitudes greater than 15% screen height.

9.2 Results

Sample 1

Metallurgically this was not a good sample. The material exhibits high levels of magnetism in its entire surface. Weld free areas show lower level of magnetism and any signals of significance were recorded for both active and remanent fields using the probes 3C03 and AD01 respectively.

Welded Areas – Signals were obtained from the welded areas but there was no correlation between the visually observed areas of corrosion. It was concluded that the phase selective

corrosion was insignificant in depth and that the heat-affected areas with magnetic signatures need to be investigated.

Sample 2

The cast header section was mapped and numbered for scanning location. Each area was inspected from both surfaces [corroded face and face remote to corrosion] and signal recorded.

Inspection from the corroded face using the Remanent and Active probe [3C03, AD01] identified the presence of corrosion without much difficulty.

The inspection from the remote side produced some result using the Remanent probe. It was however the Active probe, AD01, which produced most of the data –table 6. The wall thickness of the casting [30-40mm] was high this meant that using the AD01 probe will require low frequency [500Hz] excitation of the probe coil to achieve sufficient penetration of the magnetic field. The lowering of the frequency in turn has an effect on the speed at which scanning could be performed. The movement of the probe was slow to accommodate the time lag created by the use of low frequency.

Table 6 –Correlation of Magneto-resistive sensor signals to corrosion evident.

AREA	OUTER SURFACE INSPECTION RESULTS	VISUAL INSPECTION -INNER SURFACE
1	CLEAR	CLEAR
2	CLEAR	CLEAR
3	CLEAR	CLEAR
4	SMALL INDICATION FIG.62	CLEAR
5	CLEAR	CLEAR
6	LARGE INDICATION FIG.63	AREAS OF CORROSION PRESENT
7	LARGE INDICATION FIG. 64	AREAS OF CORROSION PRESENT
8	SMALL INDICATION FIG.65	AREAS OF CORROSION PRESENT
9	SMALL INDICATION FIG.66	AREAS OF CORROSION PRESENT
10	SMALL INDICATION FIG.67	CLEAR
11	CLEAR	CLEAR
12	CLEAR	CLEAR

13	CLEAR	CLEAR
14	CLEAR	CLEAR
15	CLEAR	CLEAR
16	CLEAR	CLEAR
17	CLEAR	CLEAR
18	CLEAR	CLEAR
19	CLEAR	N/A
20	CLEAR	N/A
21	SIGNIFICANT INDICATION FIG.68	AREAS OF CORROSION PRESENT
22	SIGNIFICANT INDICATION FIG.69	AREAS OF CORROSION PRESENT
23	UNSUALLY LARGE SIGNALS FIG.70	N/A
24	UNSUALLY LARGE SIGNALS FIG.71	N/A
25	CLEAR	CLEAR
26	CLEAR	N/A
27	CLEAR	CLEAR
28	CLEAR	CLEAR
29	CLEAR	CLEAR
30	CLEAR	CLEAR
31	SIGNIFICANT INDICATION FIG.72	AREAS OF CORROSION PRESENT
32	SIGNIFICANT INDICATION FIG.73	AREAS OF CORROSION PRESENT
33	LARGE INDICATION FIG. 74	AREAS OF CORROSION PRESENT

34	LARGE INDICATION FIG. 75	AREAS OF CORROSION PRESENT
35	CLEAR	CLEAR
36	CLEAR	CLEAR
37	CLEAR	CLEAR
38	CLEAR	CLEAR
39	CLEAR	CLEAR

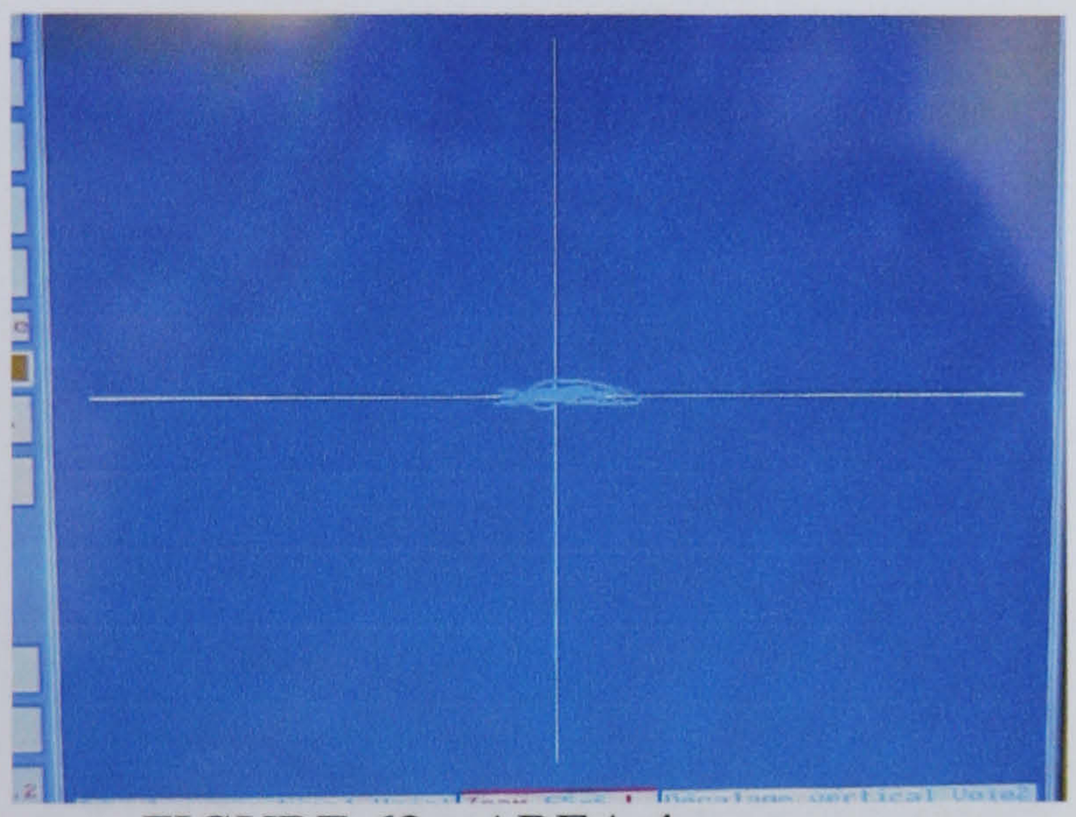

FIGURE 62 - AREA 4

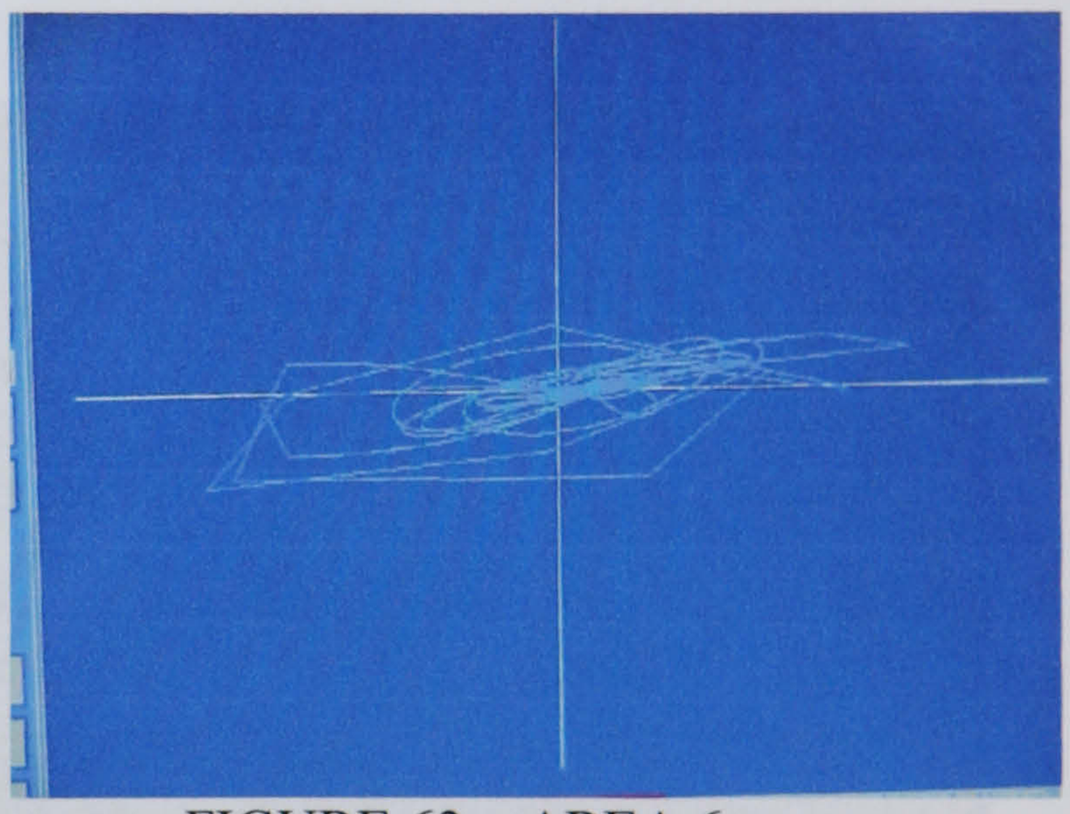

FIGURE 63 – AREA 6

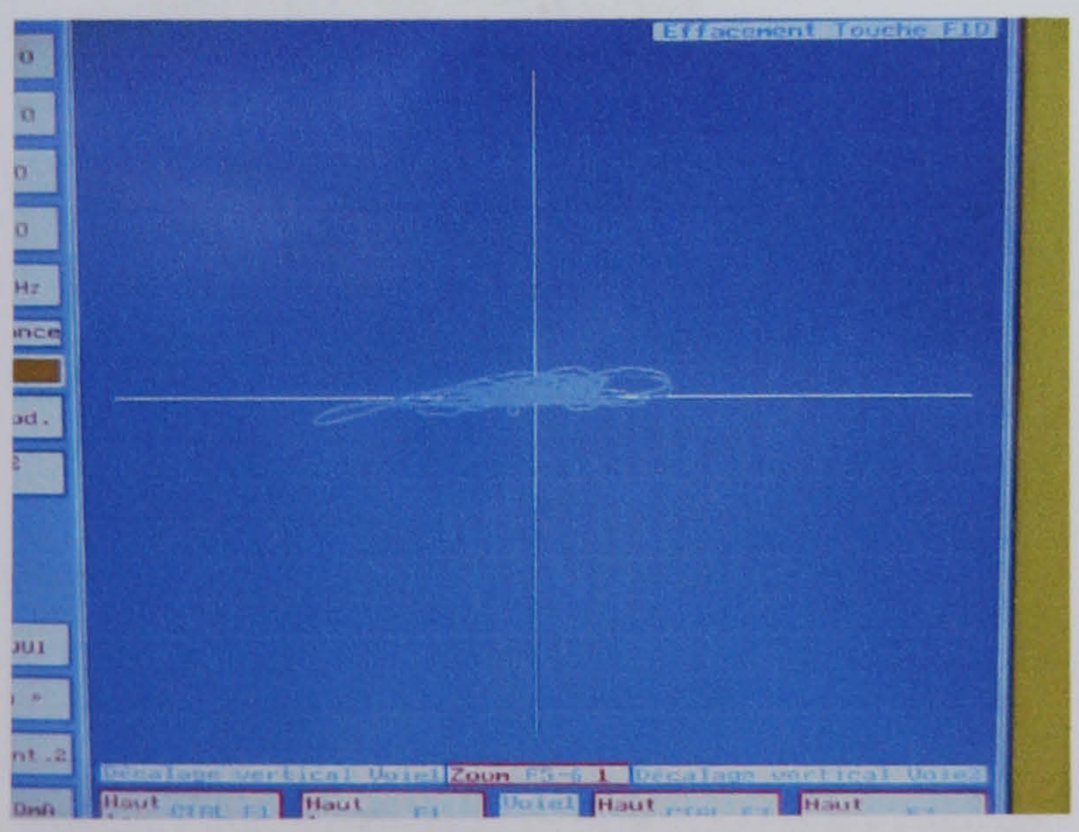

FIGURE 64 – AREA 7

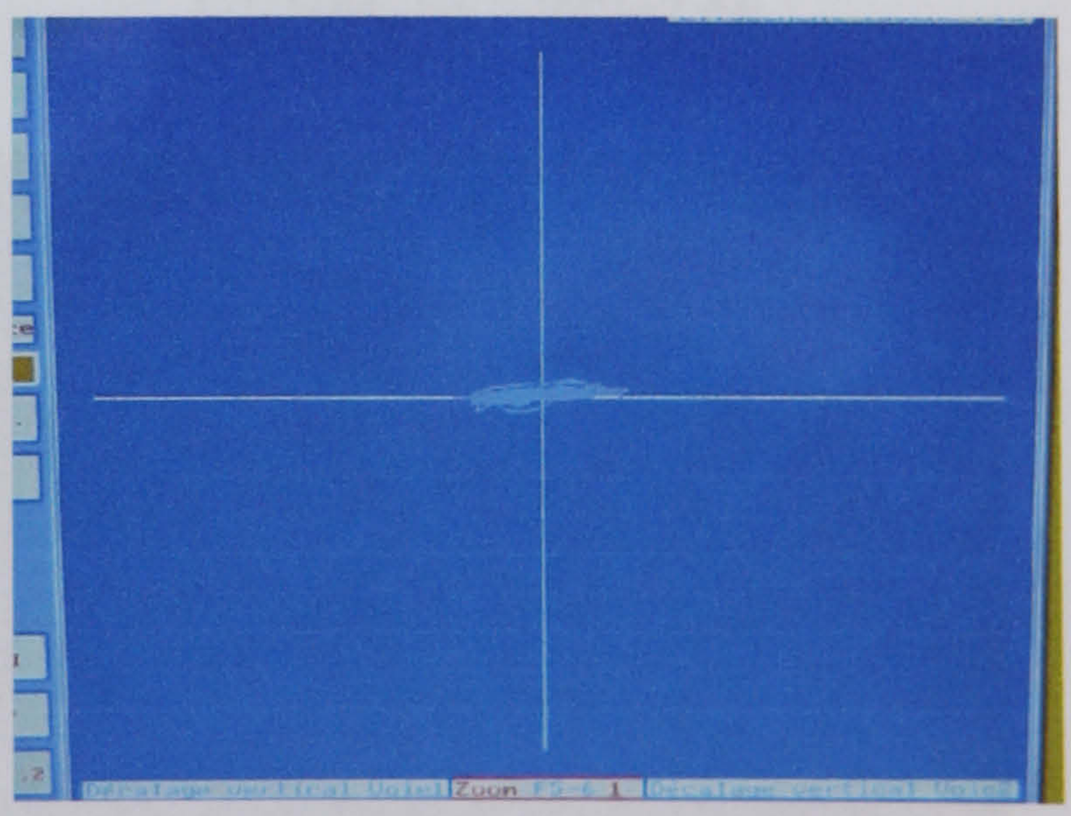

FIGURE 65 – AREA 8

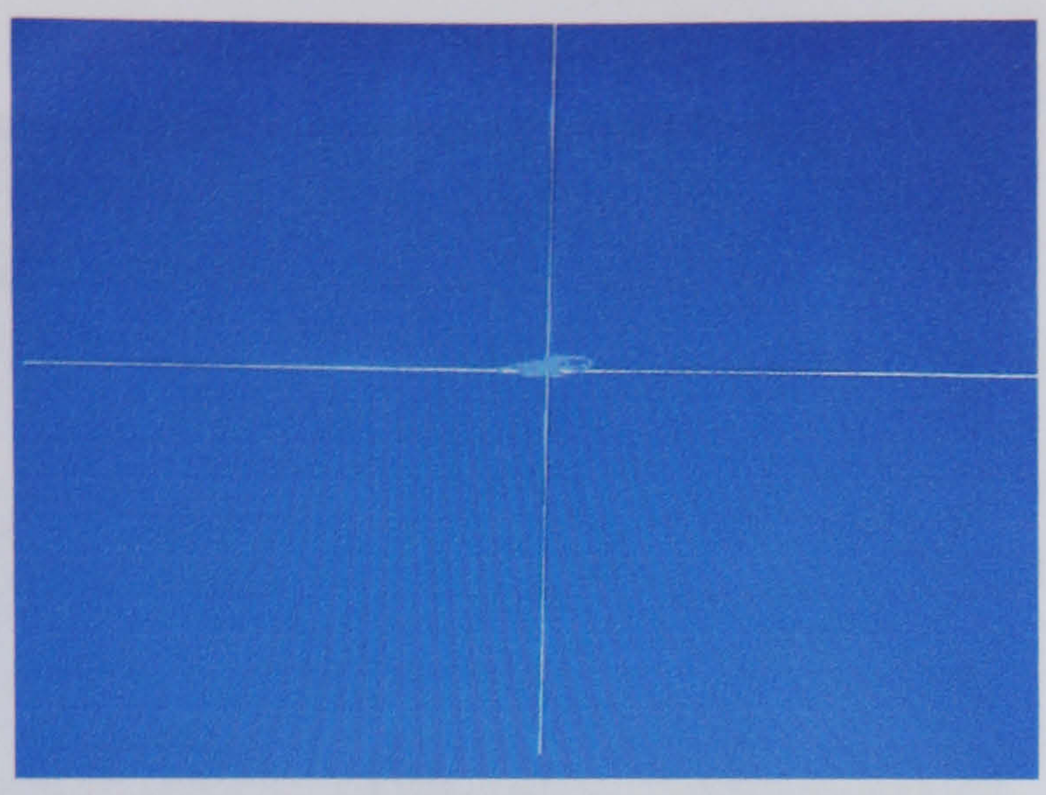

FIGURE 66 – AREA 9

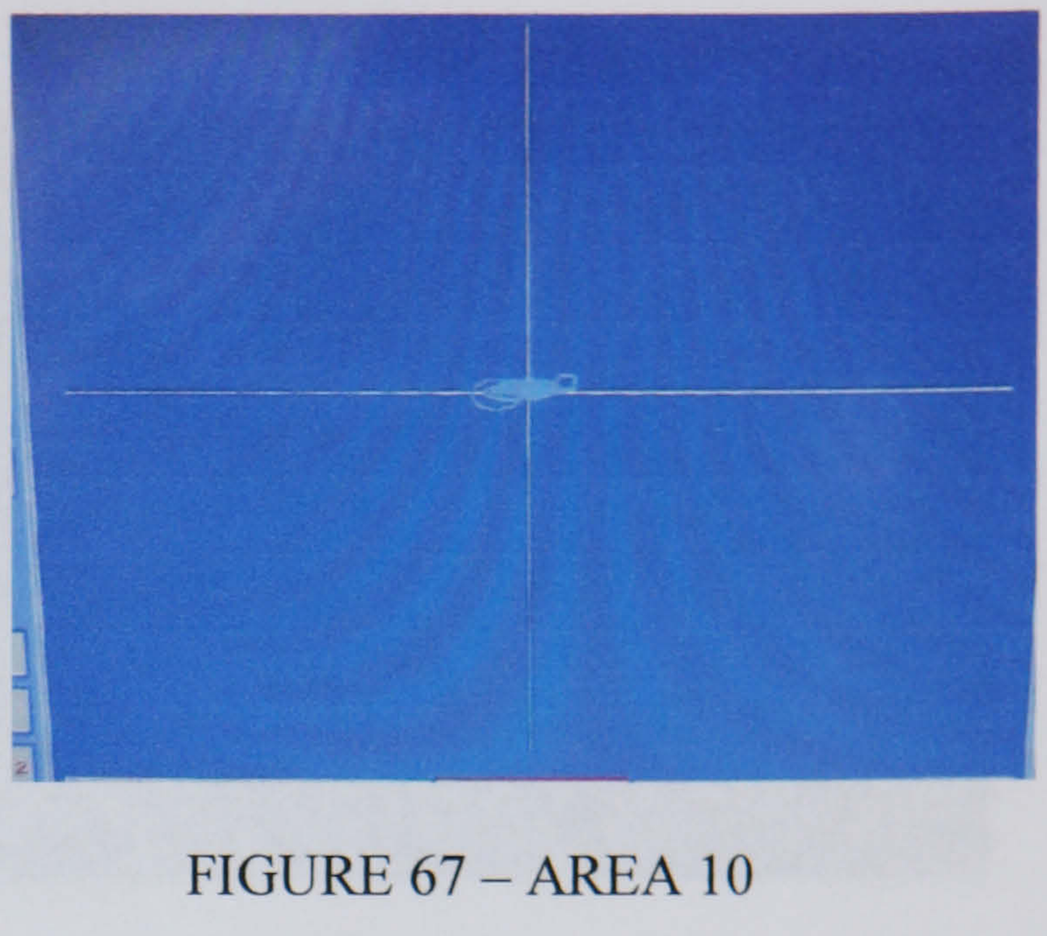

FIGURE 67 – AREA 10

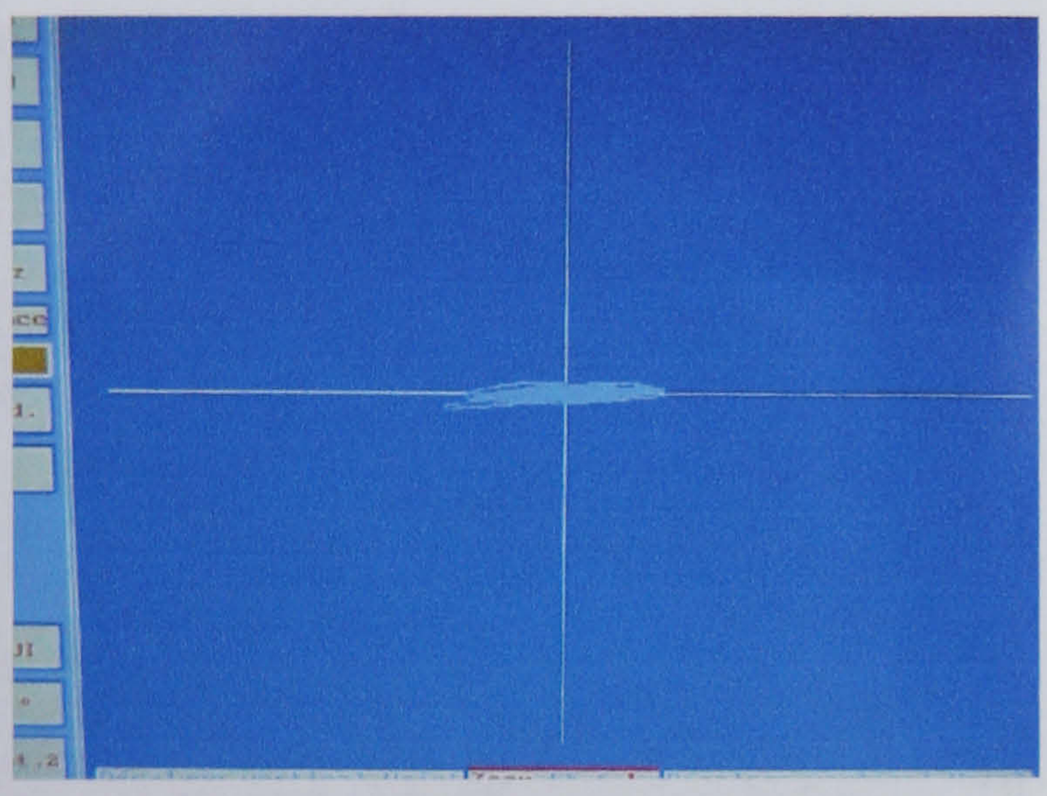

FIGURE 68 – AREA21

FIGURE 69 – AREA 22

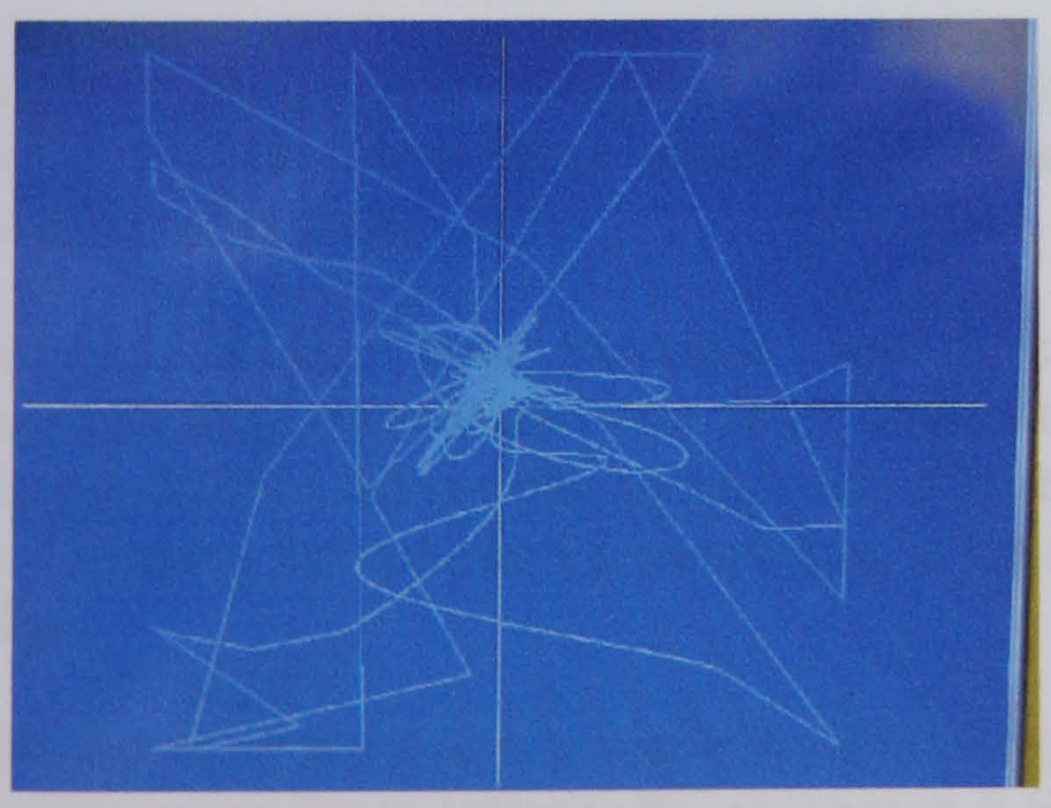

FIGURE 70 - AREA 23

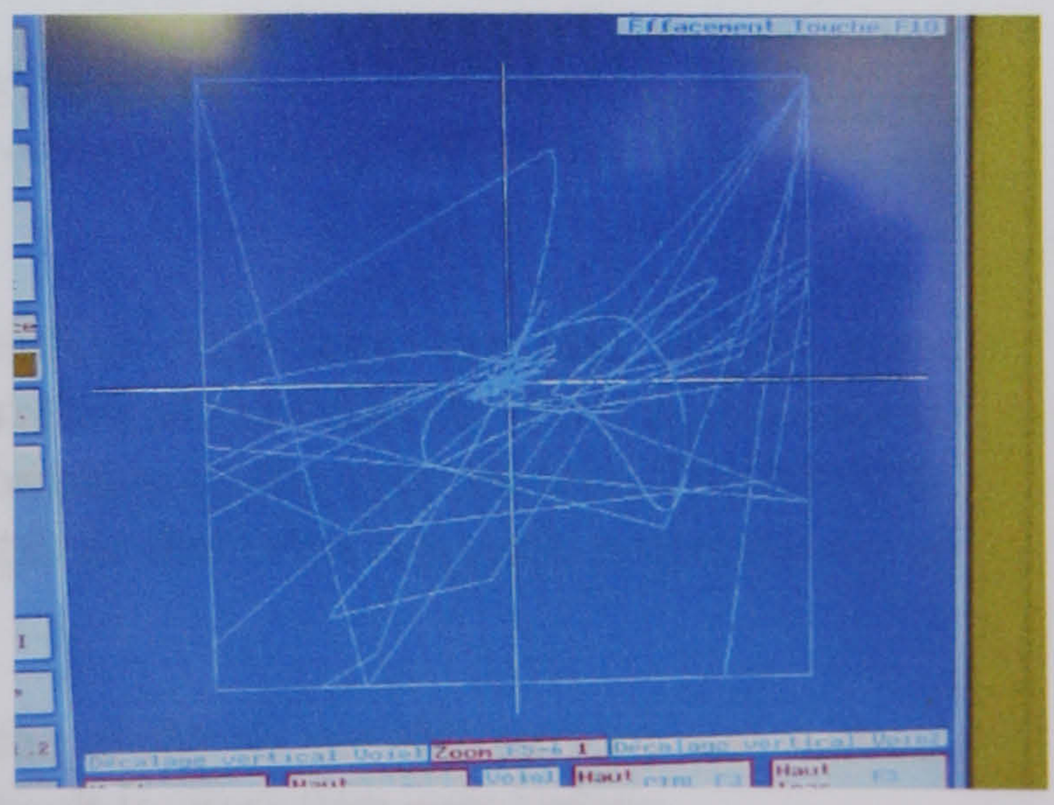

FIGURE 71 – AREA 24

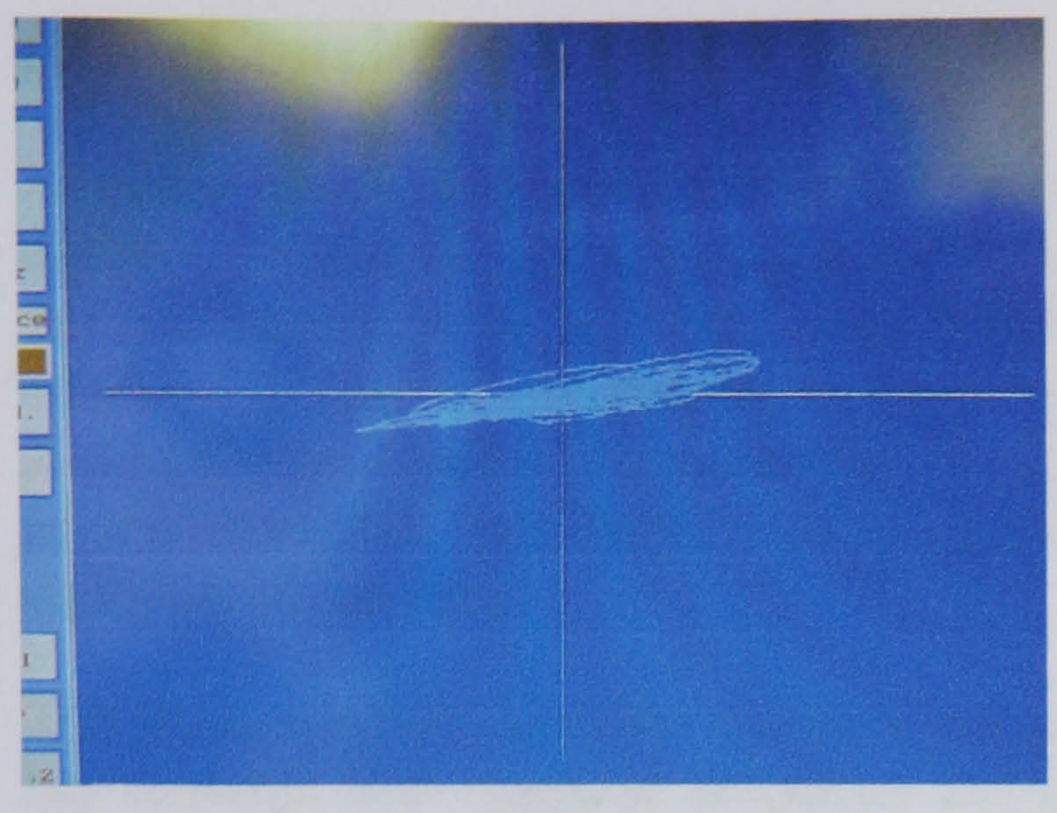

FIGURE 72 – AREA 31

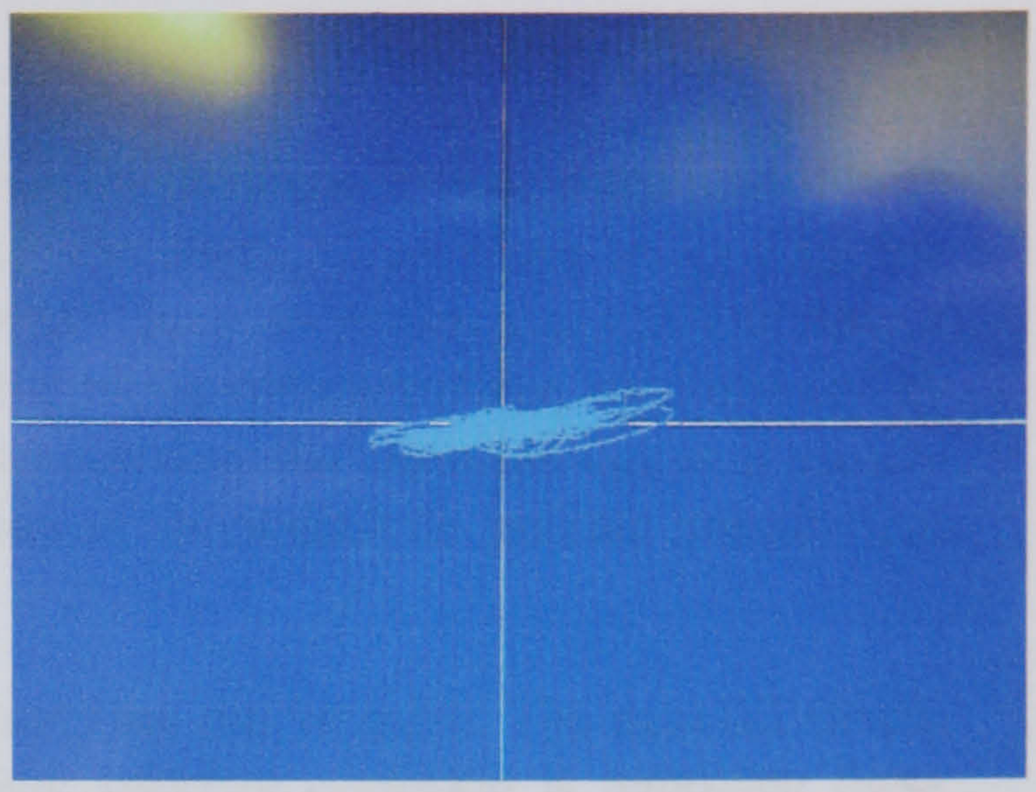

FIGURE 73 – AREA 32

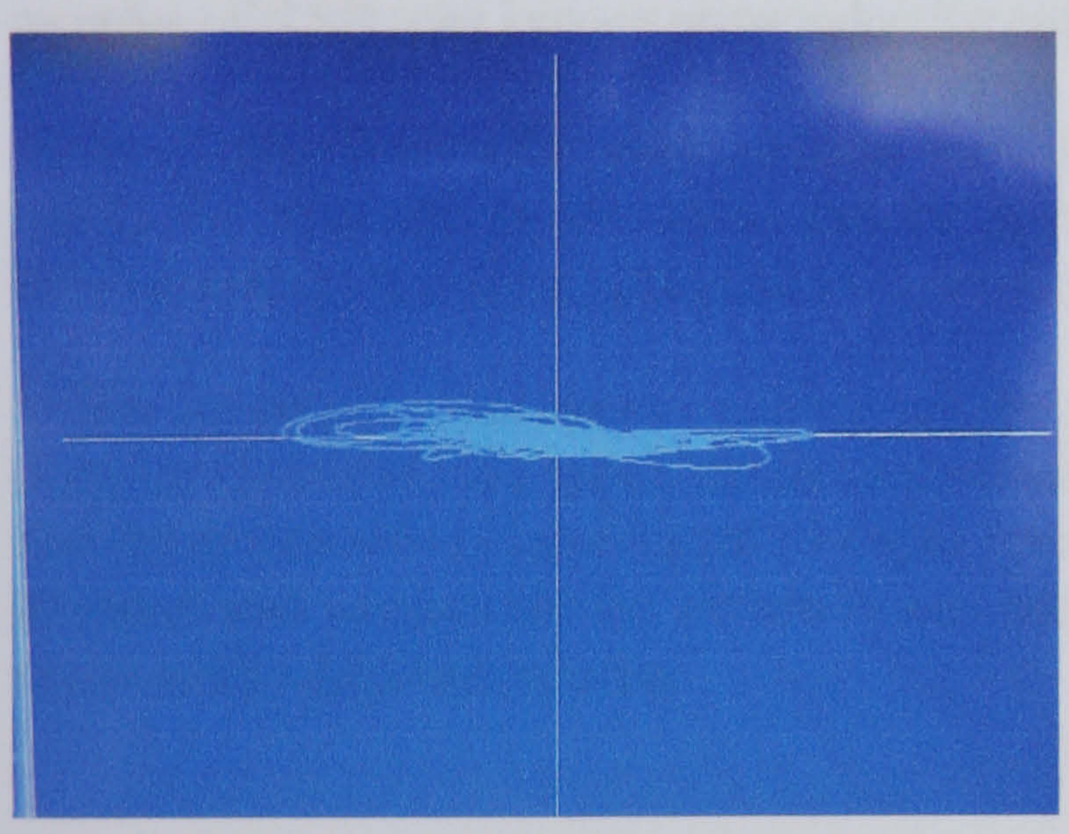

FIGURE 74 – AREA 33

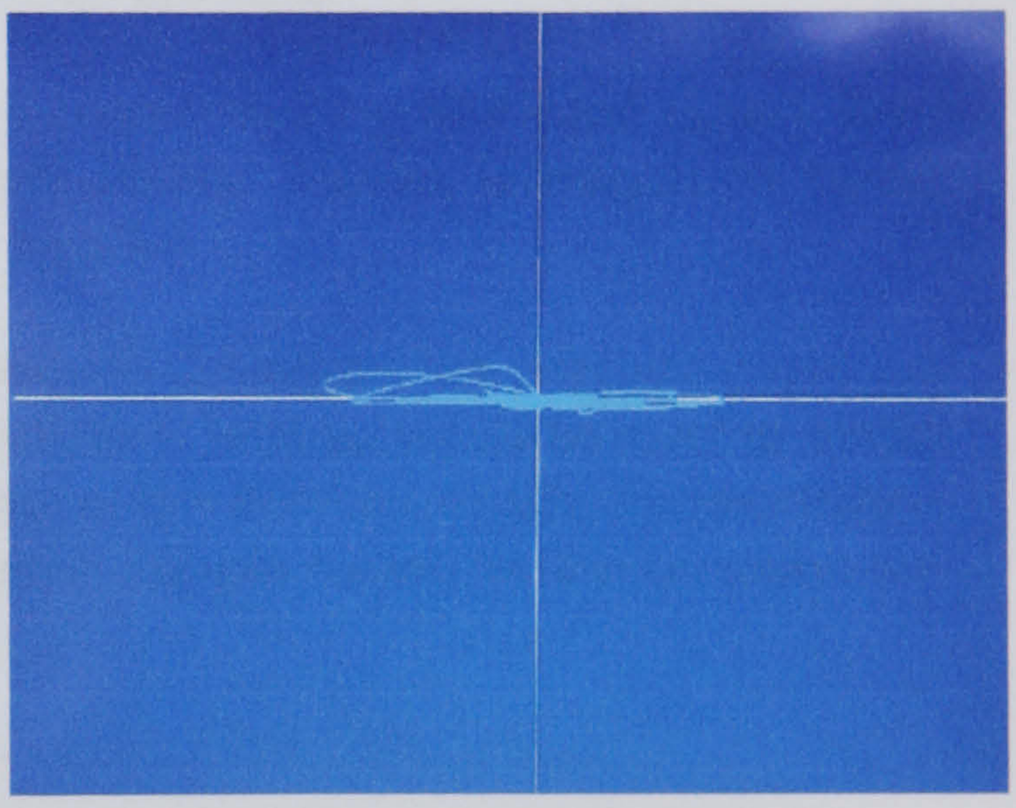

FIGURE 75 – AREA 34

All other areas of the casting not listed in the table above proved to be clear of, or show no significant indications when tested with Maxwell equipment using either the Remanent or Active probes [3C03, AD01].

As can be seen from the table there is correlation with corrosion and signals from corresponding areas at the outer face. Closer examination showed that the exact positioning of signals obtained did not directly correspond to the corrosion on the opposite face. This could be due to either the corrosion is meandering in the sample or that other magnetic properties are at play.

The extent of corrosion is unknown and without the ability to cut the samples and without reference samples to calibrate the equipment, it is difficult to draw firm conclusions.

9.4 Conclusion

As stated earlier the phase selective corrosion of Nickel aluminium Bronze is associated with κ_{III} phase, which occurs, in complex microstructures. The depth of the attack varies with size and distribution of the microstructures, and that coarser microstructures can result in deeper attacks. The corrosion mechanism is that of dealloying of the complex phase. accompanied by re-deposition of copper, thus retaining the grains surrounding the corroded κ_{III} as a spongy porous mass with little deformation or discolouration of the surface to indicate visually that corrosion has occurred.

The phase selective corrosion problem as stated is not easy one to solve. The material clearly has elements with magnetic properties and the phase selective corrosion is removing these elements. The material therefore has property changes that should and are, as it appears detectable. What was difficult was to quantify the detections; this clearly can only occur if samples of NAB with known phase selective corrosion are provided.

Maxwell and Eddy Flux examinations were further complicated by additional signals from within the material, which could not be investigated further. Further investigations would involve sectioning and metallurgical evaluation of the samples.

Whilst the results from remote surface are not quantifiable the initial work suggests inspection from the corrosion side would be more promising. Reference samples would be easer to obtain and detections would have signal to depth relationship as this does not require the penetration of many mm of material for detection and the material changes caused by the corrosion are closer to the detection sources.

9.5 Recommendations

It is clear that to provide conclusive evidence and quantifiable results from any technique evaluation, then samples of Nickel Aluminium Bronze with known corrosion are necessary.

The work carried out so far suggests that Maxwell examinations of thin section from remote side are feasible. However for definitive results then investigation of the other factors producing indications would be necessary.

Alternative method worthy of consideration in evaluating phase selective corrosion of NAB is that of ultrasonic spectroscopy.

10. FINAL COMMENTS

The traditional methods of Non-destructive inspection of non-ferrous casting, namely Ultrasonic, Radiography and Penetrants, failed to detect the specific discontinuities encountered in both Copper Nickel Chromium [CNC] and Nickel Aluminium Bronze [NAB]. The two studies offered in this report were conducted to find an NDT method that could not only detect but also evaluate the discontinuities such that the casting could be assessed for its fitness for purpose.

In an effort to have any success in applying or developing existing NDT methods, depends on understanding the morphology of what we are trying to find. Thus identifying the nature and material characteristics of the discontinuity became an equally important part of this work as to its detection.

Copper Nickel Chromium Castings [CNC]

In the case of CNC material the extensive metallurgical examinations identified the discontinuity to be oxides of Titanium, Zirconium and Silicon. The most insidious being oxides that produced thin linear type discontinuities.

After much consideration the method finalised for examining CNC castings was that of Eddy Current Testing. The application of eddy current was divided into high frequency surface detection and low frequency subsurface examination. Whilst the application of Eddy Current did not provide a complete solution, subsurface examination being limited to 10mm only, the good mechanical properties of the CNC material particularly its high toughness value helped to formulate a new philosophy on acceptance for castings where the thickness exceeded the eddy current penetrated values.

The fatigue trial conducted by Ministry of Defence laboratories showed that propagation of crack or linear type defects was minimal. Even linear type defects with 80% through wall depth did not propagate when subjected to fatigue cycles consistent with the products intended purpose. It was concluded therefore that the limited depth of examination for thick casting would suffice as a 10mm band around the product can be assessed to set defect levels. Eddy current test produces ECTP 5 for surface flaw detection and ECTP7 for subsurface examination were implemented.

Nickel Aluminium Bronze [NAB]

The selective phase corrosion of NAB is well documented since mid-1960's and the main mechanism of corrosion id that of dealloying of complex microstructures dominated by the kappa three phase [κ_{III}] a nickel aluminium structure with copper and nickel in solution. The presence of corrosion is not easy to recognise as the corroded material remaining is a spongy porous mass with little discoloration. The material properties of the affected area are much lower thus necessitating the detection and assessment on the amount corrosion present.

The application of the new electromagnetic methods will prove useful provided that corrosion assessment can be made from the corroded surface. The insurmountable task has been to detect and assess the corrosion from the surface remote to the corroded surface.

If detection and assessment from the corroded face is accepted then using the new eddy current/magneto-resistive sensors with Maxwell equipment and with appropriate samples will provide a method by with which quantitative evaluations can be made of this specific corrosion problem.

NAB is used extensively in the marine world and the industry is looking to find a suitable means of detection and assessment of selective phase corrosion.

REFERENCES

1. Powell C, ' Development of cast Copper-Nickel-Chromium alloy for Naval Service'. Journal of Metal and Materials, Dec 1990.

2. Dulay D.S, ' Defects and Non-destructive Testing Investment Casting'. Edited by P. R. Beely & R. F. Smart, the institute of Materials, University Press, Cambridge, UK.

3. Thomas, W.E., An Analytic Approach to Penetrant Performance. 1963 Lester Honor Lecture, Nondestructive Testing, Vol. 21, No. 6, Nov.-Dec. 1963, pp. 354-368

4. Clark, R., Dover, W.D., and Bond, L.J., The Effect of Crack Closure on the Reliability of NDT Predictions of Crack Size, NDT International, Vol. 20. No. 5, Guildford, United Kingdom, Butterworth Scientific Limited, October 1987. pp. 269-275.

5. Lovejoy D., ' Penetrant Testing A practical Guide', Chapman & Hall London UK 1990.

6. De Graaf, E. and De Rijk, P., Comparison Between Reliability. Sensitivity, and Accuracy of Nondestructive Inspection Methods, 13th Symposium on Nondestructive Evaluation Proceedings, San Antonio, TX, published by NTIAC, Southwest Research Institute, San Antonio, TX, April 1981, pp. 311-322.

7. Williams, H.J., Shockley, W. and Kittel. C. "Studies of the Propagation Velocity of Ferromagnetic Domain Boundary", Physical Review, Vol. 80, 1950.

8. F.B. Doane & C.E. Betz., 'Principles of Magnaflux'

9. Foerster F., ' Principles of Eddy Current Testing', Report No 132, Germany 1989

10. Hagemaier D. J, 'Eddy Current Impedance Plane analysis', Materials Evalaution, USA, Feb 1983

11. Dulay D.S., ' © NDT Consultants - Eddy Current Level I & II training notes', 1987.

12. Halmshaw R., ' Non-destructive Testing'. Edward Arnald, London UK 1987.

13. NES 824 Part1 Issue 2 May 1989, ' Copper Nickel Chromium sand castings and ingots', Part 1. MOD - Naval Engineering Standard.

14. Hall J.R., ' Investigation of defects in NES 824 Adapter Cover Casting produced at Rosyth Royal dockyard'. Mod Report R696/1 March 1991.

15. Plumb F.J., ' Summary Report into the examination of Heat Affected Zone Cracking in High Strength Cupro Nickel Chromium alloy NES 824', MOD report Naval Base Portsmouth TM 89021, 1989.

16. Gavin S.A, "The effect of impurities on the ductility of cupro-nickel alloy over a range of temperature". Ph. D Thesis, 1978, Cranfield University.

17. NDT Handbook, Second Edition Volume Three 'Radiography and Radiation Testing'. ASNT 1985

18. Neiderberger, R. B, " Composition and Heat treatment Effects on Dealuminisation of Aluminium Bronzes", Modern Castings, Vol 45, No.2 (1964)

19. Cooper, J.F. Private Communication Ministry of Defence. (1980)

20. Jackson, J.D., Classical Electrodynamics, pp. 210, 296-298, John Wiley &Sons,1975.

21. Libby H.L, "Introduction to Electromagnetic Nondestructive Test Methods", John Wiley & Sons, 1971.

22. NVE Sensor Engineering and Application Notes, Nonvolatile Electronics, INC.,1997.

23. Charlton, P.C. "A Theoretical and Experimental Study of the Magnetic Flux Leakage Method for the Analysis of Corrosion Defects in Carbon Steel Plate." February1995, Thesis -University of the West of England (Bristol).

24. Atherton, D.L. " Finite element calculation of magnetic flux leakage signals", NDT International, Vol 20, No.4, pp235-238, Aug. 1987

25. B. Wincheski, J.P. Fulton, S. Nath, M. Namkung, and J.W. Simpson, "Self-Nulling Eddy Current Probe for Surface and Subsurface Flaw Detection," *in Materials Evaluation*, Vol. 52/Number 1 (January 1994).

Appendix 1

Report from Babcock Technology Centre

' ASSESSMENT OF UT INSPECTABILITY OF Cu-Ni-Cr CASTINGS FOR BAe SEMA'.

BY

M FLYNN

SEPT. 1992

Babcock
Technology Centre

;SESSMENT OF UT INSPECTABILITY OF
u-Ni-Cr CASTINGS FOR BAe SEMA

/

FLYNN

PORT CLASS	:BABCOCK CONFIDENTIAL	CUSTOMER	: BAe SEMA
3COCK REPORT	: E/92/043	CUSTOMER REF	: ORDER M443/92/C2827/2
ɔ	: 6261	DATE	: SEPTEMBER 1992
?IC/D Number	: 78624/D001	STAFF NO.	: 0174
)NSOR	:ENGINEERING	SUBJECT CODE	: 71

Engineering Investigation Report

SUMMARY

The report describes work carried out to assess the cause of problems associated with the ultrasonic inspection of cast Cu-Ni-Cr material. It describes measurements made to assess attenuation, scattering, and beam distortion, with a view to determining the extent to which it is worthwhile pursuing an ultrasonic method for the inspection of this material. Metallographic examinations are described from which assessment of ultrasonic properties as a function of material microstructure were attempted.

The work has concentrated on the types of techniques which are normally applied for austenitic weld UT, where attenuation and noise levels are also high. While these techniques have been found to have some useful capability for inspection of the Cu-Ni-Cr material the sensitivity generally remains lower than is likely to be acceptable for contract inspections.

Recommendations for further work include the assessment of probes procured or designed specifically for Cu-Ni-Cr casting inspection and signal processing techniques.

WRITTEN BY : M Flynn STAFF NO: 0174

CHECKED BY : M. Flynn pp. B.W.O. Shepherd

APPROVED BY : MATERIALS TESTING MANAGER

The information in this report was compiled using procedures approved to ISO 9001

1. INTRODUCTION

BAe SEMA, under contract to the MOD, have been assessing the potential of volumetric techniques for the inspection of Cu-Ni-Cr castings. Radiography is considered to have inherent limitations for the detection of the type of defect of particular concern, viz. oxide inclusion networks. This leaves ultrasonics as the only practicable fully volumetric inspection technique.

The material has been reported as being very difficult to inspect ultrasonically, with evidence of high effective attenuation and high noise levels. These effects, which can vary locally, have been attributed to the coarse anisotropic grain structure.

High effective attenuation and high noise levels are also associated with the ultrasonic inspection of austenitic welds, an area in which Babcock Technology Centre have extensive experience. Babcock were therefore requested to undertake a systematic investigation of the attenuation, noise and beam skewing levels within the material and to correlate these effects to the microstructure. This was considered the most effective way of determining whether improvement in UT capability was a realistic proposition and if so what the basis of improved UT techniques might be.

2. TESTPIECES

Three blocks manufactured from cast Cu-Ni-Cr material were supplied by BAe SEMA, with the intention that if possible each should represent a different level of effective attenuation. Side drilled holes were machined into each block to provide ultrasonic targets at varying depths. The testpieces are shown in Figure 1.

The specimens were progressively machined to smaller thicknesses (see Figure 2), with ultrasonic measurements being repeated at each stage, in order to build up a picture of the effect on the beam of the varying material microstructure. Microstructure was determined by chemically etching and photographing specimen surfaces.

3. TESTPIECE MICROSTRUCTURE ASSESSMENT

Prior to any ultrasonic measurements being made, the three testpieces had all six surfaces chemically etched to show the grain structure present. These prepared surfaces were photographed, and these photographs are given in Figures 4, 5 and 6. Figure 3 defines surface numbers.

Testpiece #1 exhibits two distinct structures. Near most of the top surface (surface #4), long columnar grains are observed running vertically. This extends to a depth of approximately 10-15mm. The rest of the specimen consists of equiaxed grains of approximately equal size.

The grain size in testpiece #2 is apparently rather variable. Surface #5 exhibits a central area of small grain size, similar to areas of surface #4, testpiece #1. Surface #6 exhibits large columnar grains, evidence of which can also be seen on surface #1.

Testpiece #3 displays equiaxed grains generally of equal size. Surface #3 has some evidence of columnar grain structure.

Further assessment of microstructure was carried out at each stage of machining (see Figure 2 for machining details). Macrographs were taken of the newly exposed surfaces (Figures 7, 8 and 9) and also of the cross section at the centre line of the removed slices (Figures 10, 11 and 12). The centreline was in the plane of the angle beams applied so that these views show the grain structure along the beam path. These macrographs confirm that, with the exceptions noted above, the structure of the block material is uniform throughout.

Micrographs were also taken (at x10 magnification) of selected areas of these cross-sections. The areas photographed are defined in Figure 13, and the micrographs are given in Figures 14, 15 and 16. It was anticipated that detail not revealed in the macrographs would be apparent.

The micrographs show details of the material dendrites, the structure of which appears constant over the three blocks.

4. ULTRASONIC MEASUREMENTS

4.1. Probes

The ultrasonic properties of each of the testpieces were investigated using both angled and 0° compression wave probes. The probes used were as follows:

B2S-E 0° 2MHz 24mm ϕ single crystal

K1SM 0° 1MHz 28mm ϕ single crystal

45° 1MHz, twin crystal, 2(15mm x 25mm), focused at 45mm

60° 1MHz, twin crystal, 2(15mm x 25mm), focused at 45mm

45° 2MHz, twin crystal, 2(15mm x 25mm), focused at 60mm

60° 2MHz, twin crystal, 2(15mm x 25mm), focused at 55mm

70° 2MHz, twin crystal, 2(8mm x 13mm), focused at 15mm

70° 2MHz, twin crystal, 2(10mm x 18mm), focused at 30mm

The 0° probes are manufactured by Krautkramer, and the angled probes by RTD.

4.2. O° Compression Probe Measurements

Both 0° probes were used to measure the back-wall echo obtainable at each of six positions on each block. The six positions are defined in Figure 17. The measurements were repeated after each stage of machining. The results obtained are given in Table 1 in terms of decibels of gain required to set the back-wall echo to 80% full screen height (F.S.H.), as viewed on the flaw detector.

The echo amplitudes achieved tended to be uniform, within acceptable limits, over the three blocks. The one exception was the relatively high signals achieved on block #1, at the full thickness stage, compared with the other specimens. This is evident for both frequencies of probe. This phenomenon may be as a result of the area of columnar grains observed in this block, reducing the local effective attenuation.

Other, localised anomalies are apparent in the data. However, the material exhibits large variability in ultrasonic properties for small differences in probe position, and no conclusions can be inferred from these local effects.

This variability of back-wall signal amplitude on a given block/surface is significantly greater for the 2MHz probe, where differences of up to 13dB (Block #2, Stage T/2) can be observed. The maximum variance in the case of the 1MHz probe is 4dB.

4.3. Angled Compression Probe Measurements

4.3.1. Signal and Noise Measurements

The angled probes listed above were used to obtain signals from the various side drilled holes in the three specimens. Data collected included signal and noise amplitudes, range on the flaw detector screen, and probe stand-off from the plane of the holes.

Signal amplitude data and the corresponding signal to noise rates are given in Table 2. In order to maintain consistency between measurements made on each surface, all data was taken with the centre of the probe aligned with the centre of the testpieces. (The beams therefore passed along one of the planes from which macrographs were produced, see Section 3).

Signal to noise levels were generally poor, indicating poor detectability of the holes. The exceptions were the 70° F15 probe, and the 45° 1MHz probe. The 70° gave good results for near surface holes (especially the uppermost), whereas the 45° detected all but the uppermost hole with good signal to noise.

Generally, results were consistent across the three specimens, although some locally anomalous results appear. Using the generated signal/noise data, it is not possible to draw any general conclusions regarding the detectability of defects as a function of material microstructure.

4.3.2. Range & Stand-off Measurements

The range and stand-off measurements collected were used to plot the position of the reflectors in the testblocks. This gives an indication of the amount of beam skewing/distortion present. Diagrams showing the apparent positions of the holes as deduced from the experimental data are given in Figure 18. The RTD 60° 1MHz probe was omitted from this analysis due to its poor performance at detecting the holes. Note that the flaw detector range was calibrated using a stainless steel (304L) calibration block, and so the observed range may err by a small factor.

From the plots, it would appear that both 1MHz and 2MHz beams are distorted by the material, the angle altering as the beam penetrates the material. Distortion seems less for the 1MHz beam.

The RTD 45° 1MHz probe gives close agreement with actual hole position for all holes, though, as mentioned above, the general offsetting of the positions of plots of deeper holes implies some beam distortion. Agreement is similar for all three blocks.

The 45° and 60° 2MHz probes provide less reliable positions for the holes. The 60° 2MHz plots do not conclusively show any general distortion.

The 70° 2MHz probes accurately position near surface holes, but display what appears to be decreasing beam angle with increasing range in the material.

5. CONCLUSIONS/RECOMMENDATIONS

5.1. The microstructure of the three test specimens used generally displays equiaxed grains of uniform size. However, areas of columnar grain structure also exist.

5.2. Micrographs of the material reveal a generally uniform structure across the selected areas.

5.3. The columnar grain structure appears to display lower effective attenuation than the other observed condition.

5.4. Cu-Ni-Cr has locally highly variable attenuation for 2MHz ultrasonic beams. This variability is lessened by use of 1MHz beams.

5.5. Detectability of holes is greater for the 1MHz 45° probe than for 2MHz probes. The 70° 2MHz F15 probe gives good detectability for near surface holes.

5.6. The material structure is such that the ultrasonic beams are diverted from their true angle, which apparently increases with increasing range for the 45° 2MHz probe and decreases for the 45° 1MHz probe. The 2MHz 60° probe does not conclusively show any consistent distortion.

5.7. The optimum probes are those which, from Babcock experience in austenitic weld and casting inspection, were anticipated to be best. However, the overall sensitivity using these existing probes is likely to fall some way short of that required, even for fully optimised procedures.

The agreement between predicted and achieved probe performance supports the belief that experience gained from austenitic weld and casting UT can help to guide the development of UT techniques for Cu-Ni-Cr castings. On this basis it is considered that there is scope for achieving improvements in UT inspection capability for this material.

The two main approaches which could be adopted (possibly in parallel) are:

— Assessment of probes procured specifically for Cu-Ni-Cr casting inspection featuring e.g. stacked crystals (instead of side-by-side design), reduced crystal sizes to minimise scattering volume etc.

— Assessment of enhanced techniques incorporating signal processing techniques such as spatial averaging which should improve signal to noise ratio.

TABLES

BLOCK 1

Position	Stage T	Stage 3T/4	Stage T/2	Stage T/4
1	46	43	41	36
2	46	43	42	36
3	45	43	43	36
4	45	43	41	36
5	46	43	41	36
6	47	42	41	36

BLOCK 2

Position	Stage T	Stage 3T/4	Stage T/2	Stage T/4
1	51	46	41	36
2	51	45	42	36
3	49	46	43	36
4	50	44	44	36
5	52	45	43	36
6	48	44	41	36

BLOCK 3

Position	Stage T	Stage 3T/4	Stage T/2	Stage T/4
1	49	44	41	36
2	49	45	41	37
3	48	43	41	36
4	50	47	42	36
5	48	44	40	35
6	47	44	40	36

Figures quoted are dB to 80% FSH.

Ref. signal = 33dB to 80% FSH
(40mm thickness of A4 Block)

K1SM 0° (1MHz) PROBE MEASUREMENTS

TABLE 1A

BLOCK 1

Position	Stage T	Stage 3T/4	Stage T/2	Stage T/4
1	46	42	33	24
2	43	38	37	21
3	33	39	31	20
4	38	40	34	21
5	39	41	37	20
6	41	41	35	19

BLOCK 2

Position	Stage T	Stage 3T/4	Stage T/2	Stage T/4
1	53	40	36	19
2	51	48	44	28
3	58	42	41	26
4	48	40	28	22
5	55	42	33	26
6	48	37	33	22

BLOCK 3

Position	Stage T	Stage 3T/4	Stage T/2	Stage T/4
1	51	41	36	25
2	48	48	39	21
3	52	37	32	23
4	49	42	33	23
5	39	37	31	17
6	47	44	34	21

Figures quoted are dB to 80% FSH.

Ref. signal = 12dB to 80% FSH
(40mm thickness of A4 Block)

BS2E 0° (2MHz) PROBE MEASUREMENTS

TABLE 1B

PROBE: RTD 45° 1MHz f ≈ 45mm

REF SIG: 34dB to 80% FSH

	SIGNAL TO 80% FSH/SIGNAL TO NOISE (dB)			
BLOCK 1	**STAGE T**	**STAGE 3T/4**	**STAGE T/2**	**STAGE T/4**
TOP	ND	ND	69/4	ND
2nd TOP	57/15	57/11	61/6	
3rd TOP	58/13	59/7		
4th TOP	61/7			
BLOCK 2				
TOP	ND	ND	ND	ND
2nd TOP	61/9	61/7	61/5	
3rd TOP	61/9	58/11		
4th TOP	61/9			
BLOCK 3				
TOP	ND	ND	ND	ND
2nd TOP	63/6	59/9	59/8	
3rd TOP	56/15	58/9		
4th TOP	59/11			

ND - Not Detectable

Table 2A

PROBE: RTD 60° 2MHz f ≈ 55mm

REF SIG: 40dB TO 80% FSH

	SIGNAL TO 80% FSH/SIGNAL TO NOISE (dB)			
BLOCK 1	**STAGE T**	**STAGE 3T/4**	**STAGE T/2**	**STAGE T/4**
TOP	ND	ND	ND	ND
2nd TOP	74/7	75/5	78/3	
3rd TOP	73/8	ND		
4th TOP	ND			
BLOCK 2				
TOP	ND	ND	ND	ND
2nd TOP	75/5	74/5	72/8	
3rd TOP	76/4	ND		
4th TOP	ND			
BLOCK 3				
TOP	ND	74/7	ND	ND
2nd TOP	72/8	76/4	74/6	
3rd TOP	ND	ND		
4th TOP	ND			

ND - Not Detectable

Table 2D

PROBE: RTD 70° 2MHz f ≈ 15mm

REF SIG: 41dB TO 80% FSH

	SIGNAL TO 80% FSH/SIGNAL TO NOISE (dB)			
BLOCK 1	**STAGE T**	**STAGE 3T/4**	**STAGE T/2**	**STAGE T/4**
TOP	50/15	55/12	52/18	50/19
2nd TOP	64/6	67/4	68/4	
3rd TOP	ND	ND		
4th TOP	ND			
BLOCK 2				
TOP	58/11	54/16	51/15	54/17
2nd TOP	ND	ND	65/10	
3rd TOP	ND	ND		
4th TOP	ND			
BLOCK 3				
TOP	49/18	52/20	56/12	56/10
2nd TOP	64/10	64/9	62/14	
3rd TOP	ND	ND		
4th TOP	ND			

ND - Not Detectable

Table 2E

PROBE: RTD 60° 1MHz f ≈ 45mm

REF SIG: 51dB to 80% FSH

	SIGNAL TO 80% FSH/SIGNAL TO NOISE (dB)			
BLOCK 1	**STAGE T**	**STAGE 3T/4**	**STAGE T/2**	**STAGE T/4**
TOP	ND	ND	ND	ND
2nd TOP	70/7	ND	ND	
3rd TOP	ND	ND		
4th TOP	ND			
BLOCK 2				
TOP	ND	ND	ND	ND
2nd TOP	ND	ND	ND	
3rd TOP	ND	ND		
4th TOP	ND			
BLOCK 3				
TOP	ND	ND	ND	ND
2nd TOP	ND	ND	ND	
3rd TOP	ND	ND		
4th TOP	ND			

ND - Not Detectable

Table 2C

PROBE: RTD 45° 2MHz f ≈ 60mm

REF SIG: 37dB to 80% FSH

	SIGNAL TO 80% FSH/SIGNAL TO NOISE (dB)			
BLOCK 1	**STAGE T**	**STAGE 3T/4**	**STAGE T/2**	**STAGE T/4**
TOP	ND	ND	ND	ND
2nd TOP	70/5	65/10	ND	
3rd TOP	69/6	70/6		
4th TOP	74/8			
BLOCK 2				
TOP	ND	ND	ND	ND
2nd TOP	74/6	69/6	69/8	
3rd TOP	77/3	67/5		
4th TOP	ND			
BLOCK 3				
TOP	ND	ND	ND	ND
2nd TOP	ND	71/7	70/7	
3rd TOP	ND	ND		
4th TOP	ND			

ND - Not Detectable

Table 2B

PROBE: RTD 70° 2MHz f ≈ 30mm

REF SIG: 36dB to 80% FSH

	SIGNAL TO 80% FSH/SIGNAL TO NOISE (dB)			
BLOCK 1	**STAGE T**	**STAGE 3T/4**	**STAGE T/2**	**STAGE T/4**
TOP	66/5	69/4	70/5	65/8
2nd TOP	59/12	65/8	69/6	
3rd TOP	66/7	ND		
4th TOP	ND			
BLOCK 2				
TOP	69/7	61/12	67/4	ND
2nd TOP	69/6	66/8	ND	
3rd TOP	ND	ND		
4th TOP	ND			
BLODK 3				
TOP	64/6	62/9	ND	71/4
2nd TOP	60/8	67/7	67/9	
3rd TOP	ND	ND		
4th TOP	ND			

ND - Not Detectable

Table 2F

FIGURES

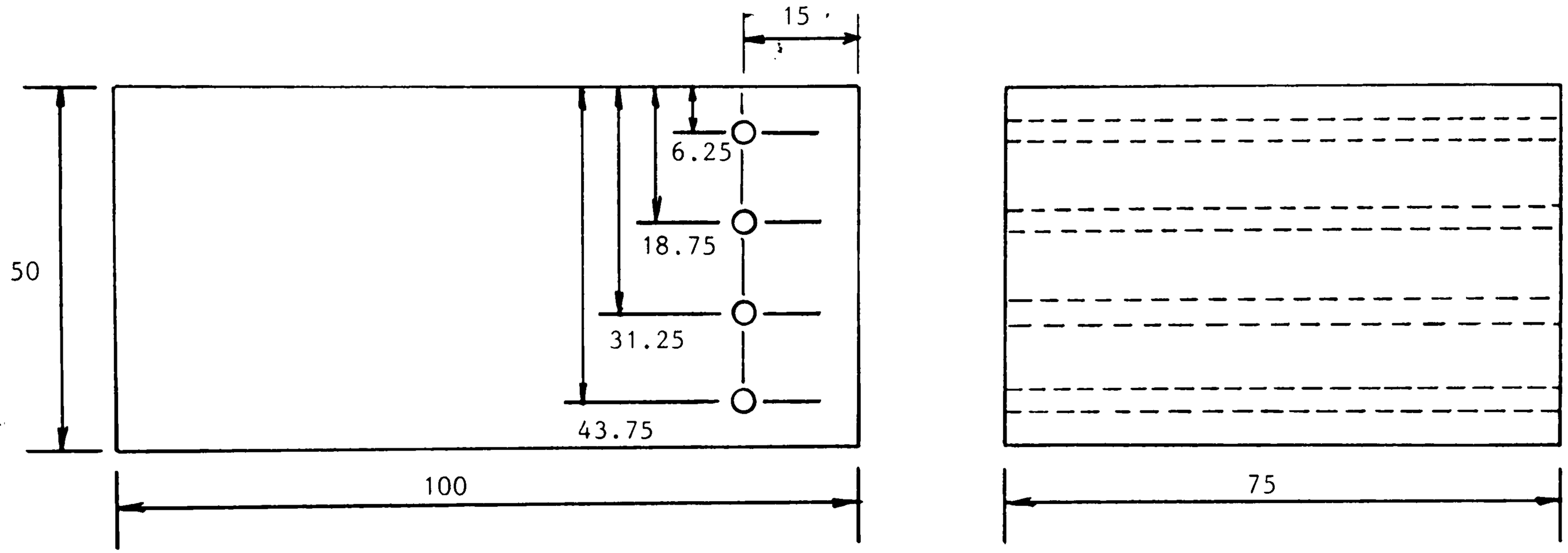

Cu-Ni-Cr Testpieces
containing 4-off 3mmØ side drilled holes. 3-off thus, ID nos 1,2&3

Figure 1

1. Progressive Machining to
   Smaller Thicknesses

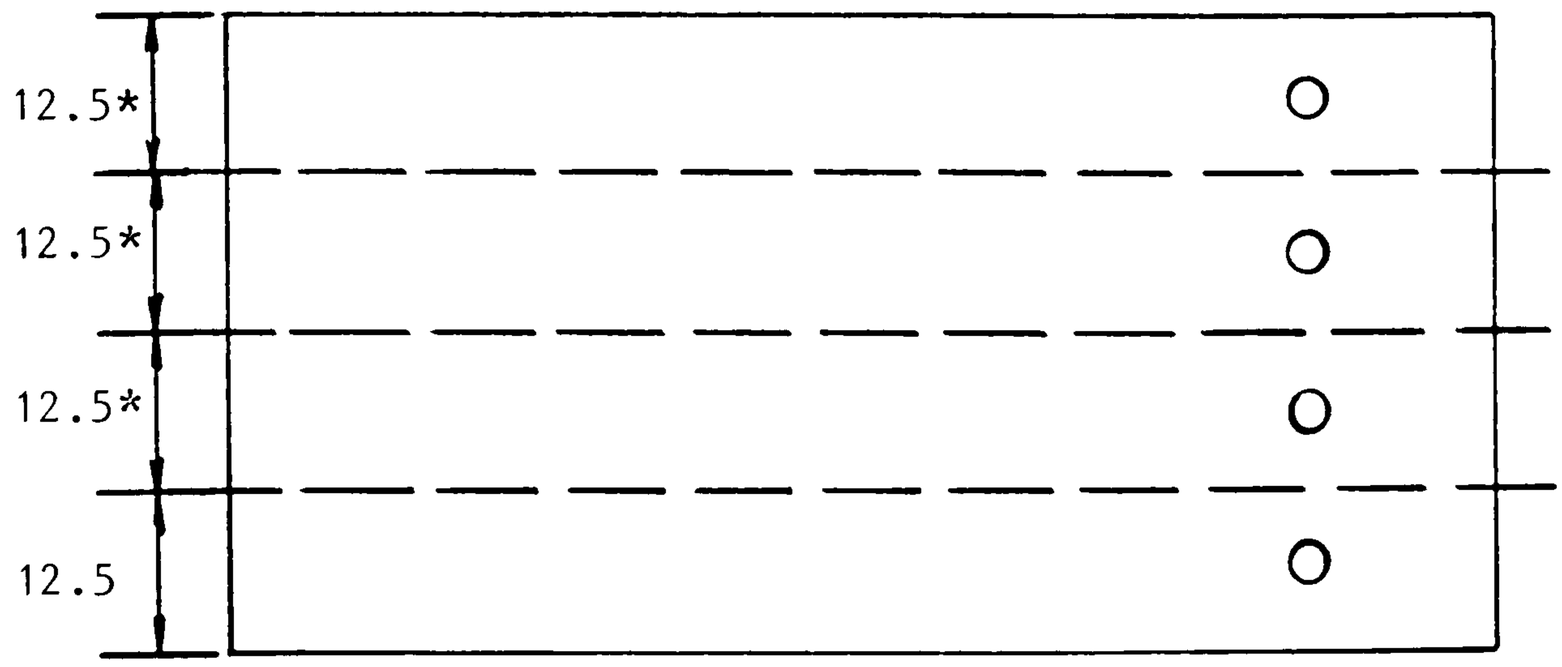

2. Machining of Slices Removed
   as Above

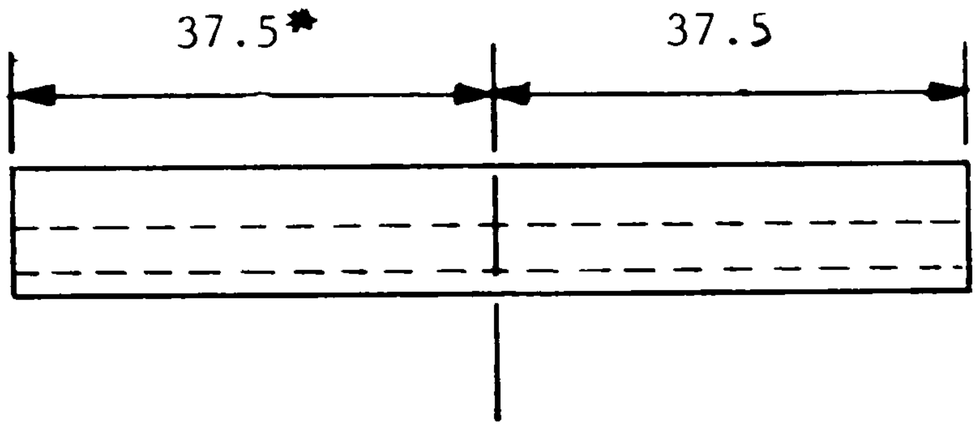

NB Dimensions marked '*' indicate the amount of material removed.

Illustration of Sequential Machining

Figure 2

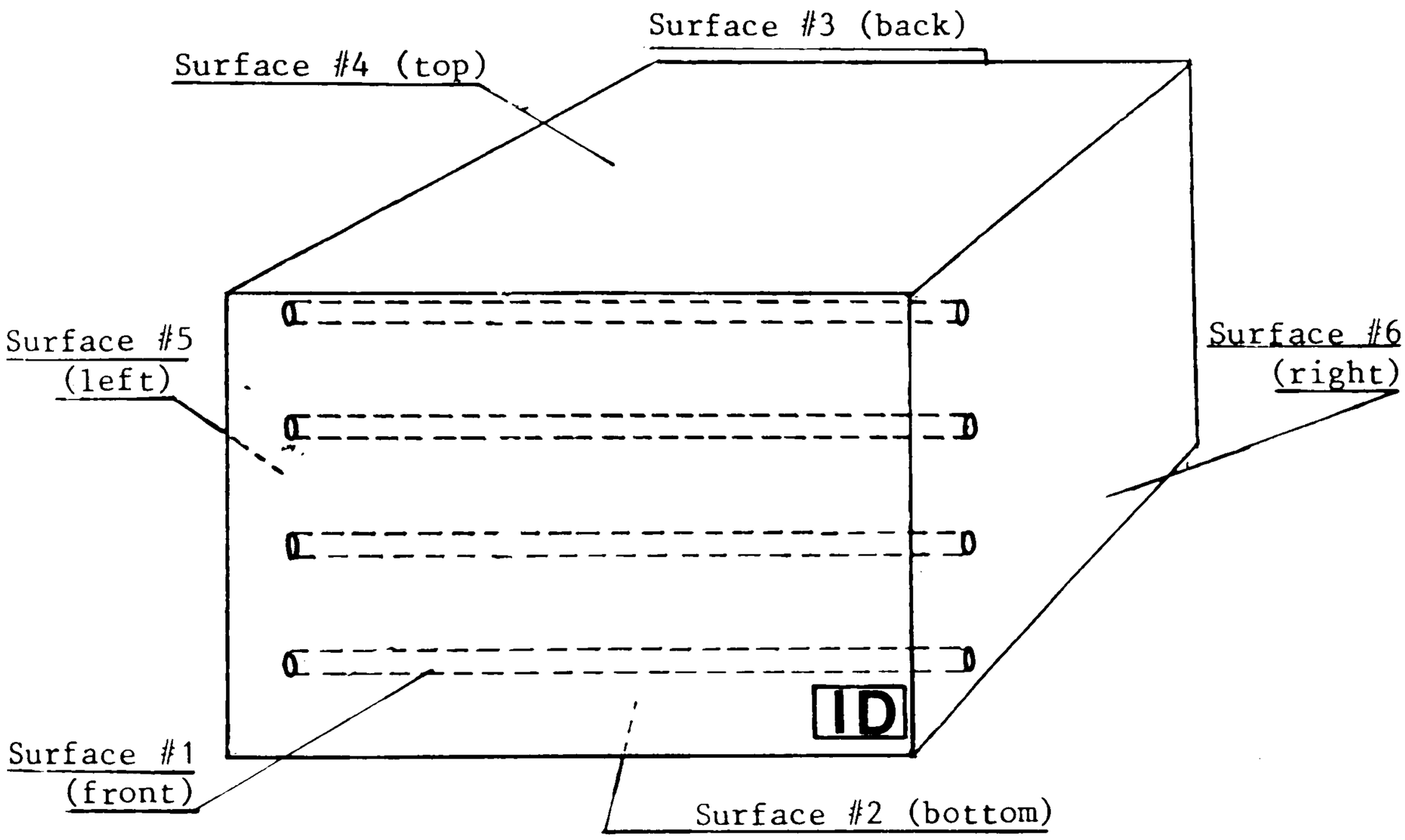

Definition of Surface Numbers

Figure 3

Appendix 2

EDDY CURRENT TEST EQUIPMENT

SURACE INSPECTION & SUBSURFACE INSPECTION

1 Surface Flaw Detection Equipment

Equipment used to carry out Eddy current surface flaw detection was as follows:

Instrument: Portable Crack Detection Unit

Probes: Austenitic – Swan neck and pencil type.

Accessories: Teflon Tape and Sheet of acetate – this is necessary for reducing wear of the probe when scanning surfaces in the as cast condition. The Teflon type is applied to the probe tip and the acetate sheet is placed on the components surface.

Equipment Details: Foerster – Defectometer 2.837

Specification

Flaw resolution	To approximately 20 μm (0.0008 inch)
Dynamic range.	20 dB in steps of 0.5 dB
Zero offset	O to 100 scale divisions (sd) in steps of 1 sd
Alarm thresholds	Two, variable in steps of 1 sd, with on/off option
Flaw indicator	Visual as segment on the LCD, acoustic on speaker or headphones, analog signal on pin in analog I/0 socket
LCD	128 x 128 pixel, with switchable back lighting, high contrast in sunlight.

Power		3x battery (alkaline "D", IEC lR20, 1.5V), or 3x Ni-CD battery (e.g. IEC KR 35/62), or external power supply (input 220 VAC, output 12 VDC; 110 VAC / 12VDC in USA)
Operating duration with batteries		>8h
Battery indicator		Warning “"BAT" if operating time is less than 10 minutes
Housing		ABS plastics, kerosene and oil resistant
Membrane keypad		10 membrane keys, dust and waterproof
Dust and *water* proofing		IP 54
Permissible ambient temperature		-10°C to +55°C (14°F to 131°F)
Permissible storage temperature		-55°C to +85 °C (-67°F to 185°F)
Permissible humidity		5% to 95%
Mass (with batteries)		0.95 kg {2.1Ib)
Connections:	Probe	Socket S-pin DIN 41524
	RS232	Connector DB-9P
	Analog I/0	Socket 6-pin DIN 45322
Accessories:	Printer cable	DB-9S to DB-25P for EPSON compatible printer
	PC cable	DB-9S to DB-9S, null modem wiring for data communication PC-to-PC
Maximum test speed		Approx. 0.1 -0.15 *m/s* (4 -6 inch/s) depending on probe characteristics.

Probe Details:	**Manufacture- Foerster UK.**
Frequency	2.0 MHz
Probe Diameter	3.00mm
Coil Diameter	– 2.00mm

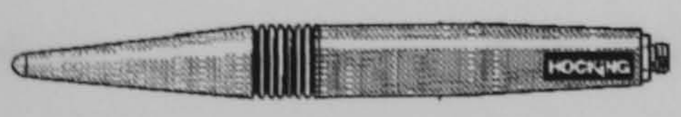

Pencil Type Probe

Swan Neck Type Probe

2 Sub-Surface Flaw Detection Equipment

Equipment used to carry out Eddy Current sub-surface flaw detection was as follows:

Instrument:	Eddy Current Phase Analysis Unit
Probes:	Specifically modified reflection type spot faced probe
Accessories:	Teflon Tape and Sheet of acetate – this is necessary for reducing wear of the probe face when scanning surfaces in the as cast condition. The Teflon type is applied to the probe face and the acetate sheet is placed on the components surface.

Equipment Details: Hocking **AV100L**

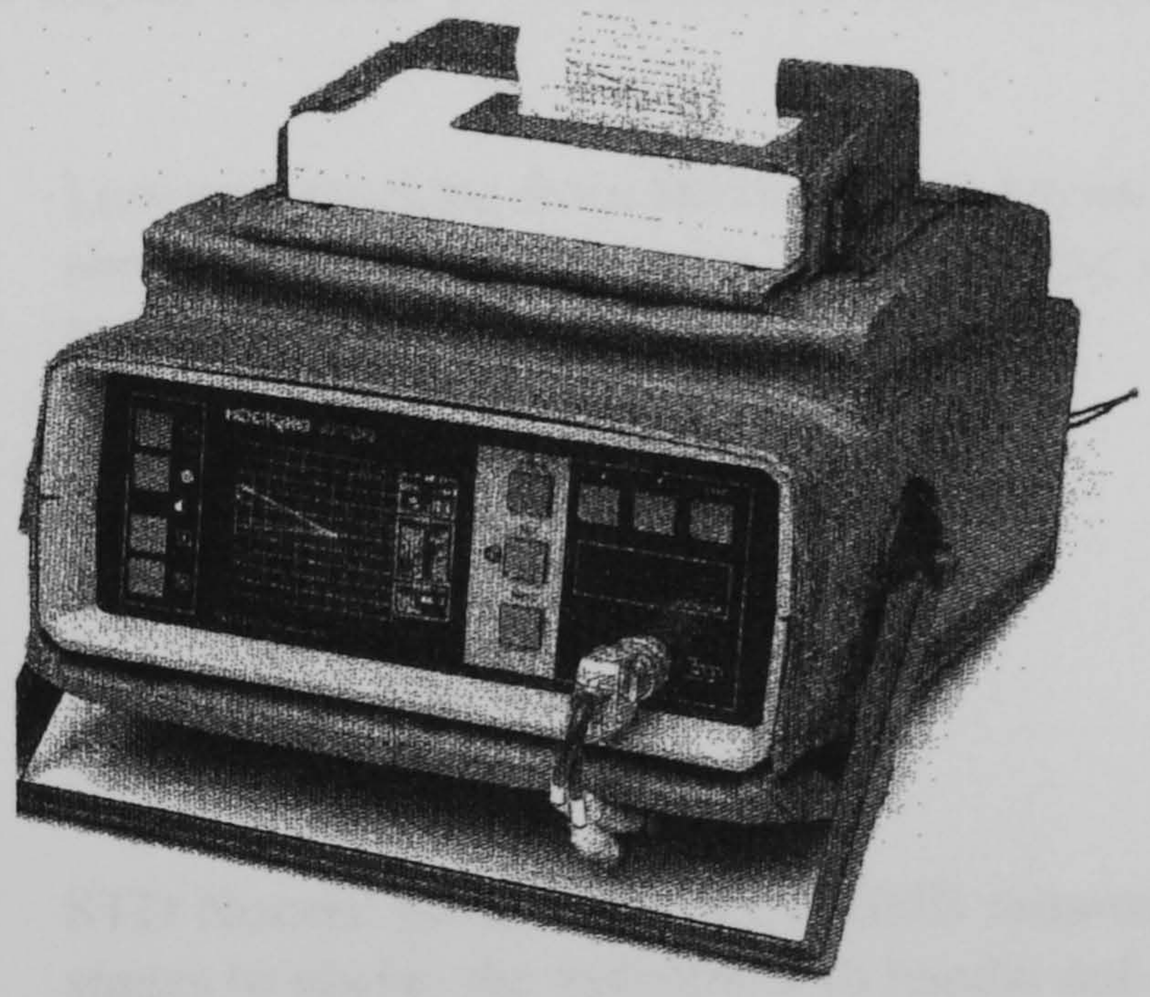

Specification:

Eddy Current Performance

Frequency Range: 80Hz to 6MHz. Crystal controlled.

Drive: ±2V into 50 ohms. Automatically increased by 6dB below 300Hz.

Gain: 10-70dB in 0.5dB steps. Sensitivity at maximum gain is 300V/ohm.

Noise: Less than 0.5 div at maximum gain for balanced load.

Phase: 0-360 degrees rotation in 0.5 degree steps.

Store: STD, constant storage, variable persistence times of' 2s, 0.5s, 0.1s. When the alarm is used and the signal exceeds the threshold the unit reverts to the constant storage mode for a short period.

Erase: Full screen erase will eliminate all signals on the screen. Depressing this control twice will remove the menu. Half screen erase will erase only the right hand half of the screen. Operating EXEC in this mode transfers the right hand half to the left hand half, this enables calibration signals to be placed on the screen while operating.

Alarm: Operates on vertical axis. Options of positive only, positive and negative, with or without audible indication.

Alarm Level: Settable from 10 to 100%.

Y:X Ratio: Adjusts the gain in the horizontal or vertical axis independently. Menu display is a ratio Y : X. Ratios are 10:1, 5.1,2.1,1:1, 1:2, 1:5, 1:10.

Automatic Fixed Filter: Low pass tracking from 80Hz-8kHz 0.5m sec time constant above 8kHz. This filter is for optimum noise and inspection speed.

HP High pass filter: STD =DC (no high pass filter)
1=2Hz 3=10Hz 5=40Hz
2 = 5Hz 4 = 20Hz

LP Low pass filter: In addition to fixed filter
STD = 250Hz 1 = 60Hz 2 = 20Hz

Input gain: STD Normal gain (70dB). Low 20dB removed from input stages to enable the instrument to handle out of balance loads.

Programming: 16 internal memories enable the 16 sets of control settings to be stored in the instrument memory. The storage procedure is to CLEAR location then SAVE. Cleared location indicated by horizontal line. Valid program indicated by filled box. Corrupted program indicated by broken line. Altered program by A. Called program by C.

Display

Resolution: 80mm x 100mm High Resolution Display, pixel size 0.25mmxO.2mm. Graticule displayed with no parallax. Working spot visible above stored signals.

Brilliance: Adjustable by control on rear. X V

Shift: Adjustable by control on rear.

Inputs/Outputs

Probe: 6-pin socket for absolute, differential or reflection probes.

Remote 25-way connector: Remote keyboard capability, separate sync arid video output.

Ancillary 25-way connector: RS232 and parallel printer output. **X Y:** Analogue horizontal and vertical inputs and output 0.5V/div.

Charger: Either 31CU11 for overnight charging or 31CU12 for quick charging can be used.

Video O/P: Composite video for TV type monitor.

Probe:

Probe Details: **Hocking – Special reflection type probe**

Frequency **300 Hz – 100KHz**

Probe Diameter **24.00mm**

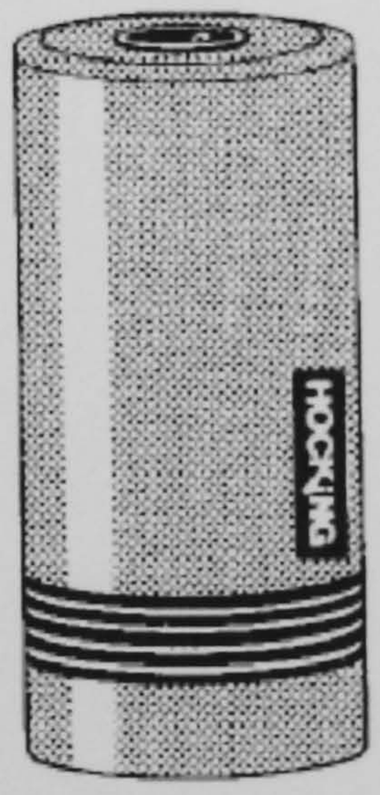

Appendix 3

EDDY CURRENT TEST PROCEDURE

ECTP5

SURFACE INSPECTION OF CAST NES 824 MATERIAL

BY

D S DULAY

NON DESTRUCTIVE TEST PROCEDURE - EDDY CURRENT INSPECTION (ECTP5)

CAST NES 824 - SURFACE DISCONTINUITIES

INDEX

1. Scope

2. Reference Documents

3. Personnel Requirements

4. Examination Coverage

5. Surface Preparation

6. Equipment

7. Calibration Procedure

8. Examination Procedure

9. Defect Reporting

ANNEX A - Details of Calibration Blocks

ECPT5

NON DESTRUCTIVE TEST PROCEDURE - EDDY CURRENT INSPECTION OF CAST NES 824 FOR SURFACE DISCONTINUITIES

SCOPE

1. a. This procedure is to be used to detect the presence of surface breaking oxide inclusion networks in High Strength Cu-Ni-Cr Alloy (NES 824) Castings. Defect Acceptance is to be evaluated in accordance with Clause 1108 of NES 824 Part 1, Issue 3.

REFERENCE DOCUMENTS

2. a. NES 729 Part 3, Issue 2 - 'Requirements for Non Destructive Examination Methods, Eddy Current'.

b. NES 824 Part 1, Issue 3 - 'Copper Nickel Chrome Sand Castings and Ingots, Production Requirements'.

PERSONNEL REQUIREMENTS

3. a. Personnel performing this examination are to have been adequately trained to the levels appropriate to their responsibilities and be capable of working to the requirements of NES 729 Part 3 and this procedure.

AREA OF EXAMINATION

4. a. All accessible areas of machined surfaces, particularly sealing surfaces and all areas of as cast surfaces in way of oxide discontinuities found by the subsurface inspection of ECTP7.

SURFACE PREPARATION

5. a. The area to be examined shall be clean, dry and free from loose scale and debris.

EQUIPMENT

6. a. All equipment shall satisfy the requirements of NES 729 Part 3 Issue 2.

b. A portable High Frequency Impedance Eddy Current Flaw Detector with Fe, NFe and Austenitic (Aust) probe facility.

c. Austenitic shielded pencil type eddy current probe.

d. Austenitic shielded right angle tip eddy current probe.

e. Deep Crack Probe (for defects greater than 4 mm in depth).

NOTE: It is recommended that PTFE or insulation tape is applied to the tip of probes to enable them to slide smoothly over surfaces and prevent wear to the tips.

Such protection shall be in place during calibration and scanning.

f. A calibration standard made from Cast NES 824 material/ see Annex A, for details.

CALIBRATION PROCEDURE

a. Check battery level of EC test equipment.

b. Connect probe and select 'Aust' operation mode.

c. Balance the probe by carrying out lift off compensation and zero compensation on one of the appropriate calibration standards ie whether for as cast or machined surface inspection. This procedure should be carried out clear of edges and slots.

d. Obtain the maximum deflection from the required slot (based on 0.1t, where 't' is the material thickness) and adjust the gain or sensitivity to give a meter reading of 80% full scale deflection.

e. Set the audio or visual alarm to trigger at a threshold level of 80% full scale deflection.

f. The equipment is now calibrated and ready for the examination procedure on either machined or as cast surfaces depending upon the calibration test blocks used.

EXAMINATION PROCEDURE

7. a. Scanning of Plane Surfaces

The following procedure is to be used for testing all areas other than edges and curved surfaces which are covered separately in paras 7a and 7b below.

(1) Place the probe away, from edges etc at the area of interest and balance the equipment by carrying out zero compensation. This should be done in more than one position to avoid the possibility of setting up on a defective area.

(2) Scan 100% of the area of interest. A scan pitch of 2mm is recommended, with the probe axis being maintained normal to the inspection surface at all times. Each area of interest should be subject to at least 2 scans whose directions are 90° to each other, for maximum sensitivity.

(3) Whilst scanning the meter reading may deviate from the zero position owing to local conductivity changes in the base material. When this happens, zero compensation is to be carried out prior to the continuation of further testing.

b. Scanning Edges

(1) Place the probe at the edge to be examined and balance the equipment. Normally zero compensation will be sufficient.

(2) Scan smoothly along the edge, preferably with an edge support/guide to maintain a constant distance and probe angle relative to the surface.

c. Scanning Curved Surfaces

When testing curved surfaces with shielded probes, under normal conditions the need to rebalance the equipment should be minimal. However if the equipment type or component geometry causes an imbalance the following procedure should be adopted to compensate.

d. Convex Surfaces

To test convex surfaces lift off compensation is carried out on the curved surface and zero compensation is carried out on a level surface.

e. Concave Surfaces

To test convex surfaces, lift off compensation is carried out on a level surface and zero compensation is carried out on the curved surface.

REPORTING OF DEFECTS

With the instrument calibrated to the appropriate 0.1t slot, all meter readings greater than 80% FSD, other than those that can be attributed to spurious indications, are to be recorded and their location marked on the casting.

Indications are to be assessed against the Acceptance Standards contained in NES 824 Part 1 Issue 3.

Record and reporting should comply, where applicable to that required by Figure 1 of NES 729 Part 3 Issue 2.

CALIBRATION BLOCKS FOR SURFACE INSPECTION

MATERIAL: DEFECT FREE CAST NES 824

BLOCK 1

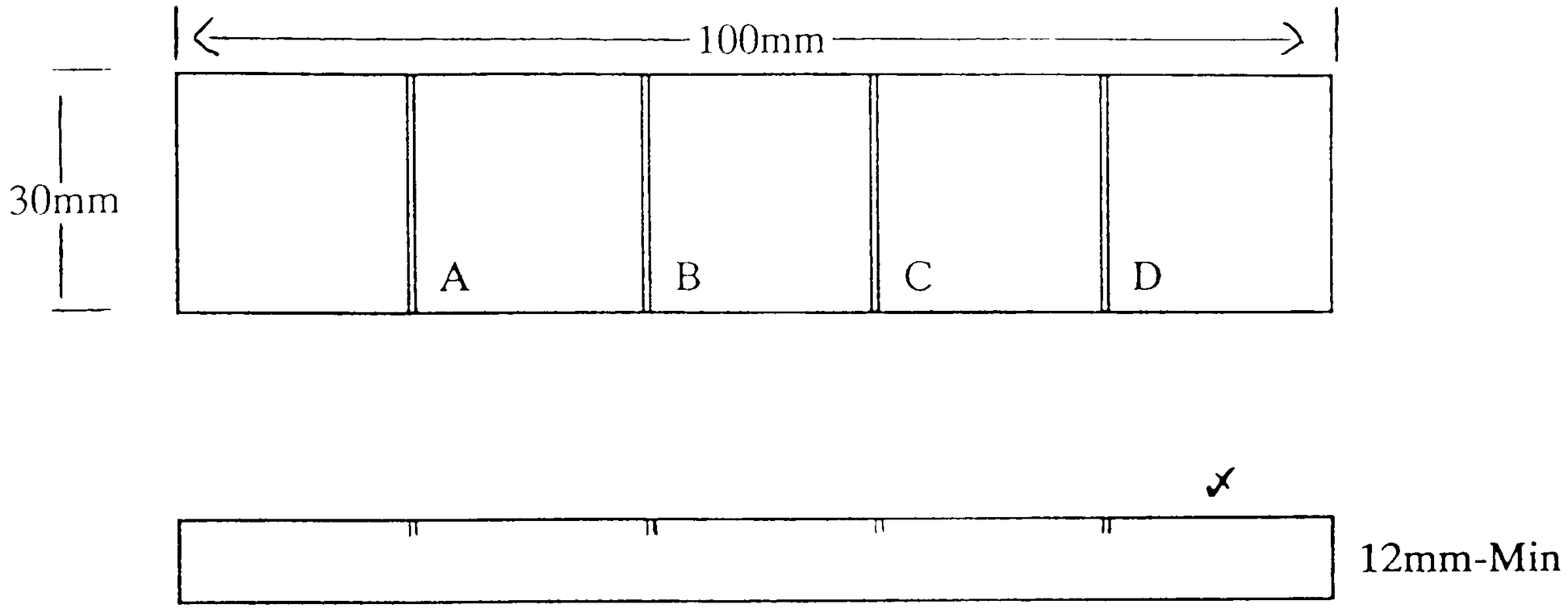

Targets A, B, C and D - Slots 1, 2, 3 and 4 - 6mm depth each approx 0.25mm width.

✓ = Machined Surface.

BLOCK 2

Similar to Block 1 except that surface ✓ is to be left in the as cast condition.

NB: Overall size of block given is for guidance only.

Appendix 4

EDDY CURRENT TEST PROCEDURE

ECTP 7

SUB-SURFACE INSPECTION OF CAST NES 824 MATERIAL TO DEPTH OF 10MM

BY

D S DULAY

NON DESTRUCTIVE TEST PROCEDURE - EDDY CURRENT INSPECTION (ECTP7)

CAST NES 824 - SUBSURFACE DISCONTINUITIES TO 10 MM BELOW THE SURFACE

INDEX

1. Scope

2. Reference Documents

3. Personnel Requirements

4. Area of Examination

5. Surface Preparation

6. Equipment

7. Calibration Procedure

8. Examination Procedure

9. Scanning Edges

10. Eddy Current Signatures

11. Reporting Defects

ANNEX A - Details of Test Blocks

ANNEX B - Typical Example of Equipment and Test Parameters use for Inspection

ANNEX C - Atlas of Eddy Current Signatures

ECTP7

NON DESTRUCTIVE TEST PROCEDURE - EDDY CURRENT INSPECTION OF CAST NES 824 FOR SUBSURFACE DISCONTINUITIES DOWN TO DEPTHS OF 10 MM

SCOPE

1. This procedure is to be used to detect the presence of subsurface oxide inclusion networks to depths of 10 mm below the surface in High Strength Cu-Ni-CR. Alloy (NES 824) Castings. Defect Acceptance is to be evaluated in accordance with Clause 1109 of NES 824 Part 1, Issue 3. It is recommended that the examination covered by this procedure is post examination of surface breaking oxide discontinuities in accordance with ECTP5.

REFERENCE DOCUMENTS

2. a. NES 729 Part 3, Issue 2 - Requirements for Non Destructive Examination Methods, Eddy Current.

b. NES 824 Part 1, Issue 3 - Copper Nickel Chrome Sand Castings and Ingots. Production requirements.

c. ECTP5 Eddy Current Test Procedure - Surface Inspection

d. ECTP6 Eddy Current Test Procedure - Subsurface Inspection (Optional Intermediate inspection)

PERSONNEL REQUIREMENTS

3. a. Personnel performing this examination are to have been adequately trained to the levels appropriate to their responsibilities and be capable of working to the requirements of NES 729, Part 3 and this procedure.

AREA OF EXAMINATION

4. a. All accessible areas of machined and as cast surfaces.

NOTE: The EC signal interpretation is better on machined surfaces as very rough surfaces are apt to introduce lift off Signals.

SURFACE PREPARATION

5. a. The area to be examined shall be clean, dry and free from loose scale and debris.

b. If the casting has an uneven surface or a surface roughness which presents scanning difficulties, it is suggested that the appropriate production authorities be

S:

consulted with a view to preparing the surface by light grinding/polishing to achieve unambiguous scanning results.

EQUIPMENT

6. a. All equipment shall satisfy the requirements of NES 729, Part 3, Issue 2.

b. A phase analysis Eddy Current Flaw Detector with a wide frequency range of 100 Hz to 3 MHz.

c. A reflection type Eddy Current probe with a frequency range of 100 Hz to 100 KHz.

NOTE: It is recommended that the PTFE or insulation tape is applied to the probe to enable it to slide smoothly over surfaces and prevent wear to the tip. Such protection shall be in place during calibration and scanning.

d. Calibration standards made from cast NES 824 material; see Annex A, for details.

e. A sheet of polythene may be used to overcome very rough surface problems and if used shall be in place during calibration and scanning.

CALIBRATION PROCEDURE

7. a. The details involved in the calibration procedure will vary to some degree, depending on the particular phase analysis instrument being used. A typical procedural example using an Institute Dr Forster DEFECTOSCOP AF 2.833.01 is shown at Annex B.

b. It is important that to avoid varying signal amplitudes, scanning speeds for both calibration and actual examination are the same for each and are to be as uniform as possible.

c. Check equipment and controls as per manufacturers instructions.

d. Connect probe via appropriate cables and adjust equipment parameters to maximise probe output.

e. Set the frequency control to 2 KHz.

f. Set the gain (dB) level to mid range (60dB)

g. Place the probe on the calibration block and balance the probe away from any discontinuity and edges. Ensure that the spot displace (ie zero position) is at the centre of the CRT.

h. Lift the probe off the calibration block and observe the direction of lift-off; adjust phase until display moves horizontally from centre point to left and off screen.

i. Pass the probe over a discontinuity, signal response should be in the vertical direction.

j. Pass the probe over the discontinuity at 5 mm depth and observe the height of the signal response.

k. Adjust the gain to achieve a discernible response from the discontinuity (approximately 2 screen divisions in height)

l. The equipment is now calibrated and ready for the examination procedure.

m. To expedite testing of the component, the use of a flaw gating system is recommended. The gate should trigger when the response to 7(k) is achieved or exceeded.

EXAMINATION PROCEDURE

8. a. The following steps are to be used for testing all areas other than edges which are covered, in paragraphs 9(a) and (b).

b. Place the probe away from edges etc, at the area of interest and balance the equipment by carrying out zero compensation.

NOTE: Equipment utilising a High Pass filter operating at other than static frequency will not require zero compensation.

c. If applicable, check the balance condition at new but similar position in case the first zero compensation was carried out on a discontinuity.

d. Scan 100% of the area of interest with 2 passes at 90° to each other. A scan pitch of ½ probe diameter and maintaining the probe normal to the surface at all times is recommended.

SCANNING EDGES

9. a. Place the probe at the edge to be examined and balance the equipment.

b. Scan smoothly along the edge, preferably, using an edge support. It is essential to keep the probe at a constant distance and angle to the edge being scanned.

REPORTING OF DEFECTS

10. To aid the interpretation of the eddy current signatures obtained during testing, reference should be made to ANNEX C which contains an Atlas of eddy current signatures for non linear and linear type discontinuities.

11. With the instrument calibrated in accordance with this procedure all discontinuities exceeding the threshold level set should be plotted and assessed in accordance with NES 824 Part 1 Issue 3. Records and report should comply, where applicable to that required by Figure 1 of NES 729 Part 3 Issue 2.

NOTE: If required the sub-surface depth of the discontinuity found can be gauged by examining the phase angle of Eddy Current signal present.

ANNEX A

CALIBRATION BLOCKS FOR SUBSURFACE INSPECTION

MATERIAL: CAST NES 824 - DEFECT FREE

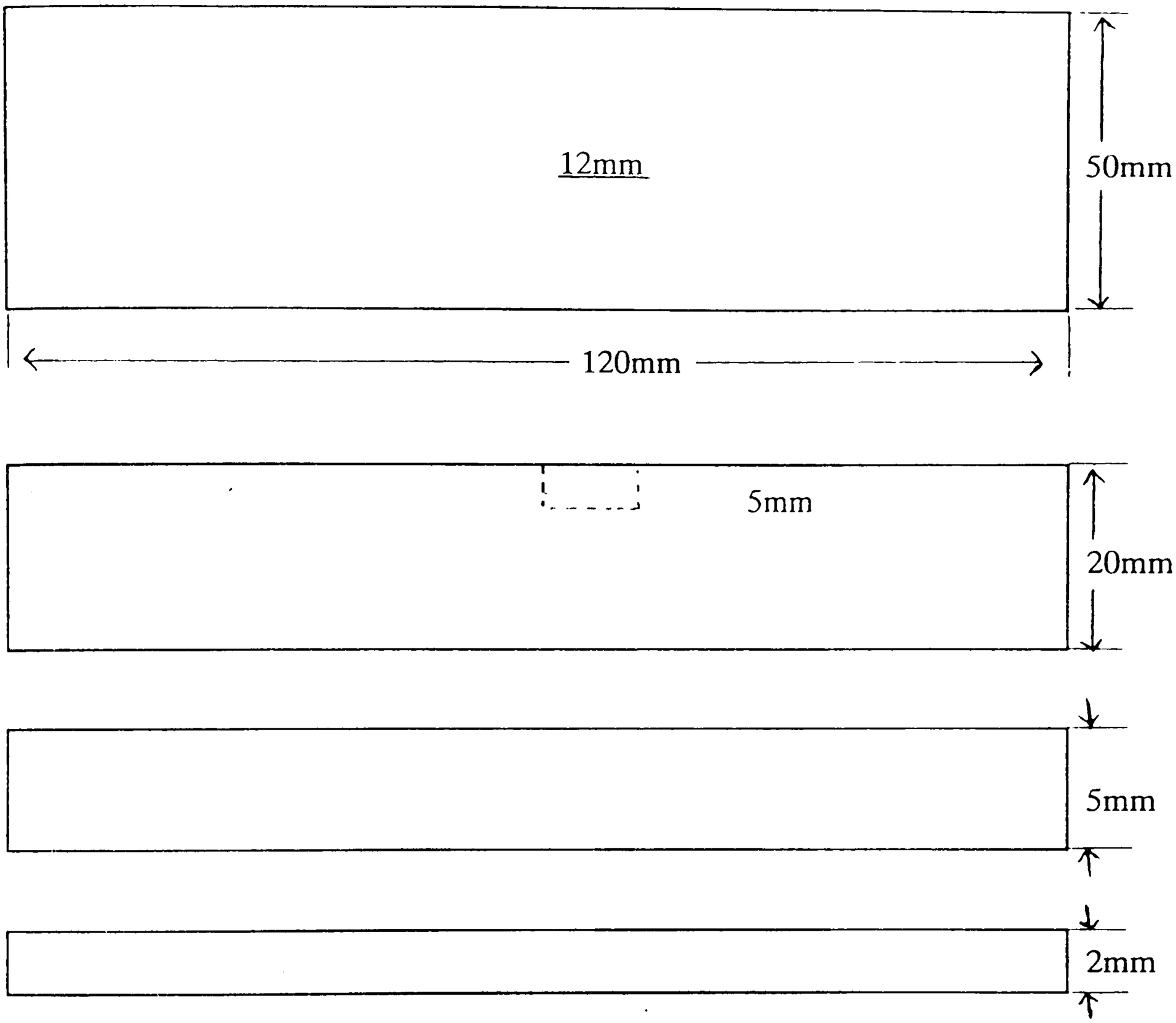

Block 50mm wide
Target EDM Slot 5mm depth approx 0.25mm width
Test coupons: 2mm x 50mm x 100mm
5mm x 50mm x 100mm
= machined surface.

NB 1: Overall size of block given is for guidance only

NB 2: The 2mm coupon is there so that the inspector can determine phase relationships if required to gauge sub-surface depths of discontinuities detected.

S

ANNEX B

EDDY CURRENT EVALUATION OF NES 824

The following are actual equipment and test parameters used for sub surface inspection of NES 824.

EQUIPMENT: INSTITUT DR FOSTER
DEFECTOSCOP AF 2.833.01

PROBE: REFLECTION TYPE
OPERATING FREQUENCY 300 Hz - 100 KHz
16 mm diameter

CABLES/ADAPTERS: CABLE; 2 832.01 0 9901
ADAPTER; 2.832.01 - 1326333

EQUIPMENT SETTINGS:

DRIVE	6
ATTENUATION	0 dB
FREQUENCY	2.0 KHz
PHASE	163 degs
GAIN	60.0 dB
Y - SPREAD	12.0 dB
HIGH PASS FILTER (HP)	0.5 Hz
LOW PASS FILTER (LP)	100 Hz
THRESHOLD TYPE	'Y' - SYMMETRICALLY
THRESHOLD SETTING	30%

CALIBRATION:

Reference: 0.010" wide slot 5mm below the surface with a 5mm height and 12mm length.

INSTITUT DR FOERSTER

DEFECTOSCOP AF 2.833 2.2 SN 25

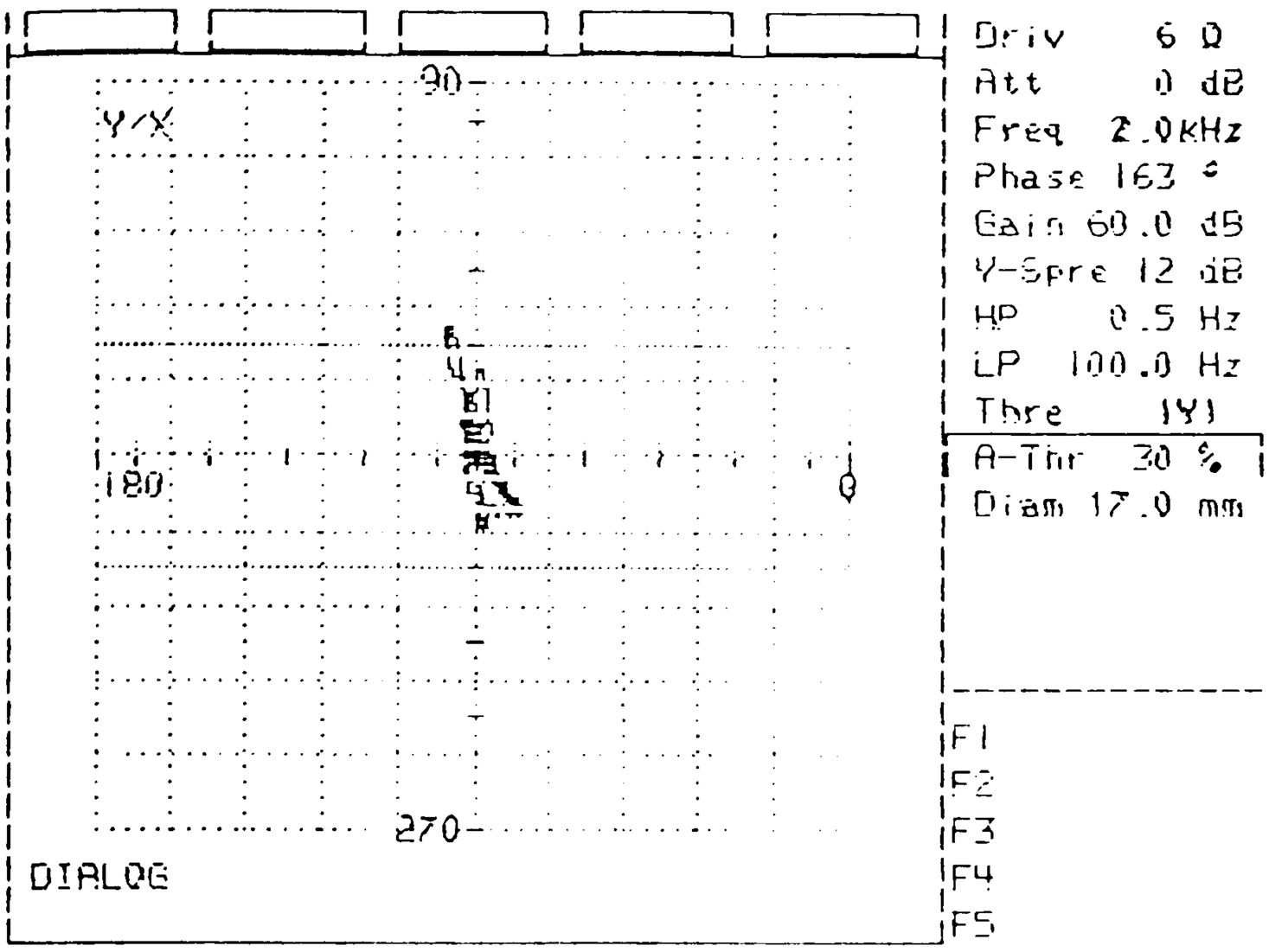

FIGURE 1: SIGNAL RESPONSE FROM REFERENCE SLOT 5 x 12mm, 5mm BELOW THE SCANNING SURFACE

ATLAS OF EDDY CURRENT SIGNATURES

VERSUS NON LINEAR

METALLURGICAL CONDITIONS

DEFECT DEPTH 0 - 5MM

OBSERVATIONS MADE DURING THE ASSESSMENT OF INDICATIONS

1. A LOOP TYPE EFFECT IS PREVALENT ON THE POSITIVE SIDE OF THE LESAJOUSE FIGURE, REGARDLESS OF WHETHER THE SIGNAL ARISES FROM SHRINKAGE OR OXIDE EFFECTS.

2. WITH SHRINKAGE THE POSITIVE ELEMENT OF THE LESAJOUSE FIGURE IS INTENSIFIED AS THE RESULT OF A SIGNIFICANT NUMBER OF IMPEDANCE CHANGES BEING DETECTED OVER A SMALL AREA.

3. WHERE OXIDE NETWORKS EXIST, THE POSITIVE ELEMENT OF THE LESAJOUSE FIGURE IS OF A LOOP TYPE WHILST THE NEGATIVE ELEMENT BECOMES INTENSIFIED.

4. IN THE MAIN, FEATHERING TYPES OF SIGNAL ARE INDICATIVE OF OXIDE NETWORKS, WHILST LINEAR TYPE SIGNALS ARE ASSOCIATED WITH SHRINKAGE OR VOIDS.

5. OXIDE INDICATIONS SHOW INTENSIFIED CENTRAL AREAS AND REINFORCEMENT OF THE NEGATIVE ELEMENT OF THE LESAJOUSE AND PORTRAY AN OVERALL FEATHERY NATURE OF SIGNAL.

6. SHRINKAGE SHOWS IN THE MAIN A LINEAR SIGNAL , THE SIGNATURE BEING INTENSIFIED IN BOTH THE POSITIVE AND NEGATIVE AREAS OF THE LESAJOUSE. THE MAIN INTENSIFICATION APPEARS IN THE POSITIVE ELEMENT.

7. DISCONTINUITIES CLOSE TO THE SURFACE TEND TO SHOW A LARGE LOOP WHICH SURROUNDS THE INTENSIFIED POSITIVE ELEMENT OF THE LESAJOUSE.

EXCEPTIONS

1. VERY FINE (MICRO) SHRINKAGE MAY AT TIMES BE CONFUSED WITH OXIDE NETWORKS DUE THE VERY SIMILAR NATURE OF THE INDICATIONS.

2. THE 0° TO 90° WINDOW ON THE DEFECTOSCOP HAS BEEN FOUND TO CONTAIN A 5mm BELOW THE SURFACE ENVELOPE AND DOES NOT PERMIT ACCURATE DEPTH DETERMINATION WITH RESPECT TO THE TYPE OF DEFECT SOUGHT.

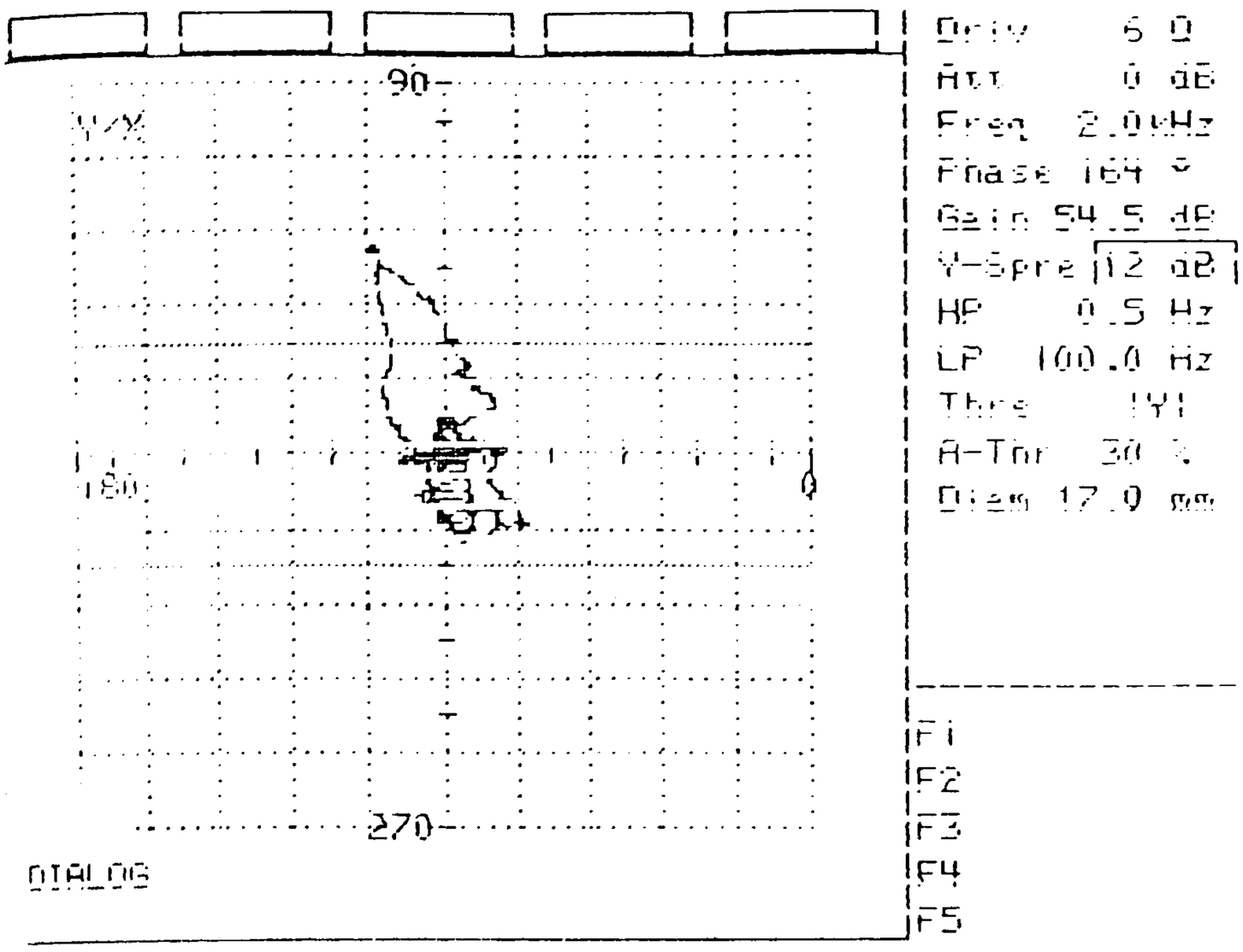

SURFACE BREAKING
OXIDE INDICATION

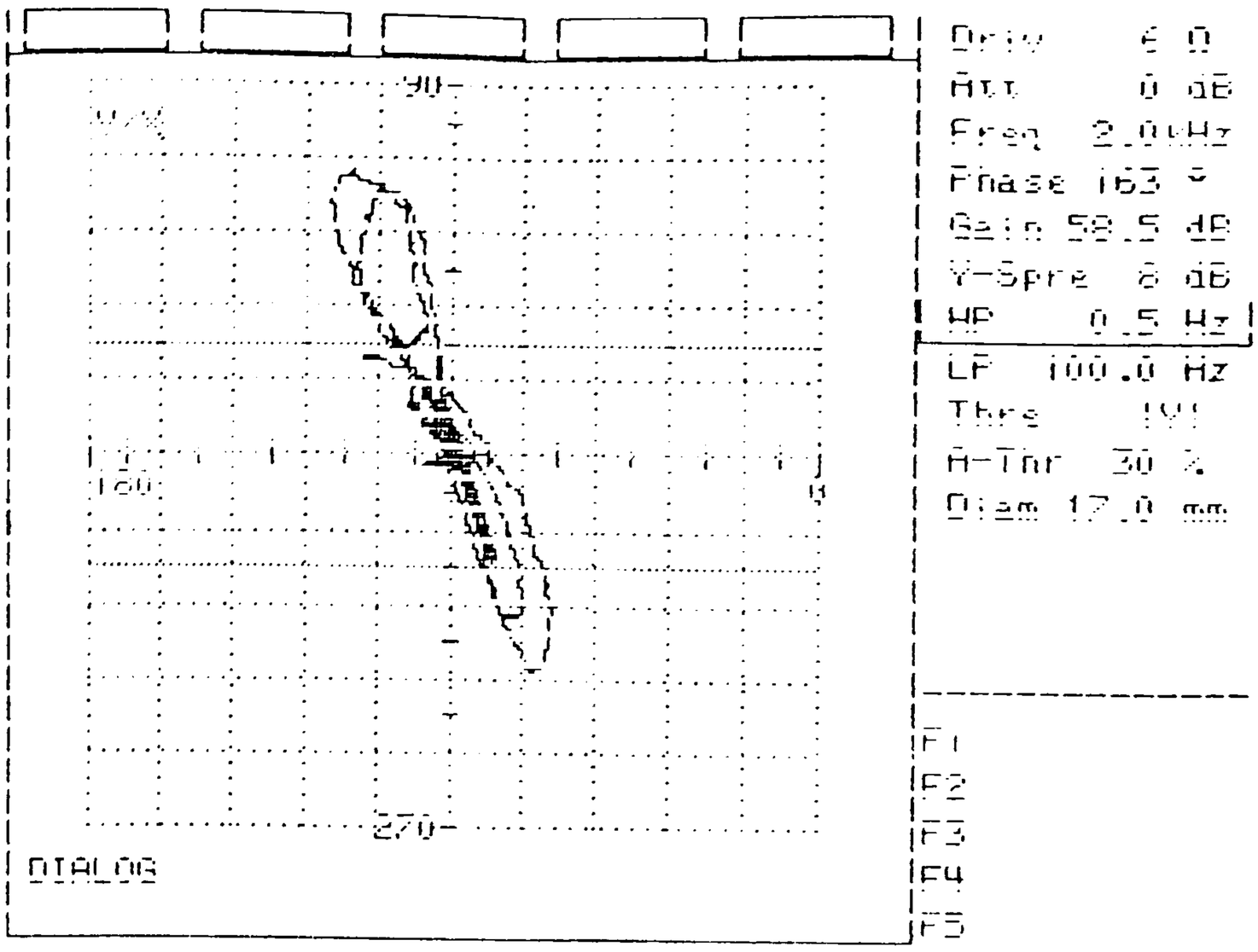

SURFACE BREAKING
OXIDE INDICATION

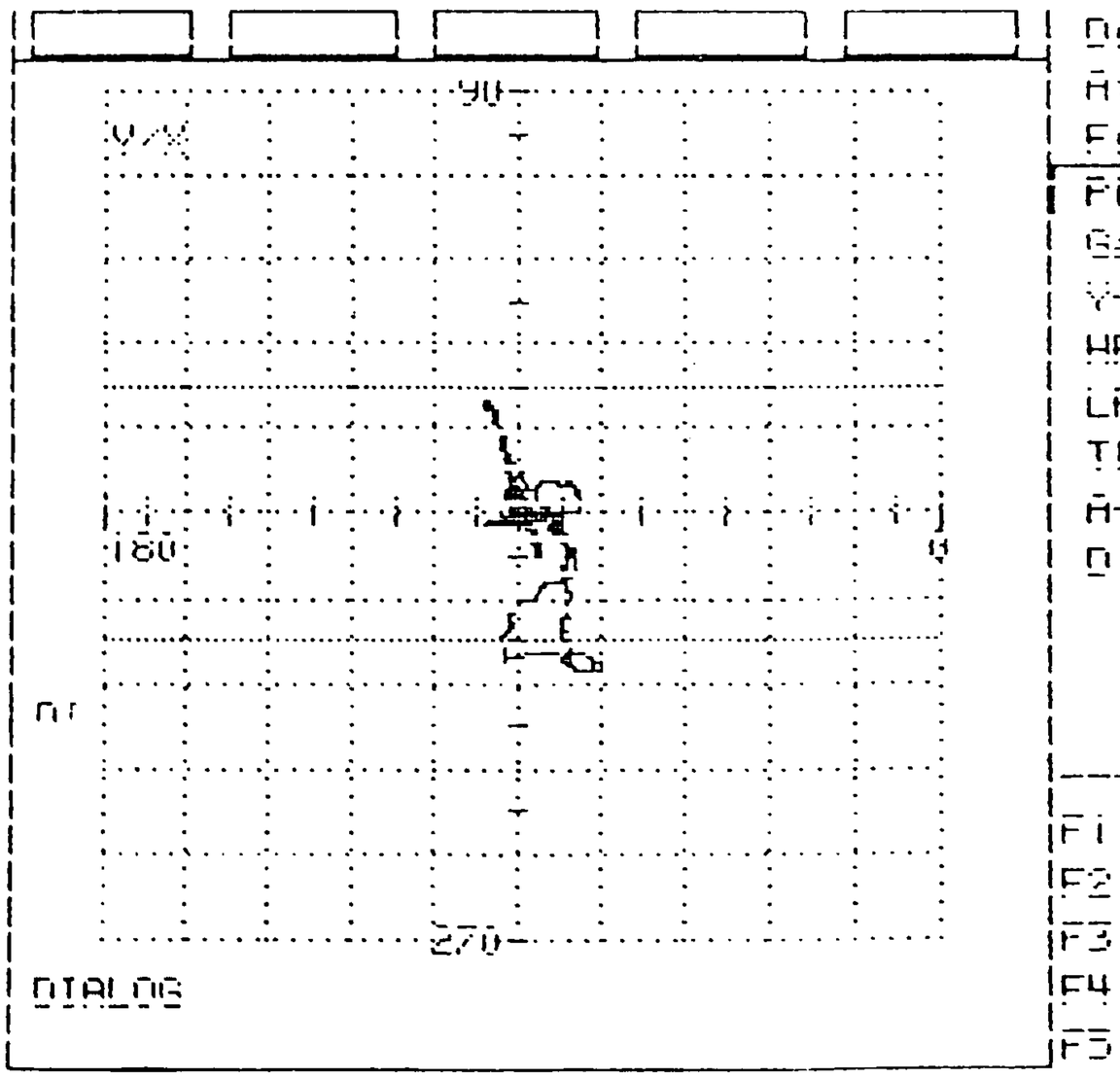

OXIDE INDICATION

SC-000-7933

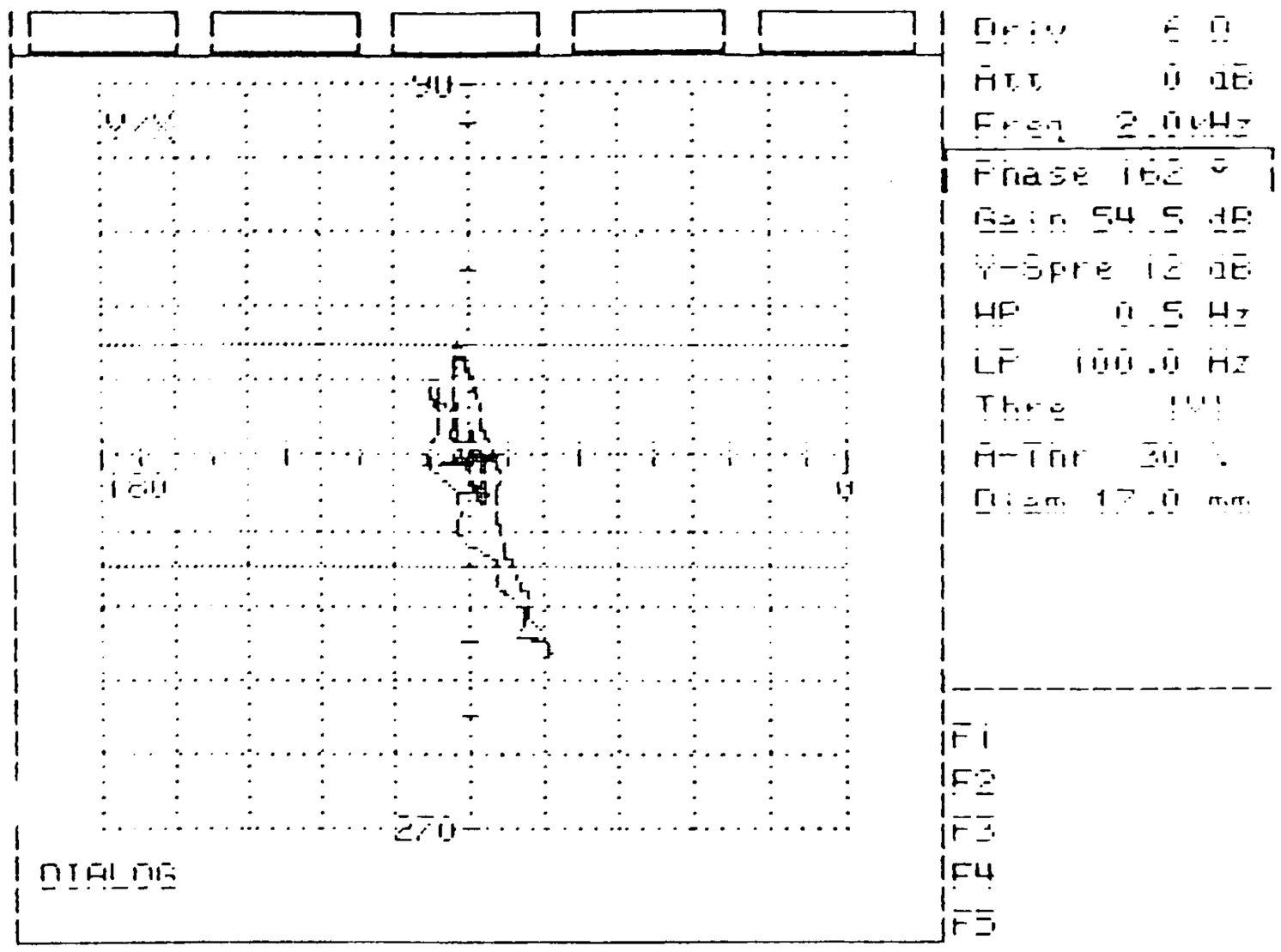

OXIDE INDICATION

SC-000-3905

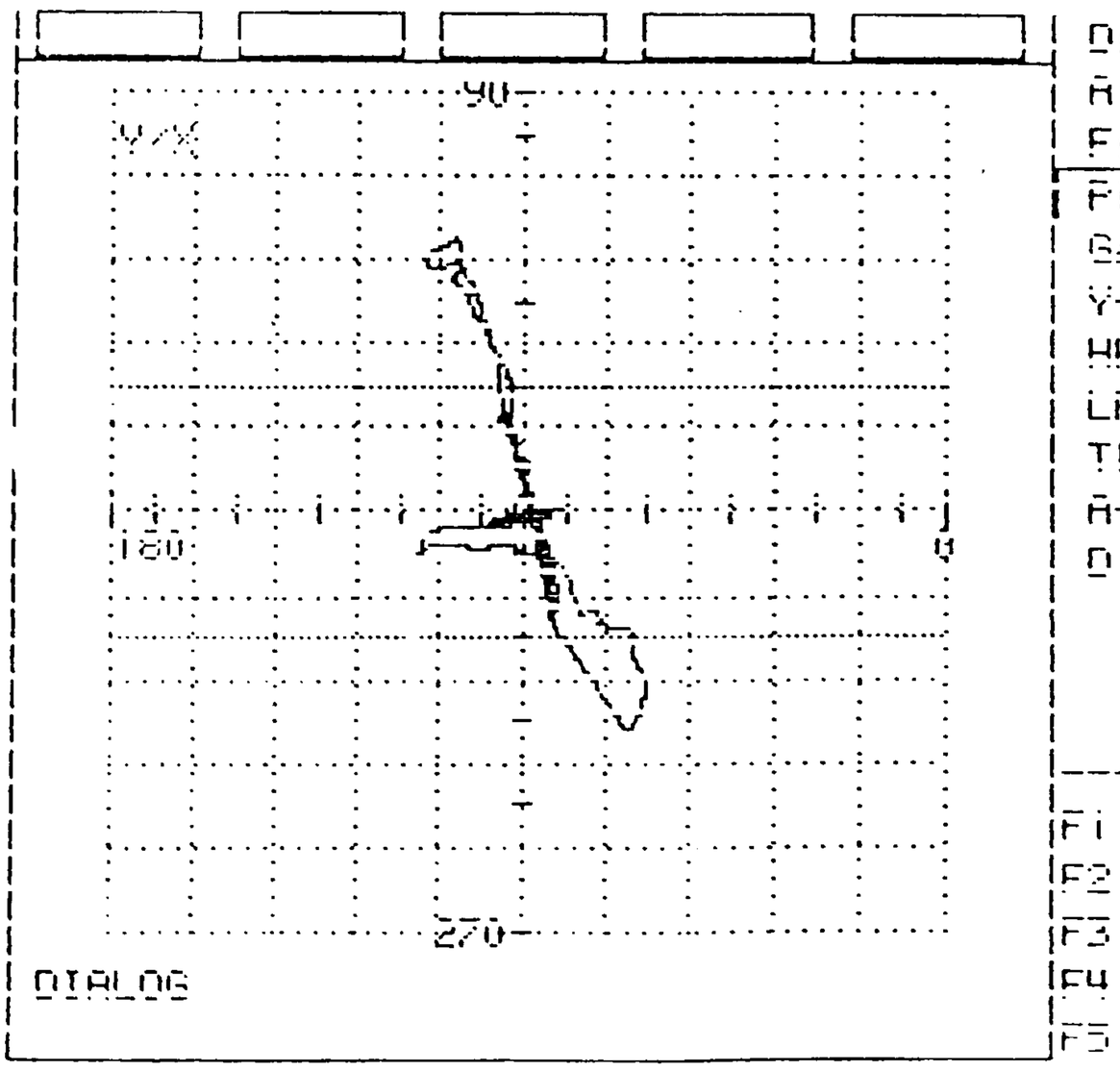

OXIDE INDIC

SC-000-8358

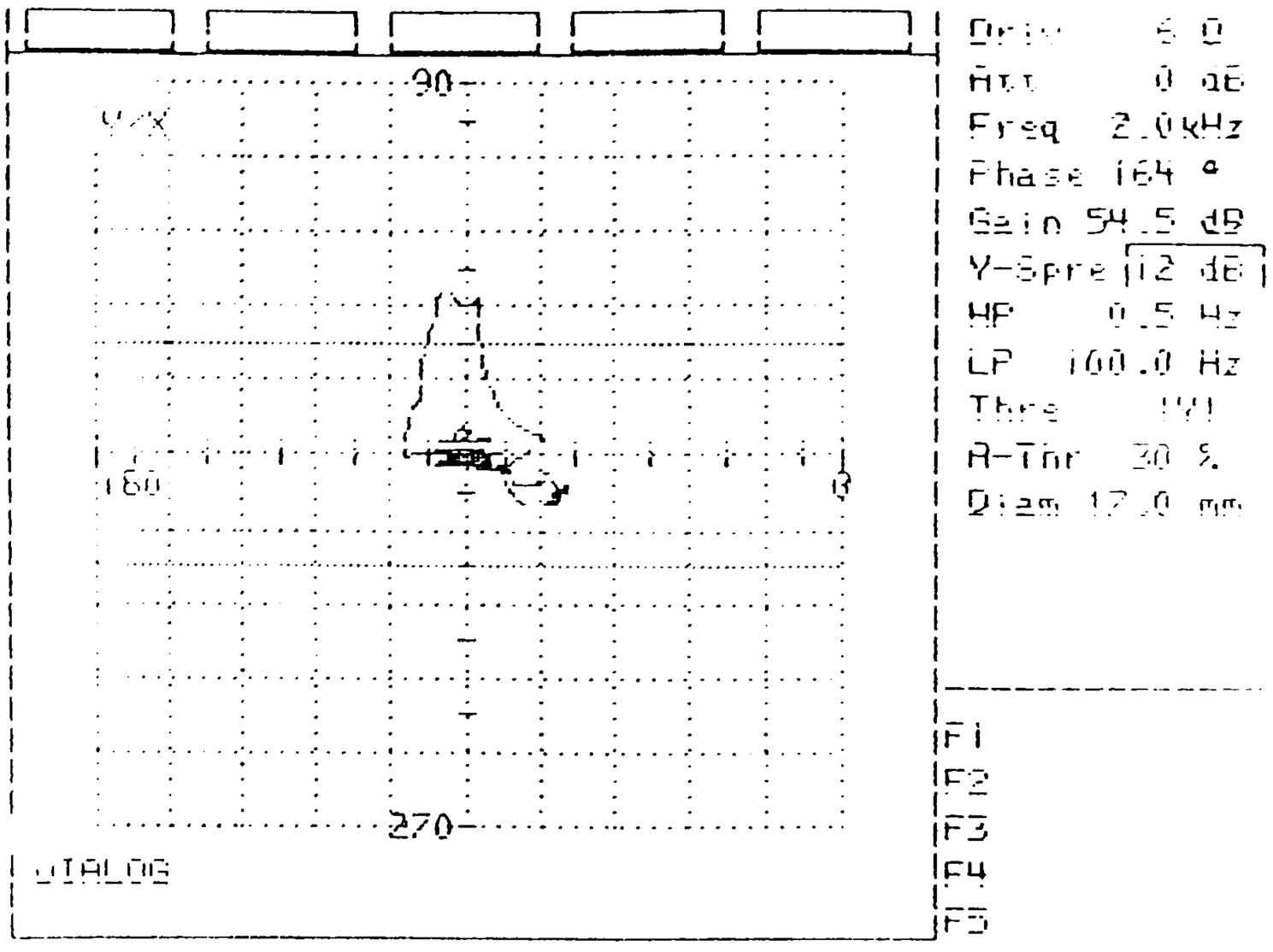

OXIDE INDICATION

SC-000-9498

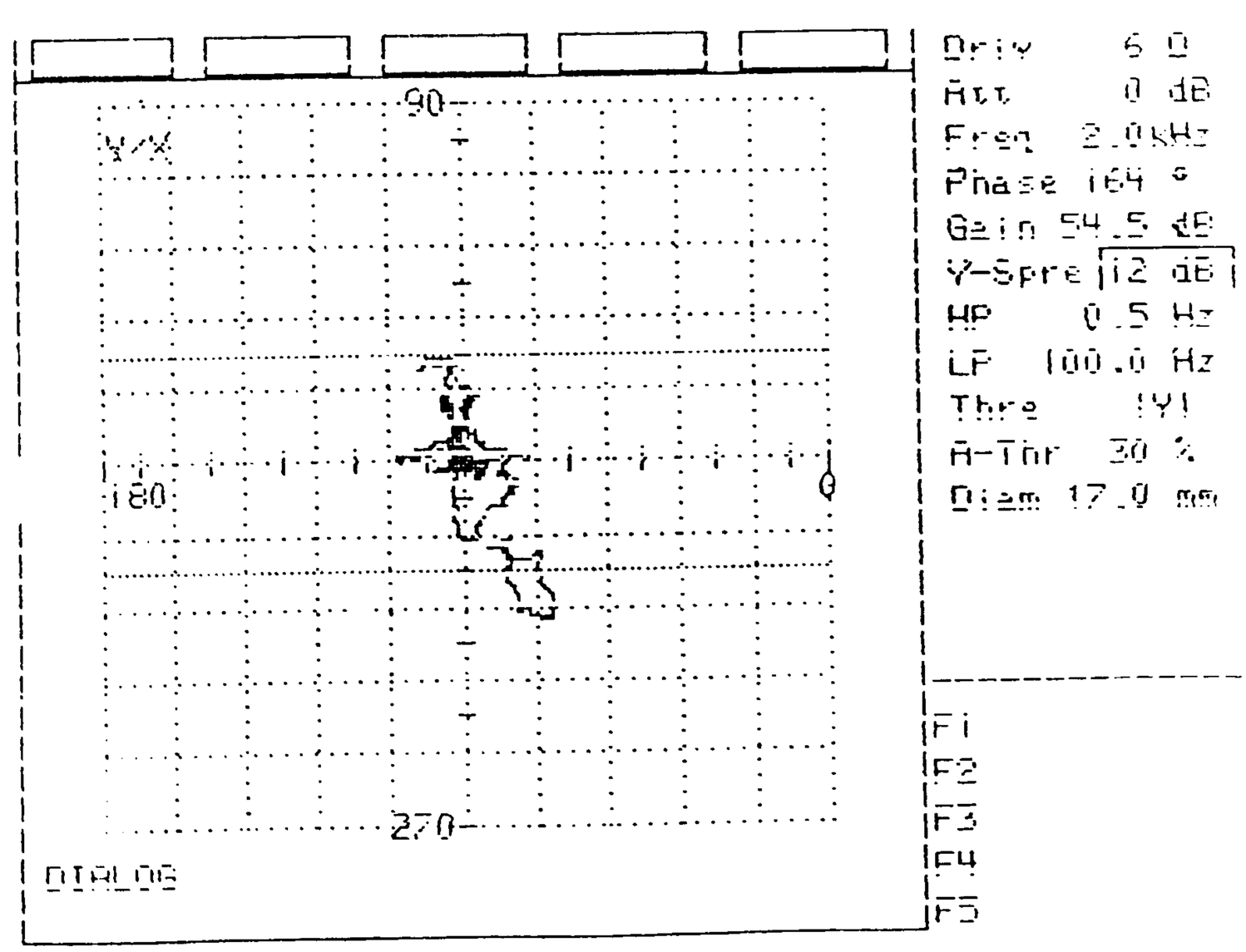

OXIDE INDICATION

SC-000-4686

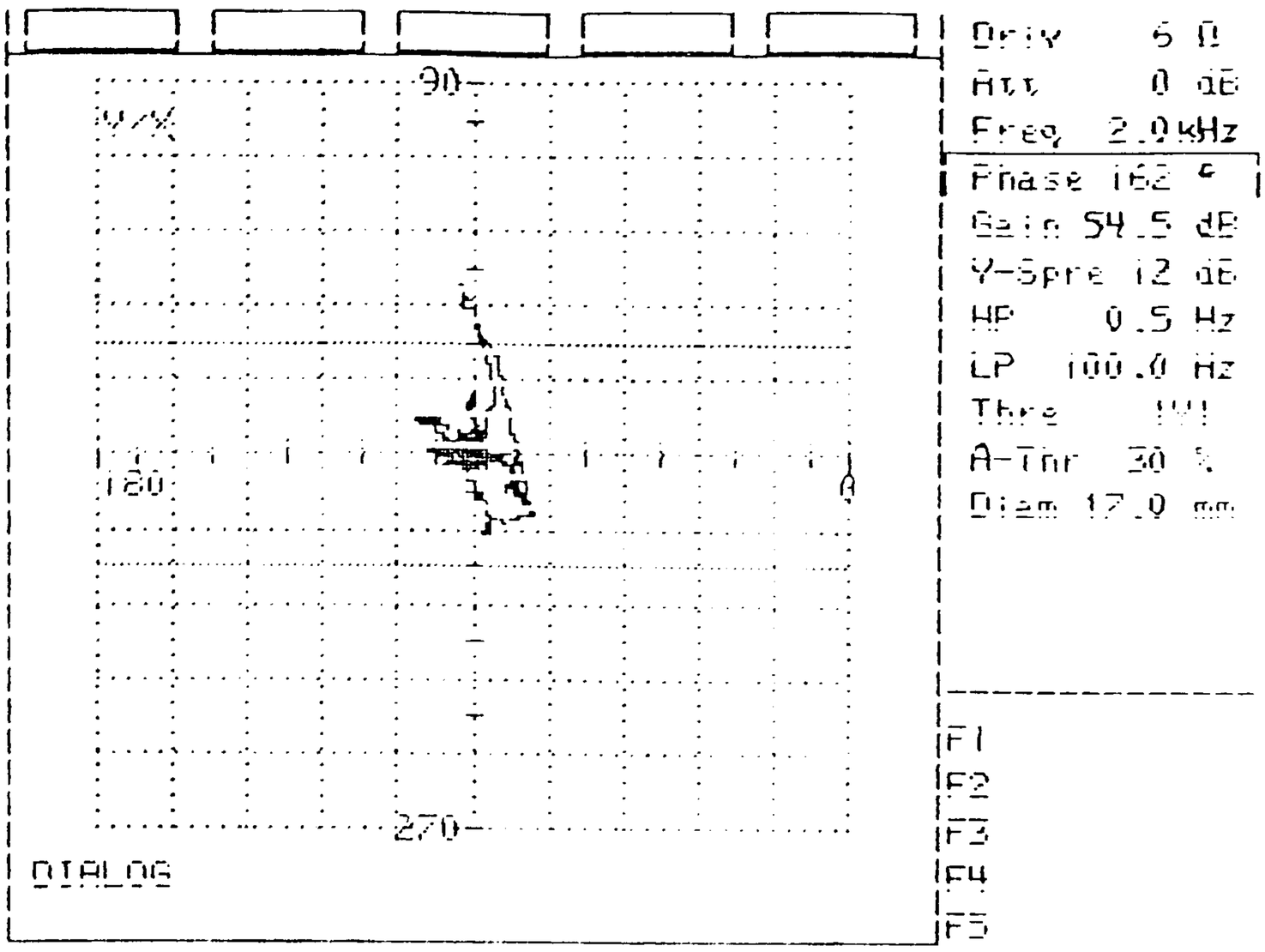

OXIDE INDICATION

SC-000-4687

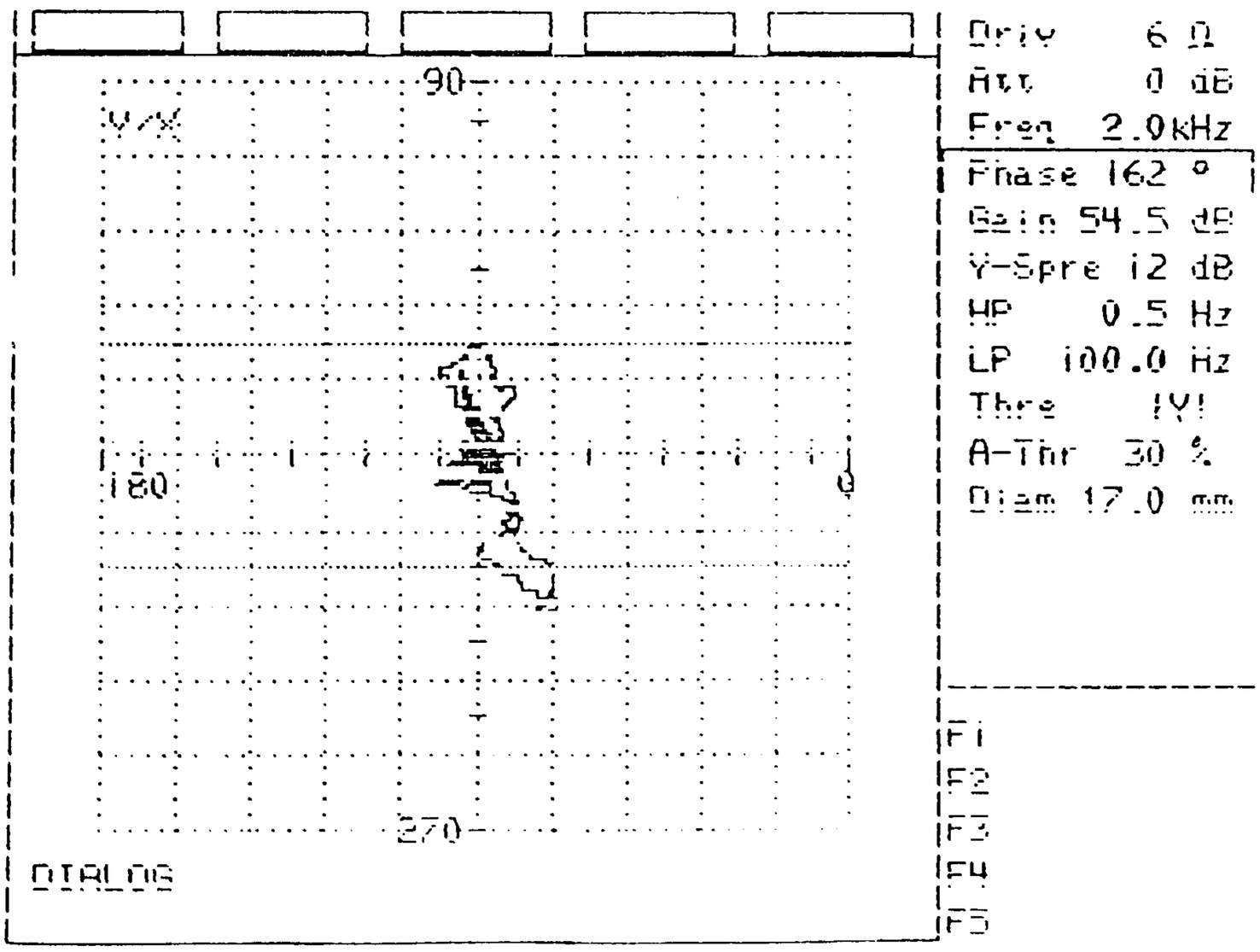

OXIDE INDICATION

SC-000-4616

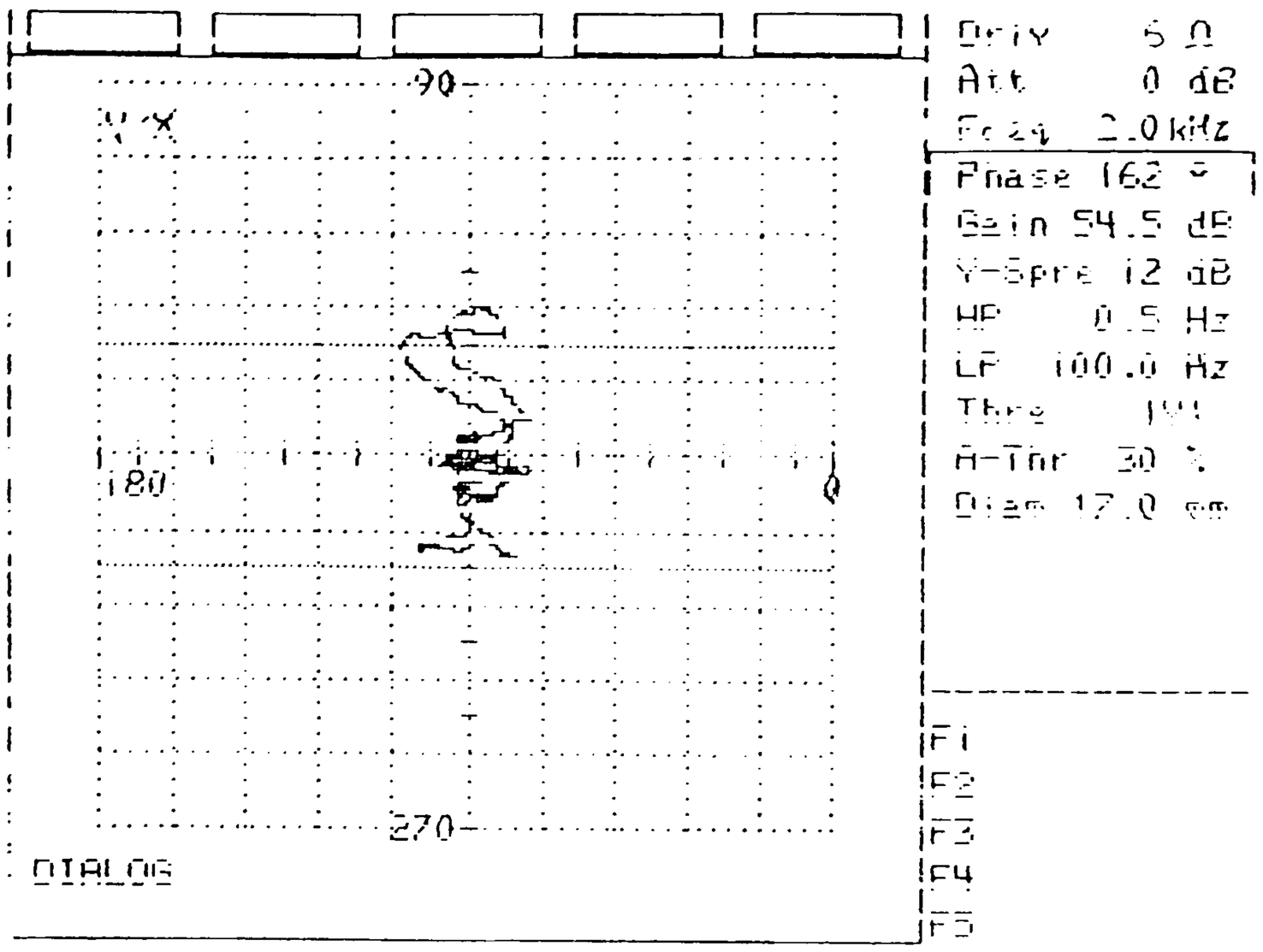

OXIDE INDICATION

SC-000-8537

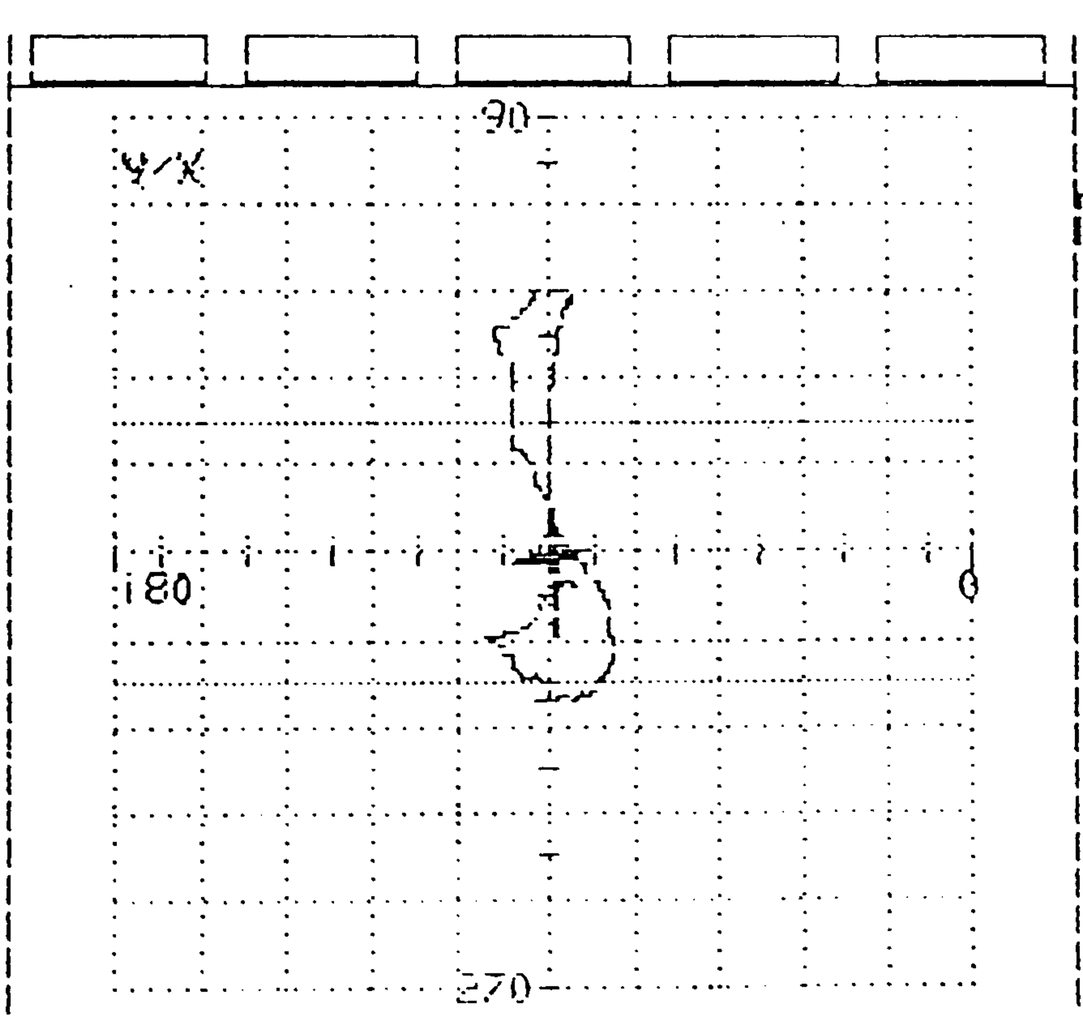

OXIDE INDICATION

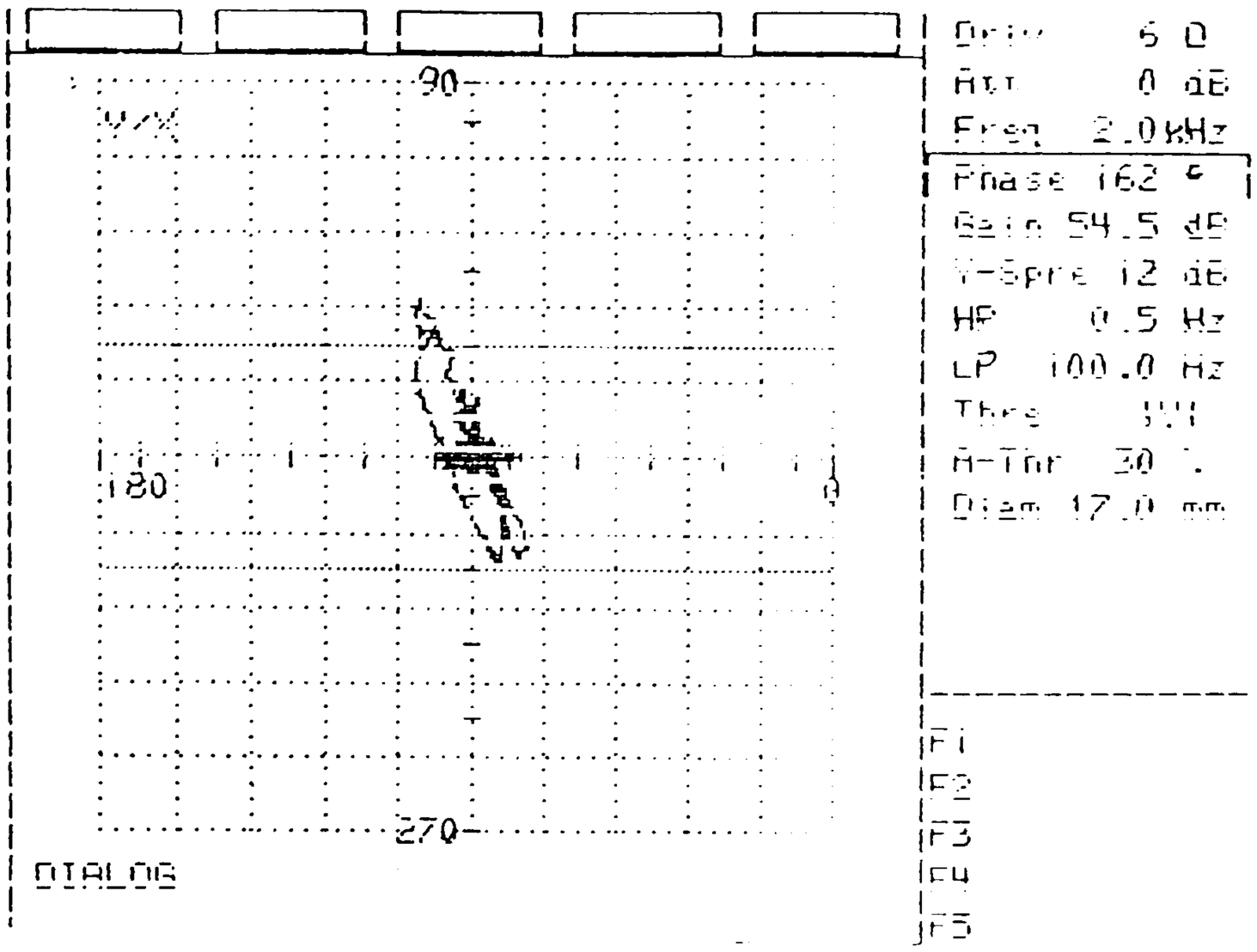

OXIDE INDICATION

SC-000-4687

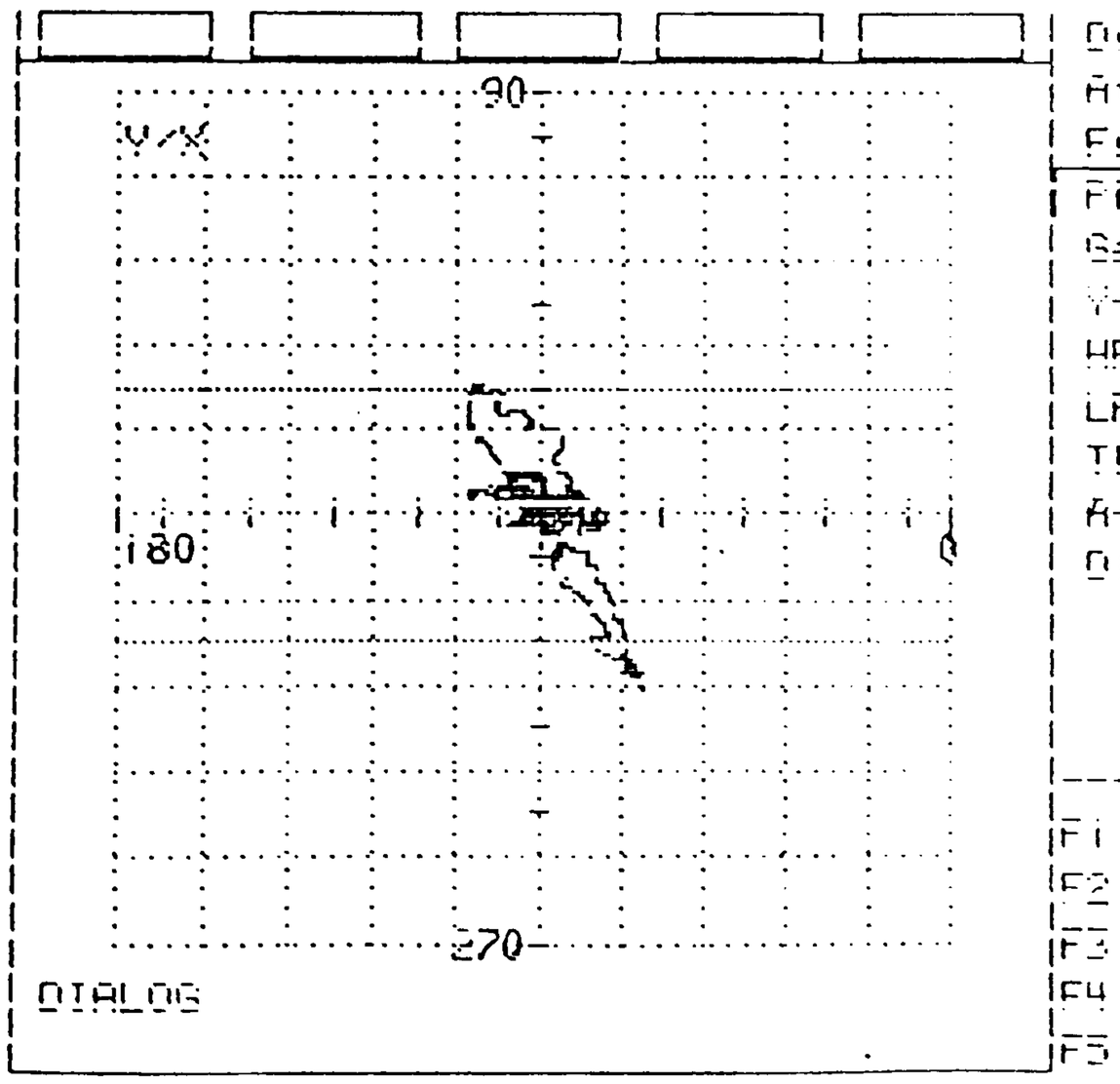

OXIDE INDICATION

SC-000-4686

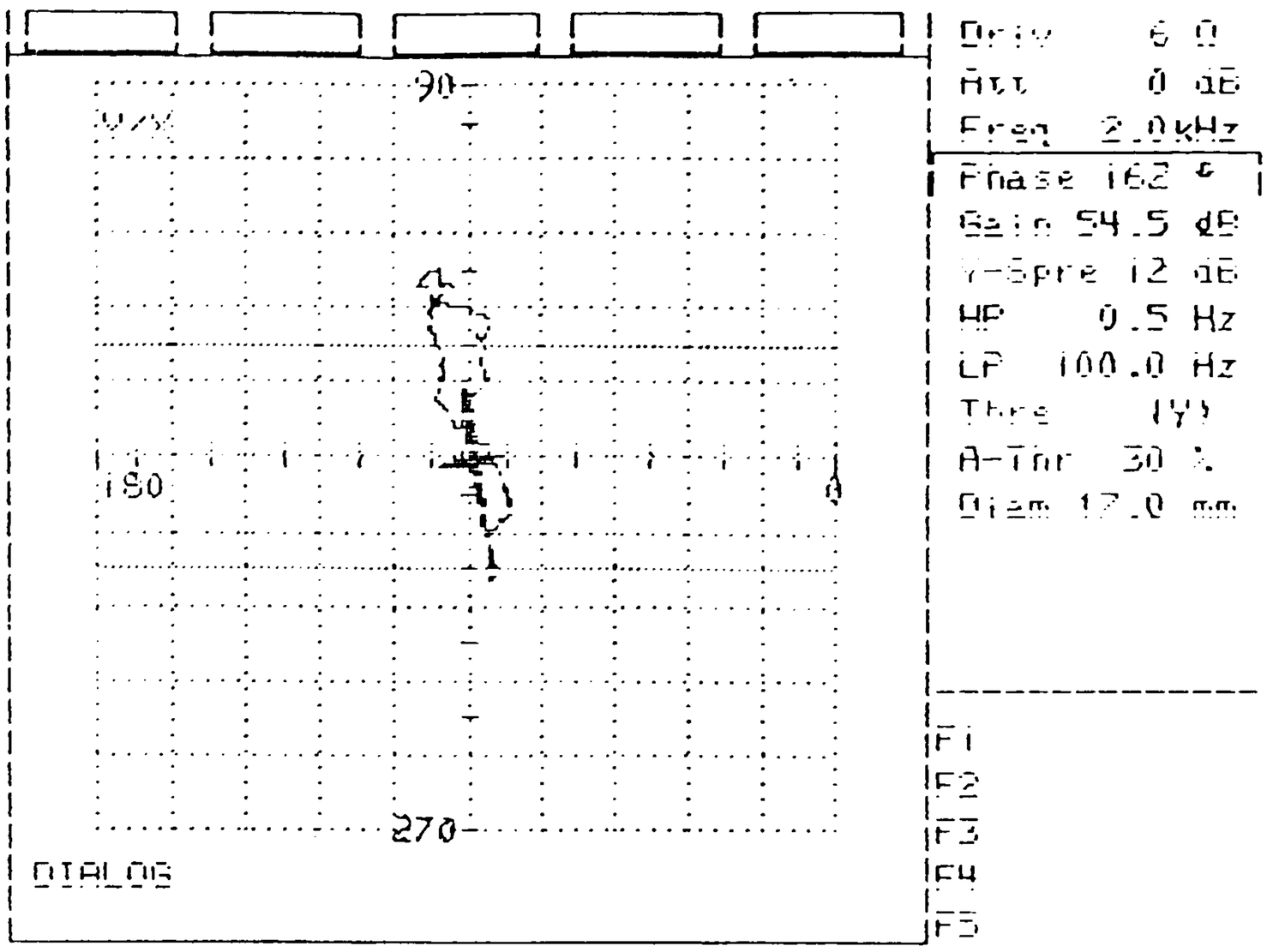

OXIDE ASSOCIATED WITH SHRINKAGE INDICATION

SC-000-4687

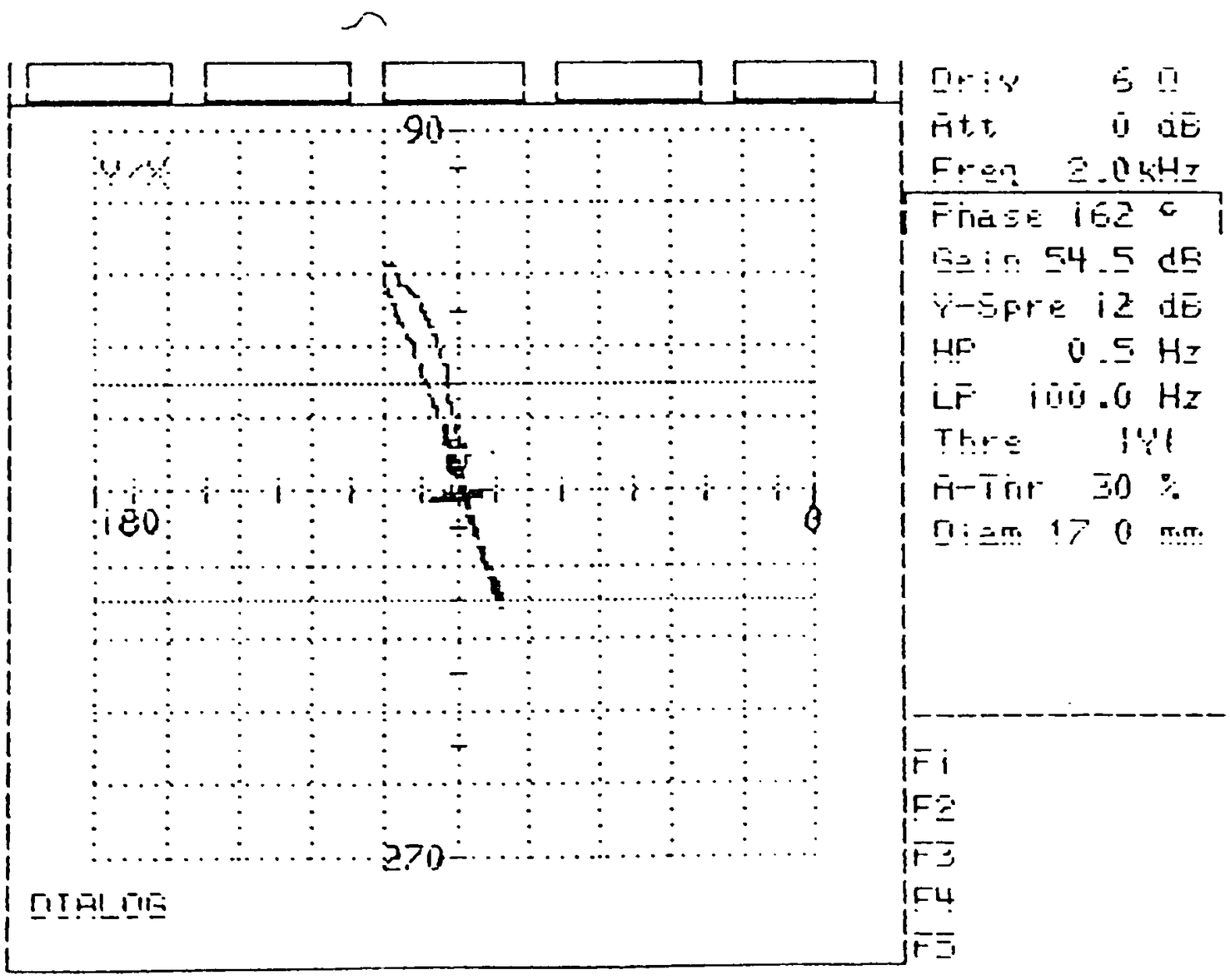

OXIDE ASSOCIATED WITH SHRINKAGE INDICATION

SC-000-9589

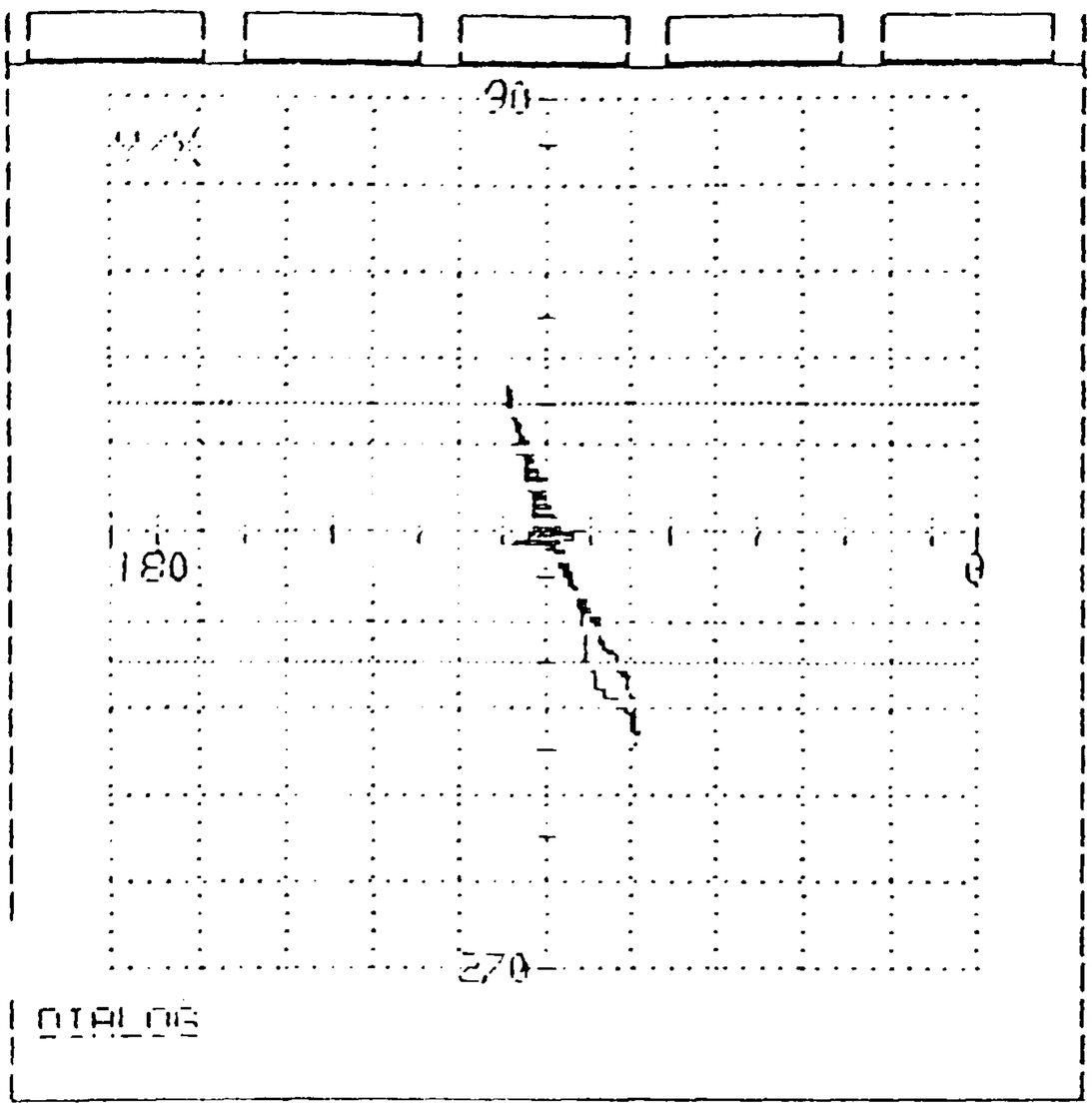

SHRINKAGE INDICATION

SC-000-9589

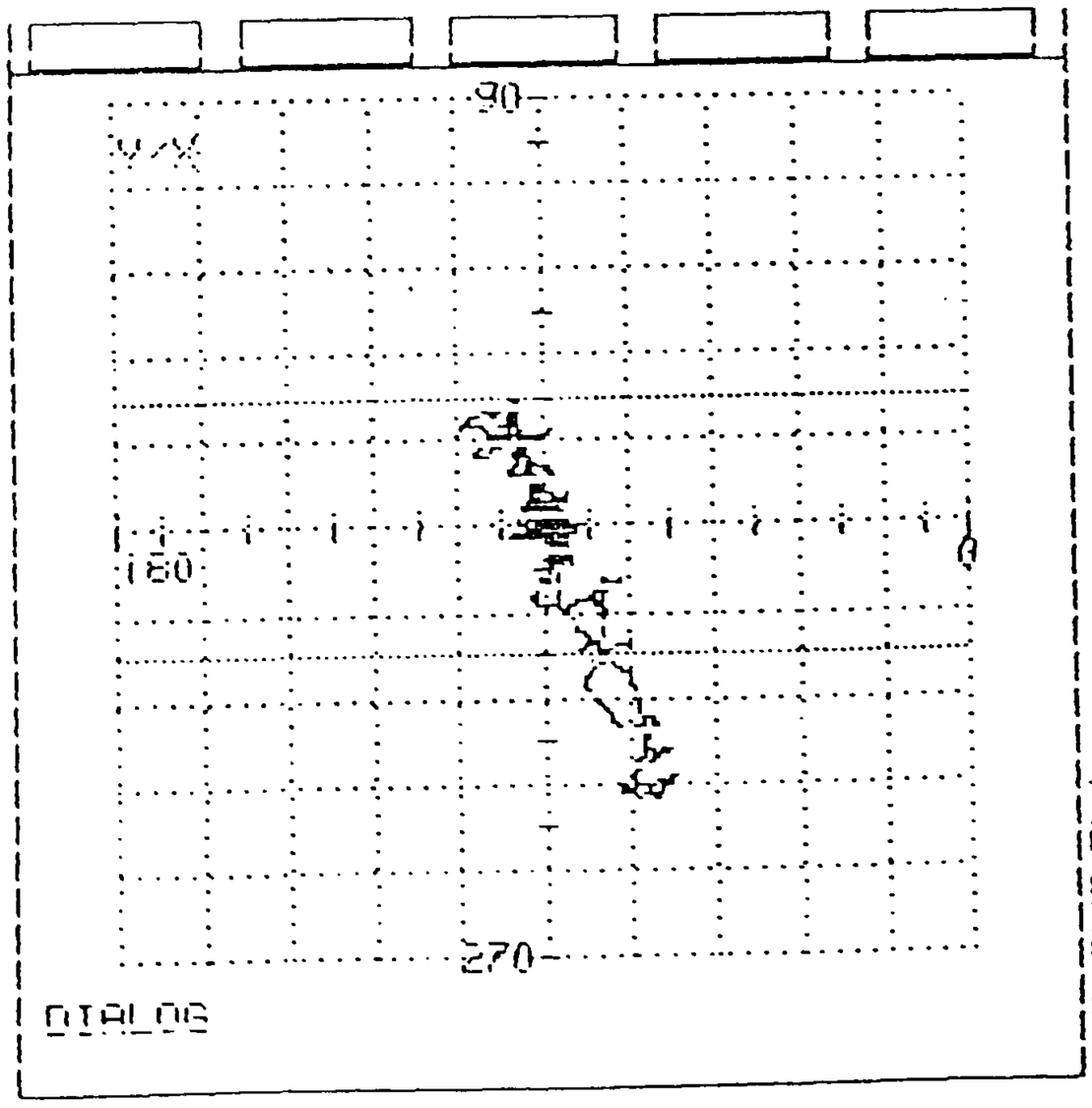

SHRINKAGE ASSOCIATED WITH OXIDE INDICATION

SC-000-7933

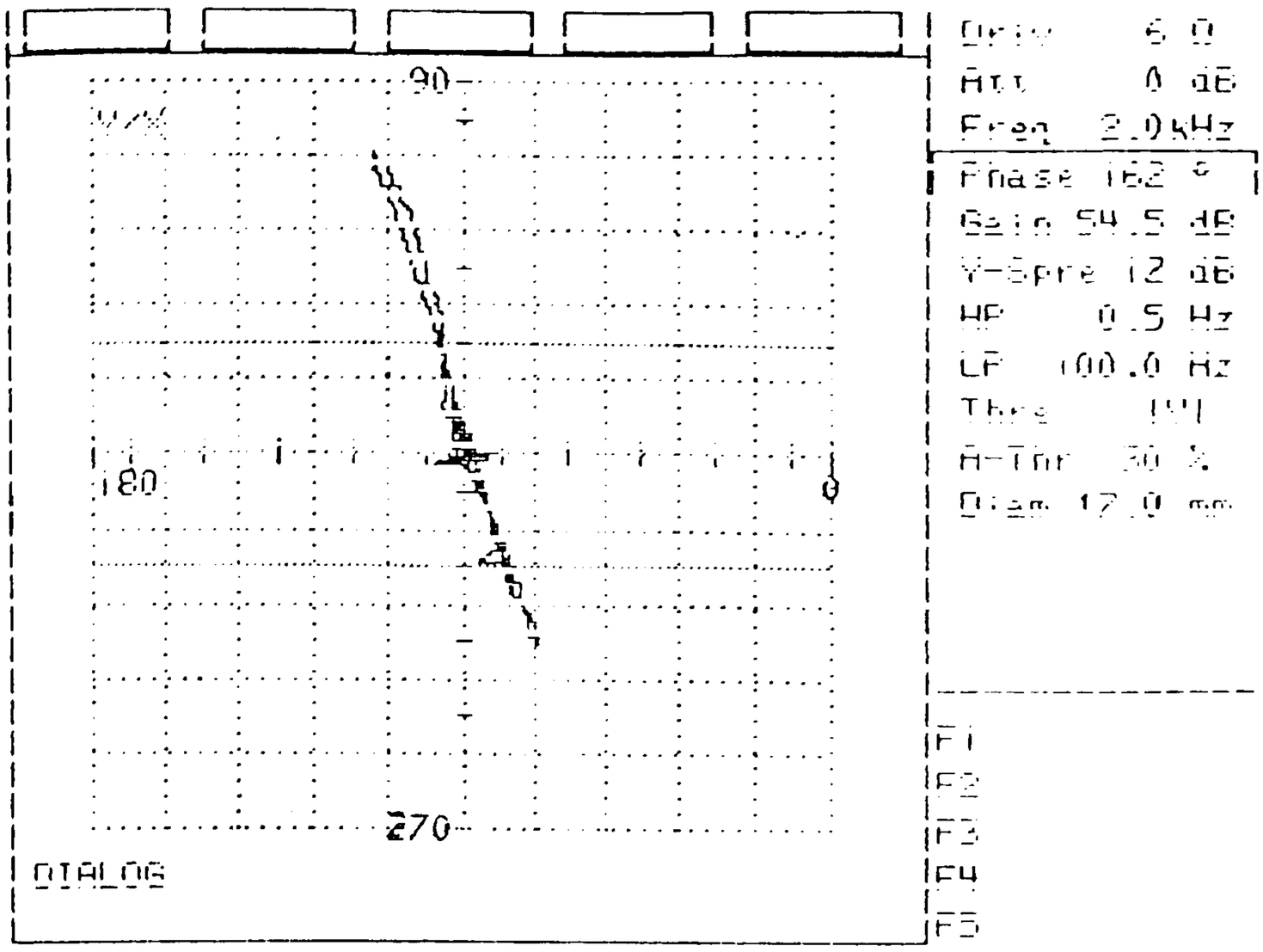

SHRINKAGE INDICATION

SC-000-3905

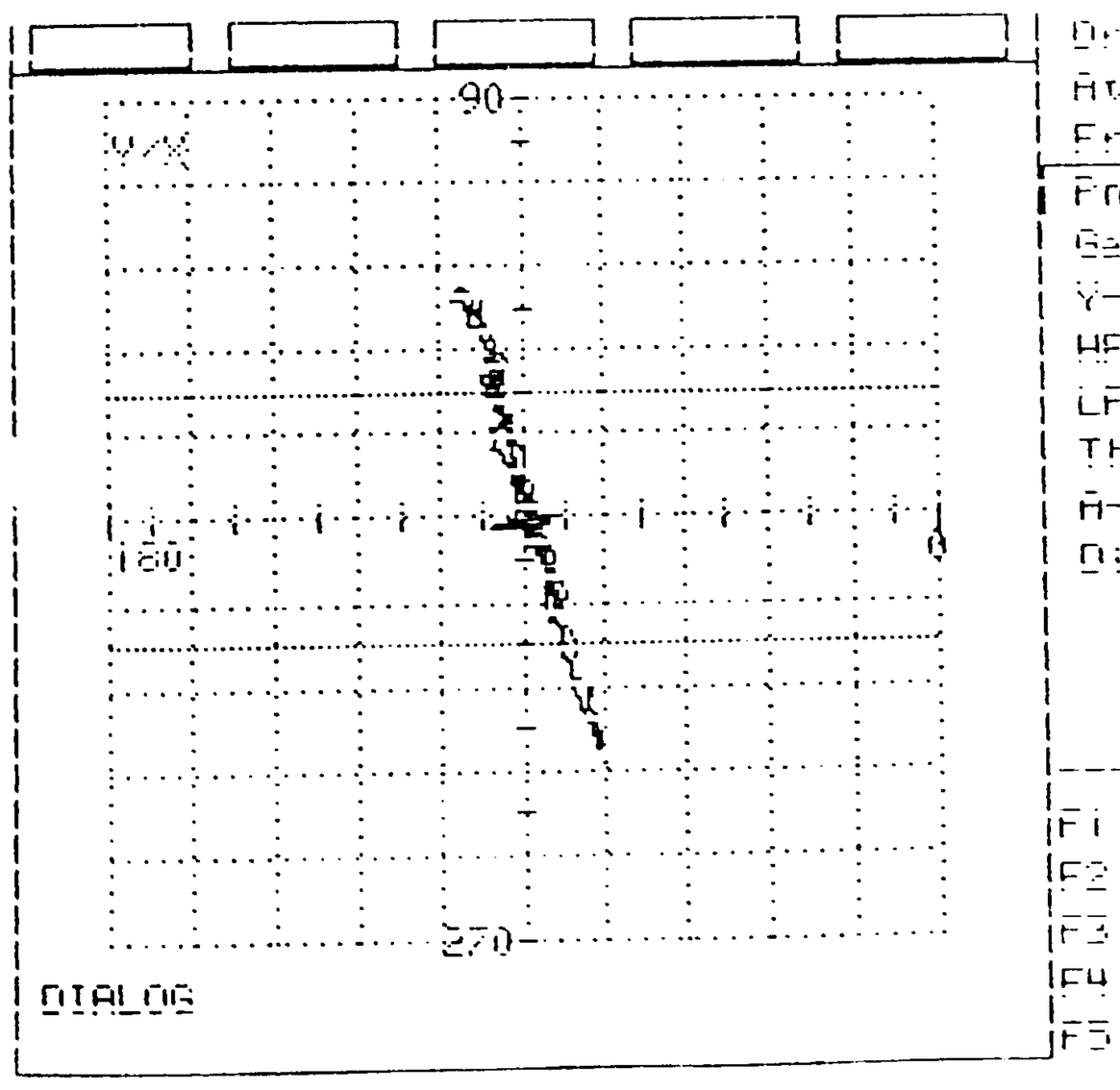

SHRINKAGE INDICATION

SC-000-9503

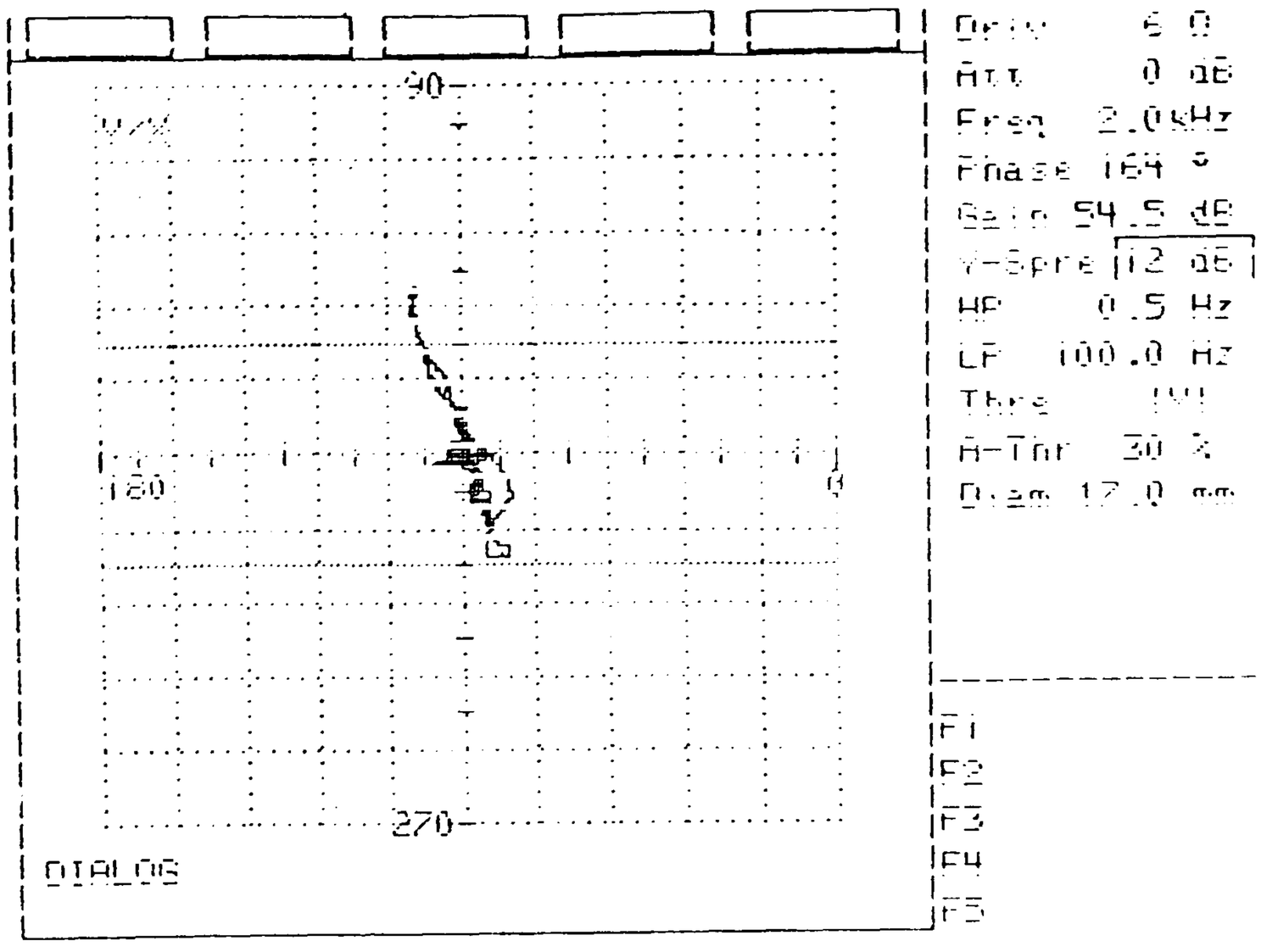

NEAR SURFACE
SHRINKAGE INDICATION

SC-000-9498

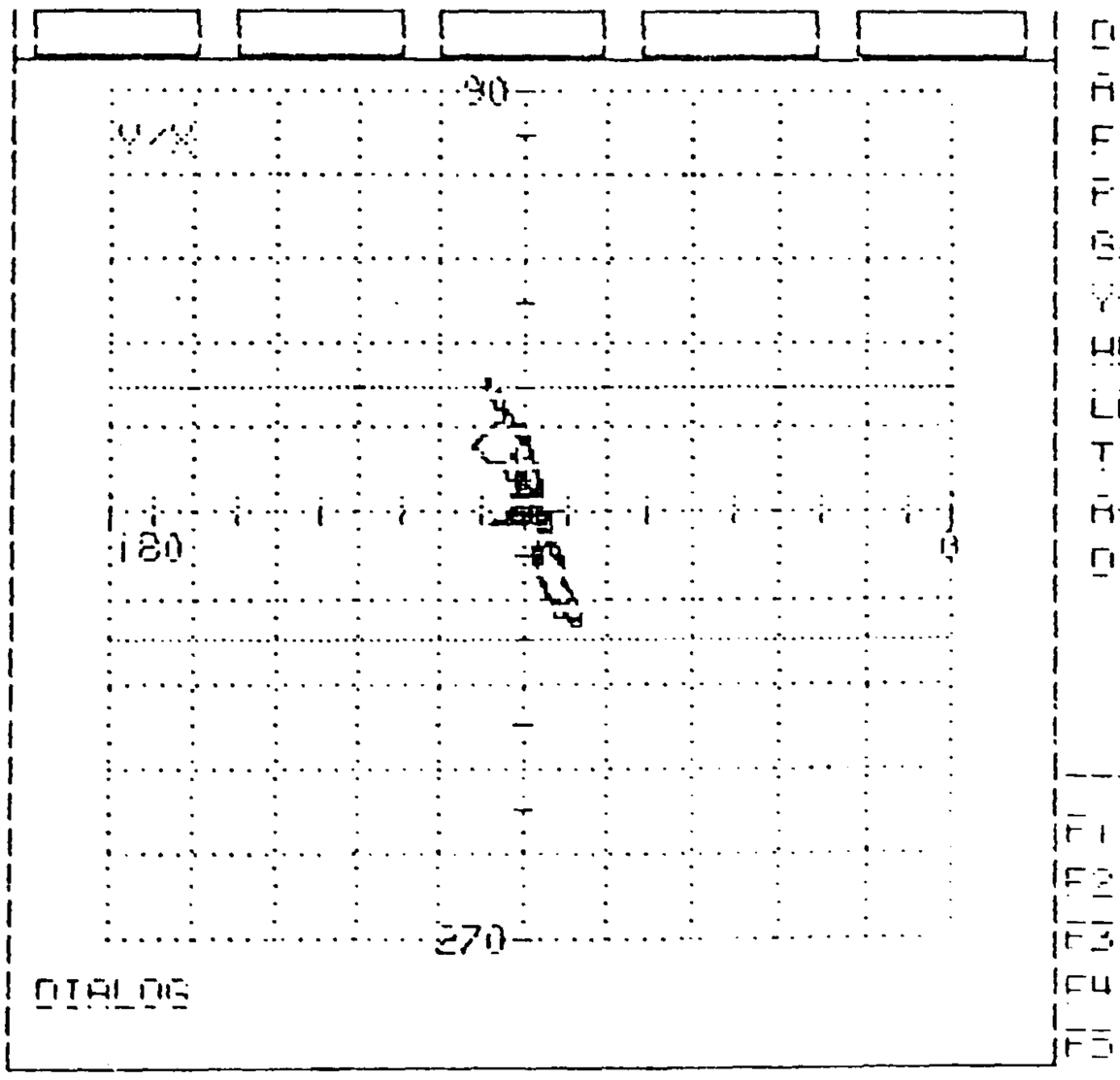

SHRINKAGE INDICATION

SC-000-9498

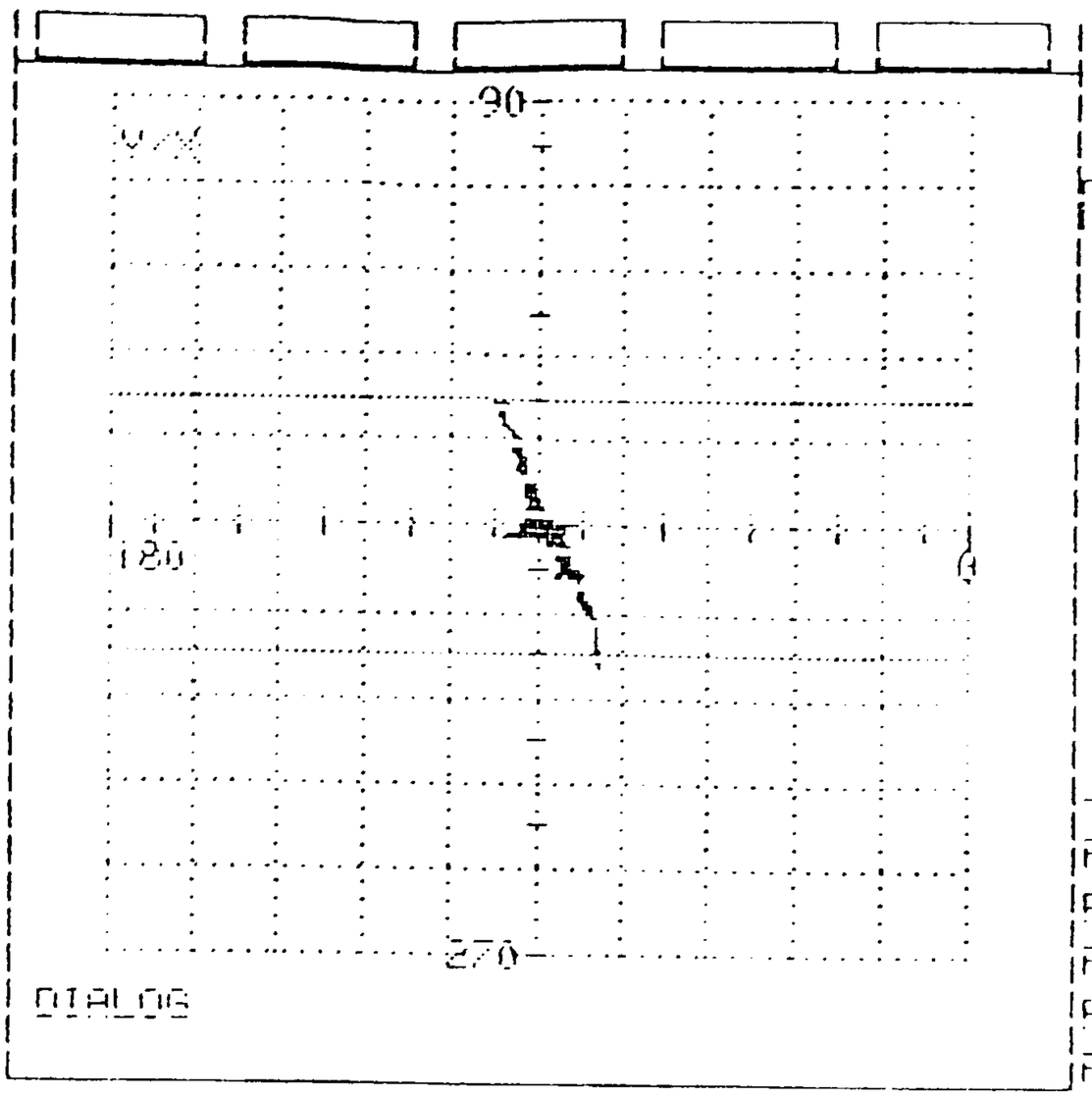

SHRINKAGE INDICATION

SC-000-8537

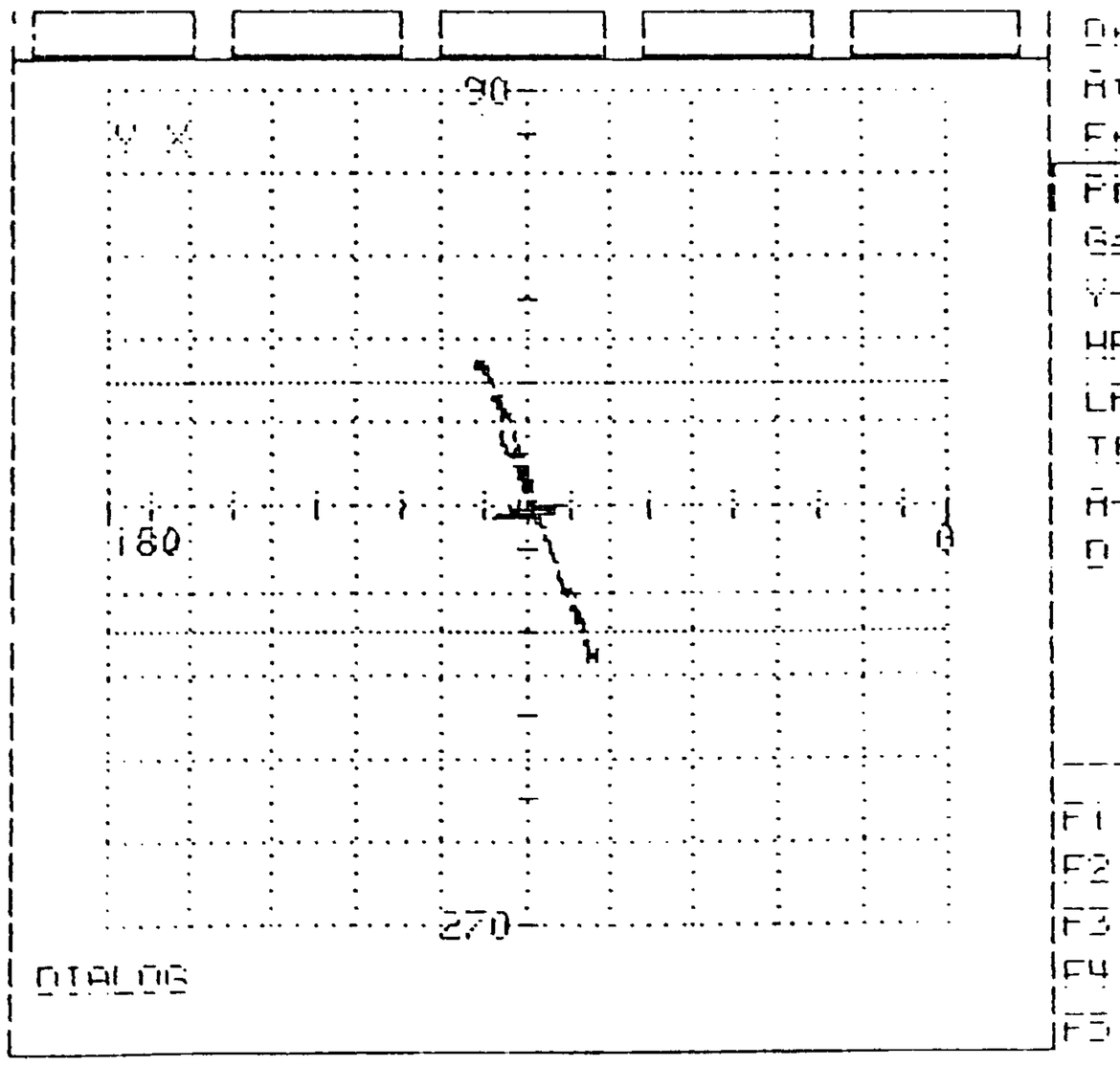

SHRINKAGE INDICATION

ATLAS OF EDDY CURRENT SIGNATURES

VERSUS LINEAR

METALLURGICAL CONDITIONS

TEST REFERENCE STANDARD WITH VARYING DEFECT HEIGHT USING 2MM , 5MM & 7MM COUPONS TO SIMULATE DEPTH.

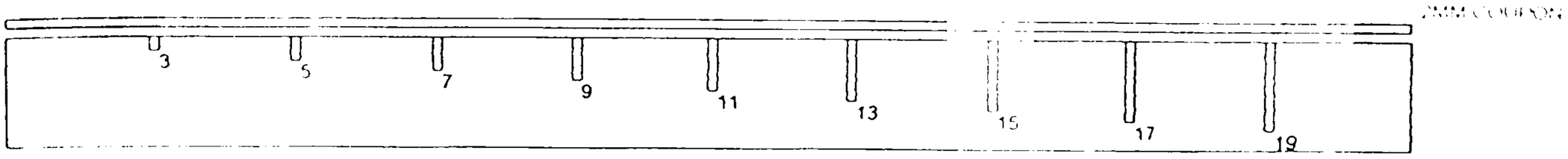

LINEAR DEFECTS AT 2MM DEPTH - VARYING DEFECT HEIGHT

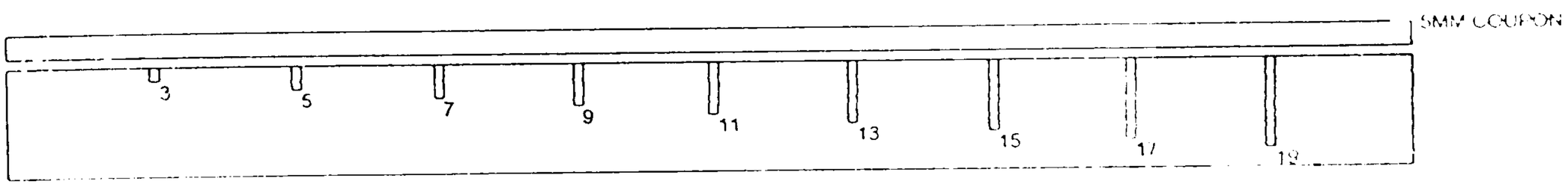

LINEAR DEFECTS AT 5MM DEPTH - VARYING DEFECT HEIGHT

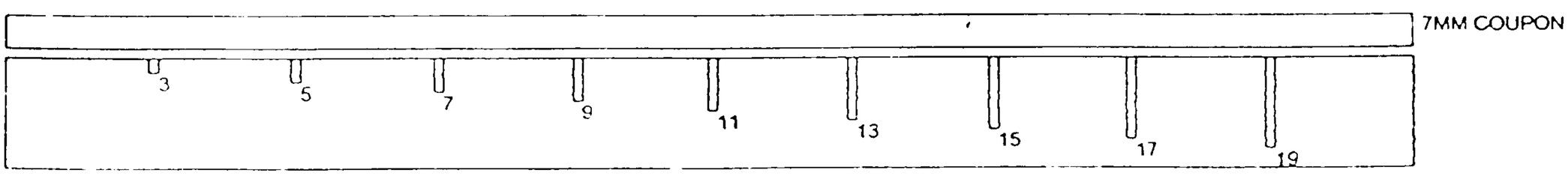

LINEAR DEFECTS AT 7MM DEPTH - VARYING DEFECT HEIGHT

INSTITUT DR.FOERSTER

DEFECTOSCOP AF 2.833 2.2 SN 25

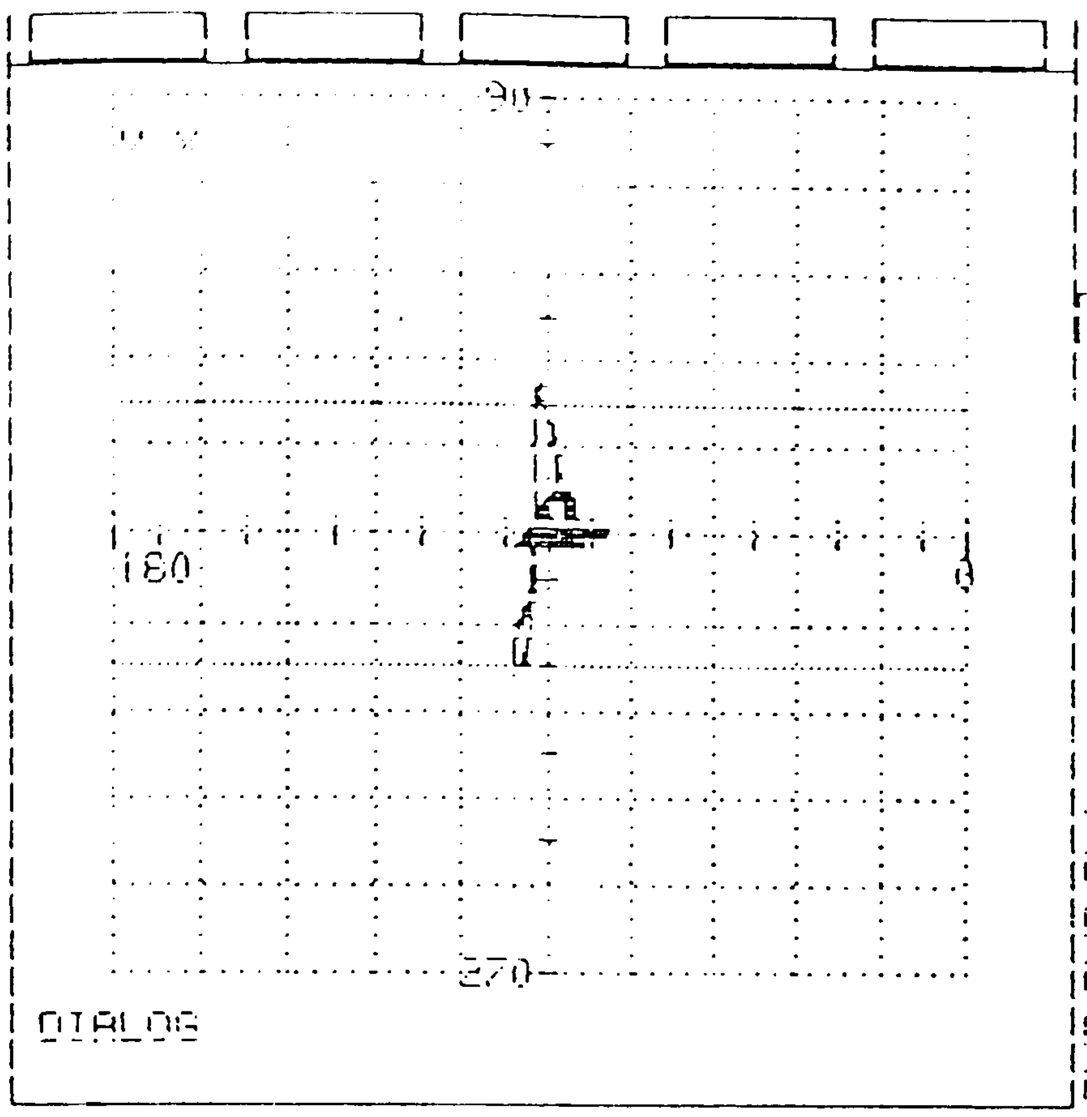

DEFECT HEIGHT 3mm AT
5mm SUBSURFACE DEPTH

INSTITUT DR.FOERSTER 02.06.95 12:56

DEFECTOSCOP AF 2.833 2.2 SN 25

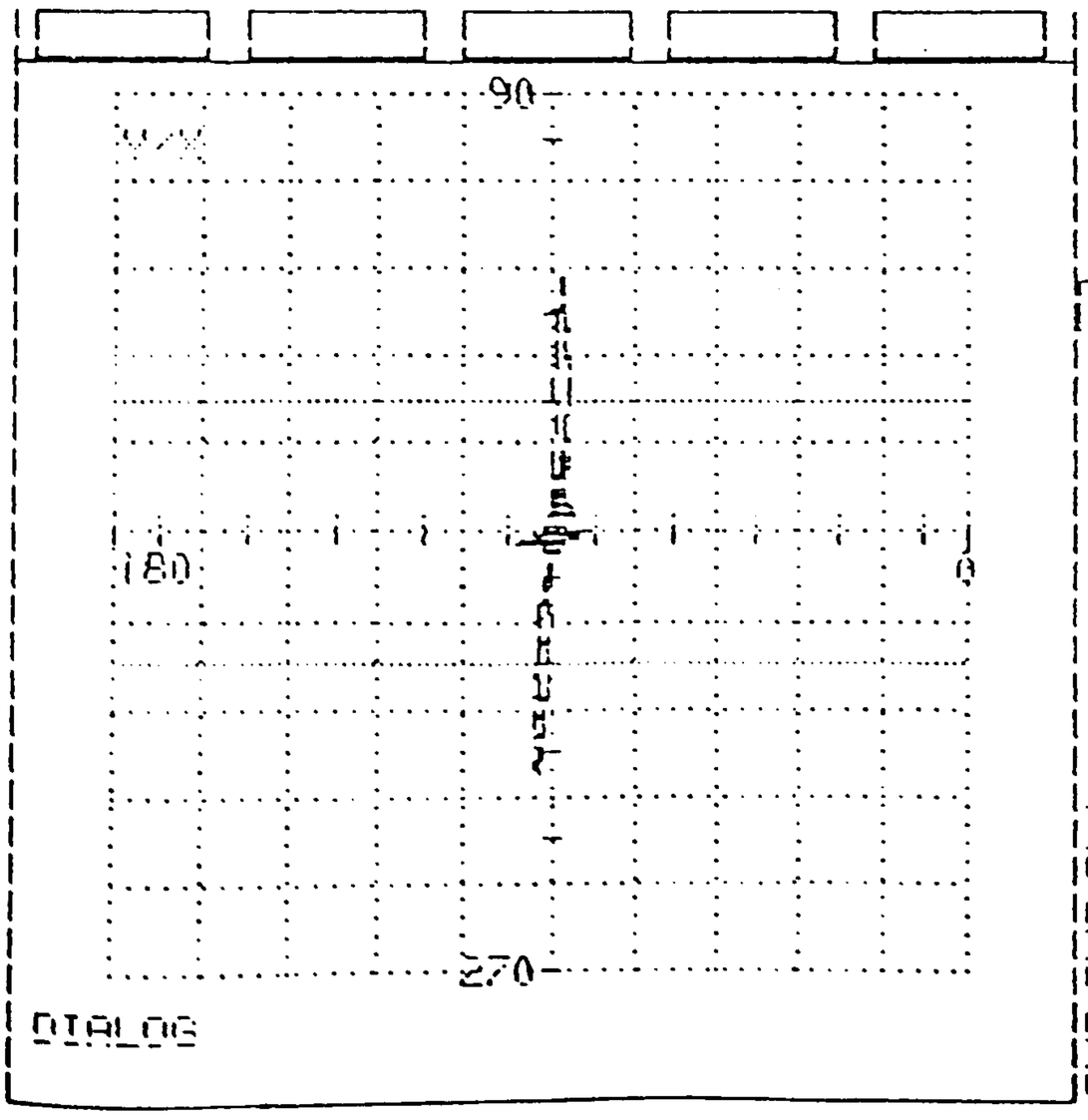

DEFECT HEIGHT 5mm AT
5mm SUBSURFACE DEPTH

INSTITUT DR.FOERSTER

DEFECTOSCOP AF 2.833 2.2 SN 25

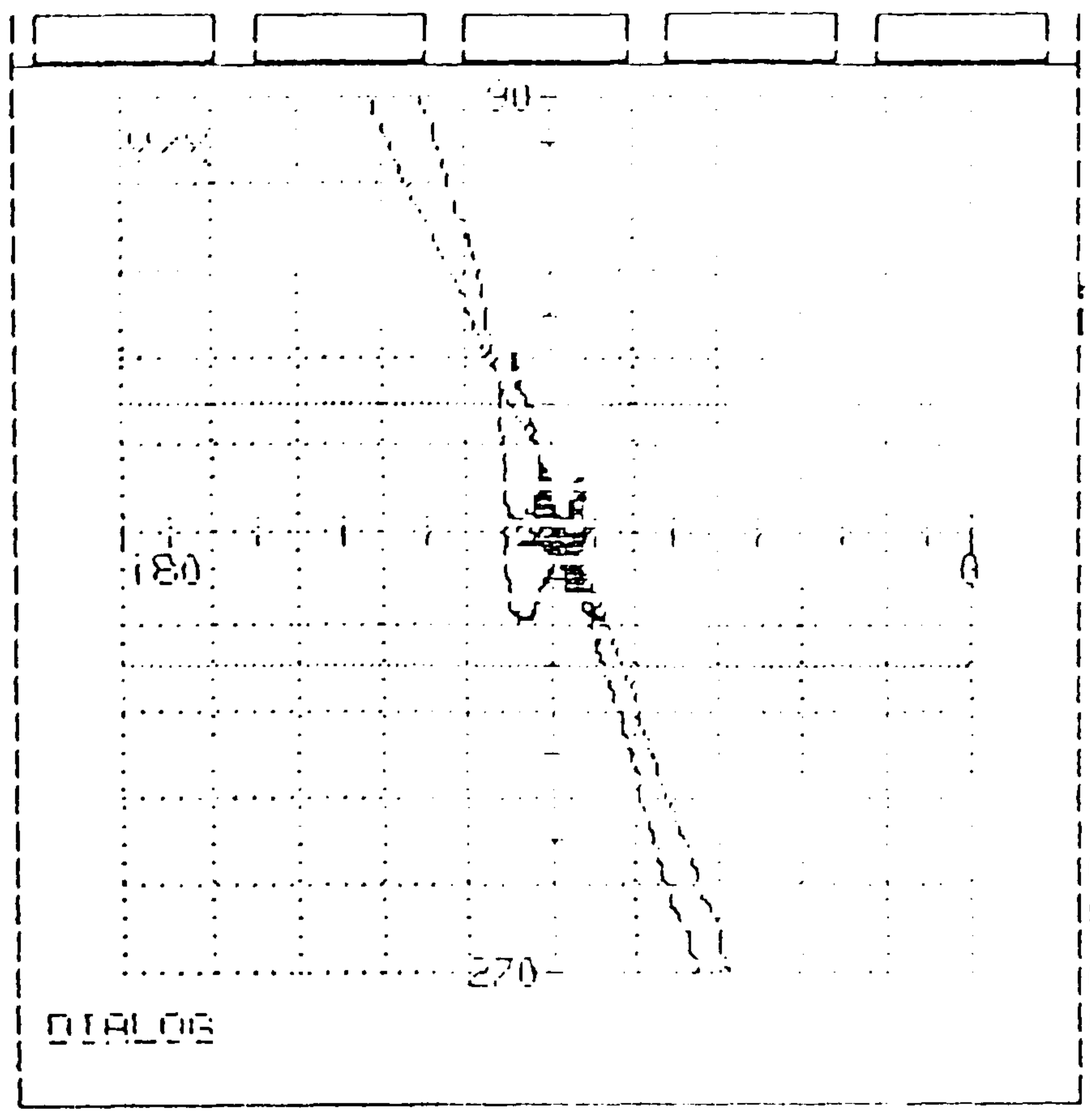

DEFECT HEIGHT 3mm AT 2mm SUBSURFACE DEPTH

INSTITUT DR.FOERSTER 02.06.95 13:44

DEFECTOSCOP AF 2.833 2.2 SN 25

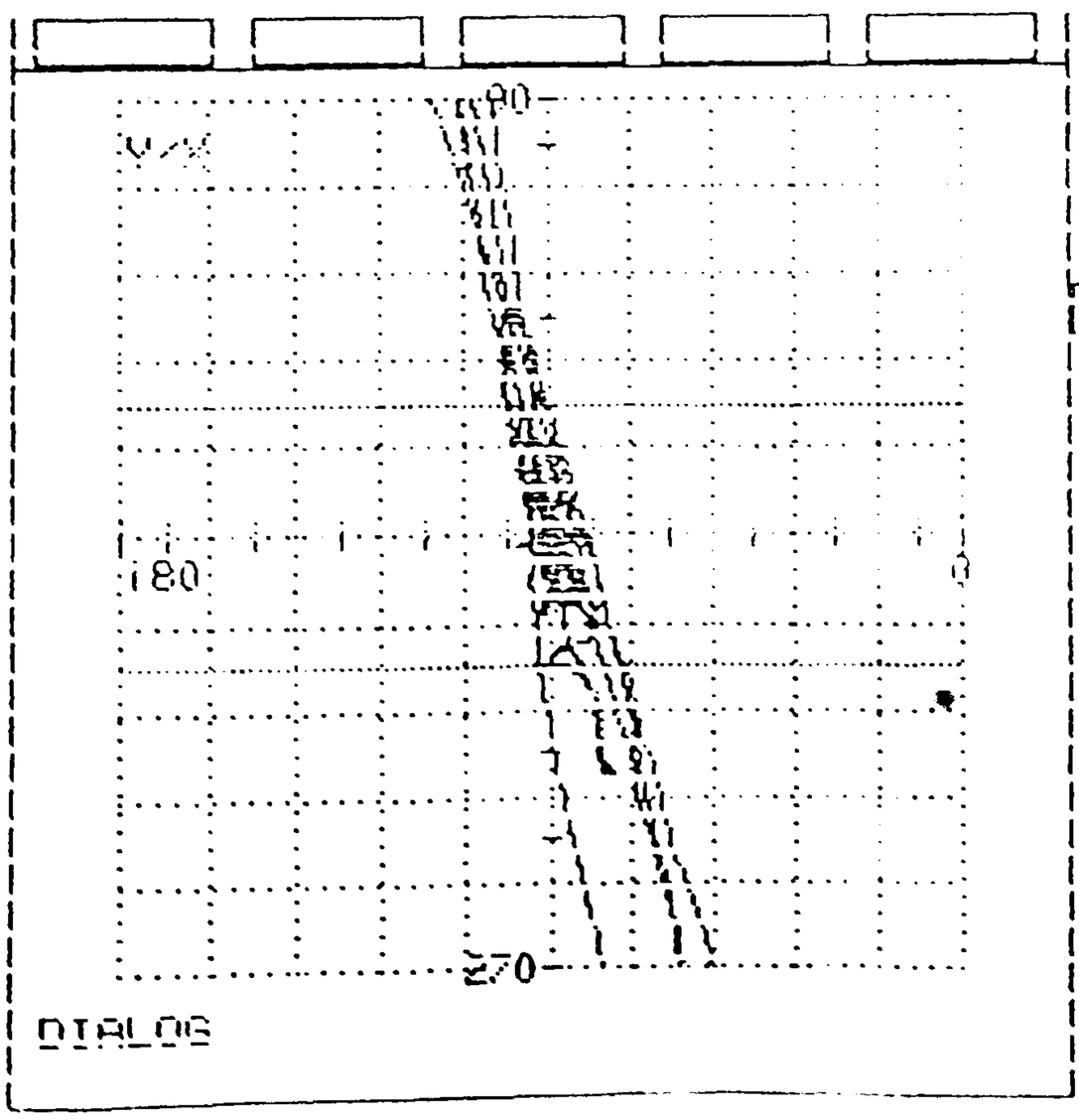

DEFECT HEIGHT 5mm AT 2mm SUBSURFACE DEPTH

INSTITUT DR.FOERSTER

DEFECTOSCOP AF 2.833 2.2 SN 25

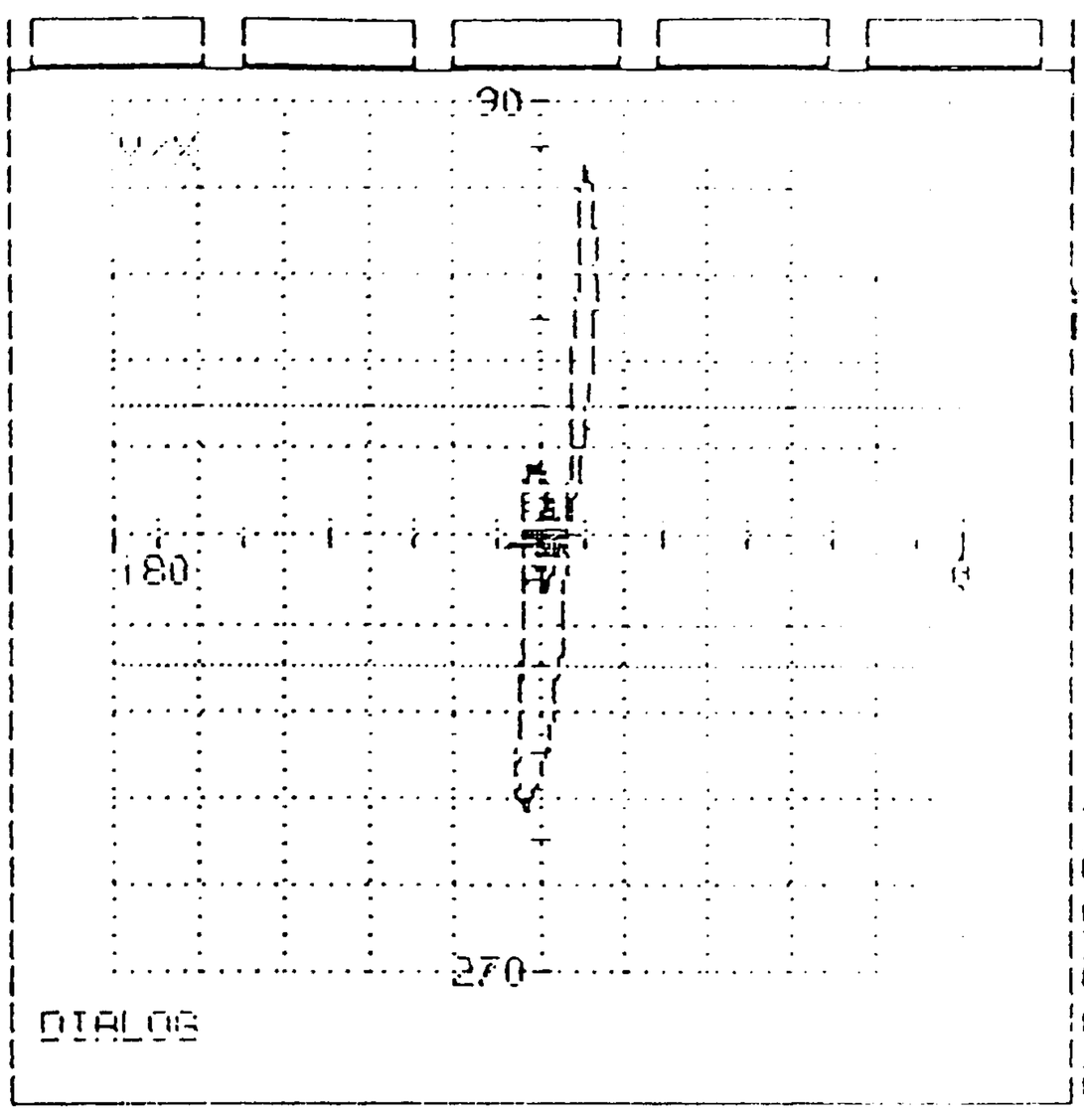

DEFECT HEIGHT 7mm AT 5mm SUBSURFACE DEPTH

INSTITUT DR.FOERSTER 02.06.95 12:58

DEFECTOSCOP AF 2.833 2.2 SN 25

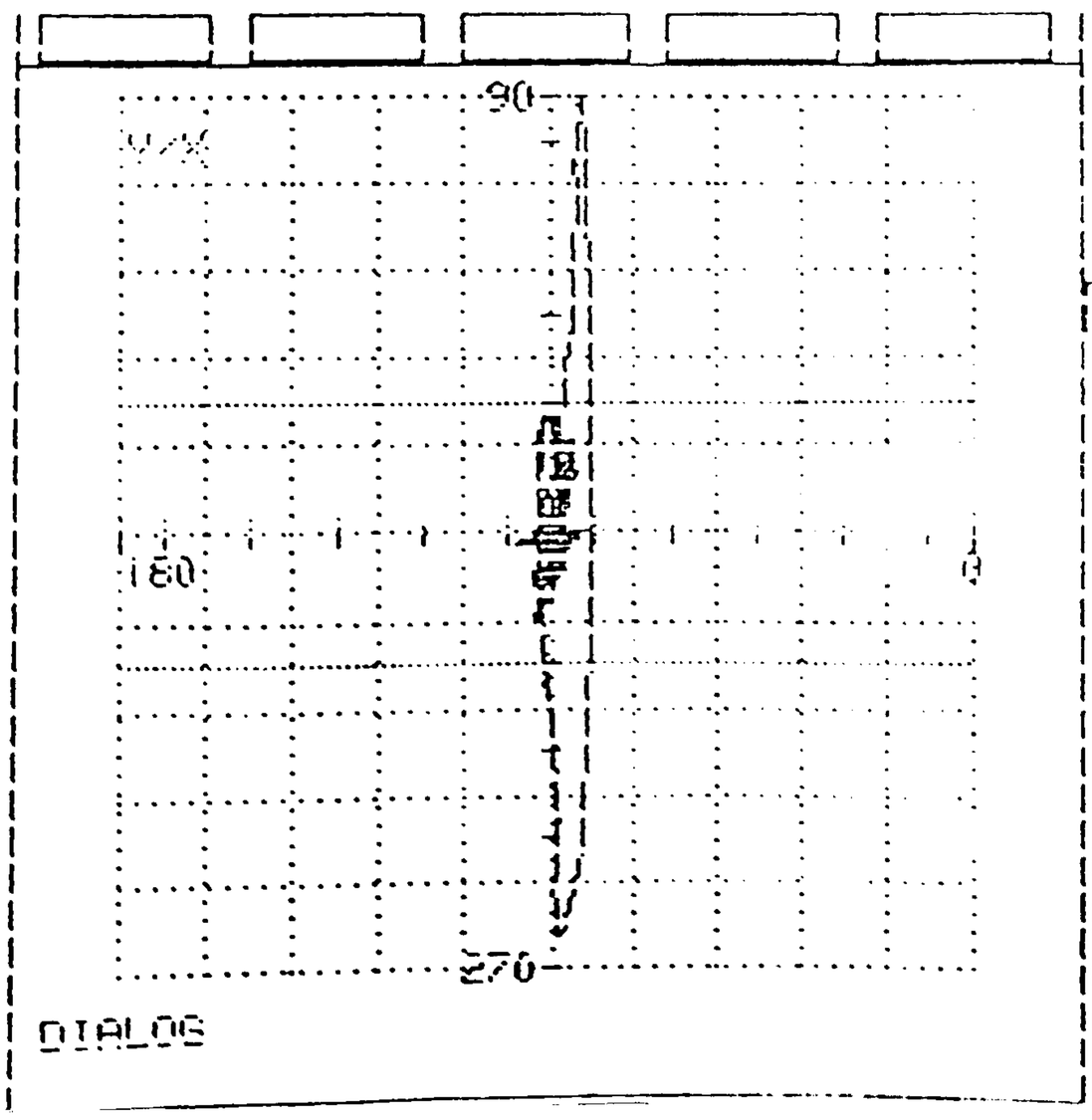

DEFECT HEIGHT 9mm AT 5mm SUBSURFACE DEPTH

INSTITUT DR.FOERSTER

DEFECTOSCOP AF 2.833 2.2 SN 25

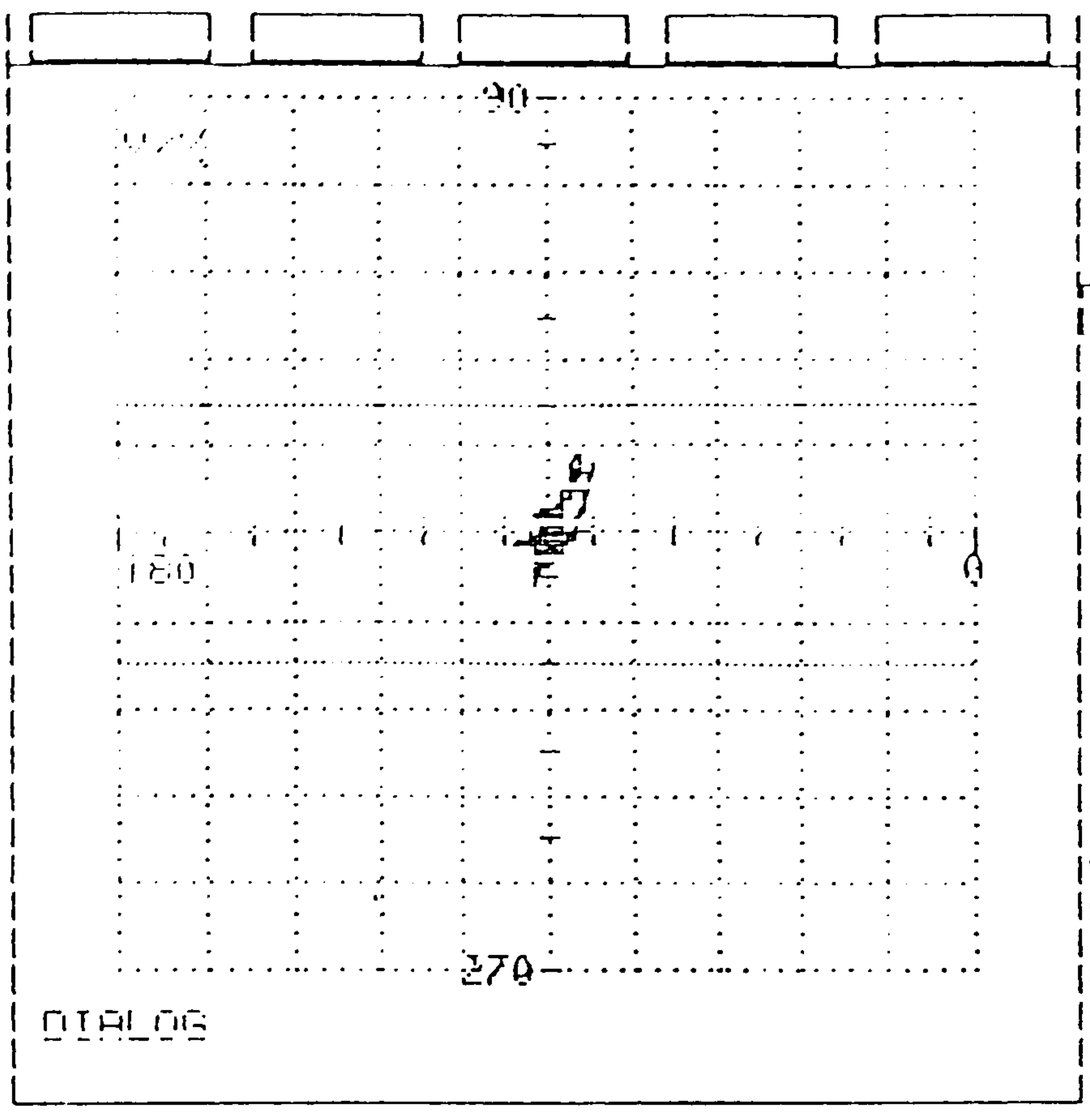

DEFECT HEIGHT 7mm AT
7mm SUBSURFACE DEPTH

INSTITUT DR.FOERSTER 02.06.95 13:40

DEFECTOSCOP AF 2.833 2.2 SN 25

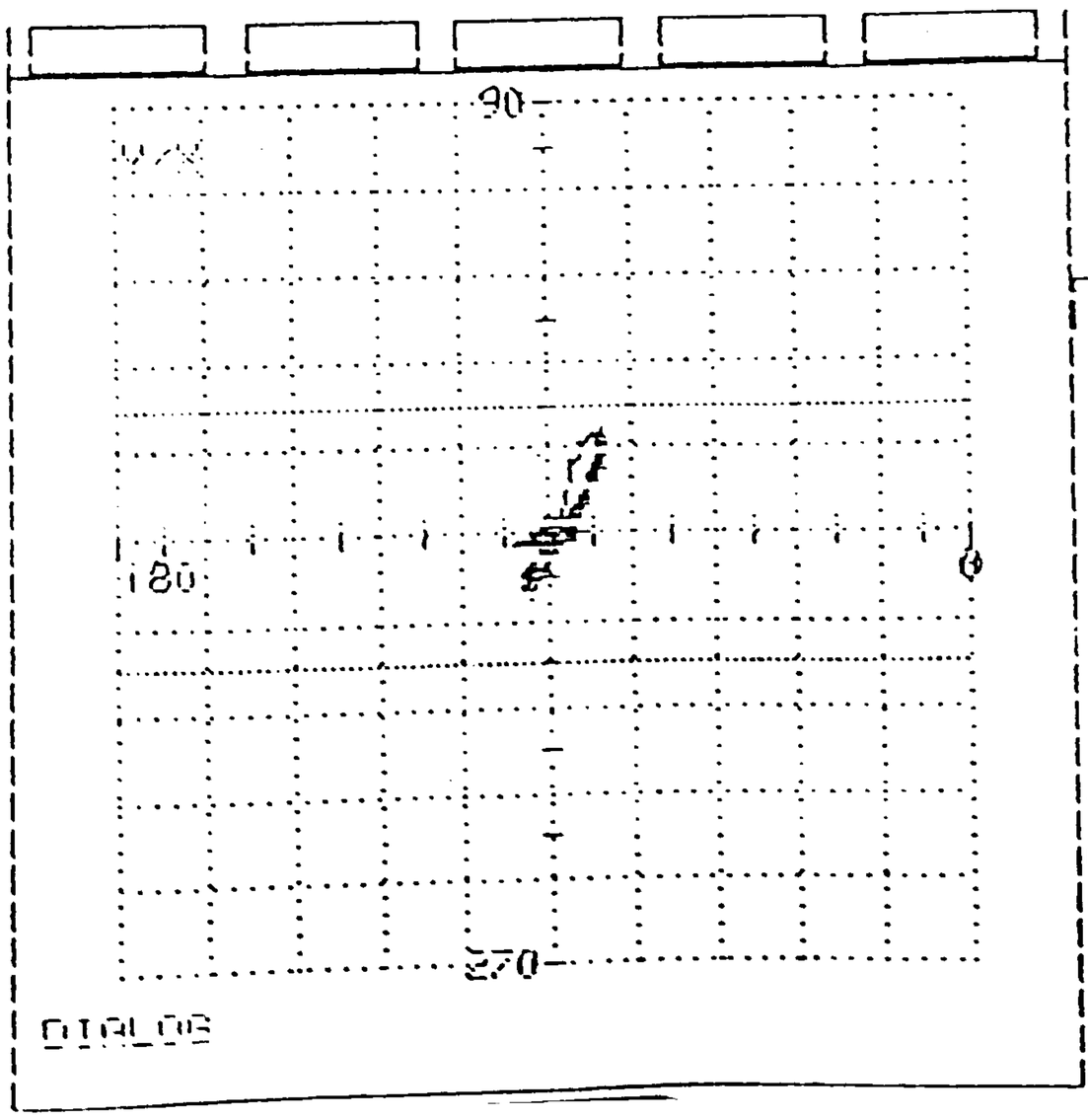

DEFECT HEIGHT 9mm AT
7mm SUBSURFACE DEPTH

Appendix 5

Report from National NDT Centre Culham

' ULTRASONIC SCANS OF NAB SAMPLE NABPC FOR BABCOCK ROSYTH/MOD'.

BY

J MOGGERIDGE

FEB. 1997

Ultrasonic scans of Nab Sample NABPC for Babcock Rosyth/MOD

J Moggeridge

February 1997

Title :	Ultrasonic scans of Nab Sample NABPC for Babcock Rosyth/MOD
Customer	
Customer reference	
Confidentiality, copyright and reproduction	Restricted - Commercial This document has been prepared by AEA Technology plc in connection with a contract to supply goods and/or services and is submitted only on the basis of strict confidentiality. The contents must not be disclosed to third parties other than in accordance with the terms of the contract.
File reference	NABPC.DOC
Reference number	

AEA Technology plc
National NDT Centre
E1 Culham
Abingdon
Oxfordshire
OX14 3DB
Telephone 01235 464065
Facsimile 01235 463799

Report Manager	Name	J Moggeridge
Approved by	Name	C E Bull
	Signature	
	Date	

Contents

1 Introduction 4

2 Method 4

3 Equipment used 5

4 Results 6

4.1 CHART 1 6
4.2 TABLE 1 7

1 Introduction

This document covers the work carried out at the National NDT Centre Culham for the Babcock Royal Dockyard, Rosyth and the Ministry of Defence, Bath. The work involved the ultrasonic scanning of a Nickel Aluminium Bronze(NAB) sample as supplied by Babcock Royal Dockyard Rosyth and the results of the examination sent to the MOD at Bath. Following the ultrasonic examination of the sample, a detailed corrosion map was to be compiled showing the position of the corrosion in the sample with respect to a datum. A µPlus computerised ultrasonic flaw detector was used for the inspection.

2 Method

The sample was divided into 8 strips, each strip being 10mm wide, see figure 1. The sample was scanned as shown in figure 1 and the data stored to floppy disc. From the data it was possible to measure the depth and position of any indications across the sample. Chart 1 shows the position of the indications across the sample, and table 1 the depth, position and nature of the indication. The actual position of any indication is central between the lines marked on the sample, see figure 1.

Figure 1

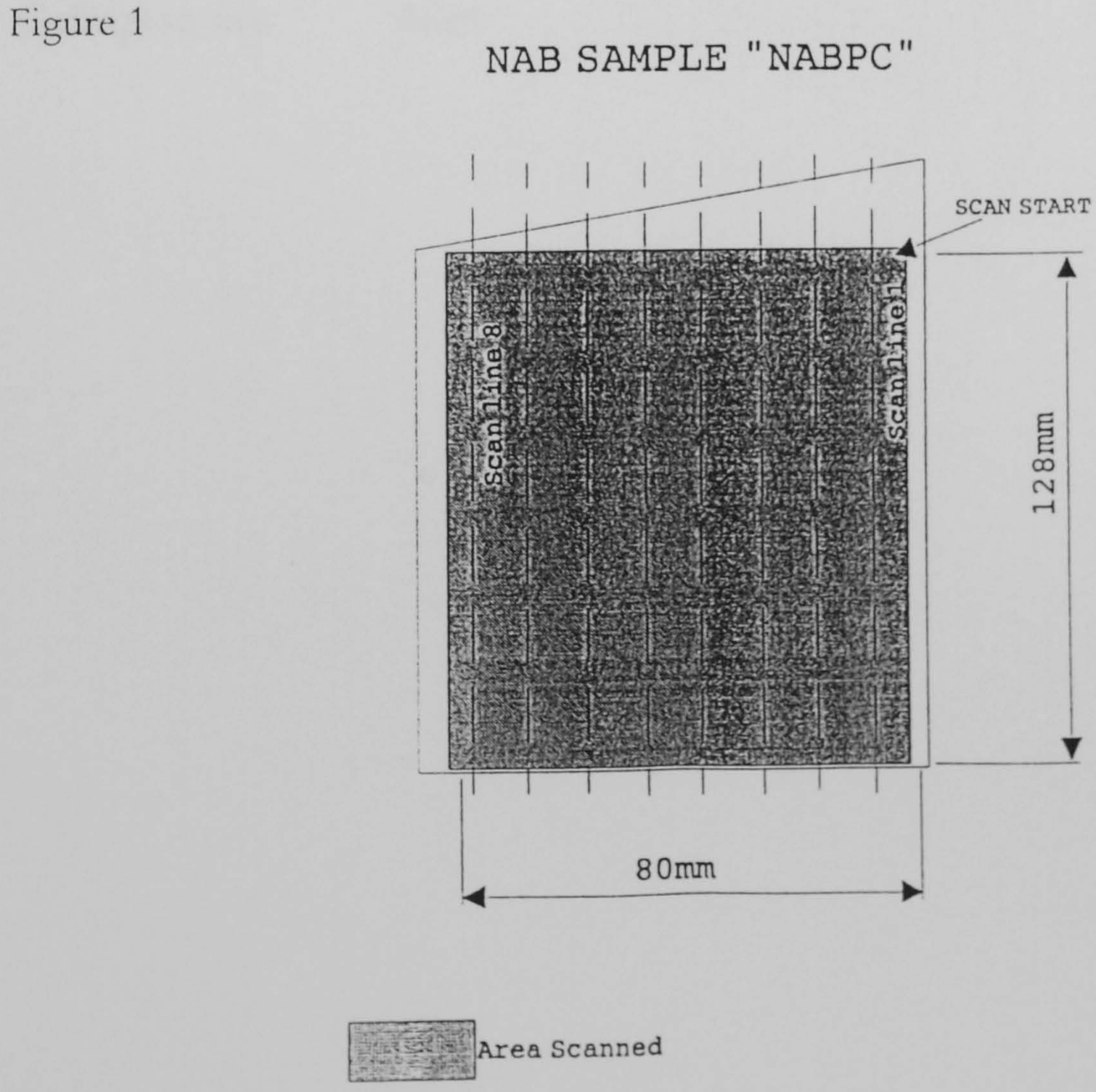

3 Equipment used

AEA technology μPlus Computerised Ultrasonic Data Collection and Analysis System.
Aerotech Alpha 2.25mhz 6mm diameter probe.
The settings of the equipment were as follows:

TX/RX	04 / 04	PRF	500Hz
Channel Gain	44dB	DAC	no
HT Voltage	200V	Probe angle	0 deg
Pulse width	120ηsec	Digitizer Start	0
High pass filter	0.5MHz	A-Scan length	20μsec
Low pass filter	10MHz	Digitizer frequency	32MHz
Rectifier	no	Averaging	16 frame
Rectifier filter	2.5MHz	Display rate	150

Scan settings:

Scan start	0
Scan finish	250
Raster spacing	0.5
Save to disk	no
Display mode	scroll
Collection mode	free run
Collection axis	Axial

4 Results

From the data collected it was possible to compile following chart and table to position the signals seen relative to the sample. Not all the signals seen in the sample were considered to be corrosion as they appeared too strong and were probably casting defects e.g. porosity.

4.1 CHART 1

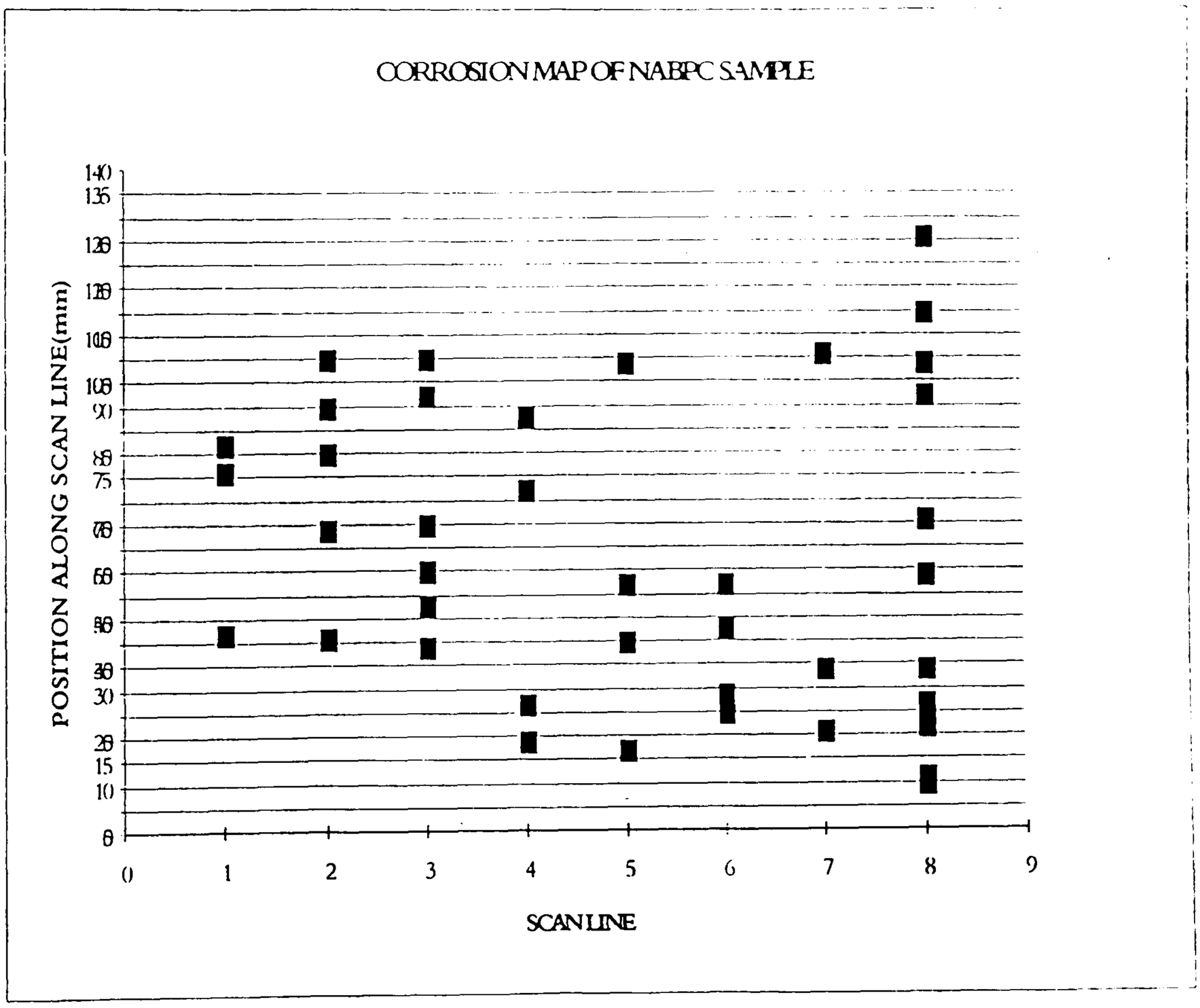

4.2 TABLE 1

Scan Line :	Position of indication from start of scan(mm)	Depth of indication from surface (mm).	Type of indication
1	42, 76, 82	20.2, 22.5, 26.5	C, C, C.
2	41, 64, 80, 90, 100.	25, 26, 19.7, 25, 26.	C, C, P, C, C.
3	39, 48, 55, 65, 92, 100.	24, 20.5, 23, 24, 18.2.	ALL CORROSION.
4	19, 27, 72, 88.	18, 28.7, 22.25, 24	P, C, C, C.
5	17, 40, 40, 52, 99.	24, 29, 24, 23, 24	ALL CORROSION.
6	25, 29, 43, 52.	19.3, 29.5, 23, 23.	P, C, C, C.
7	21, 34, 101.	21, 21, 25.	ALL CORROSION.
8	10, 11, 22, 34, 27, 54, 66, 92, 99, 110, 126.	21, 30, 22, 23.5, 29, 23, 24, 24.5, 27, 29, 21.3.	ALL CORROSION.

Legend: C = Corrosion, P= Porosity.

NAB TEST BLOCK
NDE SECTION
NTD
FASLANE
HM NAVAL BASE CLYDE

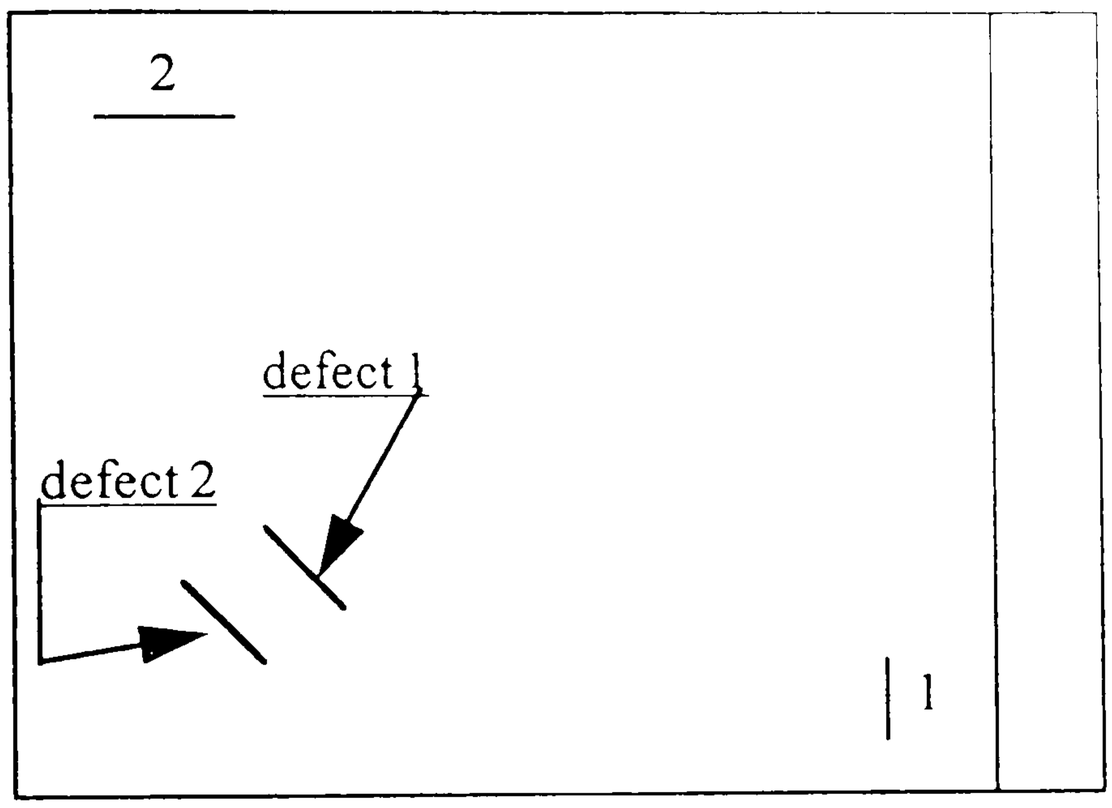

PLAN VIEW OF TEST BLOCK

DEFECT 1
POSITION FROM DATUM 1 = 75 mm
POSITION FROM DATUM 2 = 125 mm
SAMPLE THICKNESS = 17.4 mm
CORROSION PENETRATION = 2.3 mm
REMAINING SOUND MATERIAL = 15.1 mm

DEFECT 2
POSITION FROM DATUM 1 = 90 mm
POSITION FROM DATUM 2 = 135 mm
SAMPLE THICKNESS = 17.7 mm
CORROSION PENETRATION = 2.5 mm
REMAINING SOUND MATERIAL = 15.2 mm

DEFECT (2)

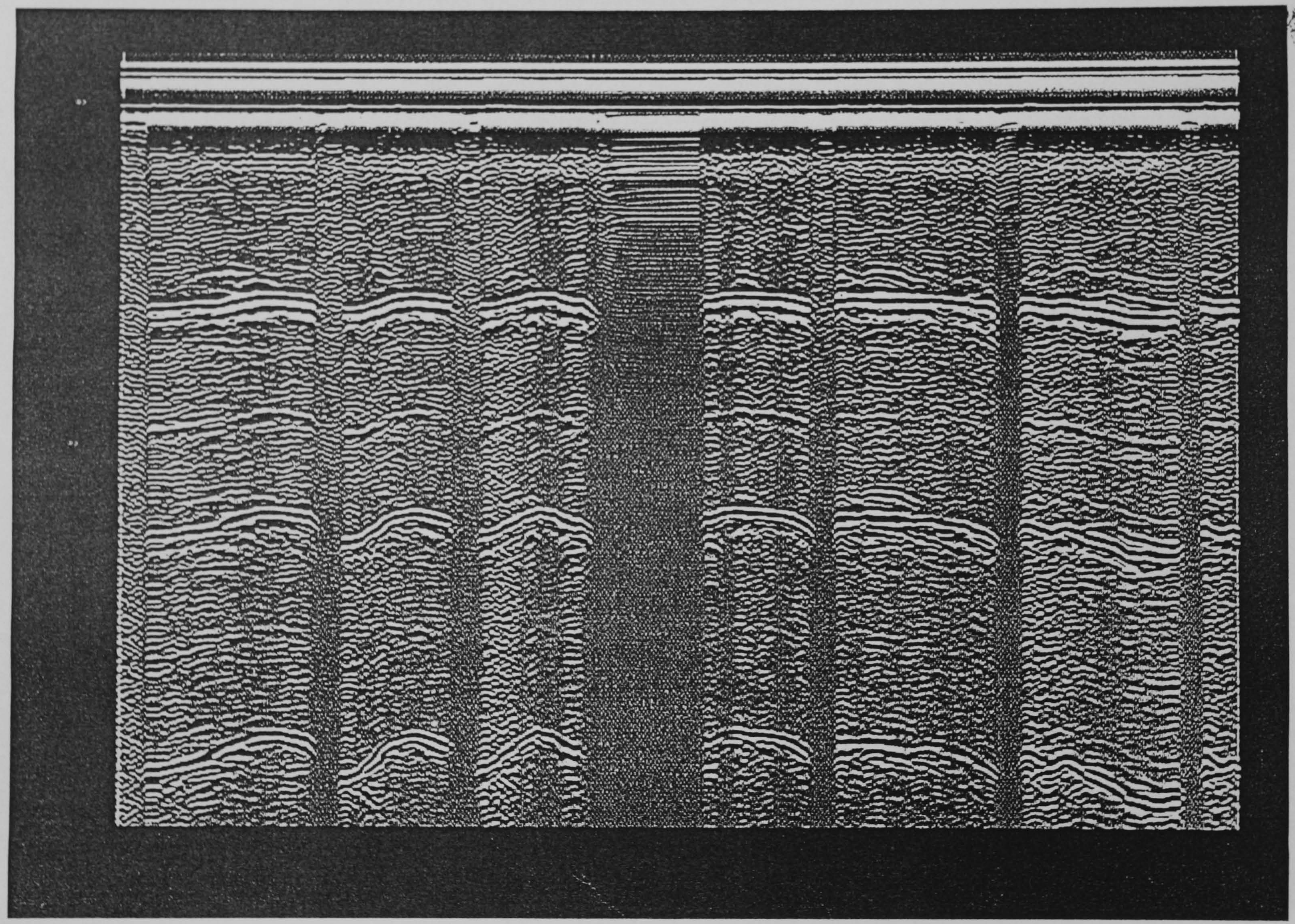

DEFECT (1)